https://ntrs.nasa.gov/search.jsp?R=19700001724 2020-03-12T04:56:07+00:00Z

N 70 11028

NASA CR 106637

CASE FILE COPY

Bell Telephone Laboratories
Research and Development Unit of the Bell System

FINAL REPORT

PARTICLE DETECTION EXPERIMENT FOR APPLICATIONS TECHNOLOGY SATELLITE 1 (ATS-1)

May 1, 1969

Contract No. NAS 5-9635

FINAL REPORT
PARTICLE DETECTION EXPERIMENT FOR APPLICATIONS TECHNOLOGY SATELLITE 1 (ATS-1)

May 1, 1969

Contract No. NAS 5-9635

Prepared by Bell Telephone Laboratories, Incorporated
Mountain Ave., Murray Hill, N. J. 07974
on behalf of Western Electric Company, Incorporated
83 Maiden Lane, New York, N. Y. 10038

Project Manager: Walter L. Brown
Project Engineer: G. L. Miller

W. M. Augustyniak H. B. Lie
I. Hayashi L. V. Medford
H. E. Kern D. A. H. Robinson
R. W. Kerr J. W. Rodgers
L. J. Lanzerotti G. H. Wheatley

for

Goddard Space Flight Center
Greenbelt, Maryland 20771

Technical Monitor: F. H. Wainscott II

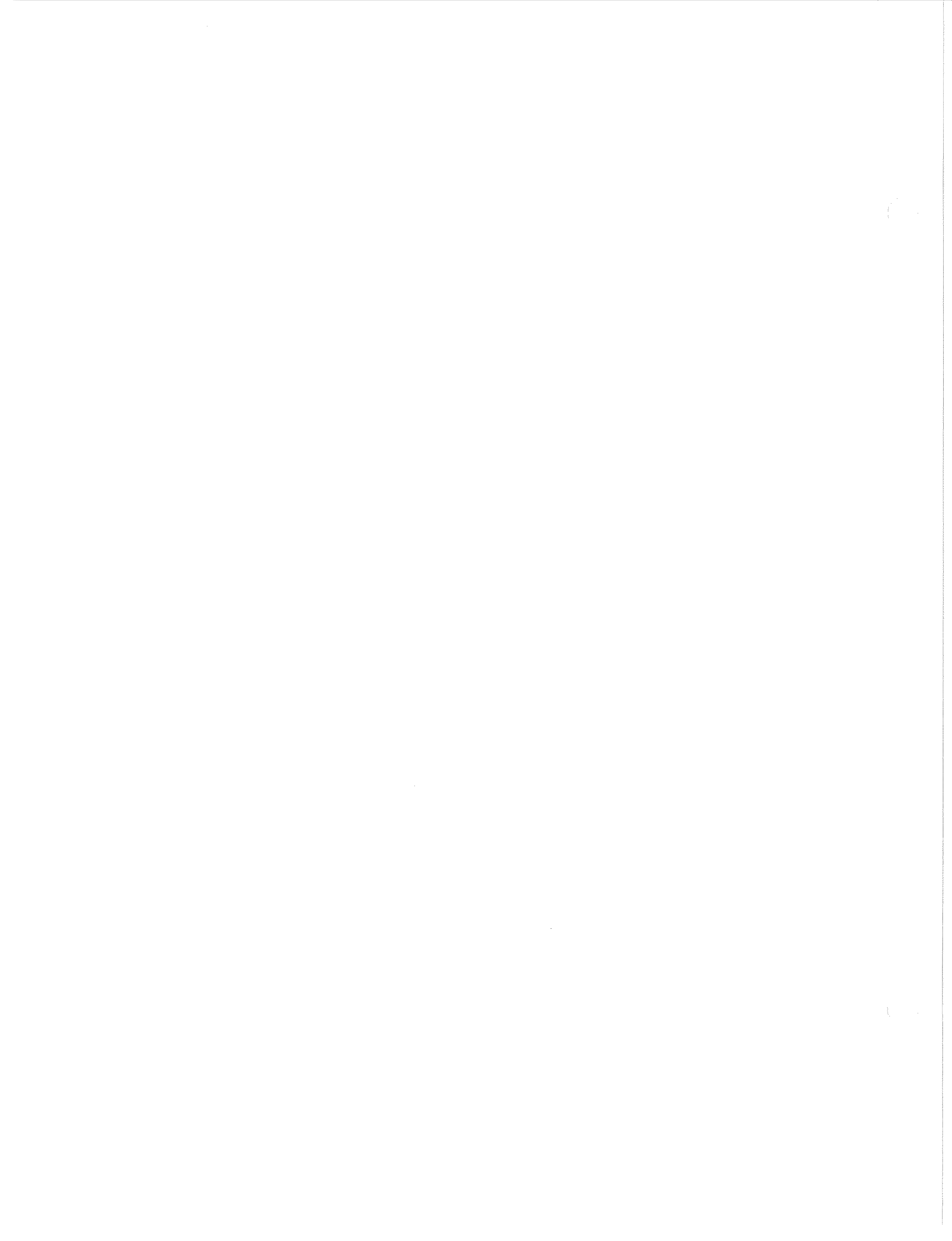

TABLE OF CONTENTS

		Page
Chapter 1.	INTRODUCTION	1-1
	1.1 Experimental Objectives	1-1
	1.2 Experimental Scheme	1-1
	1.2.1 The Detector Telescope	1-1
	1.2.2 Experimental Modes	1-2
	1.2.3 Operation of the Experiment	1-5
	1.2.4 Mode Sequence	1-5
	1.2.5 Telemetry Format	1-8
Chapter 2.	THE DETECTOR SYSTEM	2-1
	2.1 The Detector Telescope	2-1
	2.1.1 Introduction	2-1
	2.1.2 The Detector Element	2-1
	2.1.3 The Mechanical Assembly	2-5
	2.1.4 Testing	2-10
	2.2 The Radioactive In-Flight Calibration System	2-18
	2.2.1 Introduction	2-18
	2.2.2 The Rotary Solenoid	2-20
	2.2.3 Radioactive Sources	2-30
	2.3 Mount for the Detector Telescope and Calibration Solenoid	2-32
	2.3.1 Description of Construction	2-32
	2.3.2 Detector Socket and Concentric Ground	2-32
	2.3.3 The Collimation Assembly	2-35
	2.3.4 Mounting the Solenoid-Source Assembly	2-38
	2.3.5 Measurements with the Calibration System	2-39
	2.4 Detector Telescope Insertion-Extraction Tool	2-41

Page

		Page
Chapter 3.	THE ELECTRONIC SYSTEM	3-1
	3.1 Simplified Description of the Electronic System	3-1
	3.2 Circuit Design Considerations — Microcircuits	3-3
	3.3 The Analog Building Blocks	3-4
	3.3.1 The Amplifier	3-4
	3.3.2 The Zero-Crossing Discriminator	3-4
	3.3.3 Linear Gate	3-8
	3.3.4 Pulse Shaper	3-8
	3.3.5 Potentiometer Network	3-11
	3.4 The Complete Electronic System	3-11
	3.4.1 Linear Signal Processing	3-11
	3.4.2 Coincidence Evaluation	3-11
	3.4.3 Block Diagram of the Complete Experiment	3-13
	3.5 Mode Control System	3-17
	3.6 Detector Bias Supply	3-17
	3.7 The Pile-Up Rejector	3-23
	3.8 Radioactive Calibration Source Driver	3-24
	3.9 The Test Pulser	3-27
	3.10 Storage Rejectors	3-28
Chapter 4.	EXPERIMENT PACKAGE DESIGN	4-1
	4.1 Design Philosophy	4-1
	4.1.1 Electro-Mechanical Design	4-1
	4.1.2 Encapsulation Technique	4-10
	4.2 Electronic Stack and Motherboard Layout	4-10
	4.3 Mechanical Design	4-45
	4.3.1 Mechanical Interface with the EME	4-45
	4.3.2 Thermal Control	4-45
	4.3.3 Mechanical Interface with the Rice University Experiment	4-49
	4.3.4 Housing Design	4-49

Page

		Page
Chapter 5.	COMPONENTS AND RELIABILITY	5-1
	5.1 Reliability	5-1
	5.2 Components	5-1
	5.2.1 Specifications and Screening	5-1
	5.2.2 Thin-Film Integrated Circuit Fabrication and Testing	5-28
Chapter 6.	CONSTRUCTION	6-1
	6.1 Printed Circuit Boards	6-1
	6.1.1 Layout and Art Work	6-1
	6.1.2 Fabrication	6-2
	6.1.3 Preparation for Assembly	6-2
	6.2 Assembly Area	6-3
	6.3 Motherboard Assembly	6-4
	6.3.1 Parts Kits and Records	6-4
	6.3.2 Assembly Practices	6-5
	6.3.3 Soldering	6-7
	6.3.4 Testing and Trimming	6-8
	6.3.5 Inspection	6-9
	6.4 Encapsulation	6-13
	6.4.1 Integrated Circuit Encapsulation	6-13
	6.4.2 Motherboard Encapsulation	6-14
	6.4.3 Foam Planing	6-16
	6.5 Electronic Stack Assembly	6-17
	6.5.1 Preparation	6-17
	6.5.2 Harness Wiring Procedure	6-18
	6.5.3 Front End Assembly	6-20
	6.5.4 Detector Mount Assembly	6-22
	6.6 Final Assembly	6-24
Chapter 7.	GROUND SUPPORT EQUIPMENT	7-1
	7.1 General Design	7-1
	7.2 Power Supplies	7-2
	7.3 Ratemeters	7-9
	7.4 Mode Control	7-9

Page

		Page
7.5 Bias Command		7-9
7.6 Precision Pulser		7-12
7.7 Test Points		7-15
Chapter 8.	ENVIRONMENTAL TESTING	8-1
	8.1 Tests	8-1
	8.1.1 Specified Tests	8-1
	8.1.2 Additional Tests	8-1
	8.2 Experimental Checkout	8-1
	8.3 Test Sequence	8-1
	8.3.1 Thermal Cycling	8-1
	8.3.2 Vibration	8-17
	8.3.3 Bakeout	8-17
	8.3.4 Thermal Vacuum	8-17
	8.4 The Individual Tests	8-18
	8.4.1 Thermal Test Apparatus and Procedure	8-18
	8.4.2 Thermal Test Results	8-18
	8.4.3 Vibration Test Apparatus and Procedure	8-18
	8.4.4 Vibration Test Results	8-21
	8.4.5 Vibration Build-up in the Package	8-23
	8.4.6 Thermal Vacuum Test Apparatus and Procedure	8-23
	8.4.7 Thermal Vacuum Test Results	8-30
Chapter 9.	EXPERIMENT CARRYING CASE	9-1

LIST OF ILLUSTRATIONS

Figure		Page
1-1	Schematic of Detector Telescope	1-2
1-2	ΔE versus E_p for Detector 1 through 5	1-3
1-3	Simplified Block Diagram of Proposed ATS Particle Spectra Experiment	1-6
1-4	Experimental Mode Sequence	1-7
1-5	ATS/EME — Mission B Encoder Format	1-9
2-1	dE/dX Silicon Detector	2-2
2-2	Oxide Etching Fixture	2-3
2-3	Lithium-Drifted Silicon Detectors	2-5
2-4	Detector Telescope	2-6
2-5	dE/dX Detector Contact Wafer	2-8
2-6	Lithium-Drifted Silicon Detector Assembly	2-9
2-7	Thermal Vacuum Test — Effect of Temperature on Reverse Current dE/dX Detector — 25 Microns Thick	2-12
2-8	Thermal Vacuum Test — Effect of Temperature on Reverse Current dE/dX Detector — 50 Microns Thick	2-13
2-9	Thermal Vacuum Test — Effect of Temperature on Reverse Current dE/dX Detector — 100 Microns Thick	2-14
2-10	Thermal Vacuum Test — Effect of Temperature on Reverse Current Lithium-Drifted Silicon Detector — 1 mm Thick	2-15
2-11	Thermal Vacuum Test — Effect of Temperature on Reverse Current Lithium-Drifted Silicon Detector — 2 mm Thick	2-16
2-12	Reverse Current History of Lithium-Drifted Silicon Detectors	2-17
2-13	Noise History of Lithium-Drifted Silicon Detectors	2-19
2-14	Radioactive Calibration Assembly	2-20
2-15	Rotary Solenoid	2-21
2-16	Rotary Solenoid Magnetic Circuit	2-22
2-17	Solenoid Magnetic Characteristics	2-24
2-18	Bearing Torque Test	2-28
2-19	Radioactive Source Assemblies	2-31
2-20	Detector Mount Assembly	2-33
2-21	Front Ring Installation Tools	2-37
2-22	Rotary Solenoid Mounting	2-38

Figure		Page
2-23	Calibration Spectra, Alpha Particles	2-40
2-24	Detector Telescope and Insertion-Extraction Tool	2-40
3-1	Simplified Block Diagram of the Electronic System	3-2
3-2	Schematic of the Linear Amplifier	3-6
3-3	Thin-Film Linear Amplifier	3-7
3-4	Schematic of the Zero-Crossing Discriminator	3-8
3-5	Schematic of the Linear Gate	3-9
3-6	Schematic of the Pulse Shaper	3-10
3-7	Simplified Schematic of the Linear System	3-12
3-8	Simplified Schematic of the Coincidence System	3-13
3-9	Block Diagram of the Complete Experiment	3-15
3-10	Simplified Schematic of the Mode Control System	3-18
3-11	Detailed Schematic of the Mode Control System	3-19
3-12	Schematic of the Detector Bias Supply	3-21
3-13	Pileup Rejector Waveform	3-24
3-14	Schematic of the Calibration Source Driver	3-25
3-15	Schematic of the Test Pulser	3-29
4-1	BTL Particle Experiment for ATS, Block Diagram	4-3
4-2	Thin-Film Integrated Circuits	4-5
4-3	Environmental Measurements Experiment Housing and Location in the ATS-B Spacecraft	4-6
4-4	Electronic Stack, Assembly Drawing	4-7
4-5	BTL Experiment Development Model	4-9
4-6	Motherboard Dimensions	4-11
4-7	BTL Experiment Flight Model with Cover and Detector Details Removed	4-13
4-8	Motherboard 1	4-14
4-9	Motherboard 2	4-14
4-10	Motherboard 3	4-15
4-11	Motherboard 4	4-15
4-12	Motherboard 5	4-16
4-13	Motherboard 6	4-16
4-14	Motherboard 7	4-17
4-15	Motherboard 8	4-17
4-16	Motherboard 9	4-18
4-17	Motherboard 10	4-18
4-18	Motherboard 1, Schematic	4-19
4-19	Motherboard 2, Schematic	4-21
4-20	Motherboard 3, Schematic	4-23

Figure		Page
4-21	Motherboard 4, Schematic	4-25
4-22	Motherboard 5, Schematic	4-27
4-23	Motherboard 6, Schematic	4-29
4-24	Motherboard 7, Schematic	4-31
4-25	Motherboard 8, Schematic	4-33
4-26	Motherboard 9, Schematic (Sheet 1)	4-35
4-27	Motherboard 9, Schematic (Sheet 2)	4-37
4-28	Motherboard 10, Schematic (Sheet 1)	4-39
4-29	Motherboard 10, Schematic (Sheet 2)	4-41
4-30	BTL Experiment Flight Model, Front View	4-46
4-31	BTL Experiment Flight Model, Rear View	4-46
4-32	EME/BTL Experiment Interface Control Drawing	4-47
4-33	Mechanical Assembly Drawing	4-51
4-34	Front Plate and Right Side of the Experiment Housing	4-53
4-35	Right Side Drawing	4-55
4-36	Left Side Drawing	4-57
4-37	Front Plate Drawing	4-59
4-38	Back Plate Drawing	4-61
4-39	Partition Drawing	4-63
4-40	Top Cover Drawing	4-65
4-41	Bottom Cover Drawing	4-67
4-42	Ground Plane Finger Contact Drawing	4-69
4-43	Detector Mount Drawing	4-71
4-44	Test Jack Bracket Drawing	4-73
5-1	Reliability Analysis Documentation Sheets 1 - 17	5-2/ 5-18
5-2	Thin-Film Circuit Lead Bending Tool	5-30
6-1	Flight Hardware Assembly Room	6-3
6-2	Motherboard 10 Shown with its Parts Kit	6-5
6-3	Motherboard 10 During Assembly	6-6
6-4	Thin-Film Circuit Foam Encapsulation Molds	6-14
6-5	Motherboard Form Encapsulation Mold	6-15
6-6	Foam-Encapsulated Motherboard	6-16
6-7	Harness Wiring During Assembly	6-18
6-8	A Completely Wired Electronic Stack	6-20
6-9	Interlocking Shielding Partition Drawing	6-21
6-10	Vertical Shielding Baffle Drawing	6-21
6-11	A Front-End View of the Assembled Experiment	6-22

Figure		Page
6-12	Rear View of Partially Assembled Detector Mount	6-23
6-13	The Completely Assembled and Encapsulated Electronic Stack	6-25
7-1	ATS Particle Telescope Tester	7-1
7-2	Power Supply, Block Diagram	7-3
7-3	Power Supply, ±12V Regulators	7-5
7-4	Stabilized Power Supplies	7-7
7-5	Stabilized Power Supplies	7-7
7-6	Package Current Meter Wiring	7-8
7-7	Voltmeter Switch Wiring	7-8
7-8	Log Ratemeter Schematic	7-10
7-9	Mode and Command Switching	7-11
7-10	Bias Command	7-12
7-11	Mercury Pulses	7-13
7-12	Driver-Attenuator	7-17
8-1	Detector Temperature Checkout Sheet	8-2
8-2	Bias Command Checkout Sheet	8-3
8-3	Bias Monitor Checkout Sheet	8-4
8-4	Detector Bias Voltage Checkout Sheet	8-5
8-5	Mode Logic Checkout Sheet	8-6
8-6	Power Consumption Checkout Sheets 1 and 2	8-7/ 8-8
8-7	Power Supply Monitor Checkout Sheet	8-9
8-8	Threshold of Coincidence Discriminator Checkout Sheet	8-10
8-9	Threshold of 5-Channel Discriminator Checkout Sheets 1-3	8-11/ 8-13
8-10	Internal Pulser I Checkout Sheet	8-14
8-11	Internal Pulser II Checkout Sheet	8-15
8-12	Calibration Source Checkout Sheet	8-16
8-13	Vibration Fixture	8-19
8-14	Thermal Vacuum Chamber, Rear View	8-24
8-15	Thermal Vacuum Chamber, Front View	8-24
8-16	Hot Plate Filament and Thermistor	8-26
8-17	Hot Plate with Horseshoe Shroud	8-26
8-18	Photo Data System, Block Diagram	8-28
8-19	Eight-Scaler Box	8-29
9-1	Experiment Carrying Case	9-1

LIST OF TABLES

Table		Page
1-1	Mode of Operation	1-4
2-1	Treatment of Solenoid Piece Parts	2-23
3-1	Comparative Summary of Microcircuit Features	3-4
5-1	Types and Quantities of Components Used per Experiment	5-19
5-2	Specifications and Screening Programs	5-20
6-1	Inspection Procedures and Schedules	6-9
8-1	Prototype Qualification Vibration Specifications	8-21
8-2	Flight Acceptance Vibration Specifications	8-22

Chapter 1

INTRODUCTION

1.1 EXPERIMENTAL OBJECTIVES

The BTL experiment on ATS-B has been designed to measure the energy spectra of electrons and protons at the synchronous satellite altitude in order to study the systematic day-night variations in the trapped particles arising from the distortion of the earth's magnetic field by the magnetospheric boundary with the solar wind, the perturbations in the trapping associated with magnetic storms, and the long-term changes in the particles during the time of increasing solar activity. The telescope provides spectral information for electrons in the 0.4- to 3-MeV energy range and for protons in the 0.6- to 22-MeV energy range. The experiment also permits investigation of the possible existence of α particles within the magnetosphere in the energy range from approximately 6 to 85 MeV.

1.2 EXPERIMENTAL SCHEME

1.2.1 The Detector Telescope

The particle-detecting instrument is a multi-element semiconductor telescope illustrated schematically in Figure 1-1. It consists of five semiconductor wafers with a total of six active detecting elements. The first three wafers are thin, totally depleted, diffused n-on-p type silicon diodes. They are made by a planar technique in which the ambient-sensitive edge of the junction is protected by silicon dioxide. The fourth and fifth wafers are relatively thick lithium drifted p-i-n diodes. They are encapsulated together in a windowless Kovar can, using a gold-silicon alloy seal etween the can and the fourth detector wafer. This fourth wafer is divided by two angular grooves into three concentric areas. The inner two serve as independent active detecting elements as the telescope is used. The table in Figure 1-1 lists the thicknesses of the six detector elements and their effective detection areas.

The detector stack is enclosed in an aluminum shielding block through which particles have entrance via by a conical collimator with a 20° half angle. The collimator is designed with stepped baffles to minimize in-scattering of particles outside the desired acceptance geometry. Two thin foils (titanium and nickel) serve to exclude light and heat from the detector assembly.

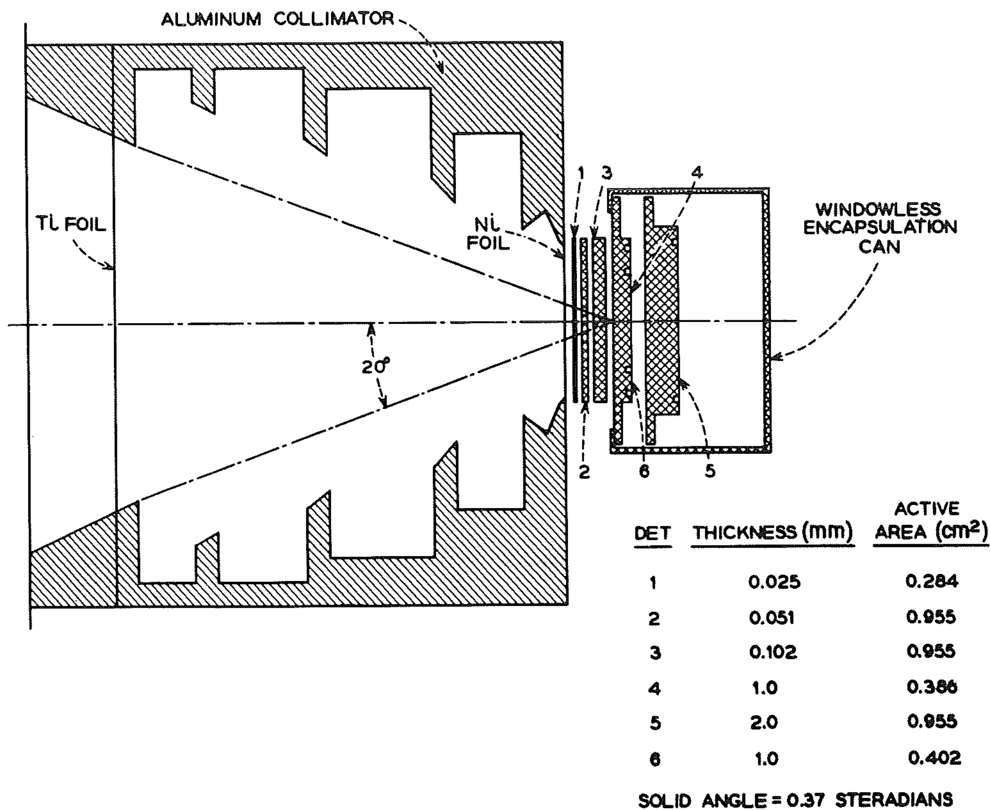

DET	THICKNESS (mm)	ACTIVE AREA (cm²)
1	0.025	0.284
2	0.051	0.955
3	0.102	0.955
4	1.0	0.366
5	2.0	0.955
6	1.0	0.402

SOLID ANGLE = 0.37 STERADIANS

Figure 1-1. Schematic of Detector Telescope

As the detector is mounted in the ATS-B satellite, it looks out perpendicular to the spin axis. Since the spin axis of the satellite is approximately parallel to the earth's rotational axis, the telescope looks out approximately perpendicular to the local magnetic field. It accepts particles with equatorial pitch angles greater than approximately 60°.

1.2.2 Experimental Modes

Figure 1-2 illustrates the energy deposited in detectors 1 through 5 due to protons axially incident on the detector stack. Each of the curves is characteristically double-valued, corresponding to particles with less and with more than enough energy to penetrate the detector. The ambiguity as to which side of the characteristic a given pulse belongs is removed in the present experiment by coincidence requirements among the detectors. The approximate minimum pulse height discrimination level for each detector is indicated by a horizontal line crossing its characteristic.

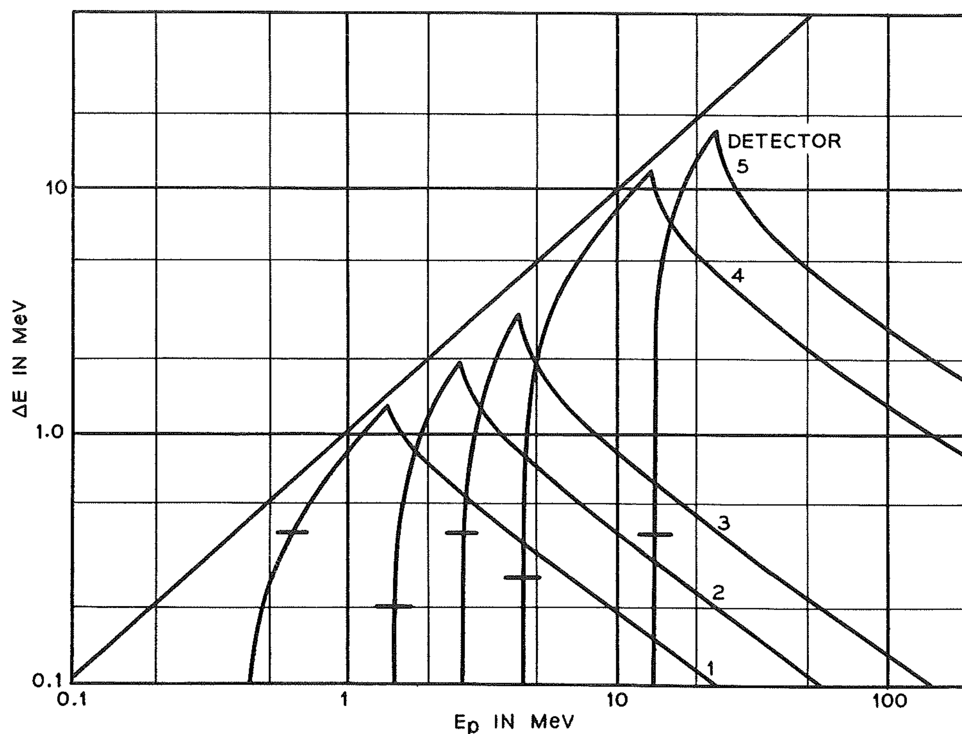

Figure 1-2. ΔE versus E_p for Detectors 1 through 5

The total proton energy range to which the instrument is sensitive extends from approximately 0.6 MeV to well above 100 MeV. The lower bound is established by the titanium and nickel entrance foils; a practical upper bound has been chosen at 100 MeV. This energy range involves a number of different coincidence possibilities, starting from a pulse in detector 1 alone, for a proton of about 1 MeV, to total penetration of the set of five detectors at proton energies above 22 MeV.

The α particle sensitivity of the instrument is nearly the same as that for protons, with all energies increased by approximately a factor of 4.

The telescope is also sensitive to electrons. The thin detectors have a low probability of stopping electrons with high enough energy to satisfy minimum pulse height requirements. This is not the case for the thick devices which thus are primarily involved in electron detection. The minimum detectable electron energy is approximately 0.4 MeV. The sensitivity of the telescope extends to very high electron energies, but the probability of complete energy absorption by the detector elements decreases as the mean electron range increases beyond 3 mm, the total thickness of detectors 4 and 5. Clear distinction of electron spectra can be made to energies of about 3 MeV. Clear distinction of electrons from protons are made on the basis of pulse height in the thin detectors. Because in most cases electrons

leave so little energy in these detectors, anti-coincidence conditions on the pulses from these devices can be used to eliminate heavy particle events.

The first column of Table 1-1 lists the nine different modes of operation which has been selected for the experiment. The second column of the table indicates the detectors involved in each of the modes of operation. The third column indicates the particles and their energy ranges which are detected in this mode. The fourth column takes note of the special requirements on the pulses.

Table 1-1
MODE OF OPERATION

Mode	Detectors Involved	Particle & Energy Ranges (MeV)	Remarks
A	1 $\bar{2}$	$0.7 < p < 1.5$ $1.8 < \alpha < 5.7$	$E_1 > .4$ MeV
B	1 2 $\bar{3}$	$1.6 < p < 2.8$ $6.0 < \alpha < 10$	$E_1 > .4$, $E_2 > .2$
C	2 3 $\bar{4}$ $\bar{6}$	$2.8 < p < 4.5$ $10.5 < \alpha < 17$	$E_2 > .2$, $E_3 > .4$
D	3 4 $\bar{5}$ $\bar{6}$	$4.5 < p < 14$ $18 < \alpha < 50$	$E_3 > .4$, $E_4 > .3$
E	2 4 5 $\bar{6}$	$14 < p < 22$ $50 < \alpha < 85$	$E_4 > .3$, $E_5 > .4$
F	$\bar{3}$ 4 5 $\bar{6}$	$22 < p < 100$	$1.2 < E_4 < 6$, $E_5 > .4$
G	4 5 $\bar{6}$	$e > 1$ MeV	$.3 < E_4 < 1.2$, $E_5 > .4$
H	$\bar{3}$ 4 $\bar{5}$ $\bar{6}$	$e < 1$ MeV	$E_4 > .3$
I	2 3 4 5 6		Singles

In the first eight modes, coincidence and/or anti-coincidence requirements are placed on the pulses that are detected. Mode I records the singles rates for detectors 2 through 6 for a check on detector noise and particle background.

In modes C through H, detector 6 is involved in anti-coincidence. This annular detector which surrounds detector 4, serves to exclude incident particles that arrive at odd angles through the detector housing and to exclude events in which a particle (particularly an electron) is scattered outside the active region of detector 4 so that its total energy is not available for analysis.

In modes C, D, E, and F, signals from detector 1 (and sometimes detector 2 or 3) are ignored although there must be coincident pulses from these detectors for

real proton or α particle events. Neglecting these additional coincident constraints increases the overall reliability of the experiment. If detector 1, 2, or 3 should fail because of noise or radiation damage, significant portions of the experiment would still be operational. Detector 4 enters in the most sensitive role since it is involved in seven of the nine modes, and in six of these as a coincident (rather than an anti-coincident) detector.

In electron mode H, the anti-coincidence on detector 3 eliminates the possibility of a proton event. In electron mode G, the additional constraint on the size of the detector 4 pulse ($0.3 \text{ MeV} < E_4 < 1.2 \text{ MeV}$) eliminates events from protons with less than 100 MeV. If detector 5 receives a pulse from a proton, the proton must necessarily have left energy greater than 1.2 MeV in detector 4 unless the proton had more than 100 MeV. The expected flux of particles with such a high energy is so low as to make this limit on the experiment unimportant.

1.2.3 Operation of the Experiment

Figure 1-3 shows the way in which the signals from the six active elements of the detector telescope are handled by the electronic system. Pulses from the detectors are amplified in amplifiers with double 1-microsecond clipping. The outputs drive coincidence circuits, the requirements of which may be changed for different experimental modes. The amplified pulses also pass through linear gates (where gain may be changed in different modes). The sum of the detector pulses which are involved in a given mode of the experiment are finally sorted in broad energy groups in a 5-channel pulse height analyzer, and routed to five 16-bit storage registers in the telemetry.

A single experimental mode (mode A or H, for example) is active during a single telemetry sequence, pulses being stored in the 5-channel registers and then read out by the telemetry at the end of the storage period. At the end of a telemetry sequence the experimental mode is changed, the storage registers are reset, and the 5-channel storage begins again under a different combination of coincidence and gating conditions corresponding to a new experimental mode. The mode sequencing is under control of the telemetry sequence clock.

1.2.4 Mode Sequence

The nine modes of the experiment do not receive equal weight in the experimental sequence, because of the greater importance of the electron and low energy proton modes for the orbit of ATS-B. The actual experimental mode sequence is shown in Figure 1-4, together with the timing signals of various lines from the telemetry sequence clock. One complete experimental sequence occupies 32 telemetry sequences. The two 16 telemetry sequence portions of this total, however, differ only in whether or not a pileup rejector is enabled or disabled (see Paragraph 3.7).

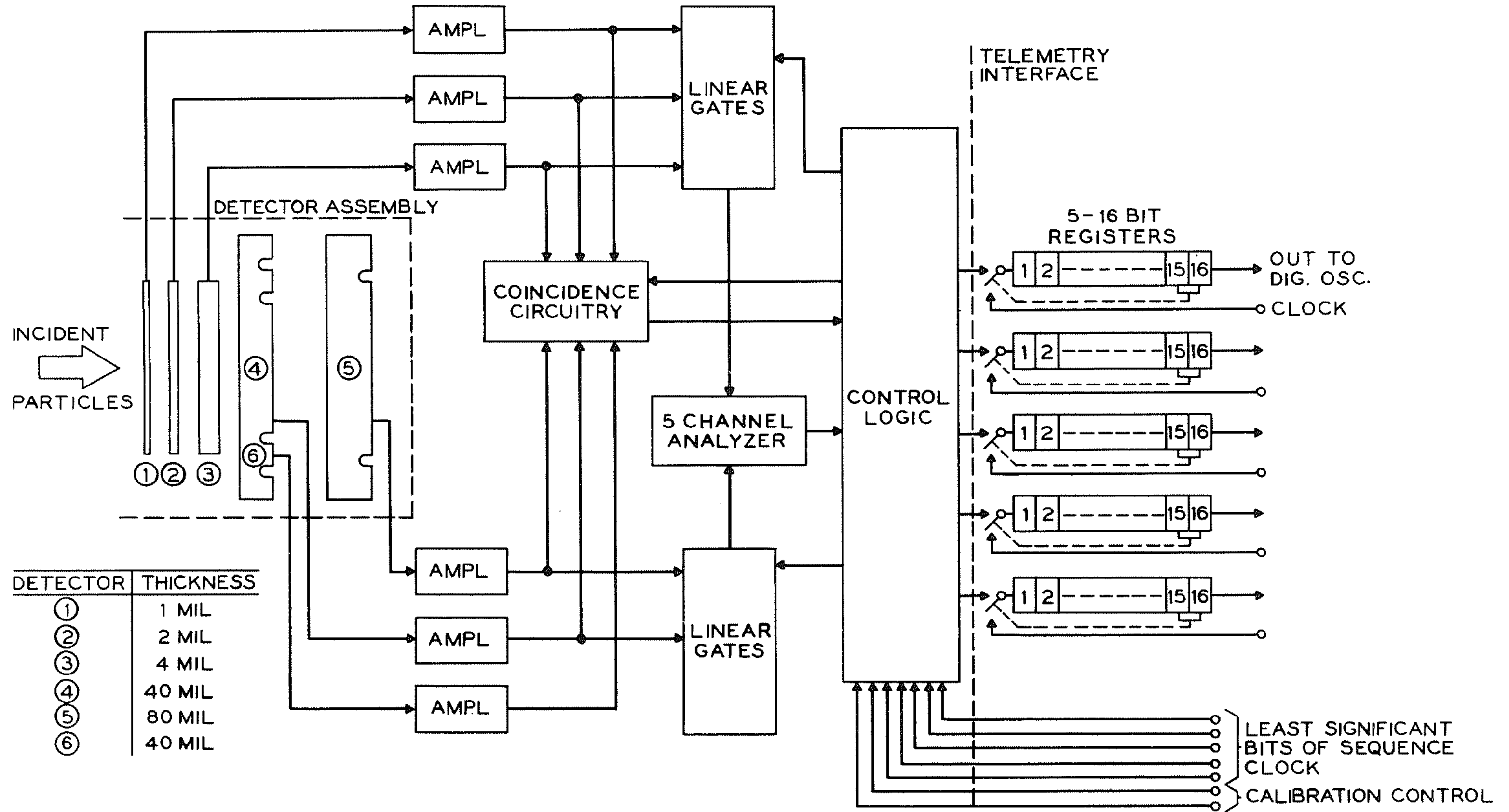

Figure 1-3. Simplified Block Diagram of Proposed ATS Particle Spectra Experiment

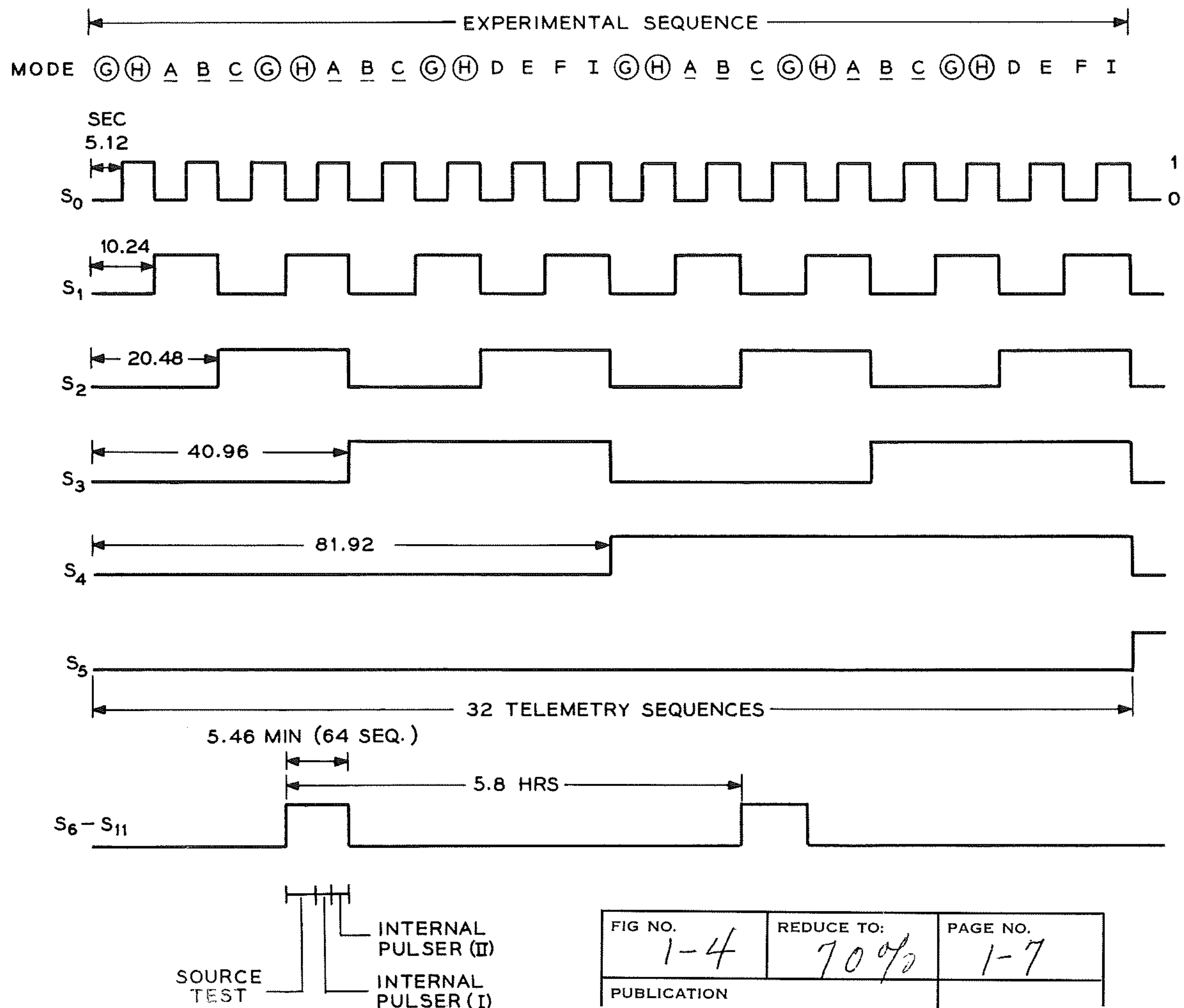

Figure 1-4. Experimental Mode Sequence

Figure 1-4 indicates a long period signal that arises from the coincidence of all sequence clock lines between S_6 and S_{11}. This signal provides a group of 64 telemetry sequences (two complete experimental sequences) once each 5.8 hours. During this 64-telemetry-sequence group, special tests are carried out in the BTL experiment. During 32 of the sequences, a radioactive calibration source (see Paragraph 2.5.2) is extended into the throat of the acceptance cone of the detector and provides alpha and beta particles for checking overall calibration of the system. During the remaining 32 telemetry sequences, test pulses are internally injected into the electronics to test the consistency of the various gain and discrimination settings. This is described in detail in Paragraph 3.9.

1.2.5 Telemetry Format

Figures 1-5(a) and (b) show the position of the BTL data in the telemetry format. The five 16-bit registers are read out once each telemetry sequence, at the end of the sequence and in the burst half of the format (Figure 1-5(a)). During the period of readout, the registers are frozen so that the readings of all five may reflect the same physically observed events.

In order to get information on a finer time scale, the middle eight of the 16 bits of register 1 are read out once each telemetry frame in the blank half of the format (Figure 1-5(b)). During the two telemetry words of each frame that this reading requires, all five registers are frozen so that all may once again reflect the same physical events. In telemetry frames 14 and 15, the middle-bit readings provide additional redundancy with the complete 16-bit readings of the register in the burst portion of the format.

The total gated time of the registers is 3.89 seconds out of the 5.12-second period of the telemetry sequence.

Figure 1-5(a) shows additional monitoring measurements provided in the telemetry for the BTL experiment. Readings are made of the detector temperature, detector bias, and of the four power supply voltages provided in the BTL packages.

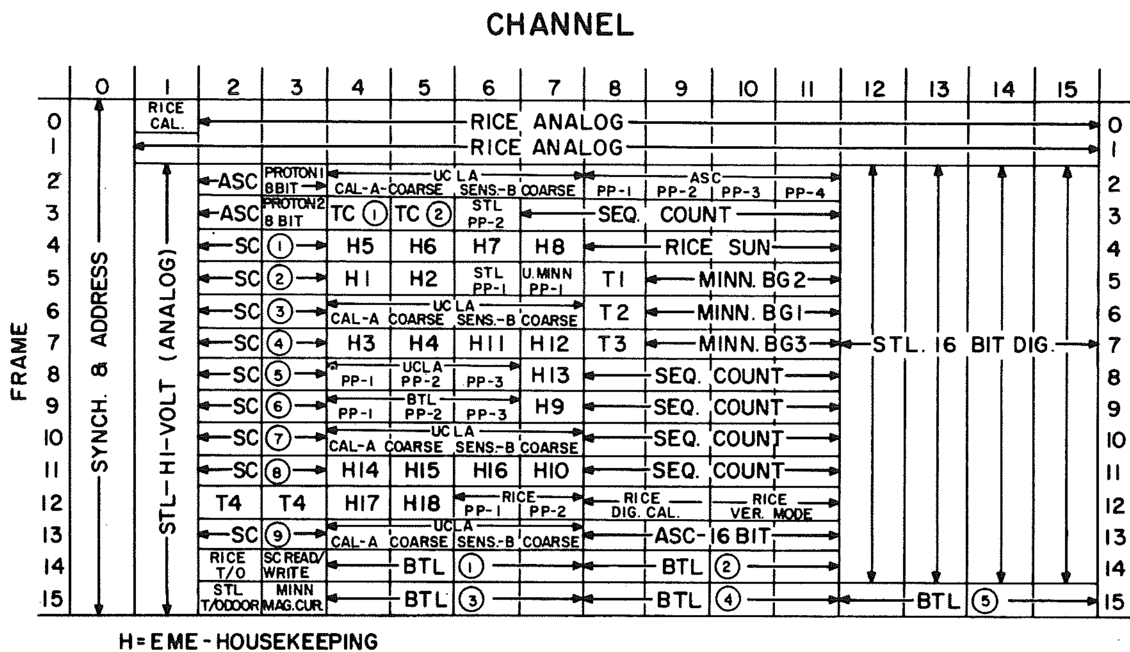

Figure 1-5(a). ATS/EME — Mission B Encoder Format (Burst)

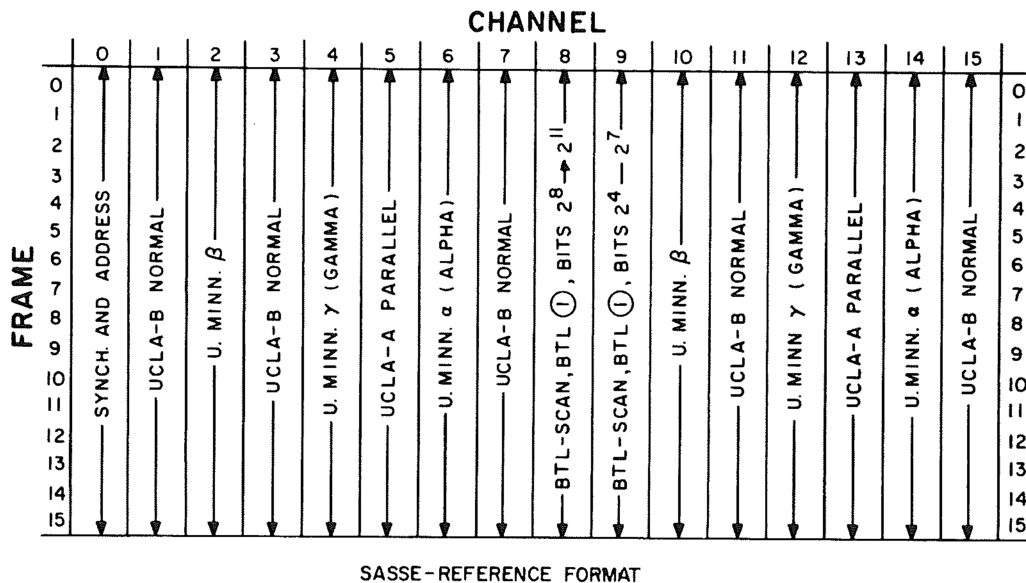

Figure 1-5(b). ATS/EME — Mission B Encoder Format (Reference)

Chapter 2

THE DETECTOR SYSTEM

2.1 THE DETECTOR TELESCOPE

2.1.1 Introduction

The multi-element silicon radiation detector telescope aboard the ATS-1 satellite was developed for experiments on charged particles in space.[1*] The telescope consists of three thin diffused p-n junction detectors 25-, 50-, and 100-microns thick, backed up by two thick lithium-drifted detectors 1-mm and 2-mm thick. The telescope has an effective area of approximately 0.4 cm^2 and, with its front collimator, has an acceptance half-angle of approximately 20 degrees. The experiment required a compact detector arrangement which had good detection characteristics for electrons, protons, and alpha particles over a wide energy range. A major effort was directed towards obtaining a structure which satisfied these requirements, was capable of withstanding launch vibrations of approximately 50 g and was electrically stable under the temperature cycling and vacuum conditions of the orbital environment. Stringent requirements were placed on the design as to weight, size, and materials. Other major considerations were the method of connection to the associated electronics and radiation damage problems.

2.1.2 The Detector Element

2.1.2.1 The dE/dX Detectors

The particle telescope requires three thin, totally depleted, semiconductor particle detectors of 25-, 50-, and 100-microns thickness. These detectors have to be physically rugged, electrically stable, and highly reliable in order to withstand the rigors of launch and operate dependably in space. They must operate at moderate reverse bias voltages to provide high internal electric fields and have low leakage currents and noise. Demountable electrical contacts were also desired, so that individual devices could be replaced should they fail during testing.

---

*A complete list of references will be found at the end of this chapter on page 2-42.

Such devices had been developed for nuclear physics experiments[2] and appeared quite suitable for use in space. They were planar-etched, oxide-passivated, phosphorus-diffused silicon devices which were both physically and electrically reliable. They could be fabricated in the quantities needed using existing techniques and equipment. Figure 2-1 shows the geometrical details of the dE/dX detectors used in the ATS-B experiment.

Fabrication. The detectors are made from p-type silicon in the resistivity range of 600 to 1200Ω cm. This resistivity range was selected to optimize the inversion layer effect common to oxide-passivated detectors.[3] Wafers are cut from the selected silicon ingots to an orientation of 8° off the <110> direction toward the <111> direction and 25° off the <110> direction toward the <100> direction. This orientation was chosen to minimize particle channeling effects.[4] They are diced to a diameter of 0.800 ± 0.002 inch and lapped to a thickness 150μ greater than the desired thickness of the finished device. The origination, cutting, dicing, and lapping are done commercially.[5]

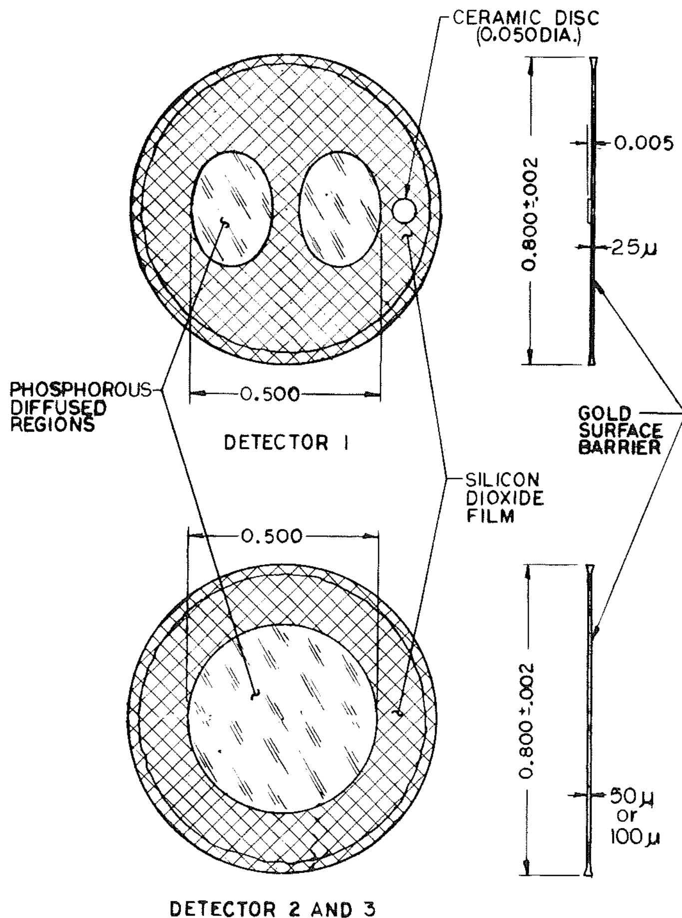

Figure 2-1. dE/dX Silicon Detector

Details of the subsequent fabrication steps have been reported previously.[2] In brief, they involve chemically etching 75μ from one side of a lapped silicon wafer, growing a 5000 Å silicon dioxide film on the wafer in high temperature steam,[6] removing the oxide on the etched side of the wafer from the area which is to be sensitive to radiation, diffusing phosphorus into this exposed silicon, etching 75μ from the back of the wafer, and evaporating a thin gold film on the back to form a surface-barrier blocking contact.[7]

To assure spatial reproducibility of the diffused region, a special fixture was designed to facilitate reproducible removal of the oxide film over specific areas (Figure 2-2). It consists of a gold-plated brass shell containing a Teflon pedestal on which an oxidized wafer is placed. Shims are placed under the pedestal to compensate for the three different wafer thicknesses. A cover plate is secured to the shell, compressing a 7/16-inch I.D. O-ring against the wafer. The assembled fixture is inverted over a cup of hydrofluoric acid, the fumes removing the exposed oxide. A 0.500-inch diameter circular area is removed from the oxide film of the 50 and 100μ devices (Figure 2-1). For the 25μ devices, two 7/32-inch I.D. O-rings are placed side by side in the cover plate and compressed against the wafer, forming two elliptical regions of ~0.050 square inches each. Reducing the active area in this way was necessary to avoid the very large capacity that such a thin device would have with a full circular area. The better of the two elliptical areas is used in the experiment.

Following diffusion, etching the back, and forming the surface barrier contact, a device is completed by evaporating a 250 Å gold film on the diffused region. In addition, a 0.005-inch thick, 0.050-inch diameter ceramic disc is fastened to the front of the 25μ detector using Eastman 910 adhesive (Figure 2-1). When the detector telescope is assembled, this small disc fits in a groove in the contact assembly and keeps the 25μ detector in proper alignment.

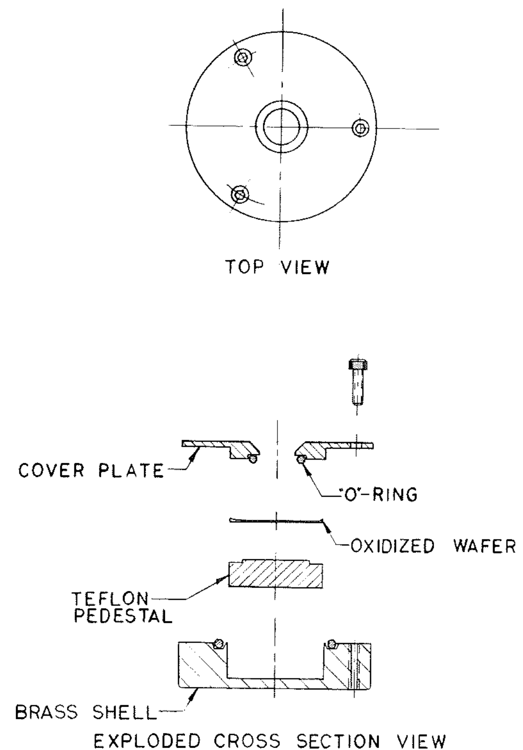

Figure 2-2. Oxide Etching Fixture

Testing and Selection. Detectors selected for space use have to meet the following electrical standards: forward resistance <5k; reverse breakdown voltage >20V above the operating point; reverse leakage current <2μa at the operating point at room temperature; no change in detector noise level at the voltage at which the detector becomes totally depleted. Experience shows that detectors either exceed or fail these specifications by wide margins — there is little middle ground. Mechanically, the detectors must be within 2.5μ of the desired thickness and have no obvious physical defects such as cracks, bumps, or pits.

The fabrication yield of detectors suitable for packaging is ~70 percent. Of those not suitable, ~30 percent are broken during fabrication, 30 percent have bad diode characteristics, 20 percent fall outside thickness specifications, 10 percent have physical defects, and 10 percent have high reverse leakage currents. Each delivered detector represents approximately six man-hours of work.

2.1.2.2 The Lithium-Drifted Detectors

Figure 2-3 is an illustration of the two lithium-drifted silicon detectors.[8] These p-i-n junction diodes are made from 200 to 400 ohm-cm boron-doped p-type silicon. The geometry of the detectors resembles that of a top hat. Lithium metal is diffused into the crown of the hat to form the n-region, and an evaporated layer of nichrome forms an ohmic contact to this n-region. As the lithium ions are drifted through the slice by application of reverse bias, these ions compensate the charge of the boron atoms and thus form the intrinsic i-region. A gold surface-barrier is evaporated onto the bottom surface of the hat to form a non-injecting p-type contact. Concentric grooves cut through the lithium diffusion into the intrinsic region divide the detectors electrically into separate regions.

The 1-mm detector has two grooves which divide it into three regions: center, anti-coincidence (ANTI-C), and guard-ring (GR). The center is the main detector, while the ANTI-C region suppresses unwanted events produced by particles that enter from the sides and by electrons scattered from the central region. The GR surrounding the center and ANTI-C regions reduces detector noise caused by surface leakage by shunting this noise directly to ground. The 1-mm silicon detector is alloy-bonded to an inner gold layer of a gold-clad Kovar can (Figure 2-3) in such a manner as to be concentric with a 15-mm hole in the can. This Au-Si eutectic seal is capable of withstanding repeated cycling between liquid nitrogen and boiling water temperatures with no evidence of leak, as determined by a helium leak-detector.

The 2-mm detector is divided by a single groove into center and GR regions. Portions of the brim are cut off to permit passage of leads from the 1-mm detector contact-wafer shown later (Figure 2-6).

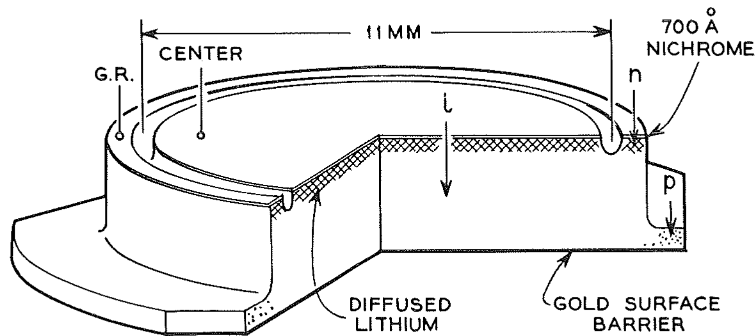

2 MM DETECTOR

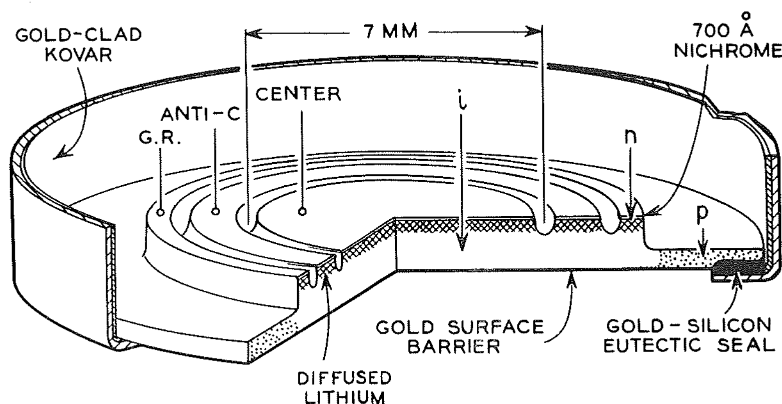

1 MM DETECTOR

Figure 2-3. Lithium-Drifted Silicon Detectors

The ambient sensitive surfaces of the detectors are protected by vacuum-encapsulation of the units in the gold-clad Kovar can. Vacuum-encapsulation is carried out in a clean stainless steel sorption-ion pump system. The encapsulation procedure has been described previously.[8]

2.1.3 The Mechanical Assembly

2.1.3.1 The Mounting Structure

The Detector Telescope Assembly is shown in an exploded view in Figure 2-4. When assembled, as shown in the insert, it is 2.54 cm long, has a diameter of 3.50 cm and weighs approximately 134 grams. The detectors are enclosed in a copper shield whose entrance has angled surfaces to minimize entry of scattered particles.

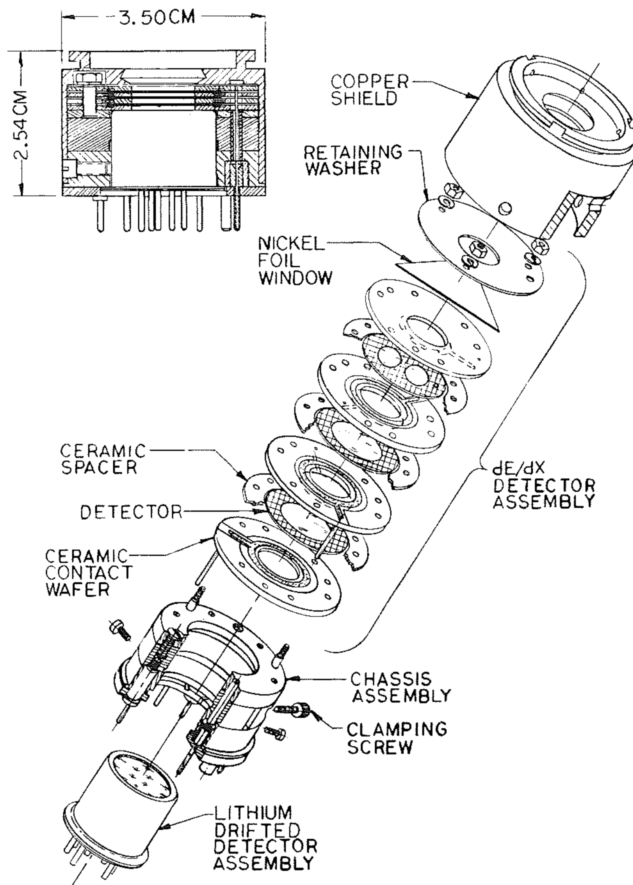

Figure 2-4. Detector Telescope

The entrance is closed with a thin nickel foil window to exclude sunlight from the light sensitive detectors. Electrical connections are made to the detectors with pressure contacts rather than bonded contacts (except for the 1-mm lithium-drifted detector) since the latter requires thermal or chemical reactions considered detrimental to the detector characteristics. Detector contact leads terminate at pins on the back of the telescope, which then conveniently plugs into the associated electronics.

The telescope is designed to meet the rigorous vibration requirements. This is accomplished by making the parts of the telescope fit together with minimum clearance and by using springs with sufficient force to maintain contact with the detectors at the maximum acceleration encountered. One telescope was subjected to vibrations of at least 70 g's in both the lateral and thrust axes, as a verification of the design. Other telescopes were continuously cycled for one month from -20°C

to +40°C at pressures of 1 x 10^{-7} Torr with a period of 24 hours with no evidence of mechanical failure.

To minimize possible contamination which might affect the stability of the detectors, only materials with good thermal vacuum qualities were used in the fabrication of the telescope.

As shown in exploded view in Figure 2-4, the detector telescope is comprised of a chassis assembly, a dE/dX detector assembly, a copper shield, and a lithium-drift detector assembly.

The chassis assembly consists of four concentric rings: three thick ones of copper and a thin one of aluminum oxide ceramic. These four parts, when assembled, retain insulating ceramic tubes and terminal pins for the contact leads of the dE/dX detectors. The front copper ring is fitted with three equally spaced copper studs which receive the dE/dX detector assembly, including the nickel foil window. All are securely held together by lock-washers and nuts threaded onto the studs. The copper shield fits snugly over these assemblies and is secured in place by three screws threaded into the back copper ring of the chassis. The telescope is complete when the lithium-drifted detector assembly is inserted into the center of the chassis and held in place by the clamping action of the split-center copper ring of the chassis assembly. Access to the clamping screw of the ring is made available by a small hole through the side of the copper shield. Proper pin alignment of the two detector assemblies is maintained by a key-and-slot arrangement. The copper parts are chrome-plated to maintain clean surfaces free from oxidation.

2.1.3.2 The dE/dX Detector Assembly

It was required that the three dE/dX detectors be closely spaced to maximize the common solid angle. In order to accomplish this, detectors are assembled between aluminum oxide ceramic wafers (Figure 2-5) which have gold-plated metalized contacts and lead wires. Concentric moats formed in the wafers provide clearance for the thick and rather irregular rims of the detectors (Figure 2-1). These moats permit the surface barrier side of a detector to lie flat on the metalized contact. The other side of the detector is contacted by a wafer equipped with a rippled spring washer. A ceramic spacer (Figure 2-4), of precise thickness, is placed between the two ceramic wafers to prevent total compression of the spring and thus control the stress placed on the thin silicon device. This surrounding spacer also prevents lateral movement of the detector.

The detectors, wafers, and spacers are assembled onto the chassis assembly (Figure 2-4) which is rigidly clamped to a workbench during the assembly operation. The first wafer is lowered over the three studs and its single contact lead is guided through a ceramic tube in the chassis assembly and into the corresponding terminal

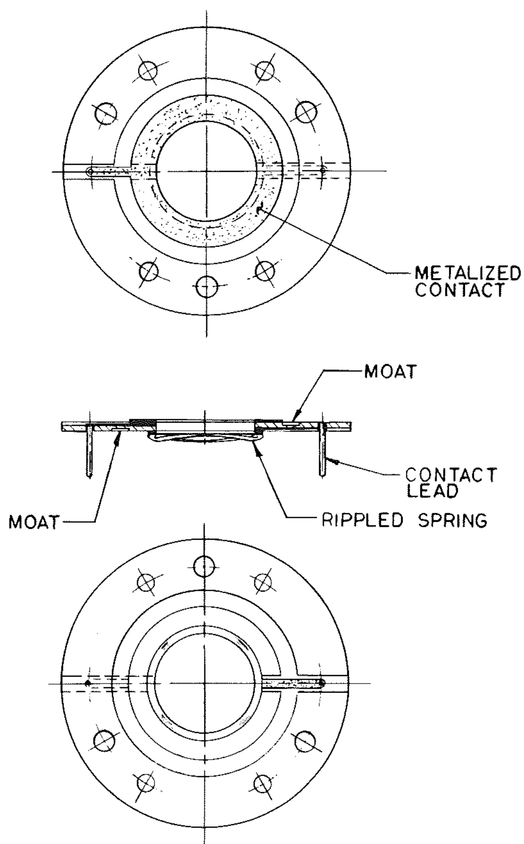

Figure 2-5. dE/dX Detector Contact Wafer

pin. This is followed by a spacer that forms a cavity into which the 100-micron detector is placed to bring together the surface barrier side of the detector and the wafer contact. Contact to the other side of the detector is made by the rippled spring on the under side of the next wafer, and the sequence is repeated with the remaining parts. The second and third wafers have two contact leads each, and the fourth only one. The nickel foil window is placed between the last ceramic wafer and the stainless steel retaining washer. The clamping nuts are threaded onto the studs and tightened with sufficient torque to flatten the lock washers. The assembly is completed by soldering the six contact leads to their corresponding terminal pins.

2.1.3.3 The Lithium-Drifted Detector Assembly

The lithium-drifted detector assembly is a windowless vacuum-encapsulated package,[8] which contains two lithium-drifted silicon detectors, 1-mm and 2-mm thick. The assembly is located in the center of the telescope and is therefore encircled by a wall of copper 8.5-mm thick. This thickness of copper is sufficient shielding against direct penetration by electrons ($<$10 MeV) and protons ($<$80 MeV) that

arrive from the side. As a result, both the radiation damage problem for the thick detectors and the generation of pulses by unwanted particles is minimized.

An illustration of the lithium-drifted silicon detector assembly is shown in Figure 2-6. The container is a Kovar can with a 15-mm diameter hole centered in the end. The inside of the can is clad with a layer of gold to which the first detector is alloyed to form a vacuum-tight seal. Contact is provided for each region of the detector by small area contacts metalized to one side of a thin (0.5 mm) aluminum oxide ceramic wafers. Shallow metalized channels connect the contacts to Kovar pins brazed near the outer edges of the wafer. Short ceramic tubes, glazed to the opposite side of the wafer, help to support the pins and provide a means for positioning the Kovar support which backs up the ceramic wafer. This support lends strength to the thin wafer and also provides an electrical contact and support for the second detector. It is essential that the detector fit snugly in the support to prevent lateral movement of the detector and thus avoid abrasion of the gold surface-barrier contact. This is accomplished by a soft gold-foil washer (0.025 to 0.050 mm thick) which folds at the edges of the detector (to form shims) as the two are pressed together into the support.

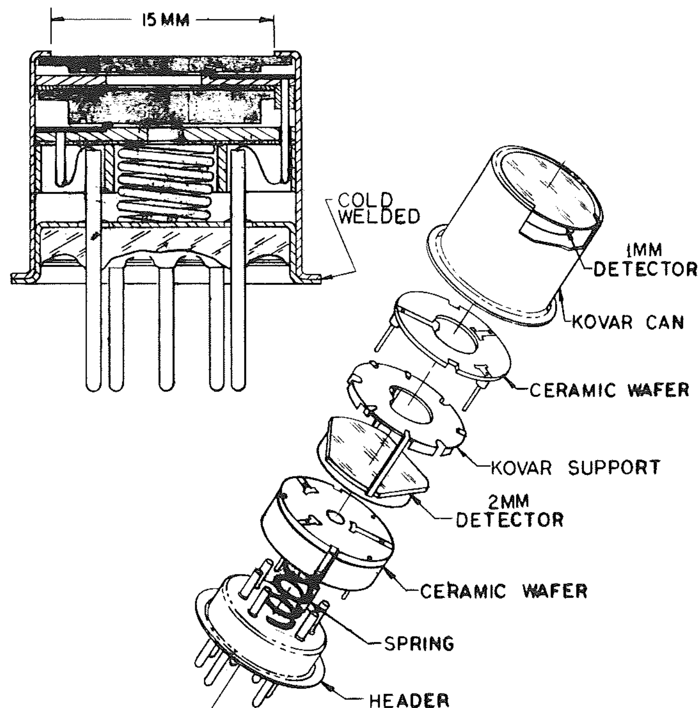

Figure 2-6. Lithium-Drifted Silicon Detector Assembly

The two regions of the second detector are contacted by the same method described previously; however, the ceramic wafer is somewhat different as it is constructed of two parts. The first part is a thin (0.9 mm) wafer containing the metalized contacts and their associated pins. This part in addition contains three holes that allow passage of the three pins from the previous wafer. The second part is quite thick (4.0 mm). It has six large-diameter (4.2 mm) holes corresponding in location to the six wafer pins and a center hole. The two ceramic parts are glazed together so that the large holes form wells. These wells confine the contact pins and their extension wires which are welded to the header pins. The center well confines the coil spring which is compressed when the header is cold-welded to the Kovar can. To protect the stability of the detectors, all parts used in the assembly are carefully cleaned, vacuum-baked, and stored in desiccators until ready for use. Assembly is carried on under clean-room conditions and is done quickly and reliably with the aid of special fixtures.

2.1.4 Testing

2.1.4.1 Vibration Testing

The detector telescope was subjected to the sinusoidal vibration levels required by Westinghouse Specification R2131, Section 3.2.13. Tests were carried out, using a Ling Model 300 vibration generator. The telescope was mounted in a fixture simulating its mounting on the satellite. The fixture was positioned to place the telescope in a desired axis of vibration, then rigidly fastened to the vibrator. Accelerometers were attached to the fixture to monitor the acceleration in three mutually perpendicular directions and also to control the applied vibration. Visicorder traces were made of all four accelerometer outputs.

The I-V characteristics, noise, and forward resistance of each detector were measured before and after the test. A comparison of these measurements was made to determine if the acceleration had any detrimental effect on the detector.

The electrical contacts to the detectors were monitored while the acceleration test was in progress. This was done by means of a bias circuit connected to each detector with cables. An intermittent contact was indicated by sharp pulses displayed on a multi-trace oscilloscope.

Vibration tests made on early development models showed that the contact springs in both the dE/dX and the lithium-drift detector assemblies required modification. These tests also indicated the need for improving the support for the three thin detectors and second lithium-drifted detector. After making these modifications, all detector assemblies successfully passed the tests at the specified levels of vibration.

2.1.4.2 Thermal Vacuum Testing

The detector telescope was temperature cycled for several weeks in a commercial thermal vacuum space simulator. Temperature was cycled continuously from -20°C to +50°C with a period of 24 hours. The detectors were reverse biased at their operating voltages. Temperature sensing was accomplished with a thermocouple attached to a copper fixture containing the telescope. Pressure in the chamber ranged from 5×10^{-8} Torr at the minimum temperature to 5×10^{-7} Torr at the maximum temperature. A switching arrangement on the bias supply permitted reverse current-voltage (I-V) characteristic measurements to be made of each detector. These measurements were made frequently to determine the reliability of the detectors. An abrupt change of the shape of the characteristic, at a given temperature, is generally accompanied by a change in the noise line-width of the detector.

The I-V characteristics for the five detectors on the ATS-B satellite are presented in Figures 2-7 through 2-11. The small change of current with increasing bias voltage at 25°C indicates, in each case, both a good surface and a good p-n junction, and is a necessary requirement for low noise. These figures show the effect of temperature on reverse current. The increase of current is due primarily to the thermal excitation of intrinsic carriers.*

In Figures 2-7 through 2-9, the "punch through" voltage is shown for each dE/dX detector to demonstrate the reliability of the gold surface barrier back contact. At this voltage, the space charge region reaches the back of the device. Failure of the back contact to block injection of noise producing minority carriers (electrons) would be indicated by a sharp increase of the current at "punch through"; however, the data shows a steady current increase out to the operating voltage and beyond.

The long-term stability of the dE/dX detectors may be judged by comparing the I-V characteristics obtained at 25°C, as shown in Figures 2-7, 2-8, and 2-9. After many months of shelf-aging and environmental testing, these characteristic measurements with related noise and forward resistance measurements indicate no significant degradation of the detectors.

2.1.4.3 History of Lithium-Drifted Detector Characteristics

Reverse Current History. Life tests were run with reverse bias of 200 volts on all regions of both the 1-mm and 2-mm detectors. The reverse current history of each region is shown in Figure 2-12. Current is expressed in microamperes

---

*A detailed discussion of this question will be published separately by H. E. Kern.

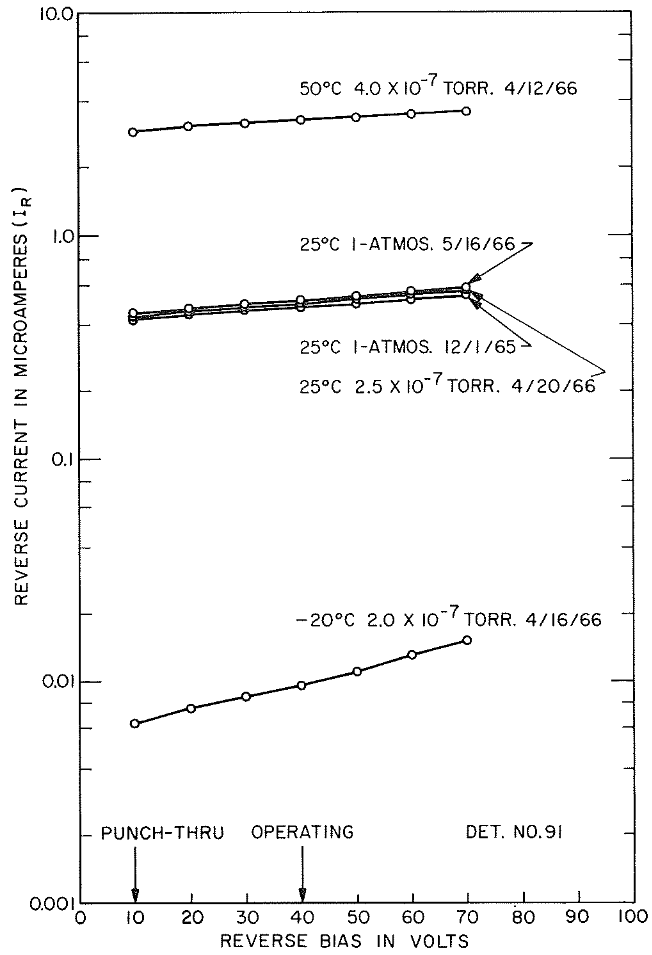

Figure 2-7. Thermal Vacuum Test — Effect of Temperature on Reverse Current dE/dX Detector — 25 Microns Thick

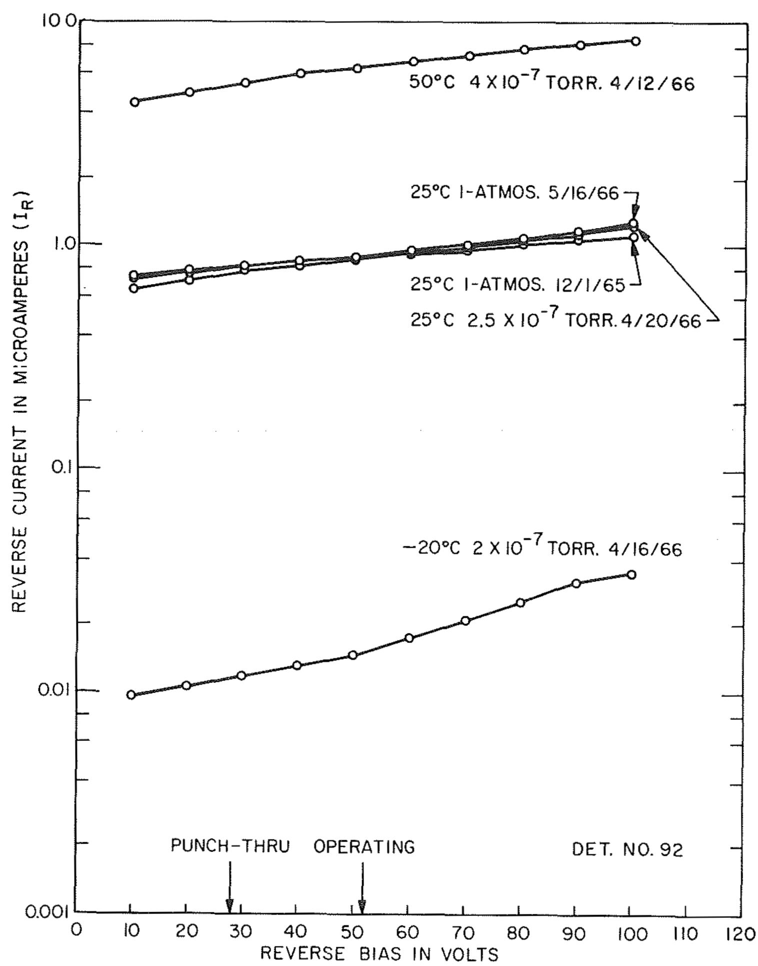

Figure 2-8. Thermal Vacuum Test — Effect of Temperature on Reverse Current dE/dX Detector — 50 Microns Thick

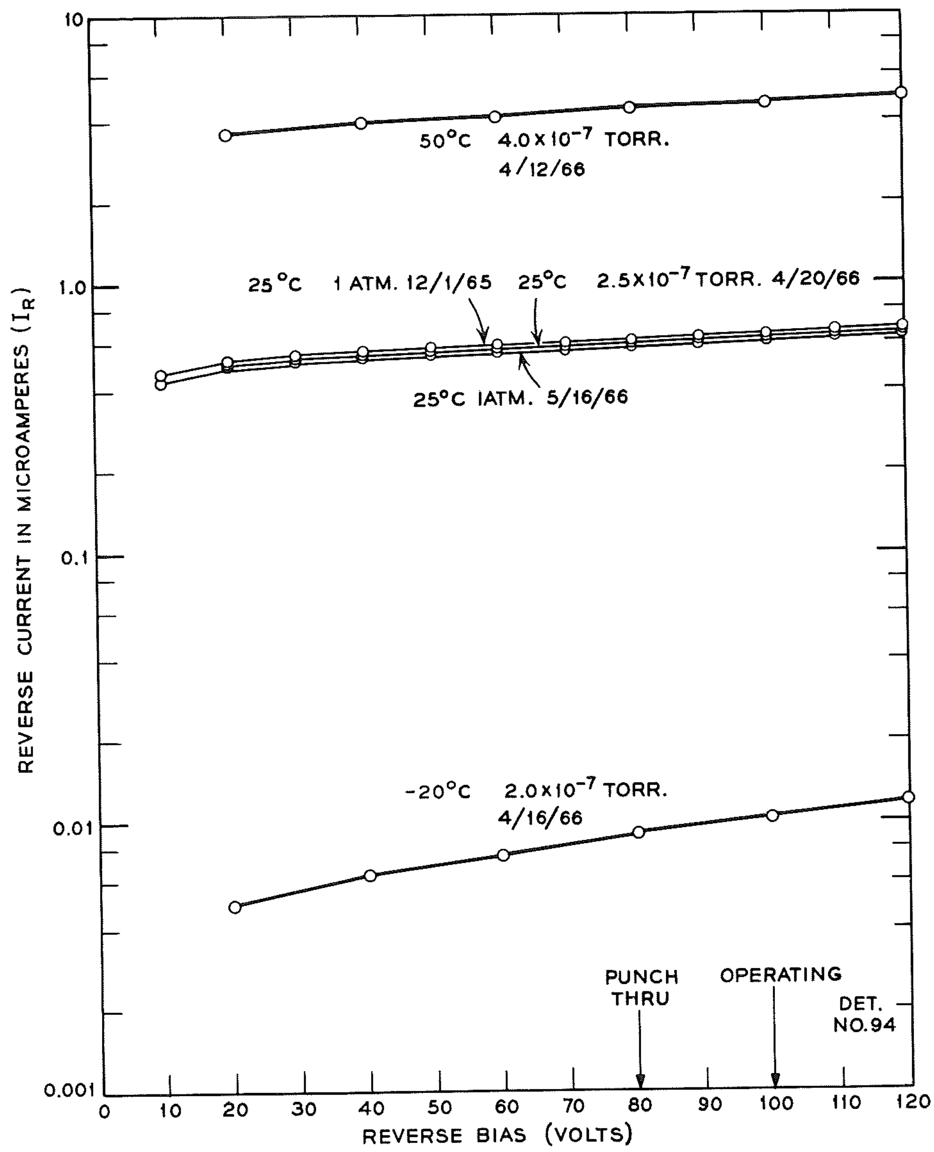

Figure 2-9. Thermal Vacuum Test — Effect of Temperature on Reverse Current dE/dX Detector — 100 Microns Thick

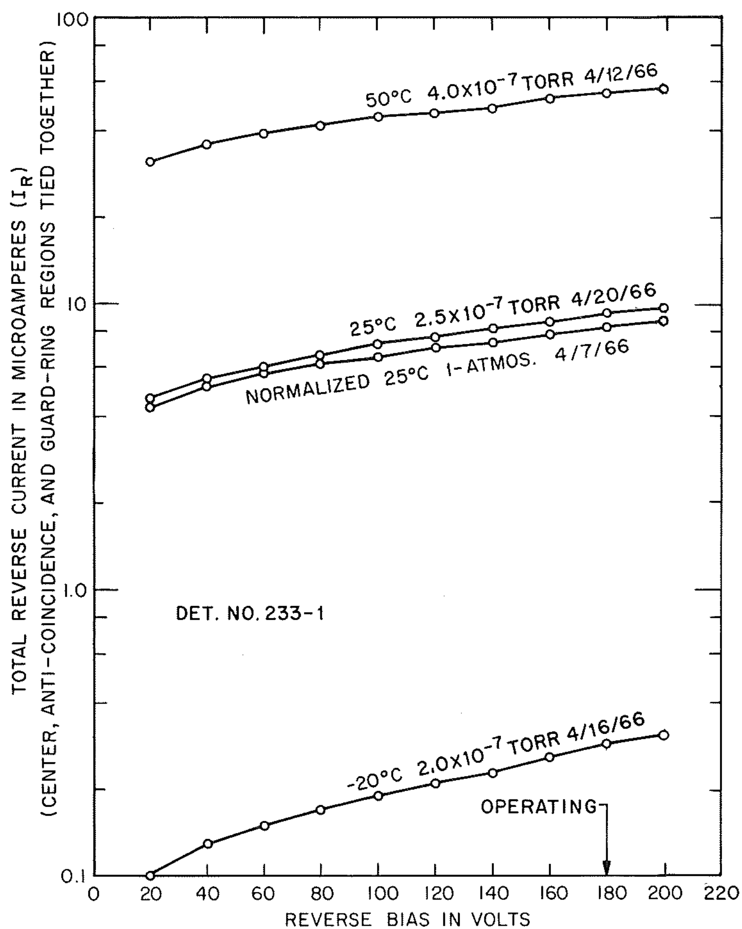

Figure 2-10. Thermal Vacuum Test — Effect of Temperature on Reverse Current Lithium-Drifted Silicon Detector — 1 mm Thick

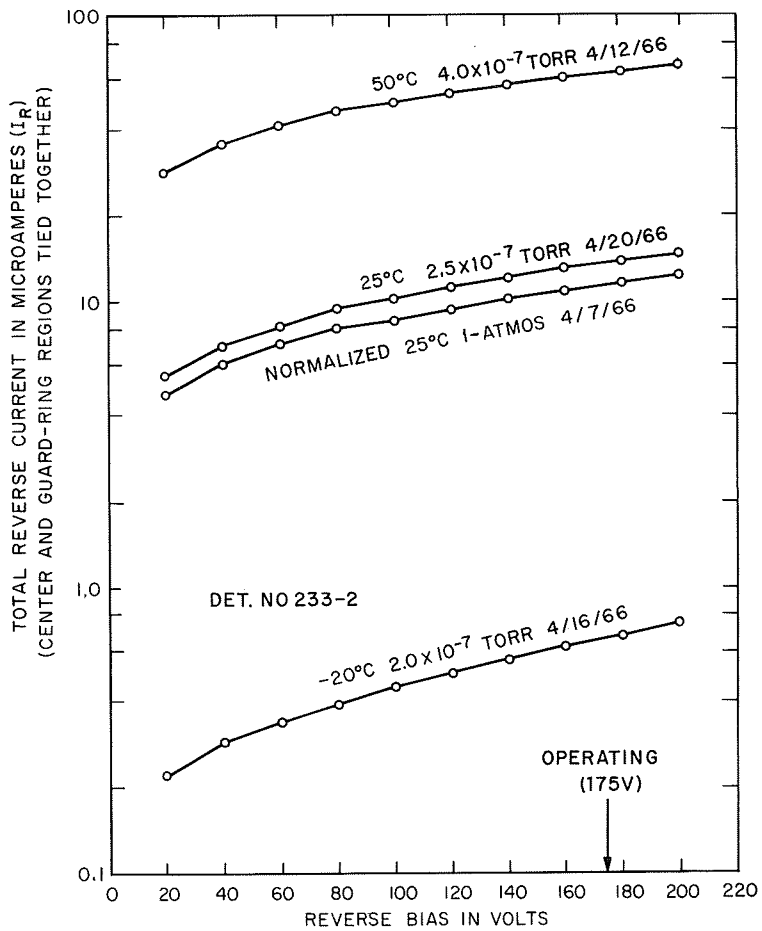

Figure 2-11. Thermal Vacuum Test — Effect of Temperature on Reverse Current Lithium-Drifted Silicon Detector — 2 mm Thick

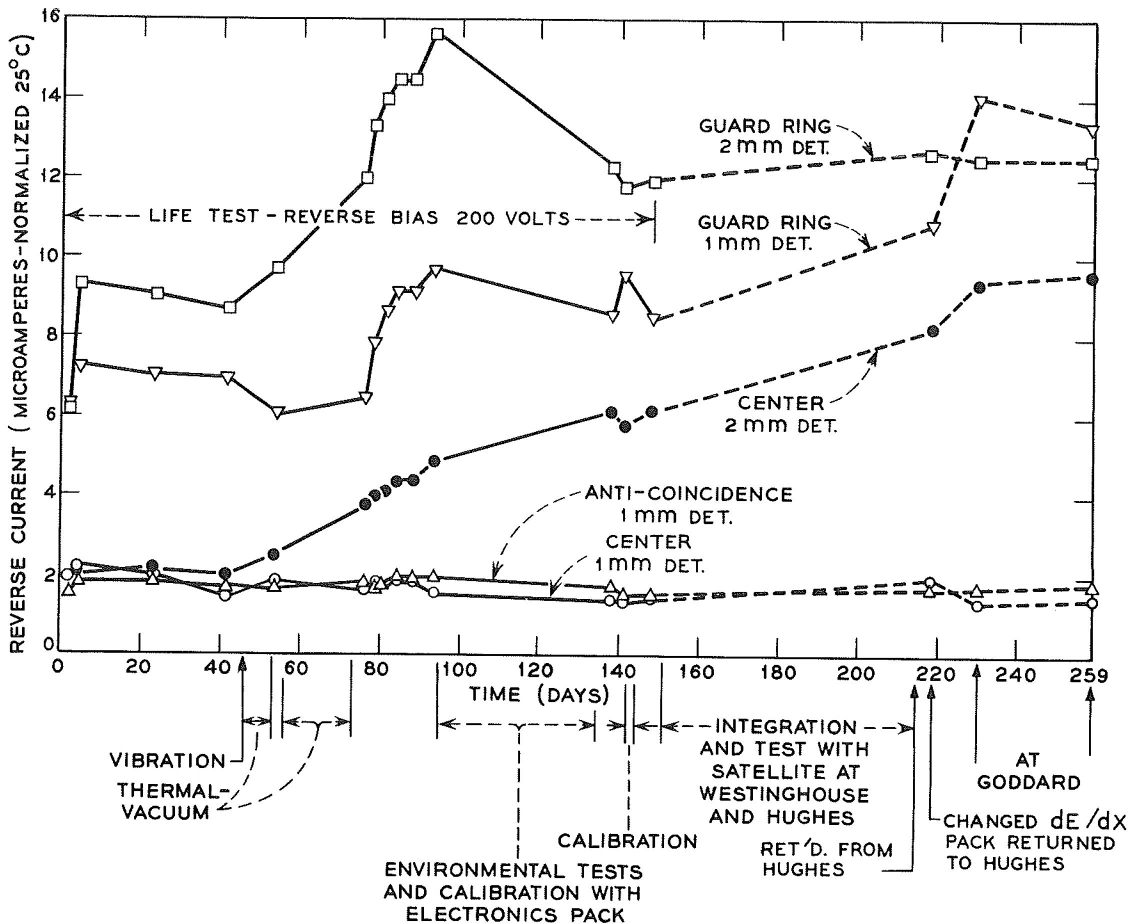

Figure 2-12. Reverse Current History of Lithium-Drifted Silicon Detectors

normalized for 25°C. Solid lines indicate operation under essentially continuous reverse bias, whereas dashed lines indicate intermittent operation with reverse bias on only during specific tests.

Results of Figure 2-12 show that the center and ANTI-C reverse currents of the 1-mm front detector remain low and very stable throughout all test periods (259 days). GR-1 behaves as intended and shunts most of the slowly increasing leakage current to ground. After completion of thermal-vacuum tests (day 73), reverse current of center (2-mm) shows an increase with time, with its GR (2-mm) shunting a large portion of current to ground. There is an indication of stabilization of reverse current between days 149 and 259 for GR-2-mm and between days 230 and 259 for Center-2-mm and GR-1-mm.

Excessive reverse currents contribute to increased electronic noise with impairment of signal-to-noise ratio. In addition, high reverse currents may produce

a significant decrease in the detector bias voltages because of IR drop in the load resistors. Such a decrease can result in a decrease in the collection efficiency. Tests at Goddard Space Center and at Cape Kennedy indicated the final measured reverse currents to be well within acceptable limits.

Noise History. Early noise data obtained on lithium-drifted detectors were expressed in units of rms volts. Later a portable detector test-set was built for measuring noise and reverse current in the field. In order to relate noise measurements more directly to the satellite electronics system, this portable "suitcase" tester was calibrated as the discrimination threshold (in KeV) at which the noise counting rate was 100 counts per second. It was desired that the 100 counts per second noise level of each active detector region be well below the coincidence discrimination threshold in the flight electronics. For the 1-mm detector, thresholds were set at 304 KeV for center and 385 KeV for ANTI-C regions, while the 2-mm center threshold was set at 390 KeV.

After appropriate calibration of the suitcase tester, the original rms noise data were converted to noise in KeV at 100 counts per second and plotted against time, as shown in Figure 2-13. This figure summarizes the noise history of each section of the 1-mm and 2-mm lithium-drifted detectors. With the exception of the sharp noise peak on day 78 (probably instrumentation error since it was observed simultaneously for both 1-mm and 2-mm detectors), the noise characteristics of all sections of the 1-mm detector remain essentially constant throughout all test periods (259 days). The final noise signal for the center 1-mm (72 KeV at 100 counts per second) lies approximately 230 KeV below its discriminator threshold. The excessive noise developed in GR-2-mm may be responsible for the slow increase in noise observed for the 2-mm center section. However, the rate of change appears slow, and at flight time the noise level of the center section was still about 250 KeV below its discriminator threshold.

2.2 THE RADIOACTIVE IN-FLIGHT CALIBRATION SYSTEM

2.2.1 Introduction

Solid-state detectors of high-energy particles require in-flight calibration to check on their performance in space. The electronic portions of an experiment can be checked with internal electronic pulses, but the calibration of the detectors themselves can only be checked with real particles. In some orbits and for some experiments, the galactic cosmic ray background may serve as such a calibration source but in a synchronous orbit and in an experiment to measure relatively low-energy particles, radioactive sources are required. Such sources may be of low activity and may be continously exposing the detectors. However, it is difficult to select

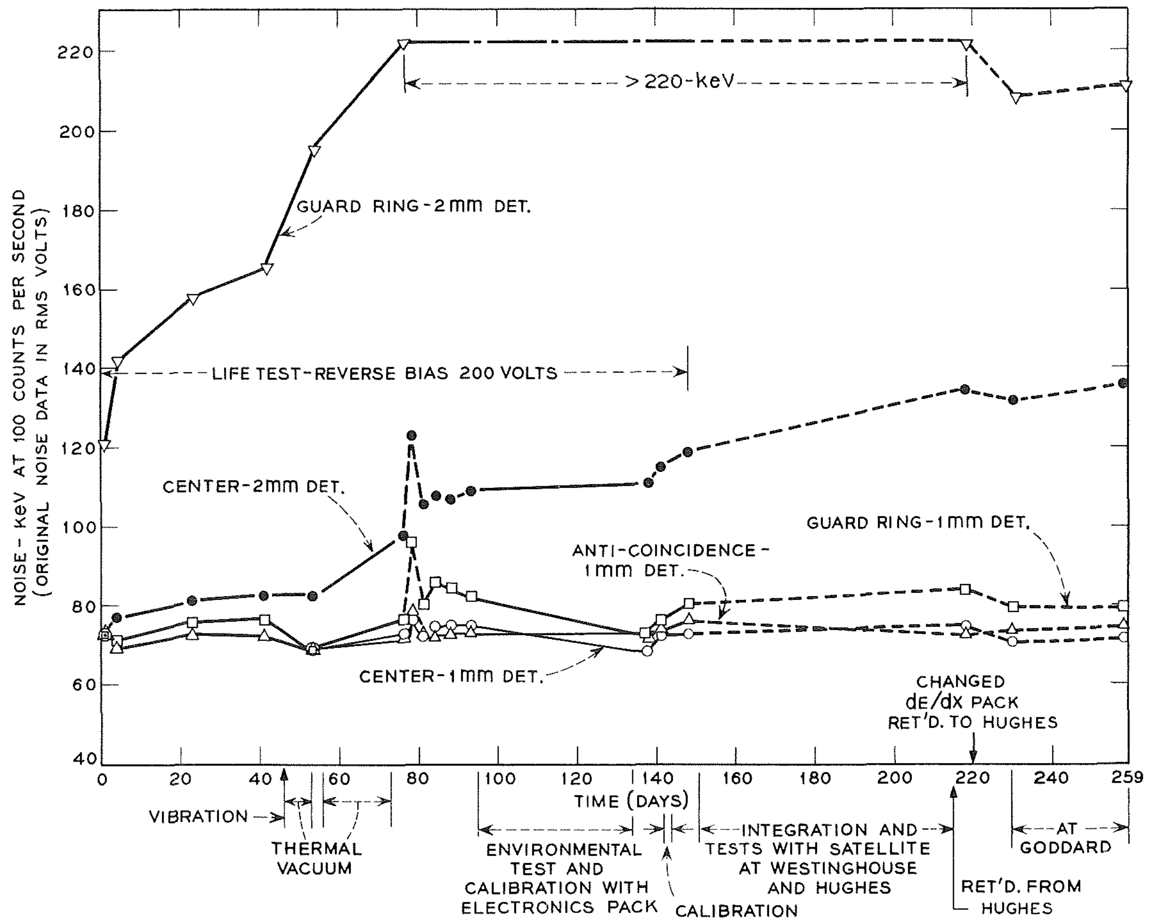

Figure 2-13. Noise History of Lithium-Drifted Silicon Detectors

low-level sources which provide adequate intensity for statistical accuracy in calibration without substantially reducing the dynamic range of the experiment. In the present experiment, in-flight calibration has been provided with higher-level alpha and beta sources which are mounted on an arm and periodically rotated into view of the detector telescope by means of a rotary solenoid. This assembly is shown in a greatly enlarged view in Figure 2-14.

The requirements of the calibration system are demanding: small size and weight, low-power consumption, rugged construction to withstand the vibration of launch, reliable lubrication in the vacuum environment of outer space, adequate

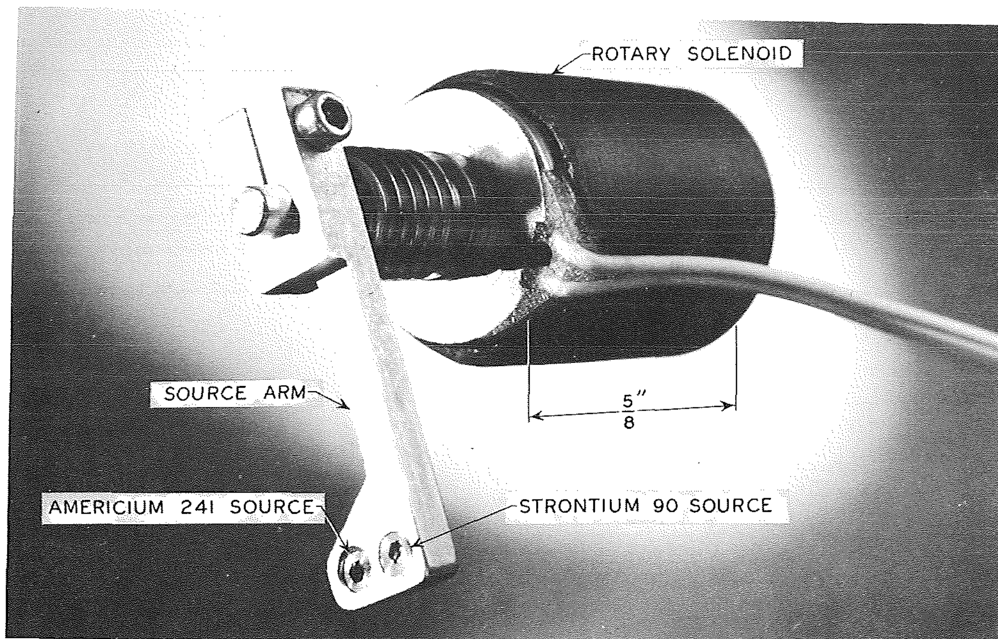

Figure 2-14. Radioactive Calibration Assembly

local shielding to provide a low background when not in the calibration mode, and low stray magnetic field from the solenoid to avoid magnetic interference with other experiments or the satellite itself. Of first order importance is reliability of operation in a satellite mission of two years duration.

2.2.2 The Rotary Solenoid

2.2.2.1 Description and Operation

Several simple devices were first constructed and evaluated, but none looked as promising for the present application as a commercially available rotary solenoid from the standpoint of size, weight, low-power consumption, and ruggedness. With modifications in fabrication, lubrication, and assembly of the commercial device, adequate reliability was achieved.

The commercial unit is a Magton, Series 11, rotary solenoid. It is manufactured by Magnuson Engineers, Inc., of San Jose, California. Its principal commercial application is as an actuator of indicator flags in the food processing industry. This device is a true rotary solenoid, and unlike some popular rotary stepping solenoids, involves no axial movement. The rotary movement is advertised to be available in any nominal sweep from 1° to 60°. The model employed in this case uses a standard 45° sweep. Figure 2-15 shows the assembled solenoid and its components in an expanded view. The total solenoid weight is slightly more than half

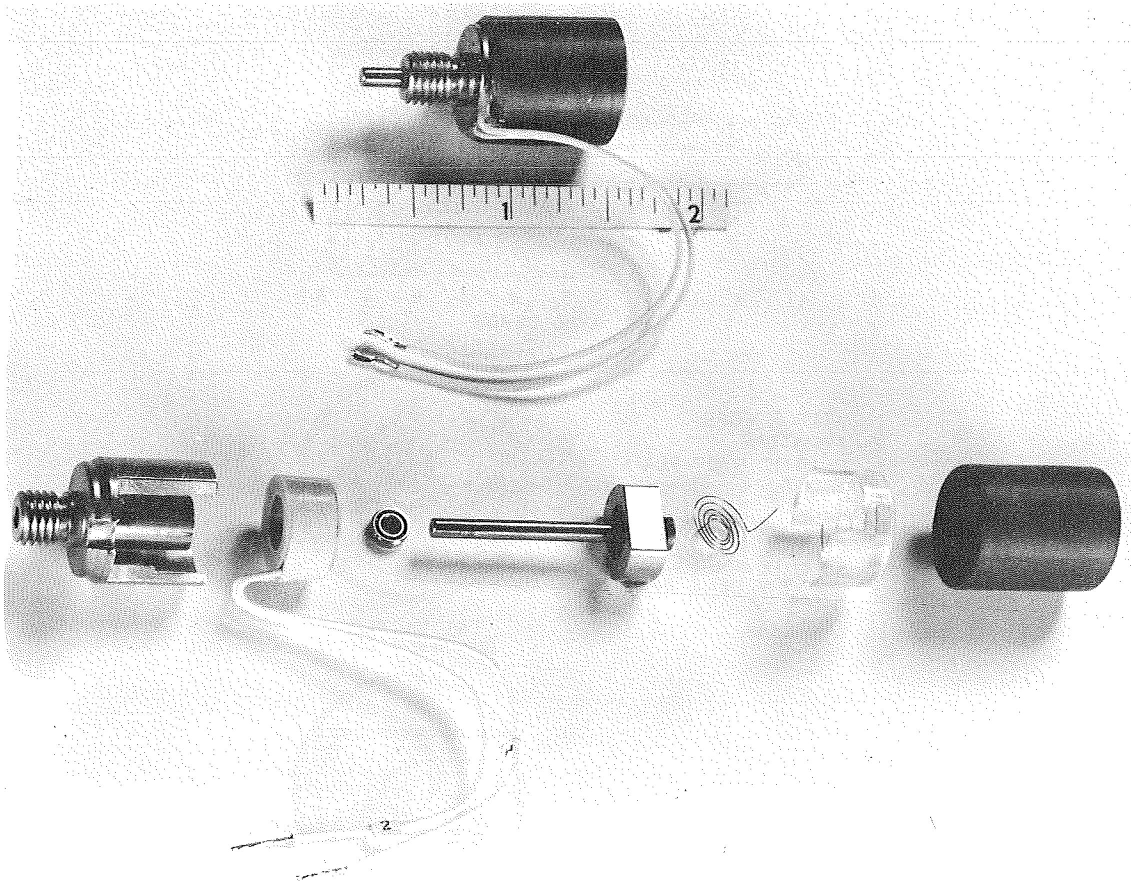

Figure 2-15. Rotary Solenoid

an ounce and the body measures 5/8 inch in diameter by 3/4 inch long. The mounting hub and the shaft add another 1/2 inch to the length.

Figure 2-16 shows two views of the solenoid and gives its nomenclature: a cross-sectional view along the axis of rotation with heavy diagonal shading outlining the magnetic iron path, and a pair of cross-sectional views perpendicular to the axis through the armature-stator air gap area. One of the pair shows the armature in the released or a retracted position; the other shows it in the actuated or extended position. The air gap is 0.010 inch in the retracted and 0.002 inch in the extended position.

When the solenoid coil is actuated, the magnetic flux density in the air gap increases sharply with decreasing gap width. This magnetic driving force causes the armature to be "pulled in" through its 45° arc. The maximum magnetomotive force is required at the start of the actuation, even though the rotation is being

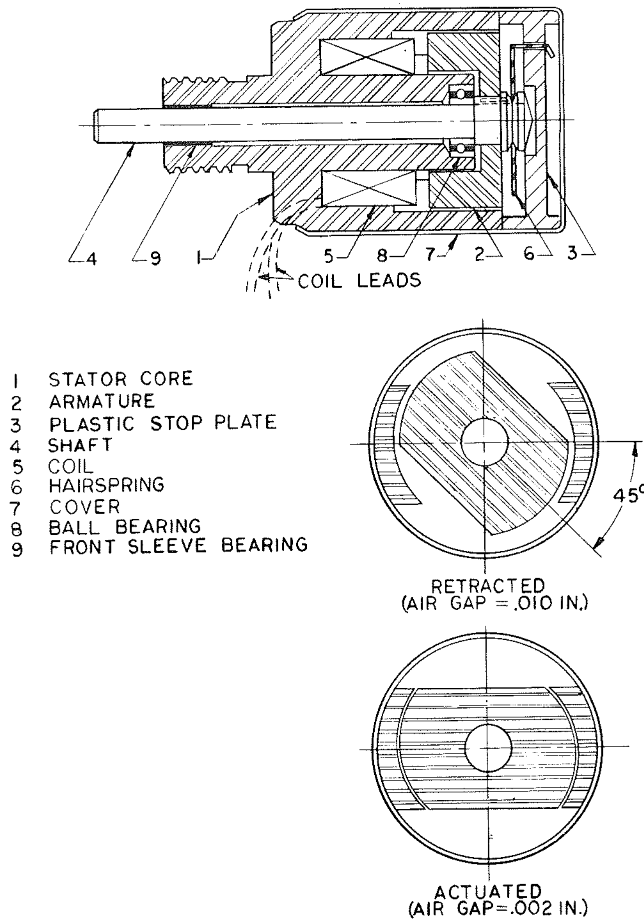

Figure 2-16. Rotary Solenoid Magnetic Circuit

increasingly resisted by hairspring tension. Conversely, in the actuated position, if the actuating power is slowly decreased, the armature stays extended until it releases, suddenly. This happens when the power reaches about one-third of the minimum power required to extend or actuate the 45° sweep.

These characteristics provide an essentially bistable device which can rotate a pair of radioactive sources from a shielded position, with power off, to a calibrating position, where they expose the detector telescope, and hold them in the calibration position with very small power consumption.

The commercially available solenoid is advertised to operate continuously at 3 watts (not in a vacuum) and develop 16 gm-cm starting torque and 27 gm-cm extended torque. Higher torques can be developed, up to 37 gm-cm, by intermittent operation at higher power levels. The minimum power requirements for a solenoid

as modified for present use but with normal hairspring tension are approximately 0.25 watts to actuate and 0.04—0.08 watts to hold extended. The torque developed at these power levels was not directly measured but could be estimated by measurements of the torque-versus-hairspring tension (see Paragraph 2.2.2.3). For a few degrees deflection, a torque of approximately 2.0 gm-cm was required and for the full 45° deflection, 3.0 gm-cm was required.

2.2.2.2 Modification and Special Treatment

Primary evaluation of the commercial solenoid was carried out on a unit which was discovered to be a discontinued model. Its replacement turned out to be somewhat inferior in operating characteristics and slightly different in design. The manufacturer gave assurances that the design change was an improvement and that the poor operating characteristics were attributable to poor manufacturing tolerances. He then agreed to tool up specially and make a limited number of units to flight tolerances with minor dimensional changes.

The units were to be left unassembled and all plating of parts deleted. Table 2-1 summarizes the special work performed on the piece parts of the solenoid assembly after delivery.

Table 2-1
TREATMENT OF SOLENOID PIECE PARTS

Part Description	Special Work Performed
Stator Core	Heat-Treat to Stress Anneal; Nickel Plate
Armature	Heat-Treat to Stress Anneal; Nickel Plate
Shaft	Replace Phosphor Bronze with Stainless Steel for MoS_2 Plating Feasibility
Ball Bearing	Special MoS_2 Plating
Sleeve Bearing	Burnish with MoS_2
Coil	Low-Impedance Winding, 115 Ohms
Hairspring	Burnish with MoS_2
Plastic Stop Plate	As Supplied
Cover	As Supplied

Stator and Armature Magnetic Properties. The stator and armature material was an alloy trade-named Ledloy A, roughly equivalent to common 1008 cold rolled steel but containing approximately 0.2 percent lead to give it a high degree of machinability. A series of B-H loop curves taken on stator core pieces* indicated

*The magnetic measurements were conducted and evaluated by E. J. Zimany, Jr. and M. S. Glass.

that some sort of heat treatment was necessary to improve the magnetic properties of the material. The dashed curve in Figure 2-17 illustrates the before heat-treatment B-H loop. The magnetic induction B, changes rather slowly with the magnetizing force H, and also saturates at a lower value than would be expected for magnetic iron. This stator was typical of all the stators before heat treatment. Installed in a solenoid, it was found that at low power the armature would assume a rotary position dependent on the applied electromagnetic force rather than at the actuated extreme. This could be attributed to the slow bend in the B-H curve.

The simplest form of heat treatment, a stress anneal at 805°C in a N_2 atmosphere, was tried first, and produced striking improvements, as indicated in the solid curve of Figure 2-17. The curve now assumes the squarer features of magnetic iron and reaches a higher B value at saturation. In addition, the assembled unit now works as a bi-stable device at low powers, as described earlier. Labeled on

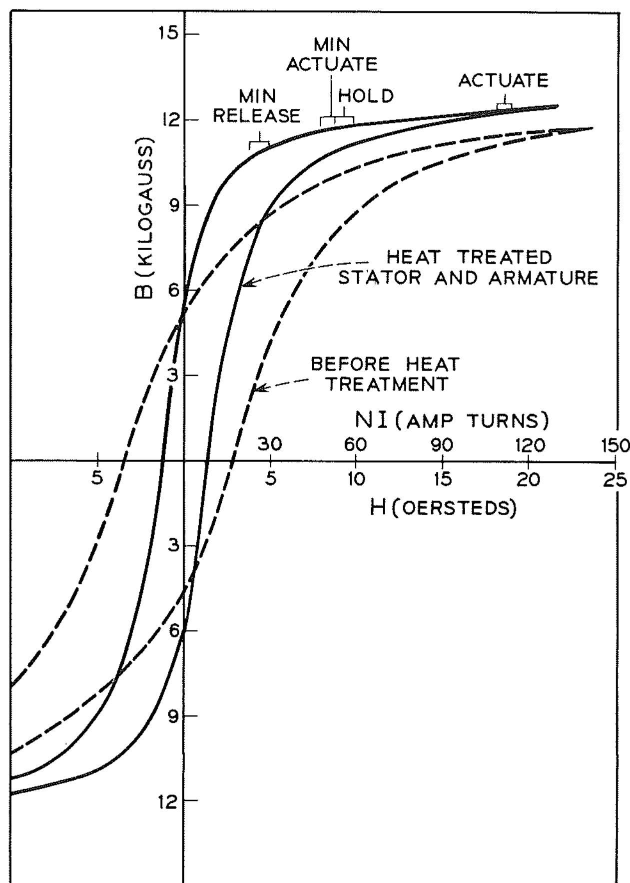

Figure 2-17. Solenoid Magnetic Characteristics

this curve are bracketed regions which show the actuation levels at which the solenoids are operated in the experiment, and the minimum operating levels for all the finished solenoids that had undergone heat treatment. Comparison of these regions indicates the operating margin that is provided.

One stator and armature set was heat-treated at a higher temperature, 830°C, in a wet H_2 atmosphere. This treatment was intended to reduce certain undesirable impurities to low levels by reaction with the hydrogen. Although no direct magnetic measurements were performed on this stator, the assembled unit was tested for minimum NI (ampere-turns) operating values. The results were identical to those after the 805°C N_2 atmosphere stress anneal; that is, a reduction of the operating minimum NI to 75 percent of the original level and a reduction of the release minimum NI to 65 percent of the original level.

A further heat treatment was tried on the same pieces at a temperature of 960°C in a dry H_2 atmosphere. As a result of being subjected to this high a temperature, the parts no longer fit together because of distortion in the most critical areas. When the unit was finally made to fit again, the minimum NI requirements remained the same. Since distortion was a certain consequence of still higher temperature treatments, it was decided to settle for the 805°C anneal.

Stator and Armature Mechanical Tolerances. For reliable bi-stable operation at low-power levels, it was found that the main air gap in the actuated position (the clearance between the armature and the stator) was very critical. A gap of 0.002 inch seems to be ideal. With a larger gap, the device was not definite in actuation at low power, whereas with a narrower gap, there was a tendency for the unit to hang up until the NI was decreased to almost zero. Also, with the narrower gap, asymmetries in the machined parts could result in the stator and armature touching in the extended position. Consequently, all stator-armature assemblies were paired for optimum clearance by using the minimum NI for the "hold" or release as a criteria. Each assembly was tried with the armature in either of the two 180° positions, and the position that resulted in the larger NI for "hold," was selected. Finally, toolmarks and burrs were removed with 600 grit cloth and the pieces were electroless nickel plated to give a 0.1- to 0.2-mil protective coating.

Bearing and Shaft Lubrication. Lubrication in outer space is a widely publicized problem. A great deal of time and effort are presently being spent trying to solve the problem of metals "cold welding" in a high vacuum. At this time, no unique solutions have been found. Most engineers agree that a solid lubricant, such as MoS_2 is the answer, but very few agree as to how to apply it to metal surfaces.

Simply impacting or burnishing MoS_2 into or onto clean metal surfaces produces good lubrication results but the amount of lubricant that can be applied in

this manner is very limited. For heavier coatings, most applications have involved the use of solid lubricants with a binder, either resin or inorganic. However, the binder may have detrimental effects on the lubrication quality or its life. Many processes used are proprietary and make preliminary evaluations difficult, since the lubrication vendor is usually reluctant to reveal the composition or the details of his process. Also, he is at liberty to change his process at his own discretion. Some of these proprietary finishes have satisfactorily met the requirements for particular applications but not for others, such as ball bearings.

The lubrication of the ball bearing parts and armature shaft of the rotary solenoid* was achieved by the use of a proprietary process still in its development stage. This process, called E3C, was developed by the Alpha Molykote Plant of the Dow Corning Corp. at Stamford, Connecticut. The E3C process deposits an electroplated MoS_2 coating of desired thickness on stainless steel and some other metals. The process for stainless steel is as follows:

Sand blast, clean and etch
Electroless Cu flash
Electroless Ag flash
Electroplate Molybdic Oxides
Convert Molybdic Oxides with high-pressure H_2S in a hot autoclave.

Machine tests showed that the lubrication qualities of E3C coatings were excellent when applied in thicknesses from 0.2 to 0.4 mils. A 0.2-mil coating of MoS_2 was applied to the armature shaft of the rotary solenoid for the lubrication of the sleeve bearing. However, this thickness was considered excessive for the ball bearing parts because of the build-up of tolerances in the very small bearing assembly.

The ball bearing assembly employed in the solenoid was one which fit on a 3/32-inch shaft and into a 3/16-inch race (Barden No. SR133 WX). The bearing balls, because of their small size, were the only parts of the assembly not plated. Since the bearing had to be plated by pieces, the Barden Corp. of Danbury, Connecticut, was contracted to handle the selection, assembly, and testing of the bearings.

The parts to be plated, the inner and outer raceways and the ball retainer pieces, were sand blasted at BTL on a rotating fixture, using S. S. White #5, 10μ, Al_2O_3 abrasive in a dental machine. Alpha Molykote then did the MoS_2 plating and sent the pieces back to BTL for evaluation and selection of suitable pieces. Good coatings were extremely difficult to achieve because of the minuteness of the pieces and the thin coatings desired, approximately 0.1 mil. Determination of the thickness of the coatings was attempted by weighing on a microbalance before and after

---

*Technical guidance and liaison assistance in connection with these lubrication problems was generously provided by G. H. Kitchen.

plating and also by "dissections" in a few cases. Neither method gave a precise measurement, but, together with a visual inspection, they helped in selection of good coatings from poor ones. The selected parts were sent to Barden where they were tested for smoothness, assembled into complete bearing assemblies, run in, and evaluated for quality by torque measurements.

The front "sleeve" bearing surface simply consisted of the armature turning in the bore of the stator mount hub section. In addition to the 0.2-mil coating of E3C MoS_2 on the shaft in this area, fine MoS_2 powder was burnished into the bore surface to further reduce any possibility of shaft seizure.

Coil Assembly. The solenoid in the ATS experiment uses a pulse of actuating power followed by a lower holding power to keep the radioactive source arm extended for 2.75 minutes every 5.3 hours. The actuating power of one watt was applied for approximately one second and did not contribute significantly to coil heating. The power consumption during the 2.75 minutes of "hold" was approximately 0.25 watts. Temperature measurements of the coil winding in a vacuum showed the coil winding average temperature did not exceed 80°C during this time. Hence, class A, 105°C polyurethane insulated wire was used. The finished nylon coil spool contained 1250 turns of #40 wire with an impedance of 115 ohms.

2.2.2.3 Final Assembly and Tests

The rotary solenoid was first loosely assembled without a coil, and the armature shaft end play was set to 0.002—0.003 inch by filing off the tip of the shaft that bears against the plastic stop plate. The hairspring was then installed on the shaft and tension was incorporated by pulling the loose end of the hairspring through one of six holes provided in the plastic stop plate. The coil was then epoxied into the stator with Resiweld #7004. After suitable baking and curing of the epoxied coil, the unit underwent electrical operating tests as described above and a torque versus angular displacement test.

The torque test was carried out by measuring the angular displacement of the armature shaft as weights were loaded and unloaded from a pulley clamped to the protruding end of the shaft with the unit assembled in a temporary cover. Figure 2-18 shows a typical torque versus angle plot of a flight solenoid. The actual torque and the slope of the curves are principally a function of the hairspring, that is, its tension and characteristics. The difference between the "loading" and "unloading" curves as well as their linearities gives the most information about friction in the unit. Since the rotary solenoid is used intermittently, the "static" torque test used here is much more meaningful than the conventional running torque test of a bearing assembly.

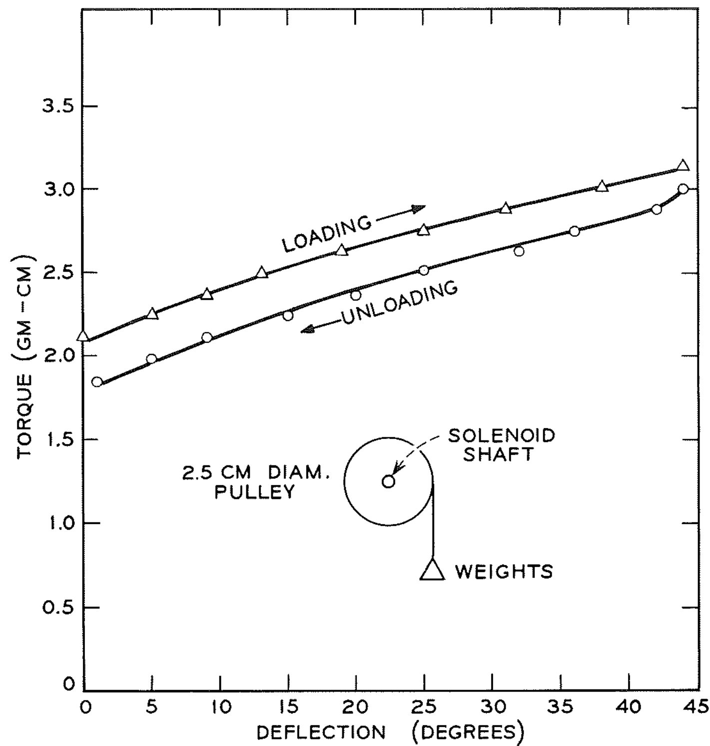

Figure 2-18. Bearing Torque Test

The unit was disassembled again for final inspection and then assembled with a permanent cover. This cover was swaged onto the stator with a hand tool and the coil extension leads were epoxied through the cover hole provided. A small teflon tube was inserted through the epoxy joint to allow outgassing of the internal parts to be vented to the outside through something besides the front sleeve bearing.

After the epoxy was cured, the entire solenoid assembly with a dummy source arm was installed on a metal dewar and placed in a vacuum station. After a mild bakeout, the solenoid was subjected to extensive electrical tests at temperatures between -30°C to +50°C. The vacuum pressure during these times were usually held to 10^{-6} Torr or better. The electrical tests consisted of the minimum NI tests as well as frequent cycling operations with a transistorized pulsed power supply simulating that of the flight electronics.

The assemblies underwent vacuum tests for periods varying from one to three days. The only potential trouble encountered was at the low temperatures where the NI for release on several solenoids became very low. This could possibly

be attributed to asymmetry or narrowing of the air gap caused by the contraction of the highly machined steel stator at these low temperatures.

2.2.2.4 Special Test Solenoids

In addition to two flight solenoids, a prototype, and a lab model for the experiment, two others were assembled to undergo special tests. The outstanding question was the bearing lubrication life in high vacuum.

The very first solenoid assembled with the bearings coated with E3C MoS_2 was utilized in a lubrication life test in the laboratory. There was no epoxy used in the assembly and the cover was machined open to allow a large area for venting the internal outgassing. These precautions and a general high state of cleanliness were aimed at achieving a high vacuum at the bearing sites. This assembly was installed in a glass chamber on a 15 liter/sec Vac Ion system on August 4, 1965. Within a few days, the vacuum pressure was less than 10^{-7} Torr and automatic cycling of the solenoid was started, using the transistorized pulsed power supply. The repetition rate was 1 minute on, 20 minutes off. This rate continued for 3 months or 7000 operations, which would be equivalent to 10 years of operations in space. Afterwards, the solenoid was alternately left idle and cycled for one to two months at a time. The unit was finally removed from the vacuum station in January 1967. The vacuum pressure had been in the low 10^{-8} Torr region during most of the test and there were no indications of the solenoid malfunctioning at any time.

The success of this particular test does not allow one to conclude that bearing seizure would have occurred in the absence of lubrication. No control experiments were done under similar conditions to determine if a solenoid assembly without lubrication, or with conventional lubrication, would fail by seizure or increased friction in the bearings.[9,10]

The second special test was designed to discover any contamination of the inside surfaces of the solenoid assembly from outgassing of its component parts, especially the epoxy. The solenoid in this test used MoS_2 burnished into the bearing surfaces but with the coil and cover epoxied and only the small teflon pumpout port to vent the inside of the solenoid to the outside. It was installed on the regular vacuum station and with vacuum pressure at 10^{-6} Torr operated in a rapid cycle 3 minutes on, 3 minutes off, for about 24 hours at -10 to -25°C and also at +40 to +50°C. Minimum NI measurements were taken frequently and showed normal operation. The solenoid was machined open after removal from the vacuum station and all internal surfaces studied under a microscope. No sticky surfaces were found anywhere, but an extremely thin "haze" appeared on the inside cover facing the coil winding. The presence of this film could only be detected by the surface reflectance before and after a wipe. This test indicates that the lubrication of moving

parts would not be affected by internal outgassing. Also, it should be pointed out that in actual operation the off periods of the solenoid are five hours as compared to three minutes during this test, thereby allowing outgassed material to be pumped off between each operation.

2.2.3 Radioactive Sources

2.2.3.1 The Overall Scheme

The choice of sources was based on the penetrating properties of the emitted particles, the absence of gamma rays, and the ease of fabrication. The Sr^{90} source used emits a beta spectrum whose maximum energy is 2.2 MeV. Beta particles with this energy will easily reach the deepest detector of the detector telescope. On the other hand, alpha particles from the Am^{241} source have very shallow penetration, in matter, even though their energy is >5.0 MeV. They will barely pass through the first thin detector of the telescope.

Both sources were made to conform to the radiological specifications set by NASA which required radioactive contamination levels far below those accepted by the AEC. The level of contamination as picked up on a "wipe" or smear on or near the sources had to stay less than $5 \times 10^{-6} \mu$ curies for alpha activity and $5 \times 10^{-5} \mu$ curies for beta activity.

For additional safety during the early electrical tests of each experiment, the sources were made readily removable from the experiment. They were electro-etched with their serial numbers for positive identification.

Figure 2-19 shows an exploded view of the assembly of the radioactive sources. Each source is set into a special machined 2-56 stainless steel socket set screw. The sources are screwed into the source arm with a conventional Allen wrench. The arm in turn is clamped to the shaft of the rotary solenoid (see Figure 2-14).

2.2.3.2 Strontium 90 Fabrication

The Sr^{90} source in its final stage is a fused pellet of $SrTiO_3$, 0.045-inch diameter by 0.020-inch thick. It is prepared by mixing a solution of $SrCl_2$ and $TiOCl_2$, adding radioactive $Sr^{90}Cl_2$ in the right strength. Out of this solution, $SrTiO\ (CrO_4)_2$ is precipitated and fired at 900°C to produce $SrTiO_3$ in a fine powder. This powder is compressed into a packed disc by the use of a die and then fired in an oven at 1300°C overnight to produce a hard, ceramic-type pellet.*

*This technique was devised, and actual pellet fabrication of the Sr^{90} source carried out, by J. D. Struthers.

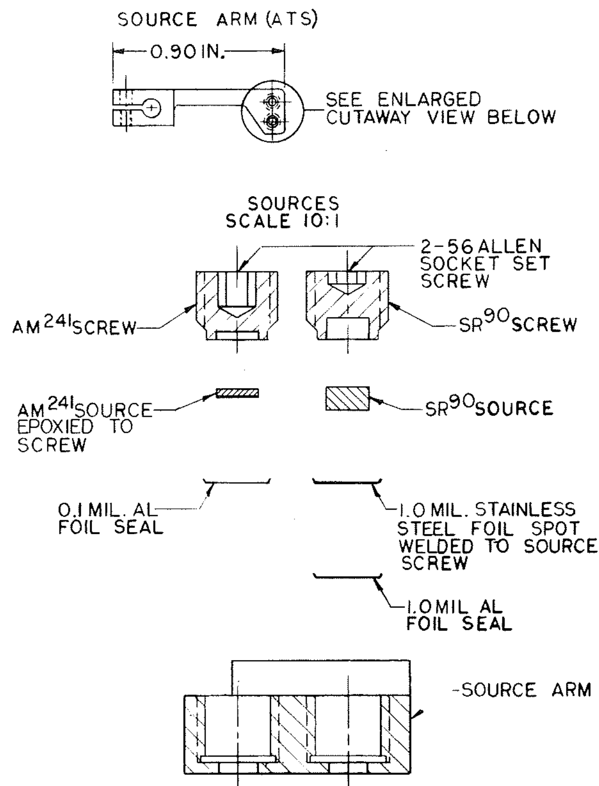

Figure 2-19. Radioactive Source Assemblies

The pellet is fitted in the machined recess in the tip of the 2-56 screw and covered with a 1.0-mil-thick stainless steel disc. This delicate assembly is held in a threaded copper block, placed between special electrodes, and the foil spot-welded to the annular rim on the screw tip. This weld does not form a hermetic seal but the stainless disc makes a sufficiently tight cover to prevent any grains of Sr^{90} from falling out of the recess. To make this assembly a sealed source, a 1.0-mil aluminum disc is placed in the bottom of the blind tapped hole in the source arm and the source assembly is screwed firmly against the foil.

2.2.3.3 Americium 241 Fabrication

The Am^{241} sources were made from strip material supplied by the U.S. Radium Corp. The process they used is as follows: Americium 241 oxide and gold are mixed and ground into a uniform mixture, then compressed into a brick and sintered in an oven. The brick is then overlayed with a thin Au layer, heated again in an oven and compressed while red hot. This piece is then cold rolled into a strip 0.003-inch thick which is subsequently mounted on a 1/16-inch thick

Ag-Au backing. A 0.001-inch Au overlay is hot press-welded into the backing and this piece is then cold rolled to a 0.006-inch thick strip. This strip is then mounted on a 0.15-inch Ag piece, overlayed with a thin Au layer, hot press-welded again, and finally cold rolled into a strip 0.006-inch thick.

A profile of the finished product is comprised of the following layers:

Bottom layer	— 0.006 inch Ag
Then	— 1-2μ Au
Active layer	— 1μ Am^{241} - Au
Overlayer	— 1μ Au

A top layer of 0.5μ Pd (or Au) is then plated over the active layer to form the final surface.

Individual 0.047-inch diameter discs were punched from the 0.006-inch thick strip. These discs were then epoxied into the recess in one of the 2-56 screws. To form a sealed source, a 0.1-mil aluminum foil was placed in the bottom of the blind tapped hole in the source arm, and the source screw run in firmly against the foil.

2.3 MOUNT FOR THE DETECTOR TELESCOPE AND CALIBRATION SOLENOID

2.3.1 Description of Construction

Figure 2-20 shows the exploded view of assembly details in and on the detector mount. The main structure is an aluminum block which has been machined to receive the detector assembly, the collimation assembly, the calibration solenoid assembly, and the detector socket and concentric ground assembly. The detector assembly is readily installed or removed through the front opening which appears near the skin of the satellite. The mechanical parts in front of the detector assembly serve to define the acceptance solid angle (full angle 40°) for the energetic particles encountered in space, to minimize scattering of particles from the collimator, to exclude light, and to retain the detector assembly firmly in its socket.

All surfaces of the aluminum detector mount were gold-plated by the Anchor Plating Co. of El Monte, California. The procedure was as follows: zincate, then plate copper, silver, and finally, hard gold. Total buildup of a surface was held to 0.0005 inch.

2.3.2 Detector Socket and Concentric Ground

A ceramic socket which receives the 15 pins of the detector telescope assembly is made from high-density aluminum oxide to maintain the clean environment

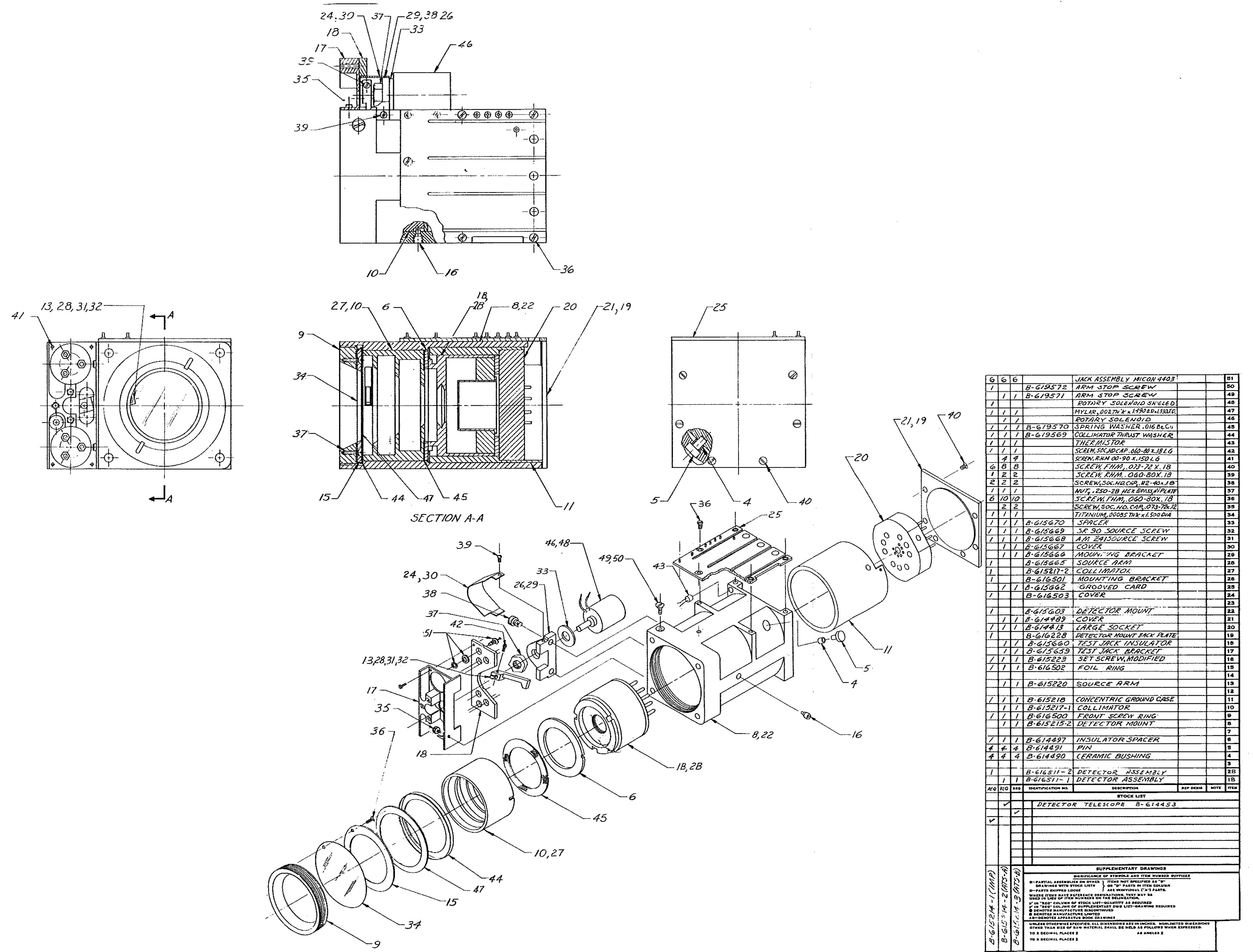

REQ	REQ	REQ	IDENTIFICATION NO.	DESCRIPTION	REF DESIG	NOTE	ITEM
6	6	6		JACK ASSEMBLY MICON 4403			51
1			B-619572	ARM STOP SCREW			50
	1	1	B-619571	ARM STOP SCREW			49
1				ROTARY SOLENOID SHIELDED			48
1	1	1		MYLAR, .002 TH'K x 1.490 O.D. x 1.330 I.D.			47
	1	1		ROTARY SOLENOID			46
1	1	1	B-619570	SPRING WASHER .016 BeCu			45
1	1	1	B-619569	COLLIMATOR THRUST WASHER			44
1	1	1		THERMISTOR			43
1	1	1		SCREW, SOC. HD. CAP .060-80 X .18 LG			42
	4	4		SCREW, RHM 00-90 X .150 LG			41
6	8	8		SCREW, FHM, .073-72 X .18			40
1	2	2		SCREW, RHM, .060-80 X .18			39
2	2	2		SCREW, SOC. HD. CAP, #2-40 x .18			38
1	1	1		NUT, .250-28 HEX BRASS, Ni PLATE			37
6	10	10		SCREW, FHM, .060-80 X .18			36
	2	2		SCREW, SOC. HD. CAP, .073-72 x .12			35
1	1	1		TITANIUM, .00035 TH'K x 1.500 DIA			34
1	1	1	B-615670	SPACER			33
1	1	1	B-615669	SR 90 SOURCE SCREW			32
1	1	1	B-615668	AM 241 SOURCE SCREW			31
	1	1	B-615667	COVER			30
	1	1	B-615666	MOUNTING BRACKET			29
1			B-615665	SOURCE ARM			28
1			B-615217-2	COLLIMATOR			27
1			B-616501	MOUNTING BRACKET			26
	1	1	B-615662	GROOVED CARD			25
1			B-616503	COVER			24
							23
1			B-615603	DETECTOR MOUNT			22
	1	1	B-614489	COVER			21
1	1	1	B-614413	LARGE SOCKET			20
1			B-616228	DETECTOR MOUNT BACK PLATE			19
	1	1	B-615660	TEST JACK INSULATOR			18
	1	1	B-615659	TEST JACK BRACKET			17
1	1	1	B-615223	SET SCREW, MODIFIED			16
1	1	1	B-616502	FOIL RING			15
							14
	1	1	B-615220	SOURCE ARM			13
							12
1	1	1	B-615218	CONCENTRIC GROUND CASE			11
	1	1	B-615217-1	COLLIMATOR			10
1	1	1	B-616500	FRONT SCREW RING			9
	1	1	B-615215-2	DETECTOR MOUNT			8
							7
1	1	1	B-614497	INSULATOR SPACER			6
4	4	4	B-614491	PIN			5
4	4	4	B-614490	CERAMIC BUSHING			4
							3
1			B-616511-2	DETECTOR ASSEMBLY			2B
	1	1	B-616511-1	DETECTOR ASSEMBLY			1B

STOCK LIST

DETECTOR TELESCOPE B-614453

Figure 2-20. Detector Mount Assembly

Page intentionally left blank

for the detectors. The socket contains gold-plated beryllium-copper contacts. The contacts are self-aligning to facilitate insertion of the telescope.

The concentric ground, item 11 in Figure 2-20, provides a noise-reducing shield surrounding the detector telescope. The shield is electrically connected to the internal electronic ground of the electronic package and insulated from the satellite or chassis ground. The concentric ground consists of an aluminum cylinder insulated on each side by a thin layer (0.5 mm) of aluminum oxide. The outside layer is applied by a plasma spray technique* and is precisely ground to form a snug fit in the aluminum telescope mount at final assembly. The inside layer of the concentric ground consists of a precision-ground ceramic tube which is fitted into the aluminum cylinder while the aluminum cylinder is heated. As the cylinder cools it shrinks to form a very tight fit on the ceramic tube. The aluminum cylinder also provides a support for the aluminum oxide ceramic socket. The two parts are secured in the telescope mount by four insulated pins. A back cover for the concentric ground is made from Fiberglas circuit board clad on each side with a layer of copper. A photoresist technique was applied to one side of the cover to leave a central area of copper surrounded by Fiberglas. This area of copper contacts the concentric ground. The copper layer on the opposite side is connected to the chassis or satellite ground by the retaining screw heads when the cover is secured in place. To complete the insulation of the shield from satellite ground, an aluminum oxide washer (item 6 in Figure 2-20) is placed between the detector telescope and the collimator. Cables from the socket to the electronics are brought through an opening machined in the concentric ground.

2.3.3 The Collimation Assembly

The front screw ring (item 9 in Figure 2-20), in addition to compressing the detector assembly in its socket, serves to hold a thin entrance foil. The entrance foil excludes the intense light of outer space. This is important in reducing the influx of heat to the region of the collimator and detectors, and in keeping light from the light-sensitive particle detectors. This second function is shared with the thin nickel foil that appears just in front of the dE/dX detector elements (see Paragraph 2.1.3.1). Even if a micrometeroid impact should drill a small hole in both foils, the probability of the sun being positioned so as to illuminate the first dE/dX detector through this pair of holes is very small. The entrance foil is 0.085-mil titanium, rolled by the Hamilton Watch Co. of Lancaster, Pennsylvania. When mounted in the front screw ring, it has an unsupported diameter of 1 inch which is stretched taut and is essentially pinhole free. Titanium exhibits tear and tensile strengths similar to those of steel.

*This technique was developed by R. G. Brandes during the Telstar program.

The durability of the mounted foils was tested in several ways. The mounted foils received vibration tests with the electronics package, but, in addition, a special test was set up to simulate the sudden decompression experienced by the foil where the fairing was jettisoned from around the satellite during launch. The pressure differential developed during this operation was estimated to be approximately 0.1 psi. The mounted foil was screwed into a dummy detector mount and placed into a large evacuated chamber. It was then subject to sudden pressure increases; as high as 0.5 psi without resulting in any sign of foil motion. Only when the chamber was suddenly brought all the way up to atmospheric pressure did the foil show signs of motion but no damage resulted. Subsequently, dead weights were placed on the foil held in a horizontal position to test its strength. Loading of 0.5 pounds on a 0.5-square-inch area produced no rupture or plastic stretching of the foil.

The thermal vacuum test of the electronics package showed that the foil experienced wrinkling at low temperatures (-10°C) and stretching at high temperatures (+40°C). Since the thermal vacuum test of the complete experiment involved only one or two complete temperature cycles, each mounted foil was additionally cycled in temperature chamber at least 24 times between temperatures of -20° and +50°C. No damage resulted to any of these foils tested. To further check the "stretching" effect, one foil that contained several pinholes was subjected to the same test to see if tearing or rupturing at the pinholes would result. Inspection of the foil with strong light under a microscope showed no change in the size of the pinholes.

The front ring is frequently screwed on and off, sometimes under torque provided by the spring washer (item 45 in Figure 2-20). Since the mating surfaces of the pieces involved with the front ring are aluminum, the problems of galling in the threads was serious and required lubrication of the threads. Silicone oil or grease were ruled out because of their migratory tendencies and the proximity of the solid-state detectors.

The male threads were finally provided with a solid lubricant surface of MoS_2, using a proprietary process of the General Magnaplate Corp. of Belleville, New Jersey. The procedure was as follows: Anodize the aluminum surface to a depth of 0.1 to 0.2 mils, leaving a porous, hard surface; follow with a vapor blast of MoS_2 particles to fill the pores and impact a 0.15 to 0.20 mil layer of MoS_2 on the surface; bake at 450°F in humid atmosphere to seal the pores of the anodized surface. The final finish is a hard surface with a generous, fully adhered coating of MoS_2. Test pieces were repeatedly screwed in and out under 35 in.-lbs. torque without any signs of deterioration of either the MoS_2 male threads or the Au plated female threads. At higher torques, ~50 in.-lbs., the aluminum threads in the detector mount started to flow.

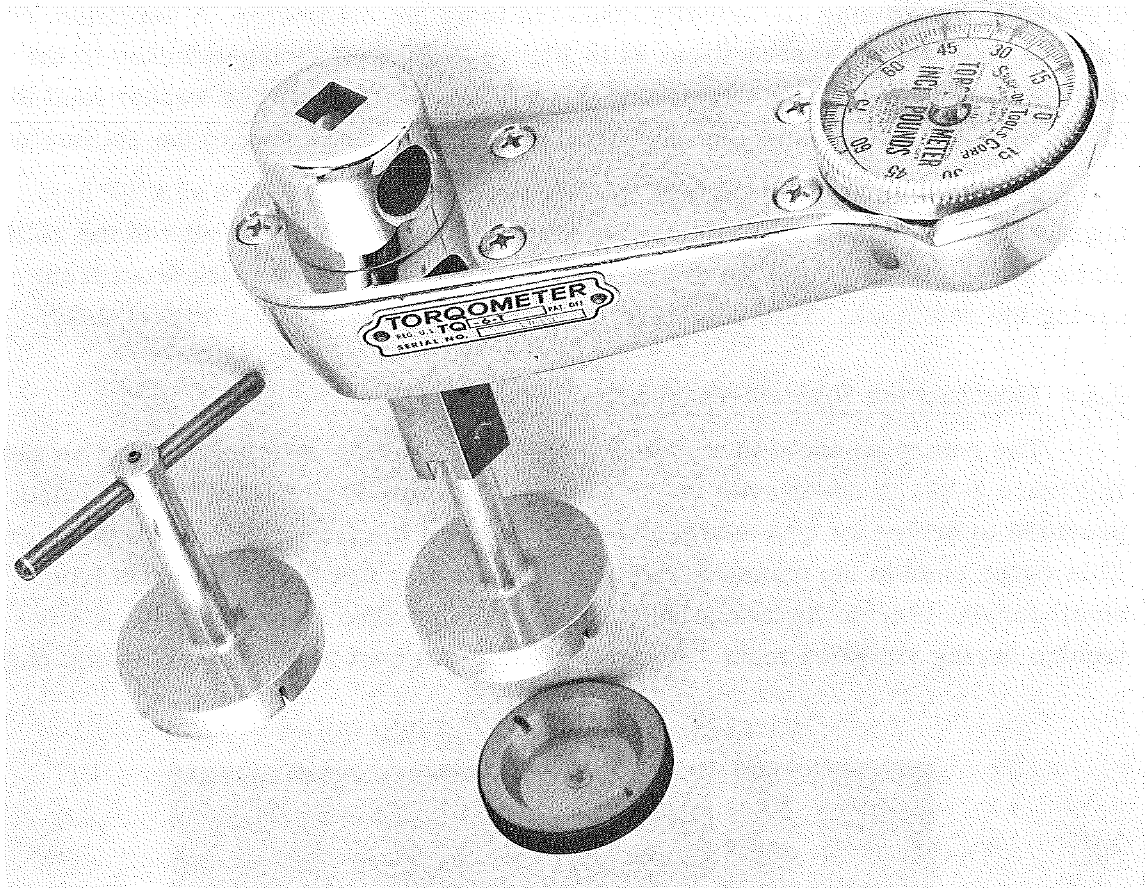

Figure 2-21. Front Ring Installation Tools

Figure 2-21 shows the tool and torquemeter used for installing and removing the front screw ring. Since the titanium is vulnerable to being pierced by any hard object, the tool was contoured to fit the exact cone angle of the front screw ring. A blade of ground stock steel protrudes from the sides of the tool cone angle to engage matching slots in the cone of the front screw ring. The T-handle tool is first used to screw in the front screw ring until the collimator starts to compress the ripple spring washer (item 45 in Figure 2-20). When the tool with attached torquemeter is substituted, and the whole collimation and detector assembly is torqued to 30-35 in.-lbs. This spring loading was incorporated to keep positive pressure on the detector assembly during the vibration of launch.

Since the collimator (item 10 in Figure 2-20) was keyed to prevent its rotation, the back of the front ring screw bore heavily against the leading edge of the collimator. Consequently, a thin mylar washer was inserted between those two

surfaces to prevent galling and provide a slip surface. However, this left the anodized front screw ring electrically insulated from the collimator. A beryllium copper "captive" thrust washer (item 44 in Figure 2-20) was spring-attached to the unanodized foil retainer ring (item 15 in Figure 2-20). This captive washer held the mylar washer in place and also electrically bridged the foil ring to the collimator.

The front ring screw defines the effective entrance aperture at a 20° half angle. Backscattering of particles into the cone is limited by the ribs in the collimator which are so placed as to prevent any particle entering at the front from seeing the detectors. This structure is visible in section A-A, of Figure 2-20.

2.3.4 Mounting the Solenoid-Source Assembly

The rotary solenoid is mounted to the outside of the detector housing as shown in Figure 2-22. A cover over the solenoid shaft (item 30 in Figure 2-20) is also provided to bridge the gap between the solenoid and the front panel of the package. This cover shields the exposed front solenoid bearing and the source arm from small foreign objects including the foam dust that is shed from the package electronics during vibration tests. The small pump-out port tube from the inside of the

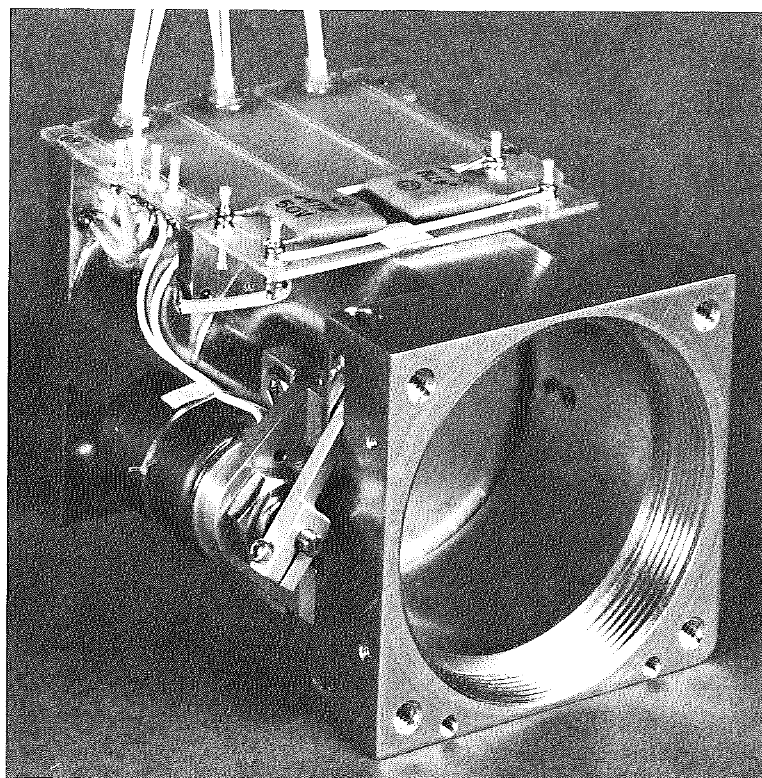

Figure 2-22. Rotary Solenoid Mounting

solenoid (see Paragraph 2.2.2.3) vents into the tunnel formed by the cover, thus providing a vent path directly to the package front panel.

The source arm extends into a slot in the detector mount body just aft of the female threads. This slot extends into and through the collimator, and its width provides a 0.010-inch to 0.015-inch clearance for passage of the source arm. With the power off and the source arm retracted, the collimator parts and the detector assembly can easily be removed and replaced. When the source arm is actuated, it extends into the open cone of the collimator to be seen by the detector assembly.

The source screws and the arm must have a firm installation because the source arm is not restrained during vibration tests and actual satellite launch. As a result, at critical frequencies the arm bangs against its physical stops.

2.3.5 Measurements with the Calibration System

It was imperative to minimize the background produced by the sources in the shielded or retracted state. Using a high intensity Sr^{90} source and a nominal 0.7-mm-thick silicon solid-state detector, counting measurements were taken in the shielded and calibrate positions. For pulse heights that the package electronics would respond to, the counting rate in the retracted position of the source was approximately 10^{-4} times the counting rate in the calibrate position. With the flight Sr^{90} source strength, this would produce about 1 to 2 cts/min in the detector, presumably from Bremsstrahlung. In the flight experiments, the Sr^{90} betas in the extended position of the solenoid arm produce measurable counts in the thickest of the dE/dX detectors and in the two lithium-drifted detectors.

The Am^{241} alpha particles have such a short range the calibrate to shielded ratio is very large and no alpha particle counts are observed in the first detector of the telescope with the source arm in the retracted position.

Figure 2-23 shows the typical spectrum for a thin Am^{241} source along with the thicker flight source, as measured by a test detector. Since the range of these alpha particles is short, approximately 1 mil in silicon, appreciable energy losses are experienced in the thin layers that appear between the source and the detector. The peak alpha energy is decreased by approximately 0.7 MeV by the absorption of energy in the Am-Au thick matrix and overlayment of Au on the matrix. (See Paragraph 2.2.3.3.) In the satellite, there will be a further energy decrease due to the 0.1-mil Al seal that covers the alpha source and the 0.025-mil Ni foil that covers the detector telescope. The expected energy loss from these two foils together is approximately 0.7 MeV, giving a final alpha particle energy of approximately 4.1 MeV at the front detector. The range of alpha particles of this energy is less than the thickness of the first dE/dX detector and thus no counts are expected in the second detector.

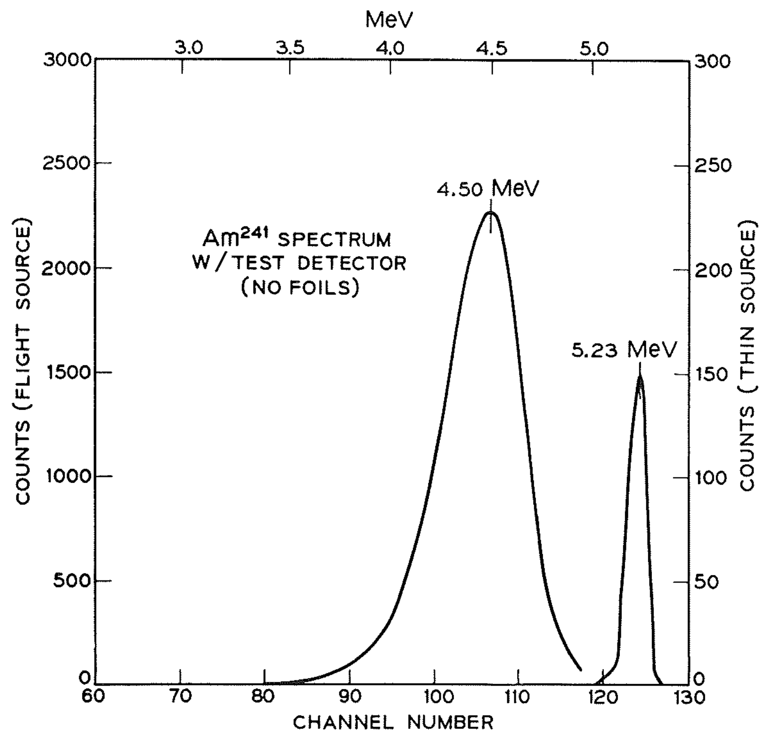

Figure 2-23. Calibration Spectra, Alpha Particles

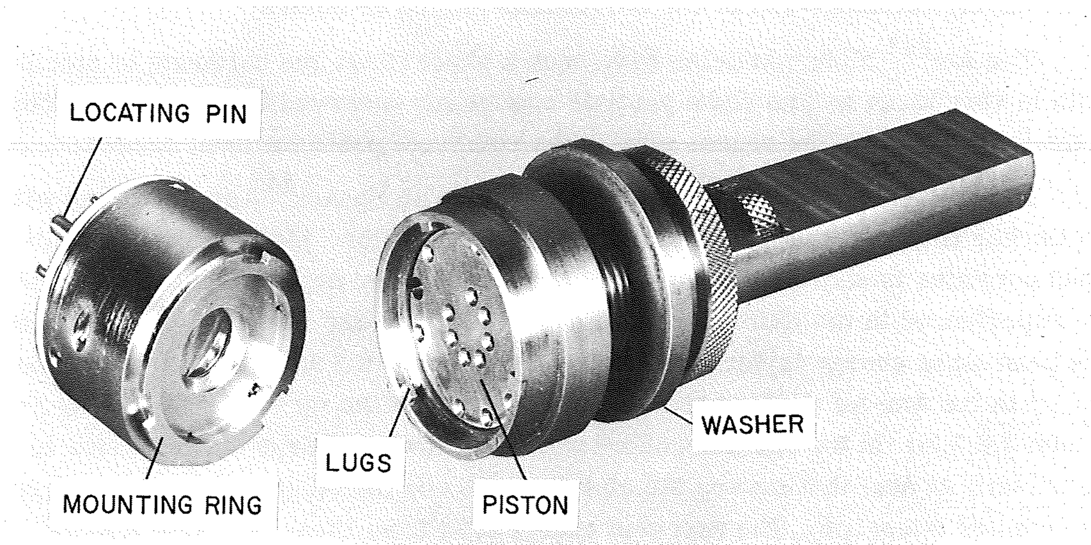

Figure 2-24. Detector Telescope and Insertion-Extraction Tool

2.4 DETECTOR TELESCOPE INSERTION-EXTRACTION TOOL

Because the ceramic socket is recessed deep in the Detector Mount (Figure 2-20) a special tool is required for inserting and extracting the Detector Telescope. The tool and telescope are shown together in Figure 2-24.

Prior to inserting the telescope into the socket, the pin arrangements of the two detector assemblies must be oriented to the hole pattern of the socket. This is accomplished by inserting the telescope into an identical pattern of holes provided on the front of the tool. The relative position of the two assemblies is maintained by cautiously tightening the clamp around the lithium-drifted detector assembly.

Following the pin orientation, the tool is engaged to the front of the telescope by three lugs which slide behind the mounting ring of the telescope. The ring is clamped tightly between the lugs and the piston by adjusting the small knurled captive nut located in the handle of the tool.

The telescope is inserted into the socket by the following method. Held securely by the tool, the telescope is placed in the entrance hole of the detector mount (Figure 2-20) and is positioned to approximately align its locating pin with the locating hole in the socket. The telescope is then carefully slid through the concentric ground until its terminal pins touch the socket. A slight rotational movement, slowly back and forth, of the telescope finds the locating hole and thus each terminal pin is aligned with its proper socket contact. Forward pressure applied to the tool forces the terminal pins into the contacts. Complete insertion of the telescope is assured by adjusting the large knurled nut until its back surface is flush with the end of the threads (partly visible in Figure 2-24). The tool is then pushed forward until the large knurled nut presses the washer against the front of the detector mount. The small knurled nut is loosened and the tool disengaged from the telescope and withdrawn from the detector mount.

The contacts in the socket are made to grip the terminal pins of the telescope firmly. As a result, and due also to the large number of terminal pins (15), a considerable force is necessary to extract the telescope from the socket. To facilitate the extraction without damage to the pins, the tool operates in the following manner. It is inserted into the detector mount and engaged with the telescope (as during insertion). The large washer on the tool is moved forward to butt against the front of the detector mount. The large knurled nut is rotated against the washer, exerting a force on the tool which extracts the telescope from the socket easily and smoothly.

REFERENCES

1. F. E. Curran, I. Hayashi, L. V. Medford, and G. L. Miller, IEEE Trans. Nuc. Sci., NS-13, No. 1, 326 (1966).
2. T. C. Madden and W. M. Gibson, IEEE Trans. Nucl. Sci., NS-11, 254 (1964).
3. T. C. Madden and W. M. Gibson, Rev. Sci. Instr. 34, 50 (1963).
4. H. E. Wegner and C. Erginsoy, IEEE Trans. Nucl. Sci. NS-12, 240 (1965).
5. Semiconductor Specialties Corp., Fair Lawn, New Jersey.
6. M. M. Atalla, E. Tannenbaum, and E. J. Scheibner, Bell System Tech. J., 38, 749 (1959).
7. P. T. Andrews, Proc. Symp. on Nucl. Instr., 93 (Academic Press, Inc., New York, 1962).
8. I. Hayashi, H. E. Kern, J. W. Rodgers, and G. H. Wheatley, IEEE Trans. Nucl. Sci., NS-13, 214 (1966).
9. P. J. Bryant, C. M. Gosselin, and L. H. Taylor, Extreme Vacuum Technology and Associated Clean Surface Studies, NASA CR-84.
10. P. M. Winslow and D. V. McIntyre, "Adhesion of Metals in the Space Environment," J. of Vac. Sci. and Tech., 3 #2, Mar.-Apr. 1966.

Chapter 3

THE ELECTRONIC SYSTEM

3.1 SIMPLIFIED DESCRIPTION OF THE ELECTRONIC SYSTEM

Figure 3-1 is a simplified block diagram of the electronic system coupled to the detector telescope. Pulse signals from each of the six active detector elements pass through linear amplifiers to a set of pulse-height discriminators and coincidence gates. For each particular experimental mode, as defined by the satellite sequence clock and decoded in the mode control logic, a set of coincidence and anticoincidence requirements is established among the detector signals. If an incident particle produces pulses which satisfy these requirements, the coincidence block of Figure 3-1 is triggered.

The linearly amplified signals are also routed through a set of linear gates. Under the control of the mode control logic the gates provide appropriate attenuation of the signals for each experimental mode. The sum of the output signals passes to a 5-channel stacked differential pulse-height analyzer whose discrimination levels are also controlled by the mode logic. In the present type of application, this type of analyzer has an advantage in that the effective width of the channels can be changed with respect to one another in different modes.

If the coincident system has fired, the outputs from the 5-channel analyzer are enabled, and the particular line (if there is one) of the five output lines corresponding to the signal amplitude sends a pulse to its register in the telemetry.

Additional elements of the electronic system are shown by the remaining blocks. A detector bias supply provides dc biasing voltages between 20 and 200 volts for the different elements of the telescope. This supply is commandable, ON or OFF. The primary bias voltage and those of the input power supply lines to the BTL package are monitored by the telementry.

For in-flight calibration of the experiment there is a radioactive source which is periodically actuated under control of a mode logic. The particles from the source check the detector-electronic system in those modes which are responsive to the alpha and beta source particles. Adjacent in time to this source calibration, a ramp test pulse generator provides pulses to all the linear amplifier inputs to test the electronic system alone.

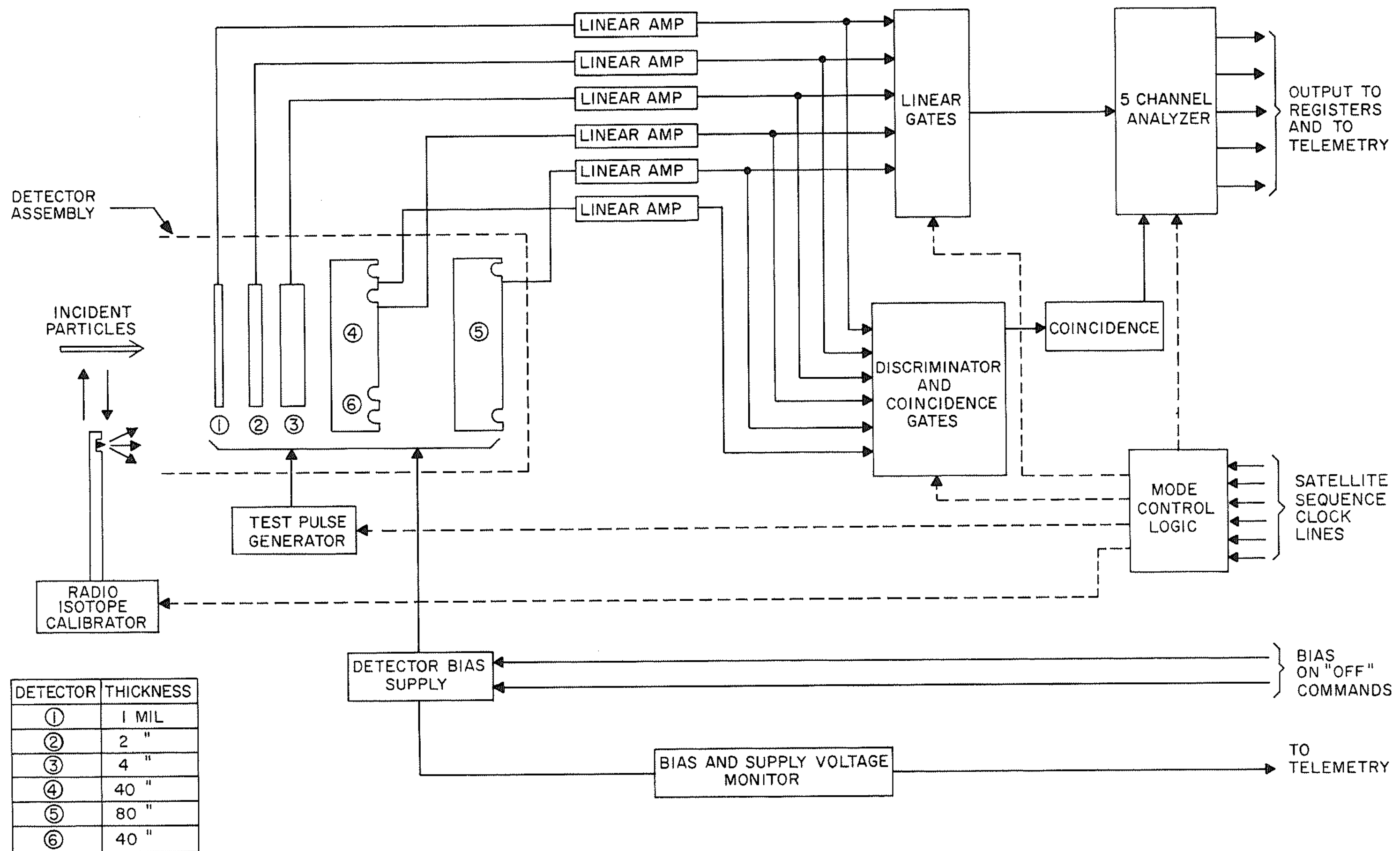

DETECTOR	THICKNESS
①	1 MIL
②	2 "
③	4 "
④	40 "
⑤	80 "
⑥	40 "

Figure 3-1. Simplified Block Diagram of the Electronic System

3.2 CIRCUIT DESIGN CONSIDERATIONS – MICROCIRCUITS

Satellite experiments impose particularly stringent demands on electronic circuitry. The equipment must operate reliably through the jarring vibrations of launch and in the inhospitable environment of space where it is exposed to ionizing radiation and temperature extremes. It is severely constrained in size, weight and power consumption, and there almost invariably exists a relatively short time from experimental concept to hardware delivery.

Any approach that can cut the design and construction time while retaining the required reliability is highly desirable. In the present experiment this led to serious consideration of the advantages of microcircuits. Particularly attractive was the possibility of choosing a small set of modules to comprise a basic set of microcircuit building blocks from which a large class of electronic systems could be constructed.

At the time of experimental design, the commercial microcircuit situation was found to be as follows:

(1) A very large number of digital microcircuits existed, exhibiting a wide range of construction forms, speed, power, etc.

(2) Extremely few analog microcircuits were available, and these were either incapable of performing the required functions or consumed too much power. (This situation is still true today, more than two years later.)

It is well known that many commercially available digital microcircuits are entirely suitable for satellite application, and in fact many such devices have been successfully used. On the other hand, it was apparent that analog microcircuits, if they were to be used, would have to be newly designed.

At this stage the question arose as to the most advantageous construction technique, monolithic or hybrid. Each of these branch into many subdivisions of technique, e.g., chip and wire, cermet, and metal film over oxide. Some broad features, however, are summarized in Table 3-1. Only if very large numbers are required (many thousands) did it seem economic to pursue the monolithic approach unless some special extenuating circumstances prevailed, such as the ability to use an existing master slice. For this reason the price entry on the monolithic side of the table indicates that the cost of such devices is either very reasonable or out of the question. In the matter of economics it was also important to bear in mind the cost of possible design changes if, for instance, a prototype exhibited poor radiation damage behavior or if a modified experimental requirement necessitated the use of transistors having a higher gain or a capability of operation at lower temperatures.

Table 3-1

COMPARATIVE SUMMARY OF MICROCIRCUIT PROPERTIES

	Monolithic	Hybrid
Size	Small	Large
Design Time	Long	Short
Radiation Damage	?	Good
Power	High	Low
Component Tolerance	?	Good
Component Stability	?	Good
Cost	Cheap or Prohibitive	Expensive

After consideration of various alternatives, the decision was made to use a configuration employing metal film resistors along with discrete capacitors and active components. There is not space to list all the considerations involved in this choice, but a few salient ones are as follows:

(1) Discrete active components permit making the best choice in terms of individual characteristics from the thousands of commercially available semiconductor devices.

(2) The size of discrete transistor packages is not such a problem as might be thought initially because each analog module has to be surrounded by a number of discrete external components.

(3) The available range of resistor values is essentially unlimited while both their temperature coefficient and drift are very low.

(4) There is no need for redesign time. A circuit having worked satisfactorily on a breadboard will, if anything, work better in thin-film form because of reduced stray capacitances.

(5) The component density is somewhat higher than that achievable with cordwood packaging. (It was concluded that this would be the next most desirable form of construction.)

(6) The flat geometry of the resulting modules is convenient for mounting on printed circuit motherboards.

(7) The cost is potentially quite low. (This advantage was not realized in practice, in part because the thin-film substrate rejection rate proved higher than anticipated.)

Important system decisions were the power supply voltages and signal amplitudes. The choices made were power supplies of ±6 and ±3 volts, and maximum signal amplitudes of ±3 volts. The availability of four supply voltages affords considerable circuit design flexibility while the choice of small signal levels allows the use of particularly simple gating arrangements as will be shown in Paragraph 3.3.3.

3.3 THE ANALOG BUILDING BLOCKS

Examination of the operations required to implement the experiment as shown in Figure 3-1 indicated a need for the set of five building block elements that are described in the following sections.

3.3.1 The Amplifier

The amplifier schematic is shown in Figure 3-2. It comprises a differential input dc-coupled operational loop. The low-frequency gain is $> 10^4$ and unity gain is at ~ 15 MHz. The amplifier was initially designed for an npn transistor having a lower collector capacitance, and being somewhat faster, than the 2N2222. However, this transistor exhibited poor radiation performance and was therefore replaced by the 2N2222. It is possible however to operate the loop with confidence at high frequencies and quite low reserve gains (e.g., 5-10). This is because the open loop gain is itself stabilized, being primarily defined by the G_m of the input pair which operate at a substantially constant current. For other applications, demanding a higher input impedance, the input pair of transistors are replaced with two 2N2844 p-channel field effect transistors.

Top and bottom views of the this film module are shown in Figure 3-3. A discussion of the fabrication techniques in contained in Paragraph 5.2.2.

3.3.2 The Zero-Crossing Discriminator

The advantages of zero-crossing discriminators for coincidence evaluation are well known. The circuit of Figure 3-4 achieves this function in a very simple way. Transistors Q1 and Q2 form a differential input. Quiescently Q3 is in saturation, Q2 is on and Q1 off. When an input signal to Q1 exceeds the threshold level set on the base of Q2 by the potentiometer R_5-R_6, Q1 turns on. The tunnel diode snaps off, turning off Q3 and completing the transfer of current from Q2 to Q1. Since Q3 is off, the base of Q2 falls to ground potential and hence the circuit reflexes when the input base reaches zero. The positive transition of the discriminator output occurs at this time and is employed in the coincidence evaluation,thus exhibiting the desired zero-crossing behavior. The vestigial amplitude dependent

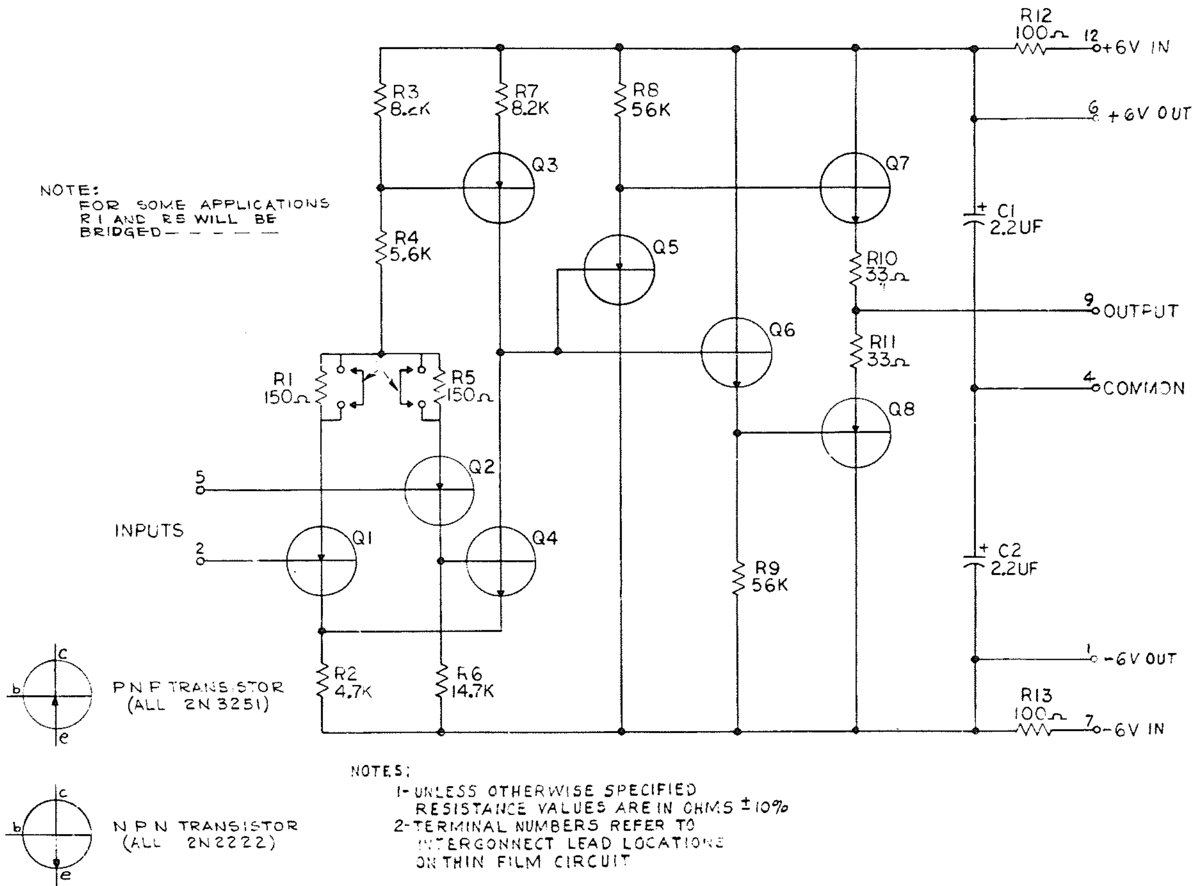

Figure 3-2. Schematic of the Linear Amplifier

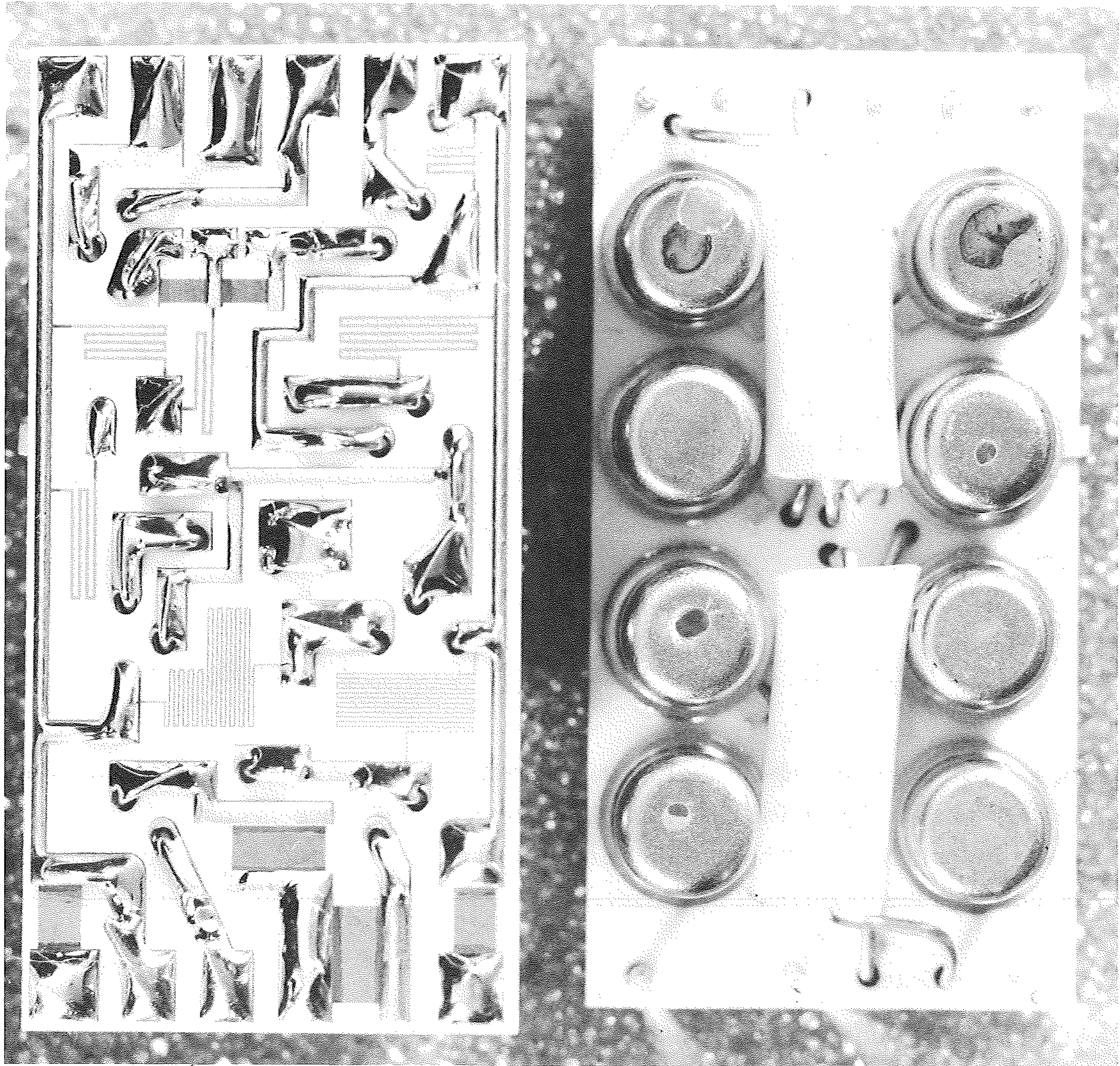

Top View Bottom View

Figure 3-3. Thin-Film Linear Amplifier

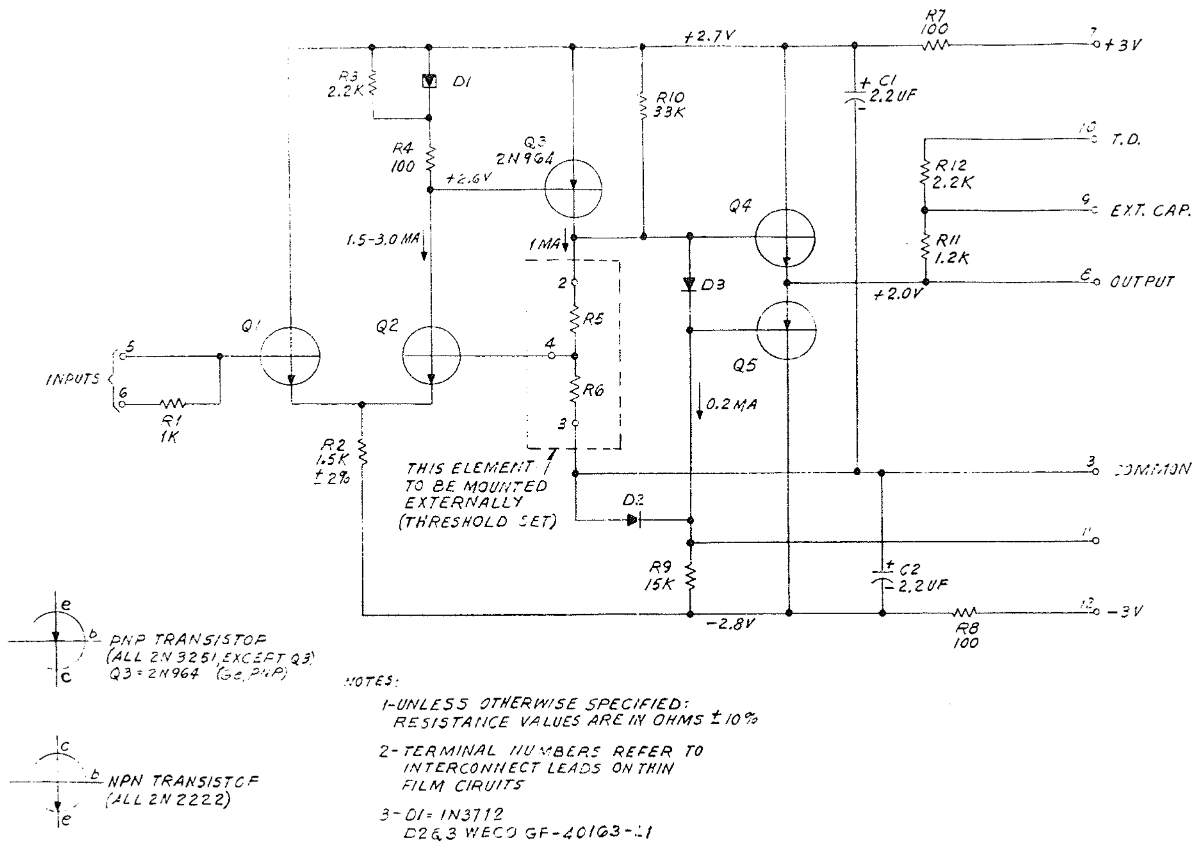

Figure 3-4. Schematic of the Zero-Crossing Discriminator

walk is < 20 ns for signals in the operating range of 0.2 to 2 volts. Also included in the circuit are facilities for providing bias for a tunnel diode, which bias is removed when the circuit fires. (The combination of a tunnel diode and discriminator is used in the coincidence evaluation circuitry.)

3.3.3 Linear Gate

One of the considerations leading to the choice of ±3-volt-maximum signal amplitudes was the possibility of using simple linear gates like that of Figure 3-5. Such gates exhibit on-to-off ratios of ~100:1 and simultaneously afford a convenient means of controlling the gain of linear systems by choosing suitable combinations of the various thin-film resistors.

3.3.4 Pulse Shaper

Figure 3-6 shows a univibrator of fixed period possessing an inhibit-input. Also included are facilities for providing a bias current for a tunnel diode as in the case of the discriminator. (Only a small number of these circuits were used in each

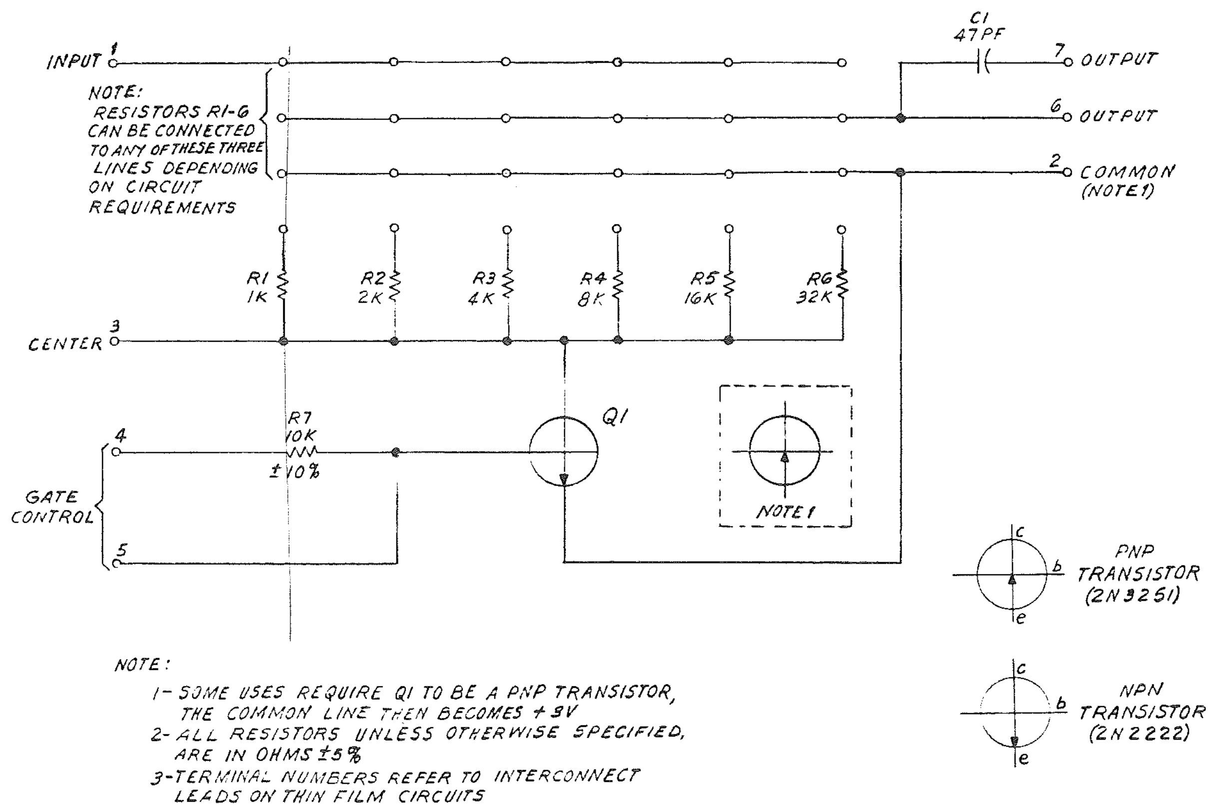

Figure 3-5. Schematic of the Linear Gate

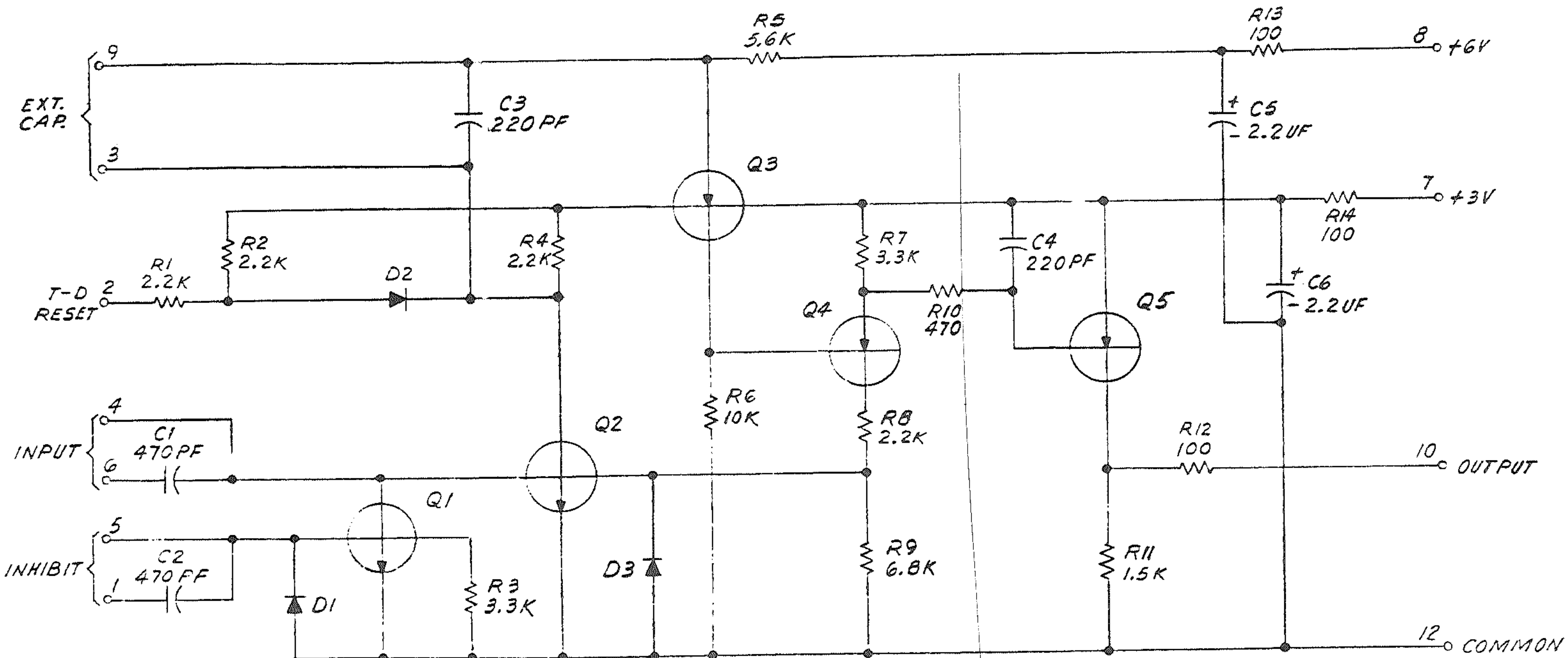

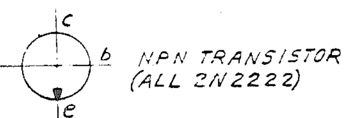

Figure 3-6. Schematic of the Pulse Shaper

satellite experiment and it is debatable whether it was really worth making them in thin film.)

3.3.5 Potentiometer Network

A small thin-film network comprising a set of binary weighted resistors was used to simulate a 3K potentiometer. By suitably bridging sets of these resistors the "slider" could be set anywhere to within ~1 percent of full scale.

When a satellite experiment was first assembled, small wire-wound 3K potentiometers were mounted at all places where adjustments needed to be made. (Examples are discriminator thresholds, amplifier gains, etc.) After all these potentiometers were adjusted for correct operation of the experiment, they were then removed, measured, and replaced with appropriate thin-film potentiometer networks.

3.4 THE COMPLETE ELECTRONIC SYSTEM

3.4.1 Linear Signal Processing

Figure 3-7 shows the way in which the amplitude or energy information is obtained by routing the appropriate signals through amplifier and linear gate circuit modules. Pulse shaping of the signals is performed with resistors and capacitors external to the amplifier modules. In Figure 3-7 two typical detector channels are illustrated. If signals from both of these detectors are of interest in a particular mode, both linear gates are opened. If one, or both, are irrelevant in a particular mode, the appropriate gates may be closed to avoid undesired contributions to the total energy signal. The 1-μs delay line is introduced in the linear chain to allow time for the coincidence system to make a decision on the input pulses.

3.4.2 Coincidence Evaluation

Figure 3-8 is a simplified schematic of the coincident system. Coincidence evaluation is achieved by using the positive-going transistions from zero-crossing discriminators to drive tunnel diode discriminators. Since the outputs to the tunnel diodes are routed via linear gates, it is possible to change the operating mode of the experiment by opening and closing these gates. The minimum coincidence resolving time is ~20 ns, but in practice it was set at a much larger values (~0.3 μs) to allow for degradation of the detector signal rise-times as a function of radiation damage in space.

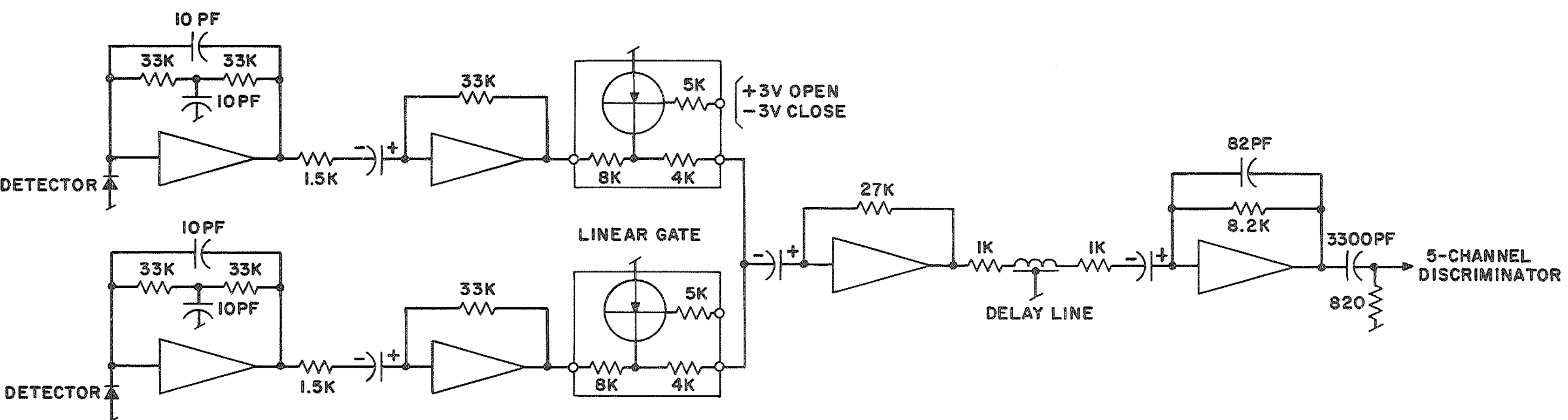

Figure 3-7. Simplified Schematic of the Linear System

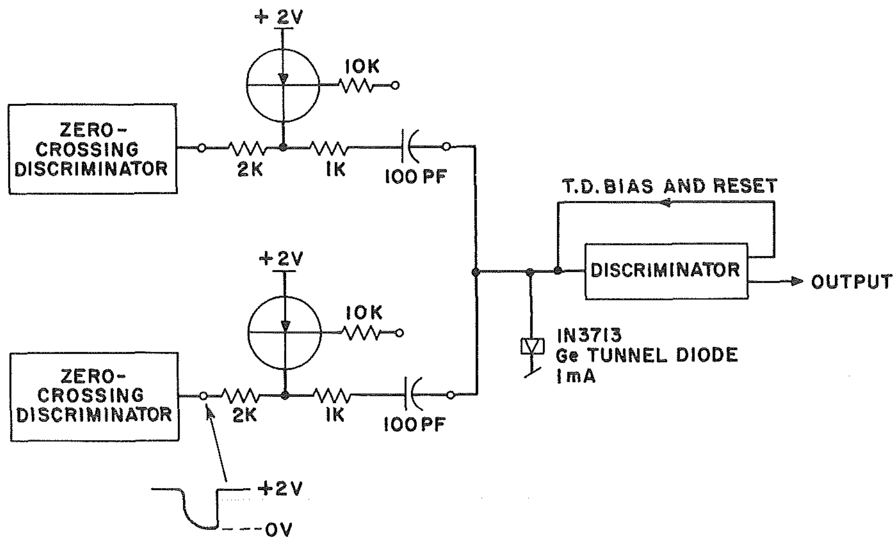

Figure 3-8. Simplified Schematic of the Coincidence System

3.4.3 Block Diagram of the Complete Experiment

The complete block diagram of the ATS-B experiment is shown in Figure 3-9. The amplifier, discriminator, gate, and shaper thin-film modules are indicated by individual blocks. The fifth type of microcircuit module, the adjustable potentiometer, is not shown in the figure. The points marked TP are test points available at a test connector on the front of the experimental package.

The routing of the linear signals can be traced in Figure 3-9 in the manner of Figure 3-7. Note that the gates are labeled with mode letters beneath them to indicate those modes in which they are open. For example, pulses from detector 1 are introduced to the 5-channel analyzer only in Modes A and B through gates G1 and G2. These two gates are adjusted to provide different gains for the two modes. Detector 4, which is included in the finally summed pulse height in the largest number of modes, has four parallel gates which provide different gain levels in different modes.

The coincident system can be traced in the manner of Figure 3-8. A coincidence discriminator is on each detector line (there are two on detectors 4 and 5 for which special conditions of pulse height are required in several modes; see Paragraph 1.2). The outputs from these discriminators pass mode-activated gates and are handled in groups in coincidence discriminators D7-D9. After secondary gating these serve to trigger shaper 6. The anticoincidence section of the system is less complicated because adjustment of the firing levels of discriminator D10 does not need to be very precise. Any single signal coming to it should fire the anticoincidence discriminator. In the coincidence case, the sum of two signals must be sufficient, but a single signal must be insufficient. (Note that detector 6 is only involved

in anticoincidence). An anticoincidence pulse serves to inhibit shaper 6. If an appropriate coincidence has occurred, the output of shaper 6 enables the output shapers of the 5-channel analyzer.

In the area of the 5-channel analyzer, an array of 24 linear gates allows adjustment of the discrimination levels of the analyzer channels in different modes. For the last two discriminators of the six involved in the 5-channel analyzer (the top of the fifth channel is closed), an additional stage of amplification is provided to stay within the 0.2- to 2-volt design range of the discriminator. A special group of gates (GD1-GD5) are provided for I mode which reads singles counts in detectors 2-6. Pulses from the coincidence discriminators of these five detectors are routed via special gates directly to the output shapers. They can trigger the shapers without an enabling pulse from shaper 6. None of the normal linear channel gates are involved in I mode.

A pile-up rejector is indicated in Figure 3-9. Its purpose is to discard linear pulses (examined just before the delay line) which have zero-crossing times that indicate the pulses are contaminated by pile-up. This circuit will be described in more detail in Paragraph 3.7. The pile-up rejector is active only half of the time as provided by the inhibit line to shaper 7 from the sequence clock line S4. When the pile-up rejector is active, its detection of a piled-up pulse serves to inhibit the firing of shaper 6 through the anticoincidence inhibit line.

The mode logic control and the test mode logic are shown in Figure 3-9 to depend on sequence clock lines S_0 through S_{6-11}. The mode control is discussed in more detail in Paragraph 3.5. The test mode logic serves to define two sequences of 32 experimental modes: In one, the radioactive calibration sources are active; in the other, an internal ramp pulser operates in either of two ramp states (see Paragraph 3.9).

The illustration shows a bias switch in the detector bias system that can be activated by command. Either of two commands is sufficient to turn the bias on, but a proper combination of a bias-off-enable command and a bias-off command are required to turn it off. This was provided for security against spurious experimental turnoff by a single misinterpreted command.

The final block of Figure 3-9 shows the commutated power supply monitor which examines the four input power supply lines on a time scale which is determined by the sequence clock lines S_4 and S_5.

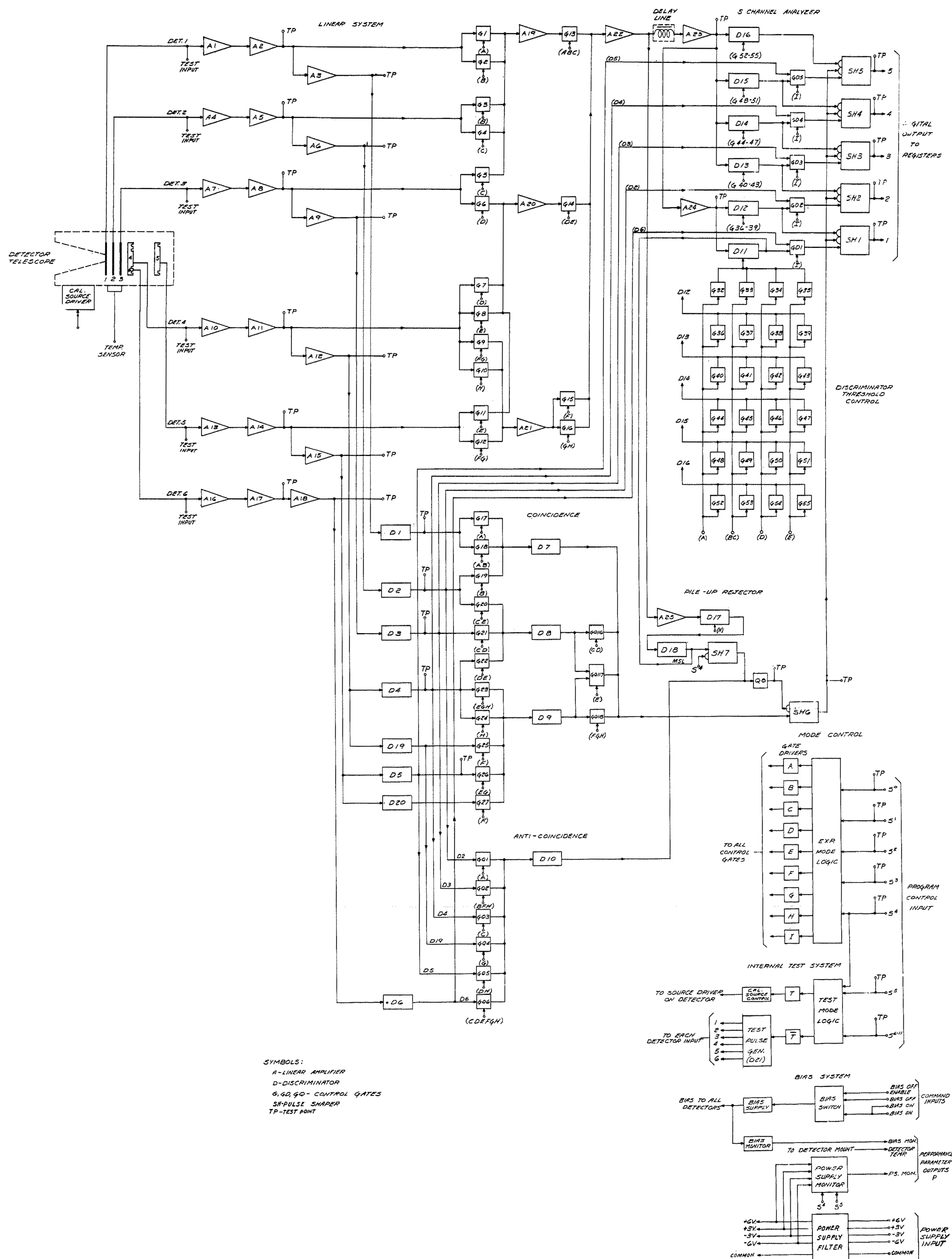

Figure 3-9. Block Diagram of the Complete Experiment

Page intentionally left blank

3.5 MODE CONTROL SYSTEM

Central to the multimode type of experiment operation employed here is the implementation of the mode control system. Provision of this control by the decoding of the satellite sequence scaler bits is convenient because

(a) These signals are already available on the spacecraft.

(b) The contents of the sequence scaler are transmitted along with the data in each telemetry sequence, thus providing mode identification.

A disadvantage of the scheme, however, is that it can only be conveniently applied if the associated telemetered data comes early or late in the telemetry sequence. If this is not the case, experimental live time is lost since data-taking must be inhibited for a substantial part of each sequence. (The worst case is that in which the telemetry of the data comes in the middle of the sequence, in which case the live time is halved.) It is obvious in any case, however, that gating must always be provided to ensure that data telemetered in one sequence corresponds to only one mode.

Generation of the mode control signals is accomplished by means of a transistor decoding tree and diode logic (to provide for the logical Or function of several modes) as indicated by Figures 3-10 and 3-11.

An important point to notice is the provision of the mode override facility. If $R_2 << R_1$ (Figure 3-10) is chosen, it is possible to control any set or subset of input control bits from the front test connector of the experimental package. This facility is invaluable in testing and debugging, particularly when the experiment is mounted in the spacecraft frame.

3.6 DETECTOR BIAS SUPPLY

A number of different bias voltages were required for the various elements of the detector telescope. These were derived from taps along the length of a Cockroft-Walton multiplier as shown in Figure 3-12. For reasons of reliability two independent supplies were employed, with their various output voltages connected together by diode or gates. It was found necessary to lock the two supplies together in frequency, via capacitor C*, to prevent beat frequencies producing serious low-frequency ripple in the high-voltage output.

A special, and unusual, feature of these supplies is that they consume low zero-load power because they are designed to oscillate in a sinewave mode. The advantages of this is that all the capacitance of the system (notably that of the HV transformer secondary) is driven resonantly and therefore consumes negligible

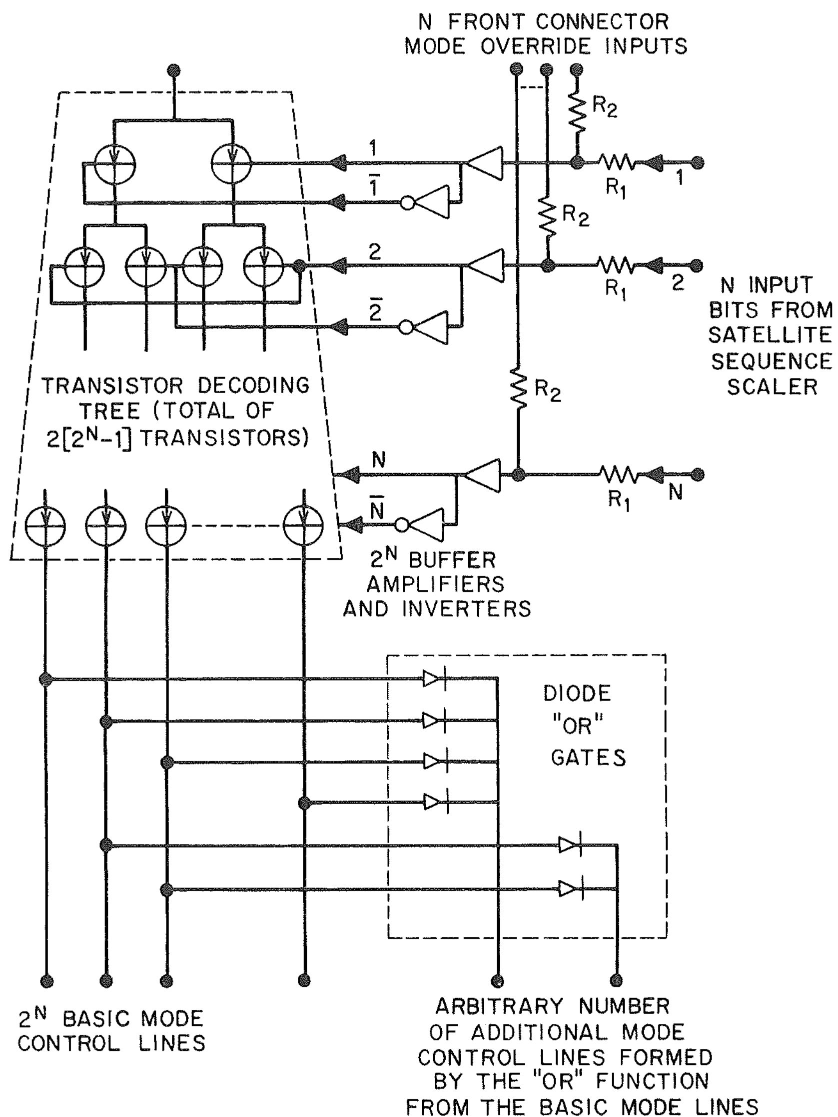

Figure 3-10. Simplified Schematic of
the Mode Control System

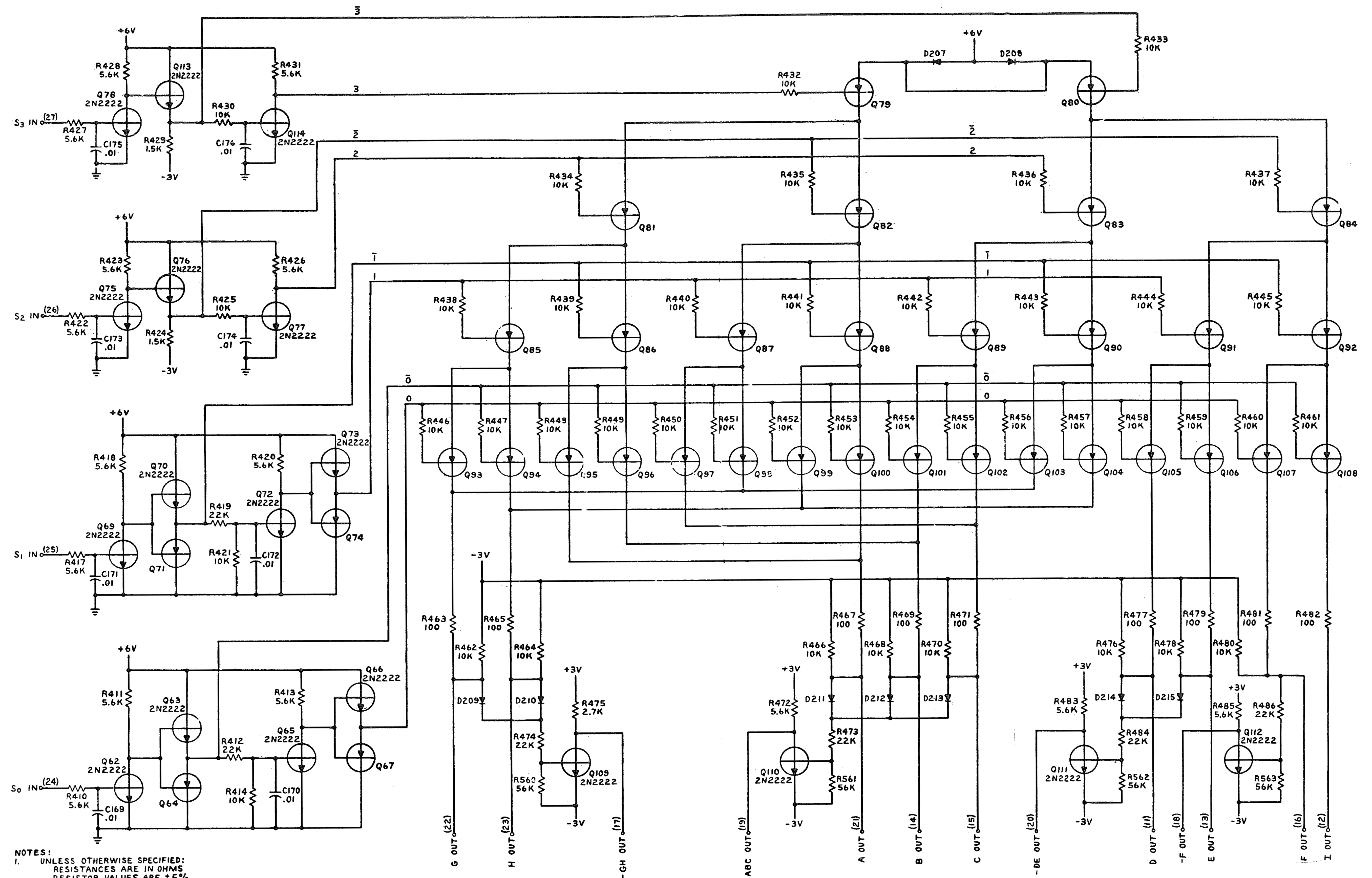

NOTES:
1. UNLESS OTHERWISE SPECIFIED:
   RESISTANCES ARE IN OHMS
   RESISTOR VALUES ARE ±5%
   RESISTORS ARE 1/4 WATT
   CAPACITANCES ARE IN MICROFARADS
   TRANSISTORS ARE 2N3251
2. SEE PARTS LIST FOR MOTHER BOARD 10 OF ATS.

Figure 3-11. Detailed Schematic of the Mode Control System

Page intentionally left blank

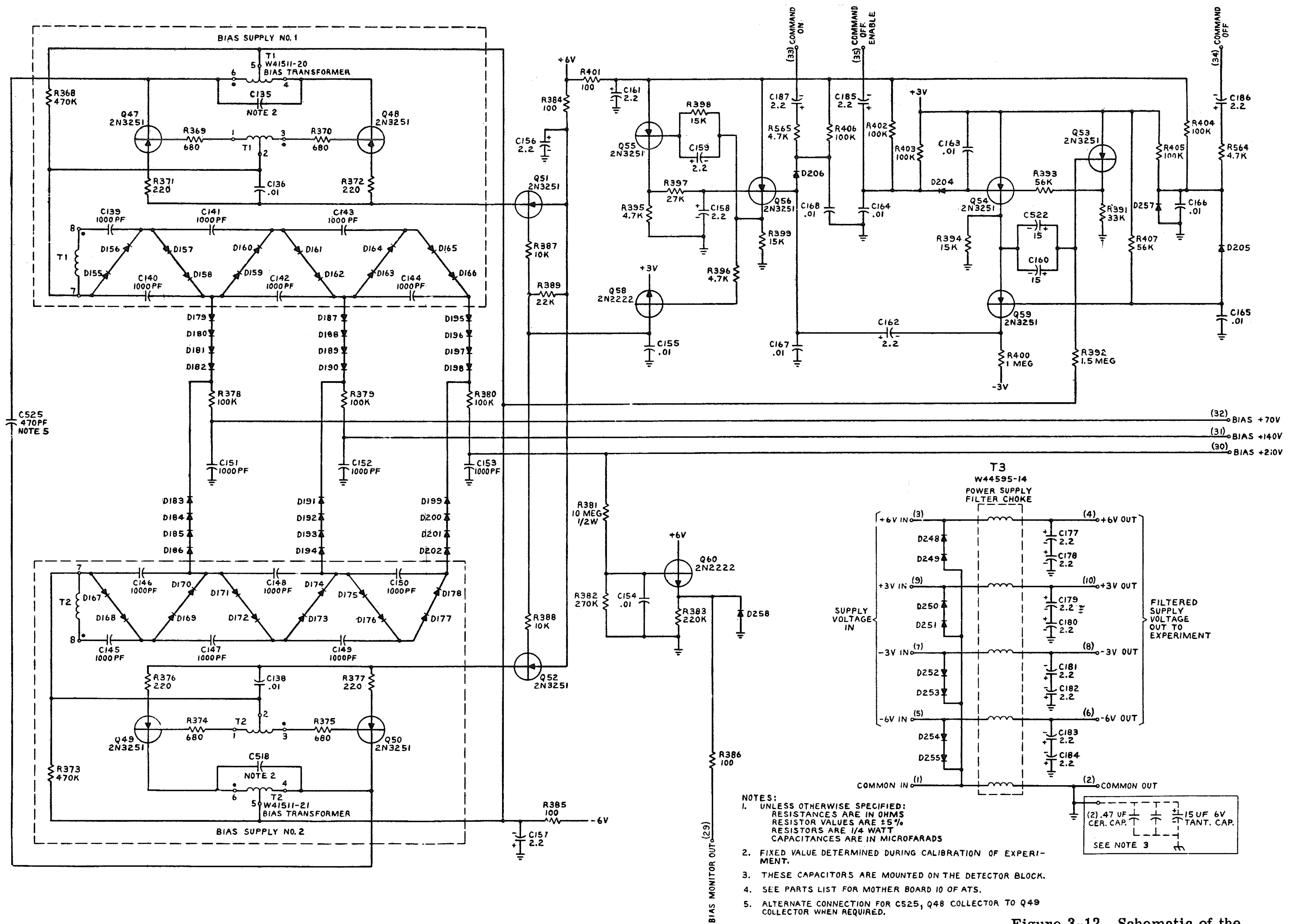

Figure 3-12. Schematic of the Detector Bias Supply

Page intentionally left blank

power. This is to be contrasted with the more usual square-wave systems in which work is done in charging and discharging the transformer secondary capacitances in each half cycle.

A high frequency of oscillation (~ 300 kHz) was chosen to simplify filtering problems and to provide a frequency above the highest frequency of interest in an associated experiment (namely, the ATS-A VLF experiment) which also employs an identical particle telescope experiment.

Since there is some evidence that it can be advantageous from noise considerations to provide periodically for the removal of the bias voltage from the detectors, provision is made to command the bias voltage on and off from the ground. For reasons of safety the OFF command must be preceded by an OFF-ENABLE command. This latter signal triggers an ~15-second-period univibrator, comprising Q53 and Q54 of Figure 3-12, which in turn enables the OFF command to turn off the bias oscillator through the switching of flip-flop Q55 and Q56. The ON command is performed by switching the control flip-flop on again.

3.7 THE PILE-UP REJECTOR

It is well known that pulse-on-pulse pile-up distorts nuclear pulse height spectral information, and a number of techniques have been developed to discriminate against such contaminated signals. The methods employed have depended on noting that the time between the start and the zero crossing of a pulse is amplitude independent and therefore the same for all uncontaminated pulses. Piled-up pulses, on the other hand, will have either a greater or lesser start-to-crossing time depending on whether the pile-up is from the left or the right. It can be demonstrated that for the present experiment the dominant effect can be expected tc be that of lengthening the start-to-crossing time. The rationale of the pile-up rejector is therefore to provide a gating signal to reject contaminated pulses, and to operate alternately with the pile-up rejector enabled and disabled. Gross differences in the resulting set of spectra then indicate when the pulse height information has been distorted by piled-up events, and due caution can be exercised in interpreting the significance of such data. If, on the other hand, no such rejector were employed it would be possible for the effects of pile-up to be misinterpreted as changes in the energy distribution of the particles under examination.

The operation of the pile-up rejector can be understood with the help of Figure 3-13. An input signal, of the form of Figure 3-13(a), is applied to a zero-crossing discriminator (see Paragraph 3.3.2) which triggers and reflexes at low levels 1 and 2 (see diagram). In the period between triggering and reflexing the

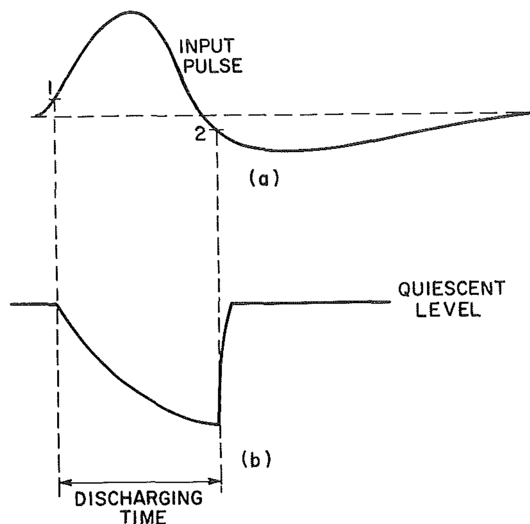

Figure 3-13. Pileup Rejector-Waveform

capacitor is discharged as indicated by Figure 3-13(b). At the instant of reflexing the capacitor is rapidly recharged back to its quiescent level. A second discriminator is used to monitor the capacitor voltage, and if it exceeds a preset negative threshold, indicating an excessively large pulse width, the second discriminator fires and inhibits the amplitude analysis of the pulse.

The two discriminators employed are labeled D17 and D18 on the block diagram of Figure 3-9, and the timing capacitor is connected to pin 11 of D17. The pulse shape discriminator is arranged to trigger if the pulse width exceeds its normal value by more than $\sim 0.3\ \mu s$.

3.8 RADIOACTIVE CALIBRATION SOURCE DRIVER

During the test period, in which bits S_{6-11} are binary "ones", and S_5 is a "one", the radioactive calibration source is deployed in front of the detector telescope.

The circuit that performs this function is shown in Figure 3-14. Here an And function is performed by Q40 and Q38, turning on Q41. This in turn drives Q44 into saturation, which then provides a negative-going signal to the emitter follower Q43 via C132 and C133. This turns on Q45 which also goes into saturation. As a result of this action almost the full supply voltage (less the sum of the drops across D151, 152 and R350, 52, etc.) appears instantaneously across the source motor solenoid, which is connected to M1, M2. This large instantaneous signal is advantageous in initiating the ON motion of the drive arm mechanism, but is not required once the arm has moved into position. For this reason the time constant of R349 and C132, 133 is arranged to slowly reduce the applied voltage from its initial value of $\sim$ 11 volts to a "holding" value of $\sim$6 volts, with a time constant of $\sim$ 1.5 seconds. This scheme of applying a large initial voltage followed by a lower holding voltage both provides more reliable source motor action and minimizes power dissipation in the solenoid during its 6-minute ON period.

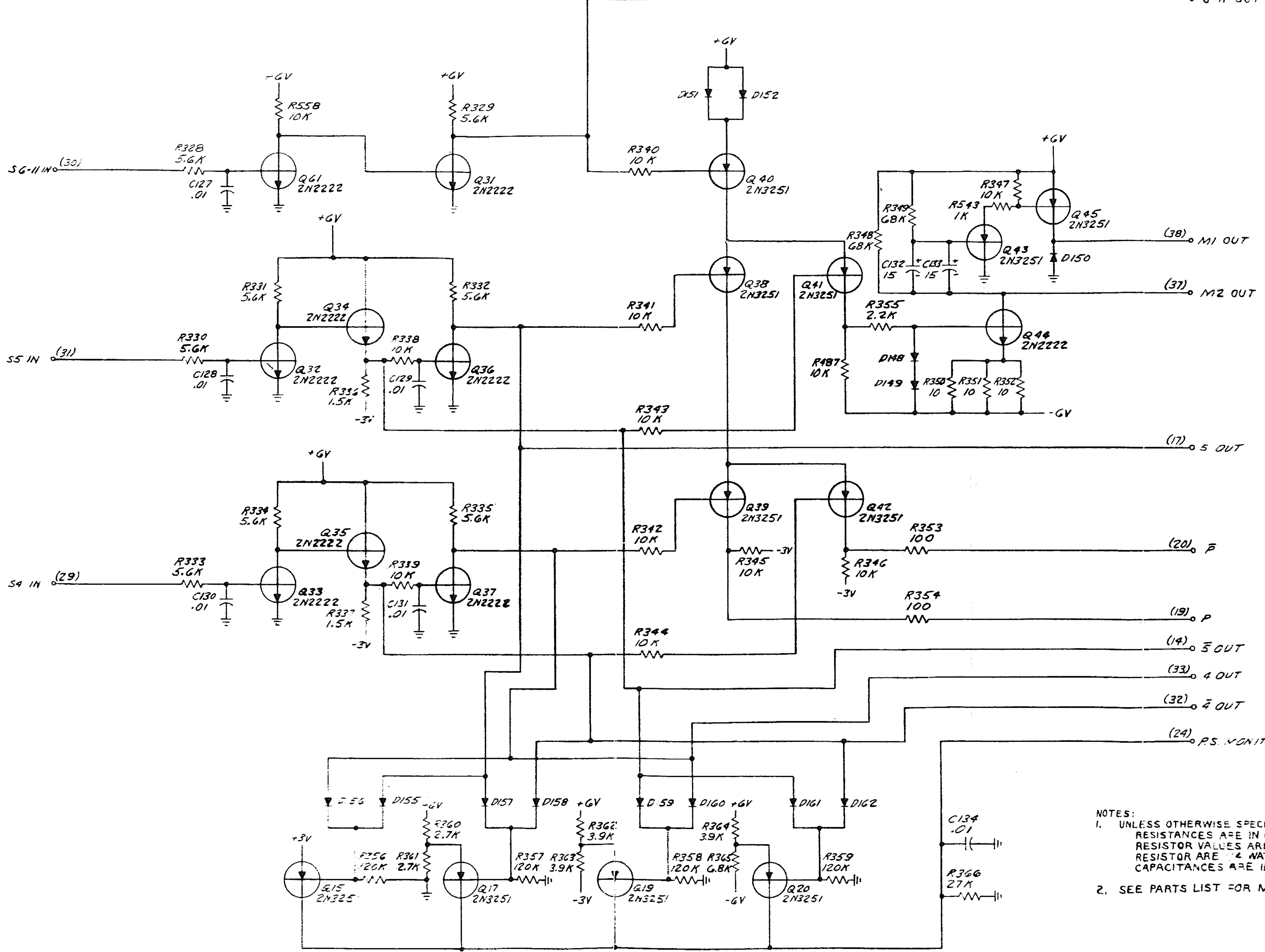

Figure 3-14. Schematic of the Calibration Source Driver

Page intentionally left blank

3.9 THE TEST PULSER

Electrical testing of the electronic system is carried out periodically by applying pulses to the preamplifier inputs. These pulses are generated by a sweeping pulse generator, and are applied to all six preamplifiers simultaneously via a set of capacitors and preset attenuators.

In addition, two different test pulser regimes are employed in turn, differing in that the signals routed to the detectors are of different amplitudes in the two cases.

By virtue of the fact that the monotonically increasing pulse train amplitudes are different in the various detectors (because of the different preset attenuators) there exists a particular range of time, in which the signals into a given detector channel are capable of satisfying its amplitude requirements (for the particular mode in which the experiment is operating). If, furthermore, these amplitude requirements are satisfied simultaneously for a number of detectors, then coincidence gating signals can be generated and the test pulser signal analyzed by the five channel analyser.

The detailed operation of the sweeping pulser can be understood with the help of the schematic, Figure 3-15. Here the two different test pulser regimes are brought into operation by either P or $\overline{P}$ being positive. If this is the case, Q21 saturates and R292 provides a constant pull-down current to the Miller integrator formed by C120 and Q22. Consequently, the input to the discriminator D21 ramps up linearly with time until it reaches $\sim +2$ volts, (set by the potential at pin 4), whereupon the discriminator fires. This turns on Q23, and hence Q22, discharging C120 and returning pin 5 to ground potential. At this point the discriminator reflexes and the cycle restarts. The length of the ramp produced in this way is ~50 ms while the return to zero takes ~ 0.5 ms.

While the ramp generator is running, the P or $\overline{P}$ signal turns off Q29, unclamping the asymmetric multivibrator formed by Q27, 28. This circuit free-runs at ~10 kHz producing pulses ~5 μs wide. These pulses in turn drive Q24 into periodic saturation, thus shunt-chopping the voltage at its collector, which voltage is supplied by the ramp generator described previously. (The diode D135 compensates for the base-emitter drop of Q23.) The presence of the capacitor C121, together with R301, guarantees that the pulses have a long-tail form and hence each produces only one signal in each detector channel.

The slope of the ramp applied to each channel is controlled by the preset attenuator R314, 316, etc. while the dual mode operation is provided by the turning on and off of Q26 and Q30 by the signals P and $\overline{P}$.

3.10 STORAGE REGISTERS

Although they are not part of the BTL experiment package, the five 16-bit registers which receive pulses from the 5-channel pulse intercept analyzer are of major importance in the operation of the experiment, and their role is thus briefly described. The registers are in the telemetry part of the EMME package and have not been constructed by BTL.

The 16-bit registers are arranged to store events for a fixed counting interval (3.89 seconds) with a storage capacity of 14 bits. If overflow of the storage capacity of the register occurs during this counting interval, that register shifts to a time mode of operation and begins to accumulate pulses from a 3 kHz clock in the telemetry. The accumulated clock pulses indicate the portion of the counting interval remaining when overflow occurs. The 15th and 16th bits of the register give a redundant indication as to whether the number stored in the 14-bit portion of the register is a number of events or a number of clock pulses. The registers are capable of receiving events at the rate of one each 3 μs.

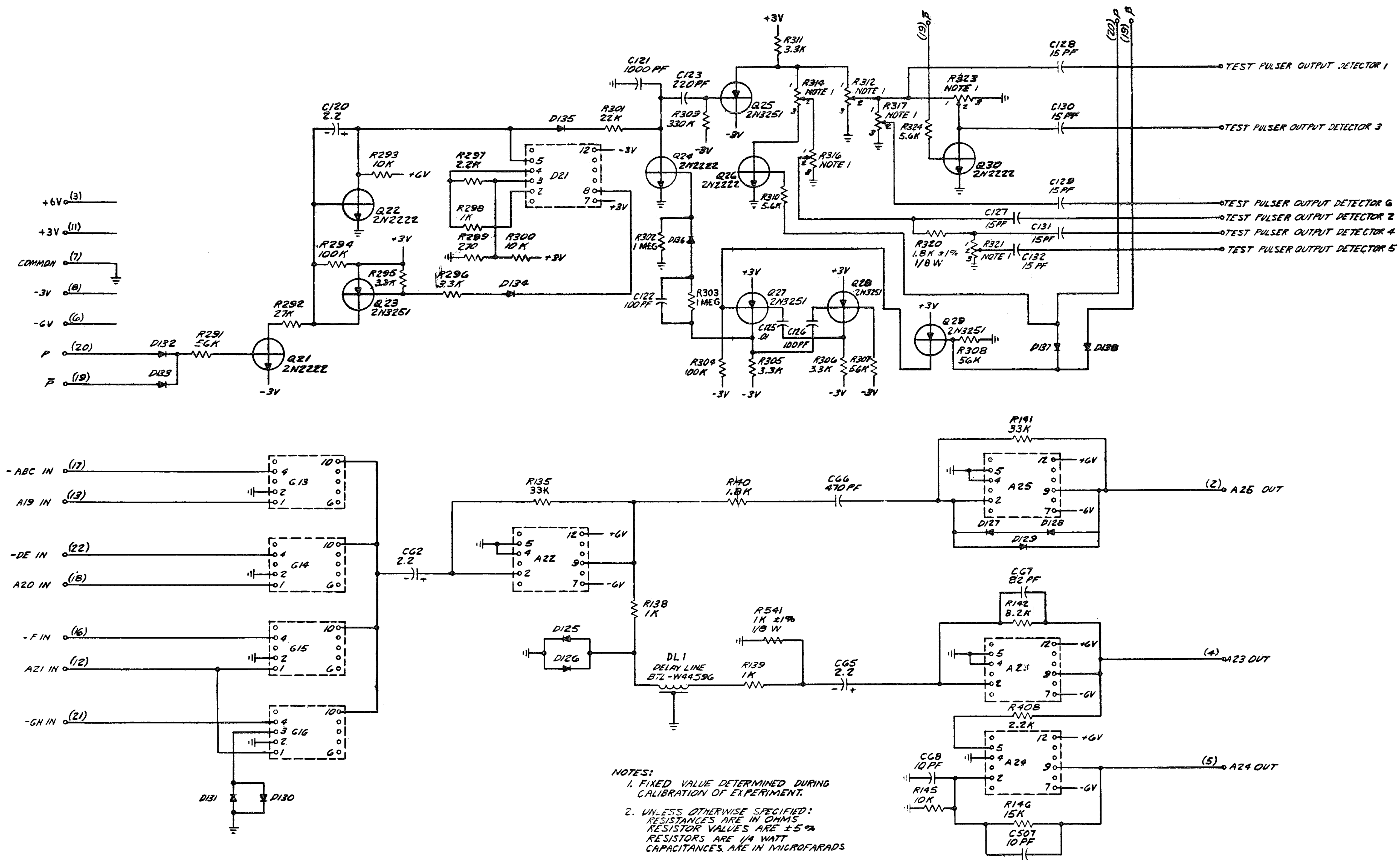

Figure 3-15. Schematic of the Test Pulser

Page intentionally left blank

Chapter 4
EXPERIMENT PACKAGE DESIGN

4.1 DESIGN PHILOSOPHY

The Bell Telephone Laboratories energetic particles experiment for ATS was more complex by an order of magnitude than any satellite experiment we had performed in the past. Our standard form of packaging had been soldered cordwood modules and two-sided wired circuit boards. It was clear at the onset of the ATS program that a far greater packaging density was required. The short program schedule also demanded an approach which would reduce design and construction time and yet retain high reliability. A hybrid system comprised of four basic integrated circuit building blocks, together with circuits using miniature discrete components on printed circuit motherboards, was adopted as the most expedient method. The block diagram of the system shows how this was accomplished in the ATS particle experiment (Figure 4-1). The system contains a total of 100 hybrid thin-film circuits of the four basic types described in Chapter 3. These are shown together in Figure 4-2: (A) is an operational amplifier, (B) a zero crossing discriminator, (C) a pulse shaper, and (E) a linear gate. The circuit shown in (D) is a potentiometer network used to replace adjustable trimming elements in flight hardware. It is made by the same basic thin-film technique but has no additional components mounted on its substrate.

4.1.1 Electro-Mechanical Design

The BTL experiment, along with others, was contained in the Westinghouse Environmental Measurements Experiment (EME) housing. This unit provided both mechanical and electrical support for the individual experiments and was integrated as a whole with the spacecraft as shown in Figure 4-3. The length and width of each package thus integrated was predetermined by the design of the EME which will be described in Paragraph 4.3.1. Height was allotted on the basis of estimated individual experiment volume requirements, constrained by the total number of experiments to be accommodated within the height of the EME housing and its window in the spacecraft skin.

A photograph of the BTL package in its flight configuration is shown later in Figure 4-30. The mechanical details of the enclosure will be described in full in Section 4.3.

The geometrical restrictions mentioned, combined with the following factors, influenced the design of the electronic package within the BTL housing:

(1) Structural considerations to meet the specified high vibration test levels (Paragraph 8.4.2).

(2) Access to all parts of the circuit for testing, modification, or repair.

(3) Isolation between portions of the electronic system sensitive to interference from internal noise sources by separation of high- and low-level circuitry onto different circuit boards.

(4) The need for an effective internal signal ground system which would reduce cross-coupling of signals and exclude external RF interference.

These conditions were best met by a stack of vertical circuit boards which are mechanically supported by bolts passing horizontally through the entire stack and sides of the housing, as shown in Figure 4-4. With this approach, good structural stiffness in the thrust axis (axis of highest vibration levels) was achieved for the least housing weight since the covers were not load-bearing and could be made thin. The housing was comprised of separately machined details which could be easily disassembled for access to the electronic stack. Interconnections between most circuit boards were made at one end only, thus permitting access to both the components and printed circuit by fanning the stack apart on a bench.

Figure 4-5 shows the inside of the BTL-owned development model, a nonflight unit constructed to verify the mechanical and electrical designs. It is included here to show the overall packaging technique since it was the only unit not encapsulated. The electronic system was divided among 10 printed circuit motherboards and so arranged that signal levels increased with each successive board, beginning at the detector mount (a large block located in the front left corner) (see Figure 4-4). Copper ground planes covering one side of each circuit board afforded good internal shielding. This combination of shielding and compartmentalizing resulted in an electronic package with no troublesome internal interference problems.

The motherboards measure 2.5 inches wide and from 6.7 to 9.6 inches long, depending on their location within the package. Full dimensional details are shown in Figure 4-6. Their main mechanical support comes from two stainless steel bolts inserted through close-fitting clearance holes along the center line of each board and the sides of the housing, as shown in Figure 4-4. The center line of the first through-bolt is just behind the detector mount, 3.2 inches from the front of the

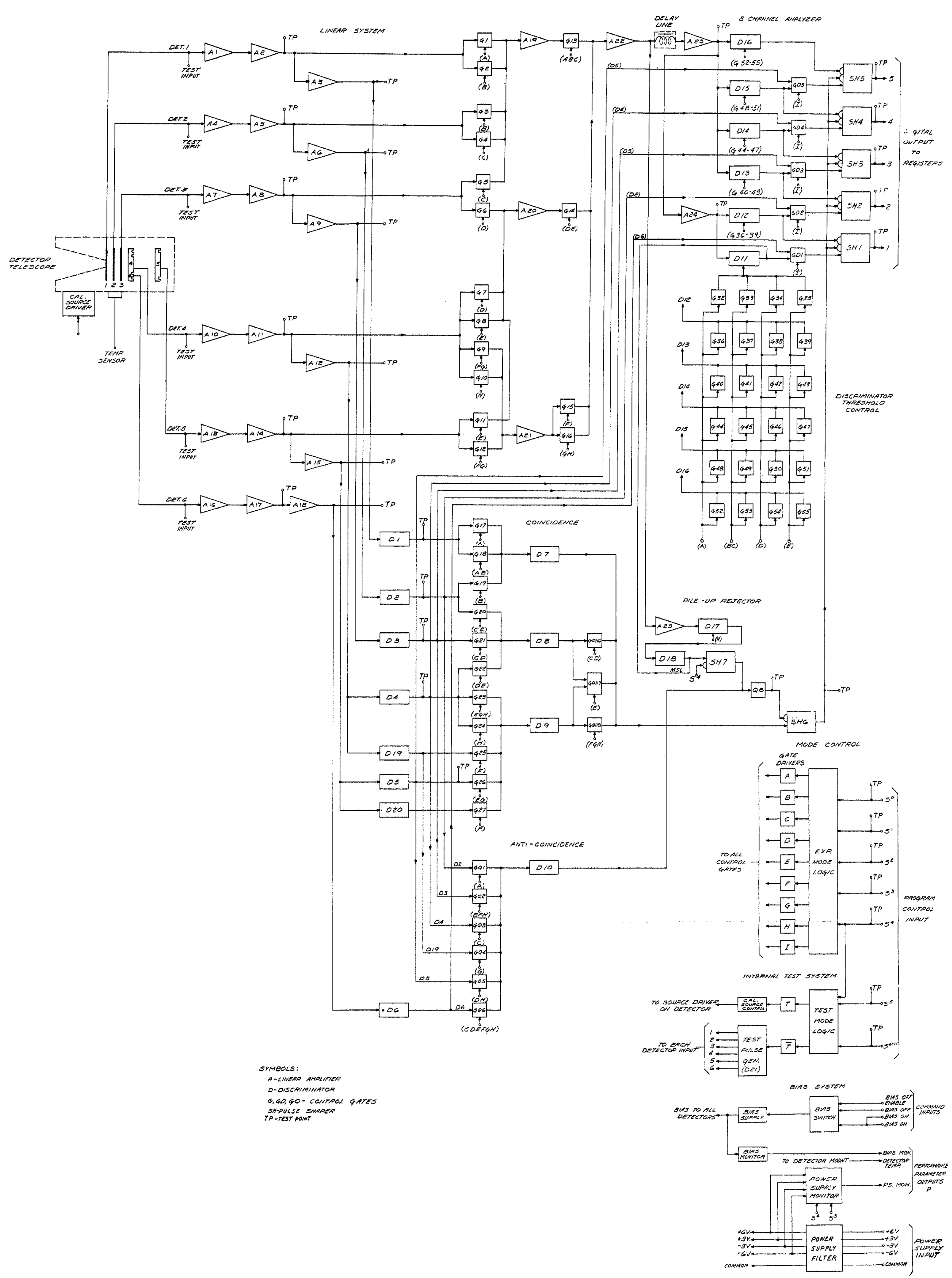

Figure 4-1. BTL Particle Experiment for ATS, Block Diagram

Page intentionally left blank

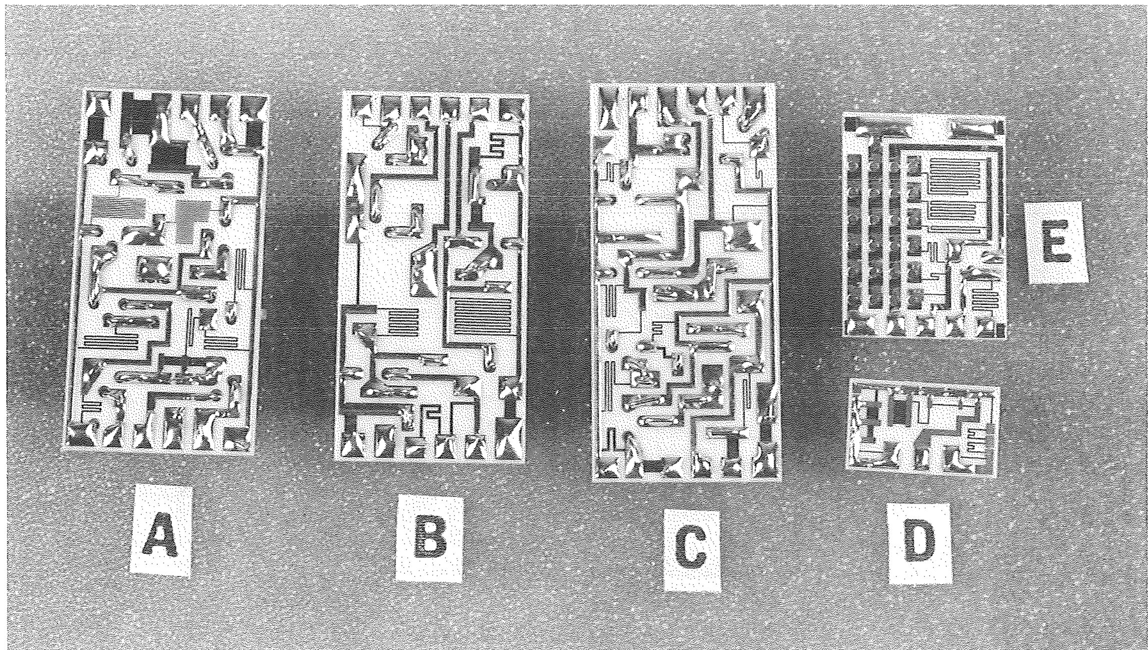

Figure 4-2. Thin-Film Integrated Circuits

experiment. Spacing between the two bolts had to be very accurately controlled on all boards and the sides of the housing to provide accurate alignment at assembly. Tubular aluminum spacers, shown in the sketch in Figure 4-4A, determined the motherboard separation in the stack which, in each case, was designed for a minimum clearance of 0.1 inch between nearest points on adjacent boards. The total thickness of the stack of spacers and boards exactly equalled the inner width of the housing. When the through-bolts were tightened, the left and right sides were clamped together to form a rigid mechanical column of boards and spacers. Further vibrational support came from polyurethane foam encapsulation in all spaces between boards, which will be described in Paragraph 4.1.2. Interconnecting harness wiring among the motherboards lay within a 0.24-inch-wide gap provided between the back ends of the boards and the inside of the housing back plate. This gap was filled with a silicon rubber foam at final assembly for vibration damping of the harness wires. Notches were machined in the rear corners of motherboards 1 through 8 to allow them to fit within a rim around the back plate as shown in the sketch in Figure 4-4A. The same arrangement was used at the front edges of boards 5 through 10 which extend inside the front plate to its inner surface, Figure 4-4C. This provided increased mechanical support during thrust axis vibration at both ends of the stack. Figure 4-4C also shows grooves cut in a boss along the inner surface of the top of the front plate and in an epoxy board strip fitted inside

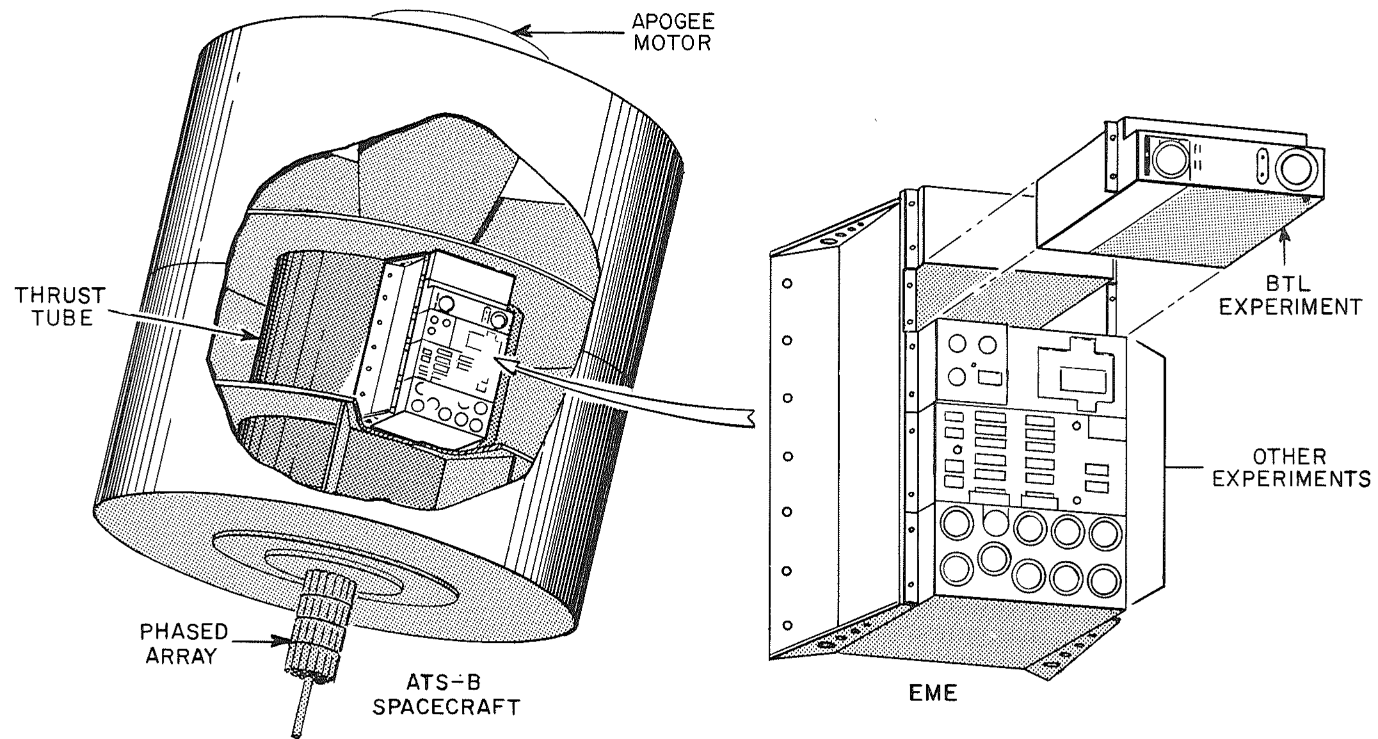

Figure 4-3. Environmental Measurements Experiment Housing and Location in the ATS-B Spacecraft

NOTES:

1- SUPPLIED BY CANNON ELECTRIC CO. SALEM, MASSACHUSETTS.

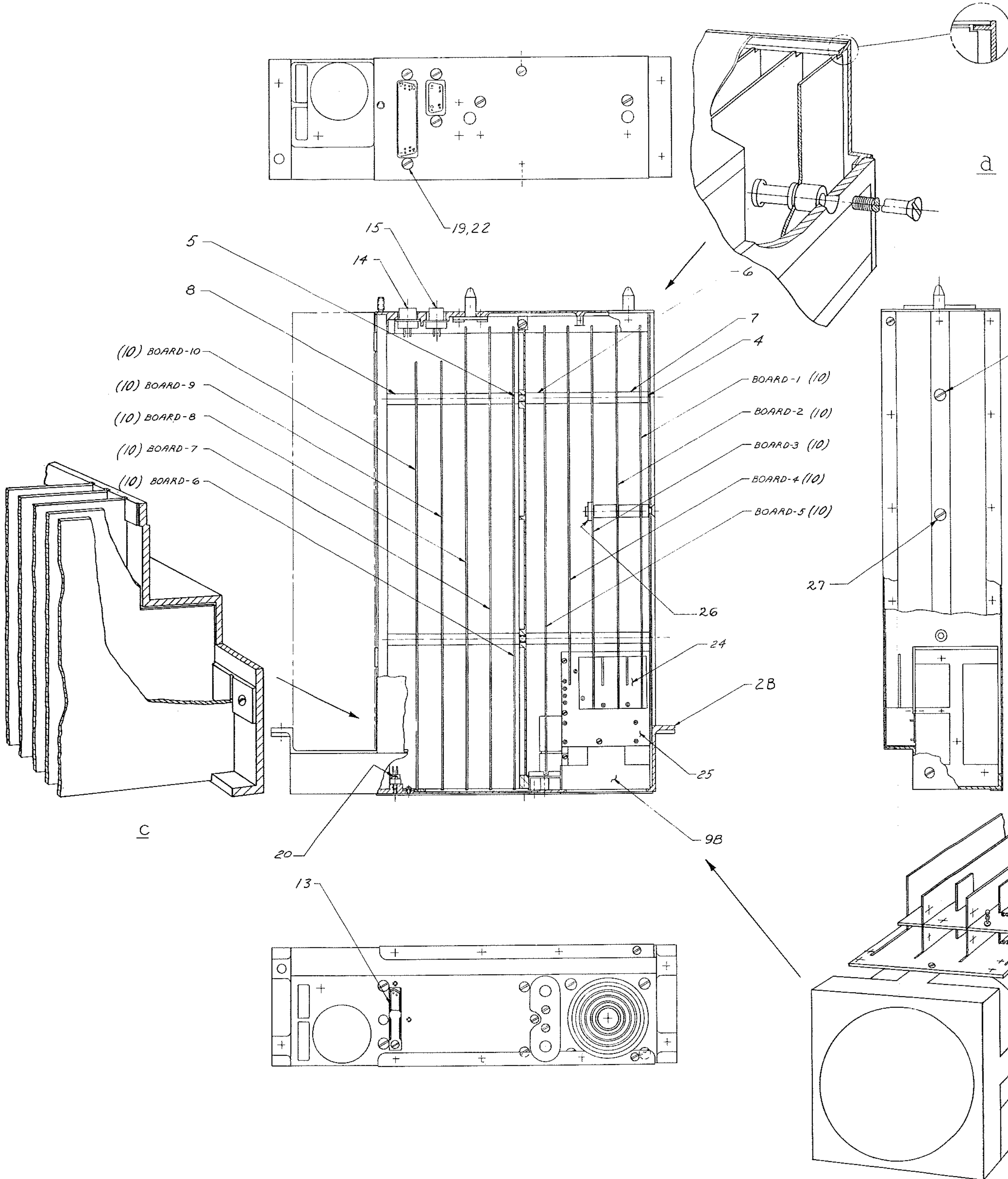

REQ	IDENTIFICATION NO.	DESCRIPTION	REF DESIG	NOTE	ITEM
1	B-619674	CENTER BOLT			27
1	B-619673	CENTER BOLT NUT			26
1		GROOVED CARD			25
1		GROOVED SHIELD			24
					23
4		NUT, HEX, .112-40, CORR. RES. STL.			22
					21
2		RHMS, 2-56 x 1/8 LG, CORR. RES. STL.			20
4		FHMS, 112-40 x .32 LG, CORR. RES. STL.			19
					18
					17
					16
1		RECPT, CAT. NO. DEM-9S		1	15
1		PLUG , CAT. NO. DBM-25P		1	14
1		PLUG , CAT. NO. MDB-37P		1	13
					12
					11
✓	B-616214	PRINTED CIRCUIT BOARDS 1 THRU 10			10
1	B-615214-3	DETECTOR MOUNT ASSY			9B
2	B-615777-3	SPACER			8
16	B-615777-2	"			7
2	B-615777-1	"			6
2	B-615776-2	"			5
2	B-615776-1	SPACER			4
2	B-614671-1	CIRCUIT BOARD SCREW			3
1	B-614632	MECHANICAL ASSY			2B
					1

Figure 4-4. Electronic Stack, Assembly Drawing

Page intentionally left blank

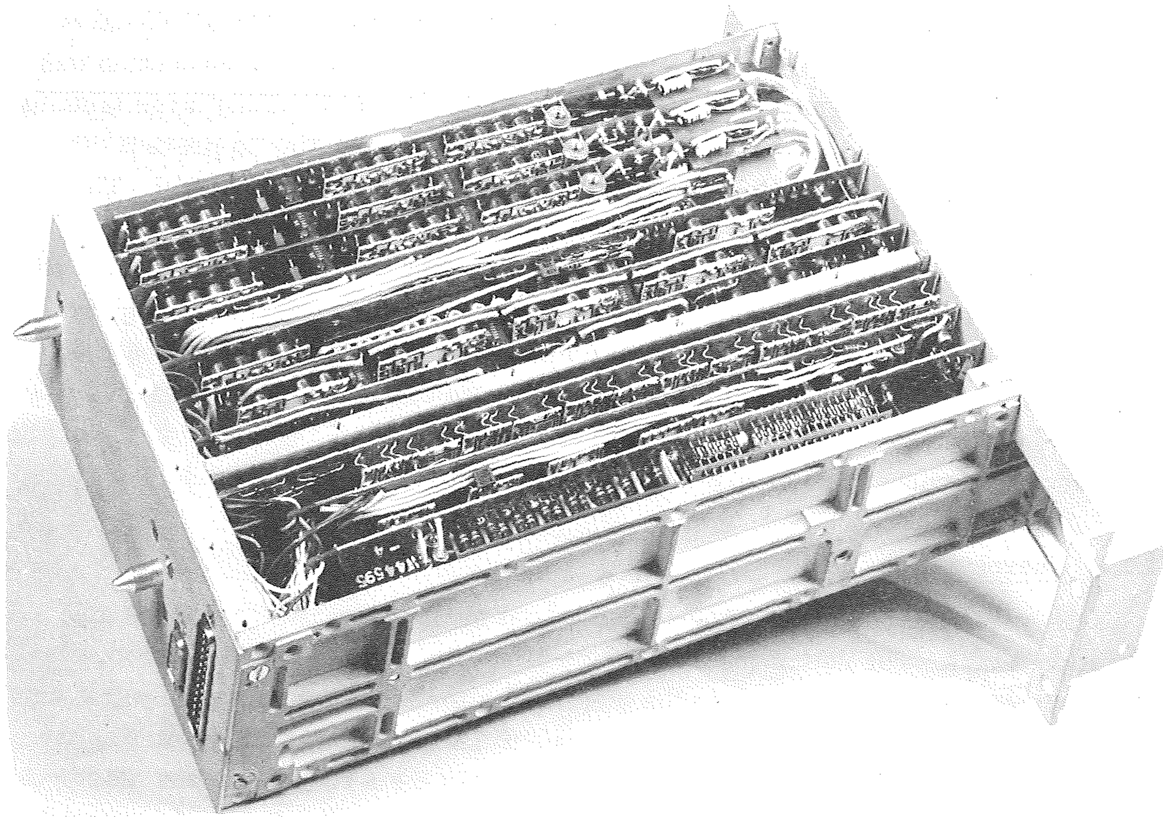

Figure 4-5. BTL Experiment Development Model

its forward portion to engage the front edges of motherboards 5 through 10 and restrict their lateral movement during vibration. This measure was required because of the greater distance between the nearest through-bolt and the front edges of these boards in this area of the stack. The rear ends of motherboards 8 and 10 were 0.57 inch shorter than the rest of the stack to allow additional space for wiring to the connectors mounted behind them on the back plate. The mechanical interface of boards 1 through 5 with the detector mount is described in Section 4.2.

Printed circuitry only appears on one side of each motherboard. On the opposite side, as much copper as possible has been retained for a ground plane. The ground plane was extended over the long edges of the boards by electroplating them with copper. When the completed stack was assembled in the housing, the ground planes on all boards were interconnected by beryllium copper finger-contact sheets

mounted under the covers. This is shown in Figure 4-7, a photograph of the package with the top cover removed. These contact sheets were electrically insulated from the covers and, together with the boards, formed a signal ground enclosure inside the chassis ground of the experiment housing. A capacitive connection was made between the two ground systems at the detector mount by using large tantalum and ceramic capacitors in parallel. There was no DC connection to prevent circulating currents which could disturb spacecraft spin and attitude control. The ground plane on each board was insulated with a bonded mylar sheet before mounting the components, as a measure of protection against the chance of short circuits to component leads occurring from the accidental inclusion of wire clippings or solder fragments. Interconnection between motherboards was made by soldered wiring to terminal lands printed along the rear edges as shown in photographs of the boards, Figures 4-8 through 4-17. These lands were also designed to mate with printed circuit connectors on a test stand described in Paragraph 6.3.4.

4.1.2 Encapsulation Technique

Polyurethane foam was chosen as the best encapsulant, in view of the high vibration levels. The use of foam in our earlier experiments had the serious disadvantage of restricting access to the electronics for troubleshooting, repairs, or modifications. Much of this hardship was due to the practice of encapsulating the entire electronic package along with the housing. In the ATS experiment, this problem was overcome by foaming the component side of each circuit board separately and leaving the printed circuit exposed for testing on the opposite side. By a procedure described in Paragraph 6.4.2, the height of the foam layer on each board was adjusted to 0.01 inch below the aluminum spacers that determine the separation between boards. Under compression in the stack, solder connections on the printed circuit side of each board were pressed into the foam on the next board. This resulted in a large area of contact between boards and greatly increased the mechanical integrity of the whole package.

All exposed wiring was encapsulated with a silicon rubber foam described in Section 6.6. This material remained flexible after cure and did not hamper access to boards which could be reached by fanning the stack apart. A completely encapsulated electronic stack is shown later in Figure 6-13.

4.2 ELECTRONIC STACK AND MOTHERBOARD LAYOUT

Layout of the motherboards was constrained by the following considerations: isolation of sensitive circuits, signal routing, packaging density, and reduction of interconnecting wiring. Interconnections were reduced by distributing mode control

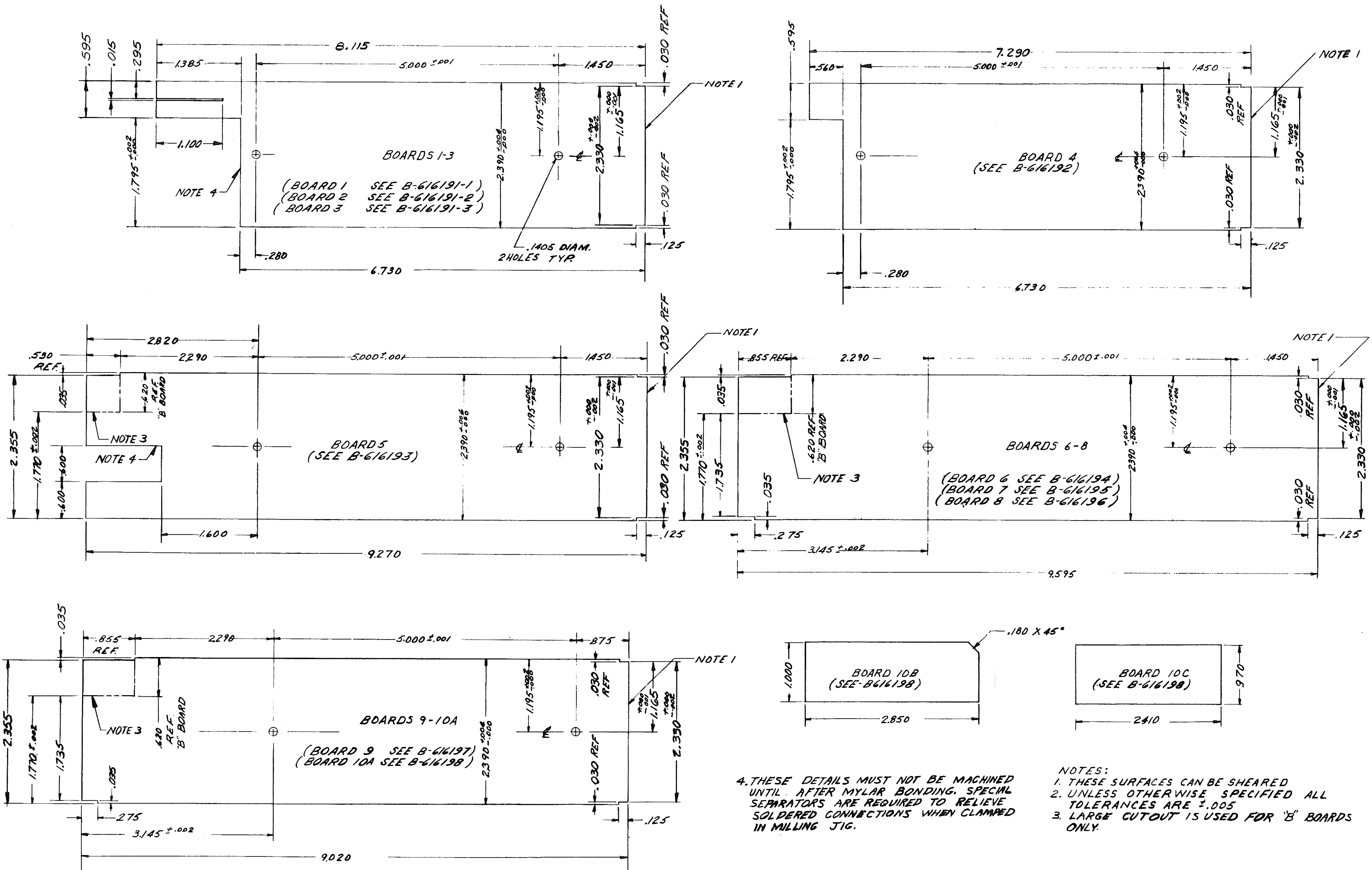

Figure 4-6. Motherboard Dimensions

Page intentionally left blank

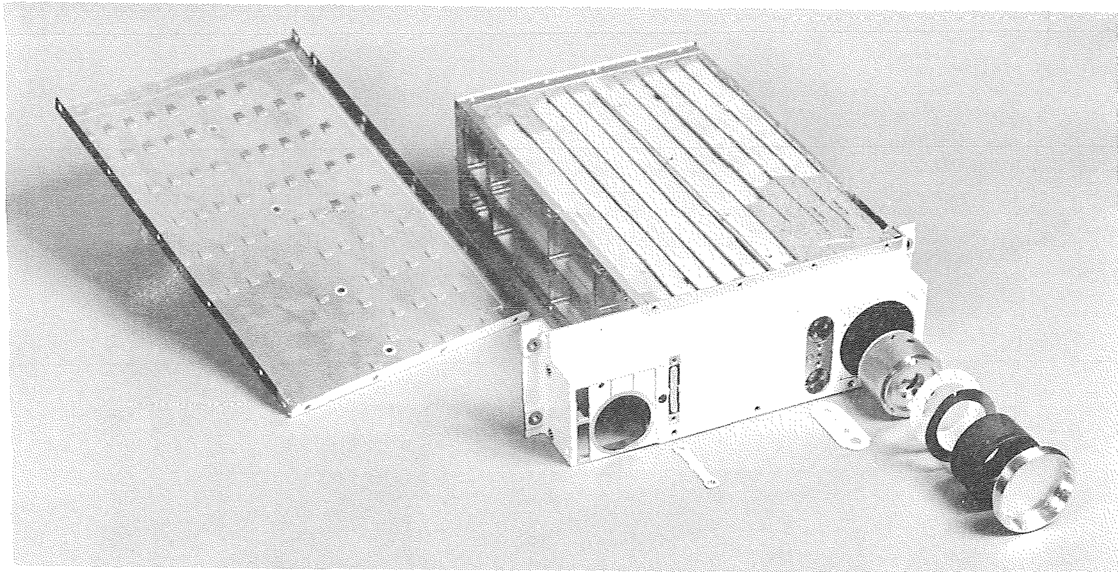

Figure 4-7. BTL Experiment Flight Model with Cover and Detector Details Removed

diode logic among the respective boards, rather than centralizing this function. Photographs of both sides of each motherboard are shown in Figures 4-8 through 4-17 and their respective circuit diagrams are shown in Figures 4-18 through 4-29.

The detector mount was located against the three inner surfaces of one front corner of the experiment housing for best mechanical support. Six linear amplifier channels, driven by the outputs of the detector telescope elements, were arranged in pairs on a group of three short printed circuit boards directly behind the detector mount. Each channel is laid out along an edge to reduce cross-coupling. Connections from the detector socket to the amplifier inputs are made as directly as possible by three groups of wires which enter the gaps between boards through an opening in the rear of the detector mount (Figure 6-12). This arrangement minimized cross-talk between the groups of detector outputs, reduced the lead length to the amplifier input terminals, and took advantage of the existing shielding between boards. An insulated concentric shield surrounding the detector cartridge within the mount and the shielded back cover plate (described in Paragraph 2.2.3) were both connected to the signal ground plane. This system prevented electrical noise on the experiment housing from coupling into the detector terminations.

Pulses from an internal calibration generator were injected into the amplifier channels in parallel with the detector inputs through small ceramic zero-temperature-coefficient coupling capacitors. The problem of shielding these sensitive inputs was

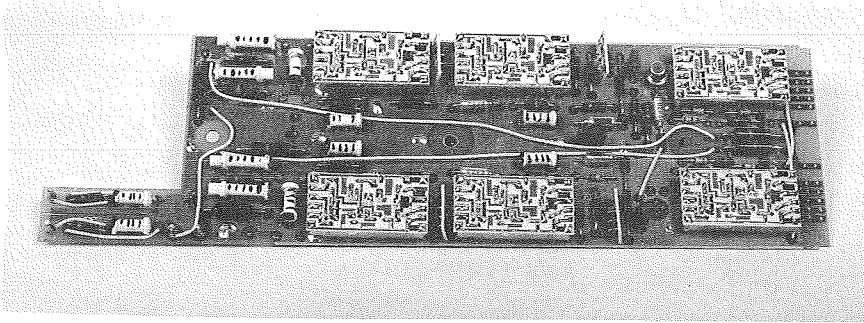

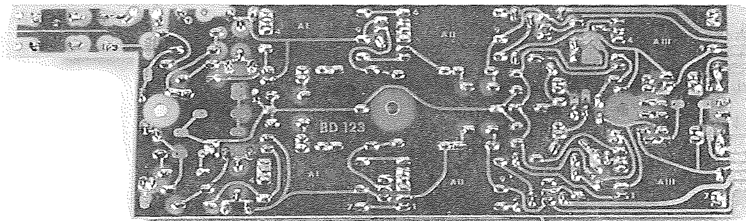

Figure 4-8. Motherboard 1

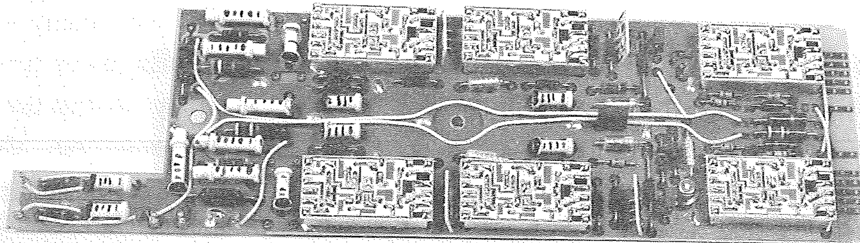

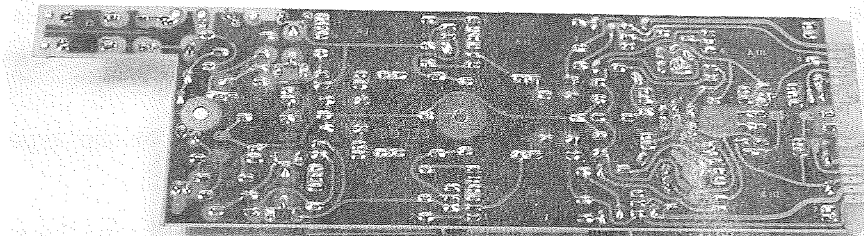

Figure 4-9. Motherboard 2

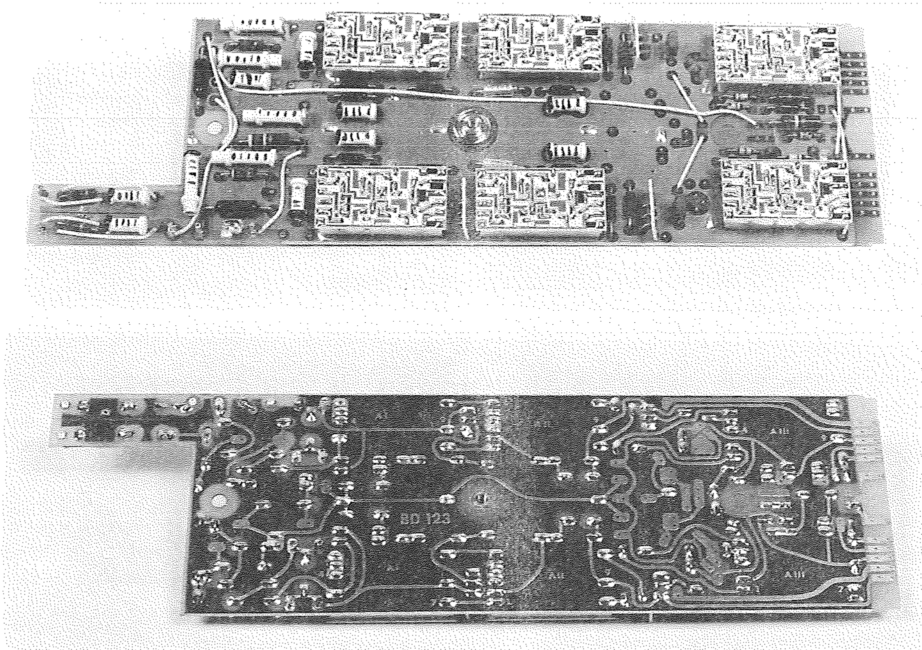

Figure 4-10. Motherboard 3

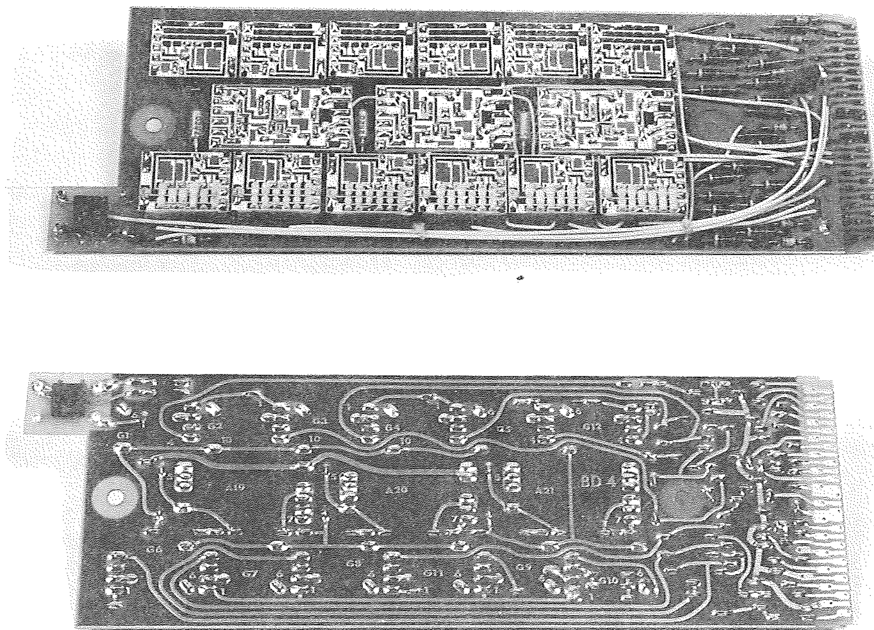

Figure 4-11. Motherboard 4

Figure 4-12. Motherboard 5

Figure 4-13. Motherboard 6

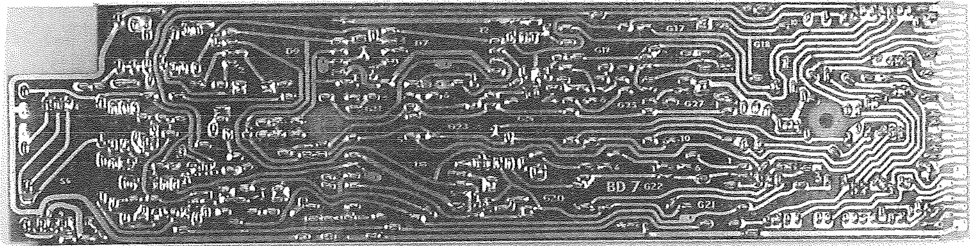

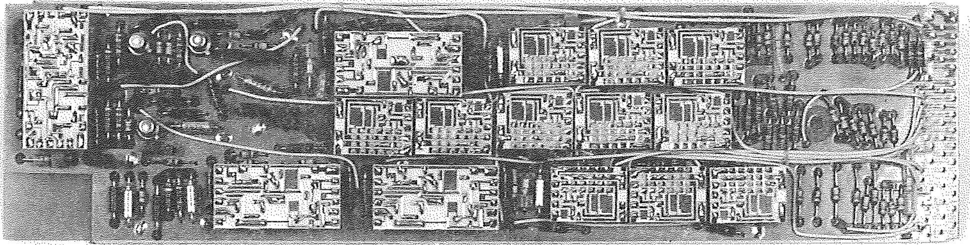

Figure 4-14. Motherboard 7

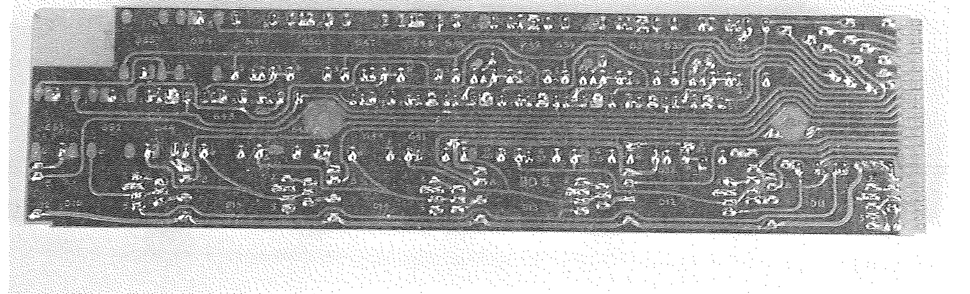

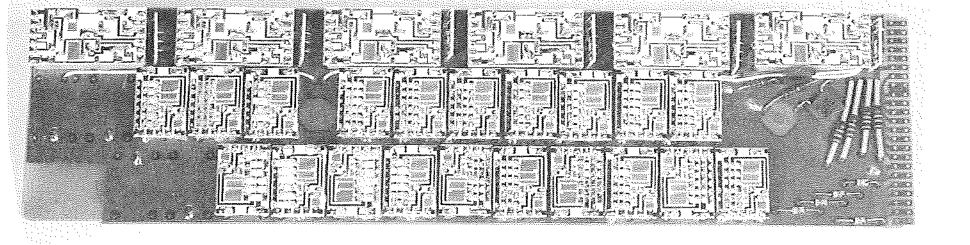

Figure 4-15. Motherboard 8

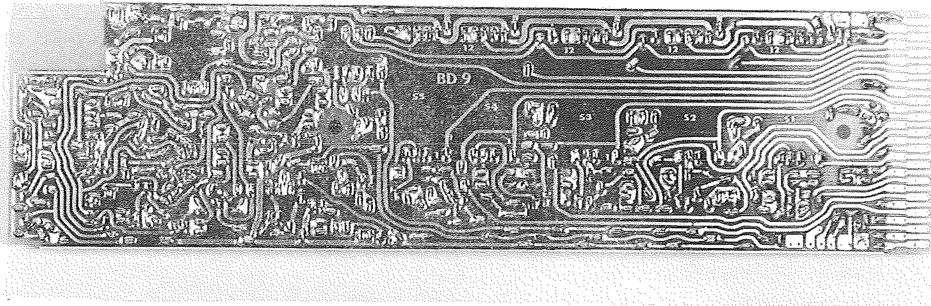

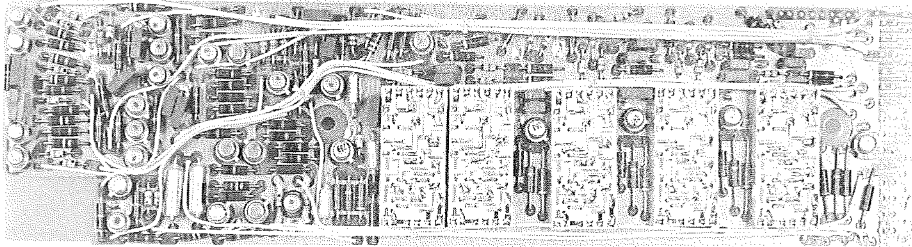

Figure 4-16. Motherboard 9

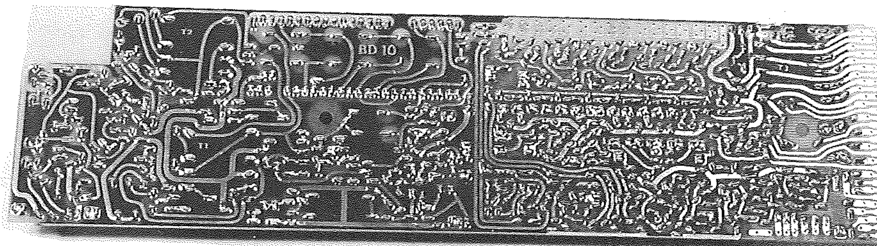

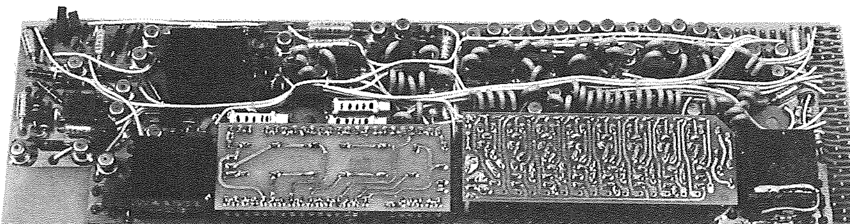

Figure 4-17. Motherboard 10

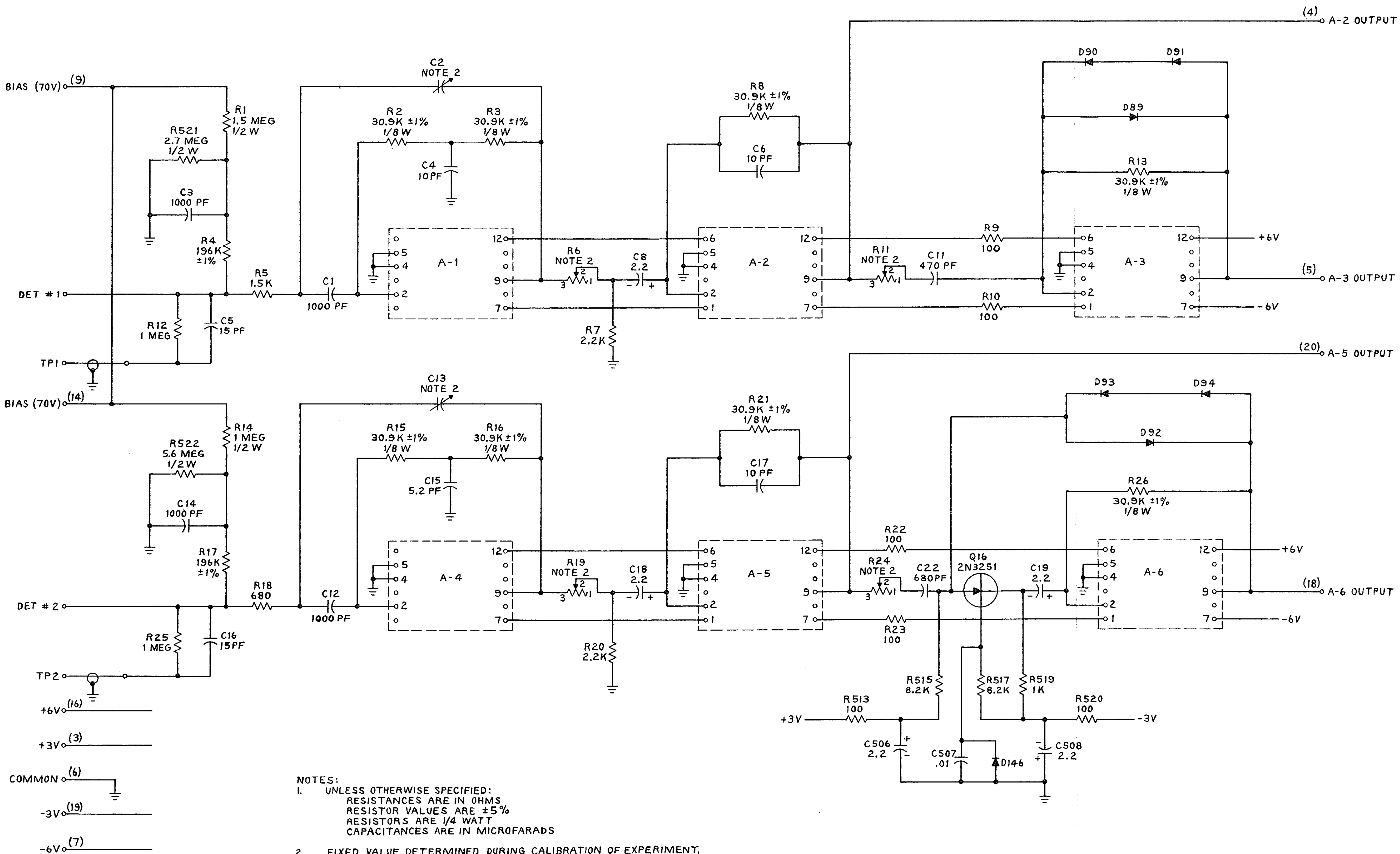

Figure 4-18. Motherboard 1, Schematic

Page intentionally left blank

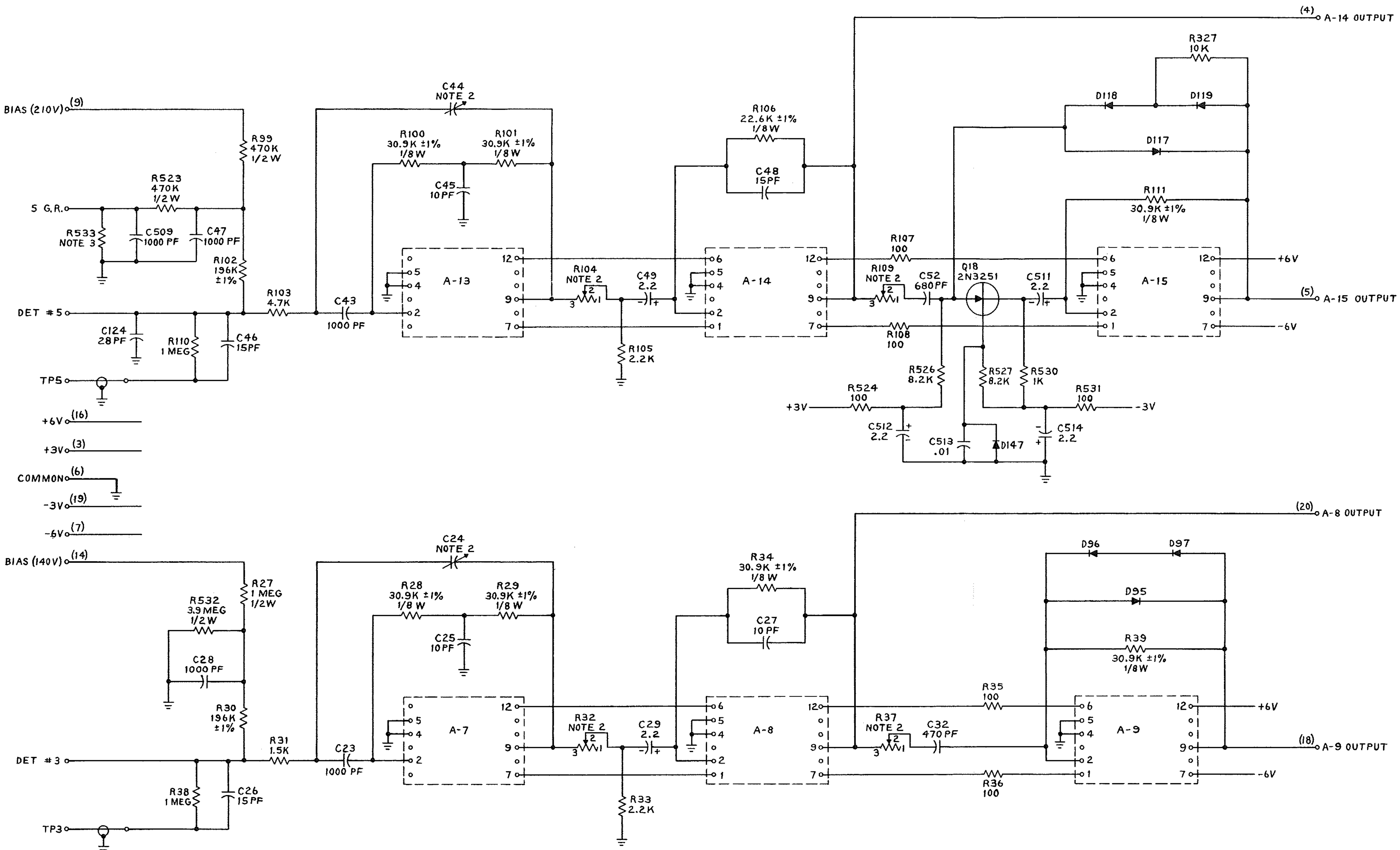

NOTES:
1. UNLESS OTHERWISE SPECIFIED:
   RESISTANCES ARE IN OHMS
   RESISTOR VALUES ARE ± 5%
   RESISTORS ARE 1/4 WATT
   CAPACITANCES ARE IN MICROFARADS
2. FIXED VALUE TO BE DETERMINED DURING CALIBRATION OF EXPERIMENT.
3. TENTATIVE COMPONENT. VALUE, IF USED, DETERMINED AS DESCRIBED IN NOTE 2.
4. SEE PARTS LIST FOR MOTHER BOARD 2 OF ATS.

Figure 4-19. Motherboard 2, Schematic

Page intentionally left blank

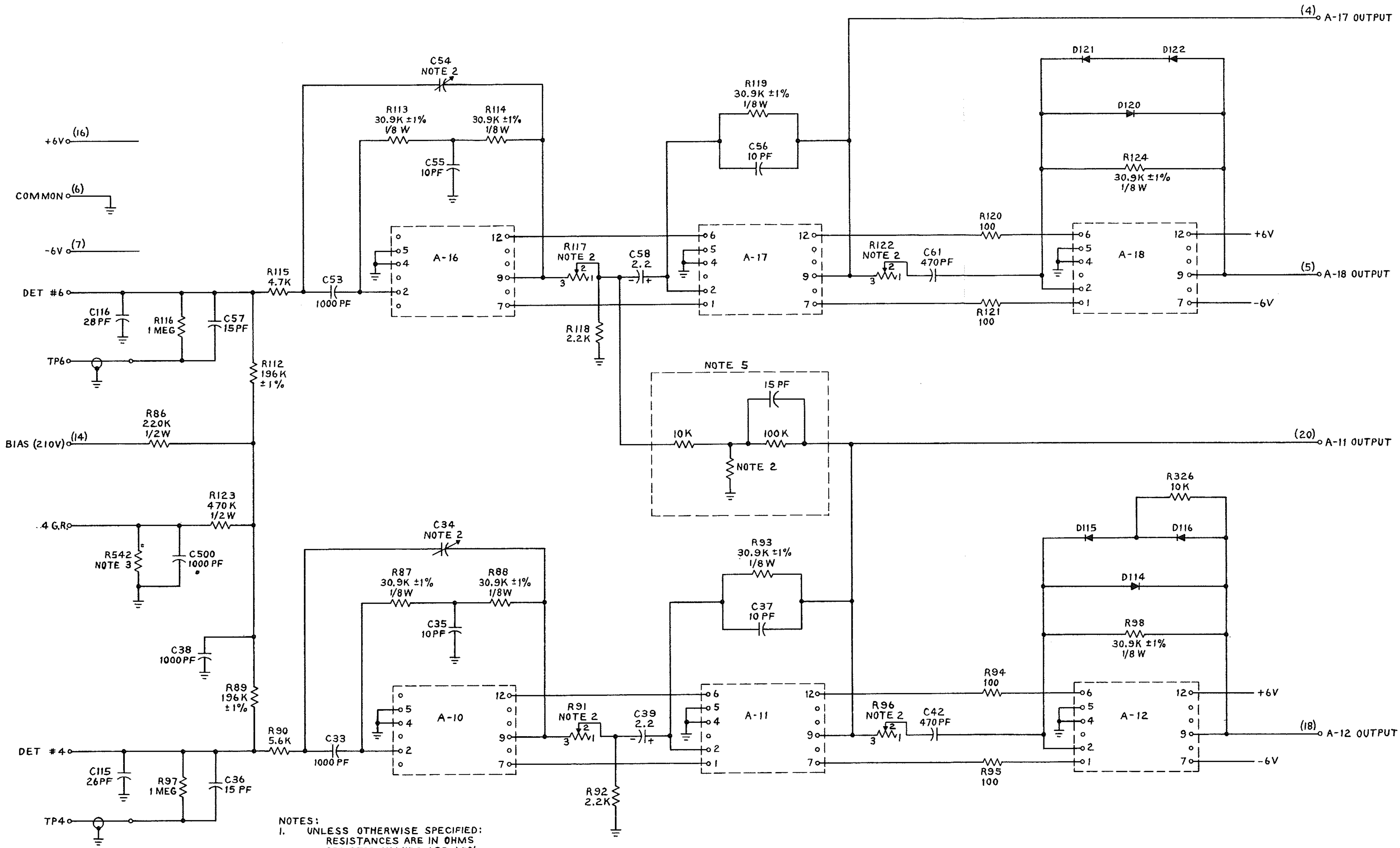

NOTES:
1. UNLESS OTHERWISE SPECIFIED:
RESISTANCES ARE IN OHMS
RESISTOR VALUES ARE ±5%
RESISTORS ARE 1/4 WATT
CAPACITANCES ARE IN MICROFARADS
2. FIXED VALUE DETERMINED DURING CALIBRATION OF EXPERIMENT.
3. TENTATIVE COMPONENT. VALUE, IF USED, DETERMINED AS DESCRIBED IN NOTE 2.
4. SEE PARTS LIST FOR MOTHER BOARD 3 OF ATS.
5. THESE COMPONENTS MAY NOT BE INSTALLED IN SYSTEM. LATER MODELS WILL HAVE THEM.

Figure 4-20. Motherboard 3, Schematic

Page intentionally left blank

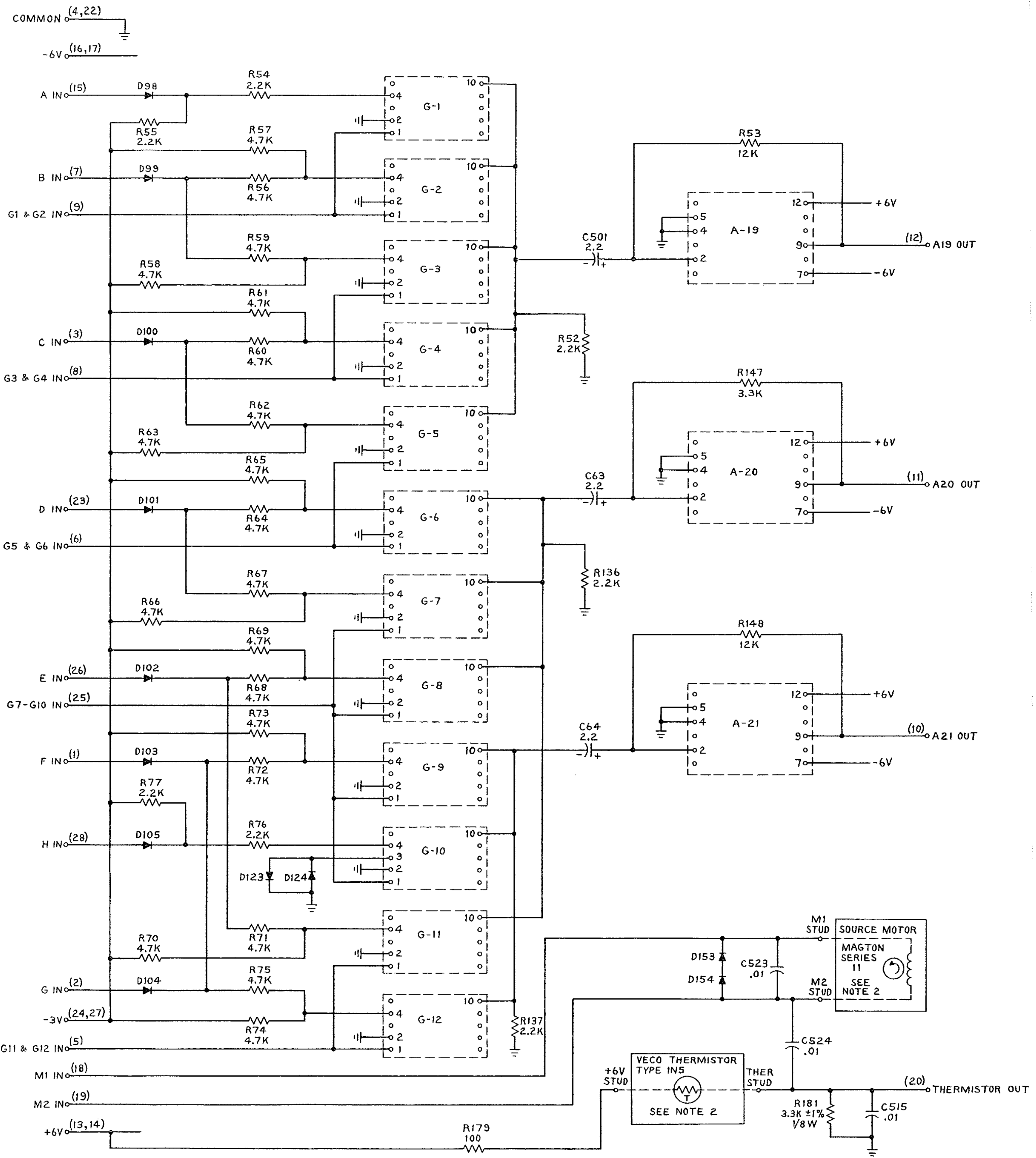

NOTES:
1. UNLESS OTHERWISE SPECIFIED:
   RESISTANCES ARE IN OHMS
   RESISTOR VALUES ARE ±5%
   RESISTORS ARE 1/4 WATT
   CAPACITANCES ARE IN MICROFARADS
2. THE THERMISTOR AND THE SOURCE MOTOR MOUNT ON THE DETECTOR BLOCK. BOTH ARE CONNECTED BY WIRE TO STUDS ON THE FRONT OF MOTHER BOARD 4.
3. SEE PARTS LIST FOR MOTHER BOARD 4 OF ATS.

Figure 4-21. Motherboard 4, Schematic

Page intentionally left blank

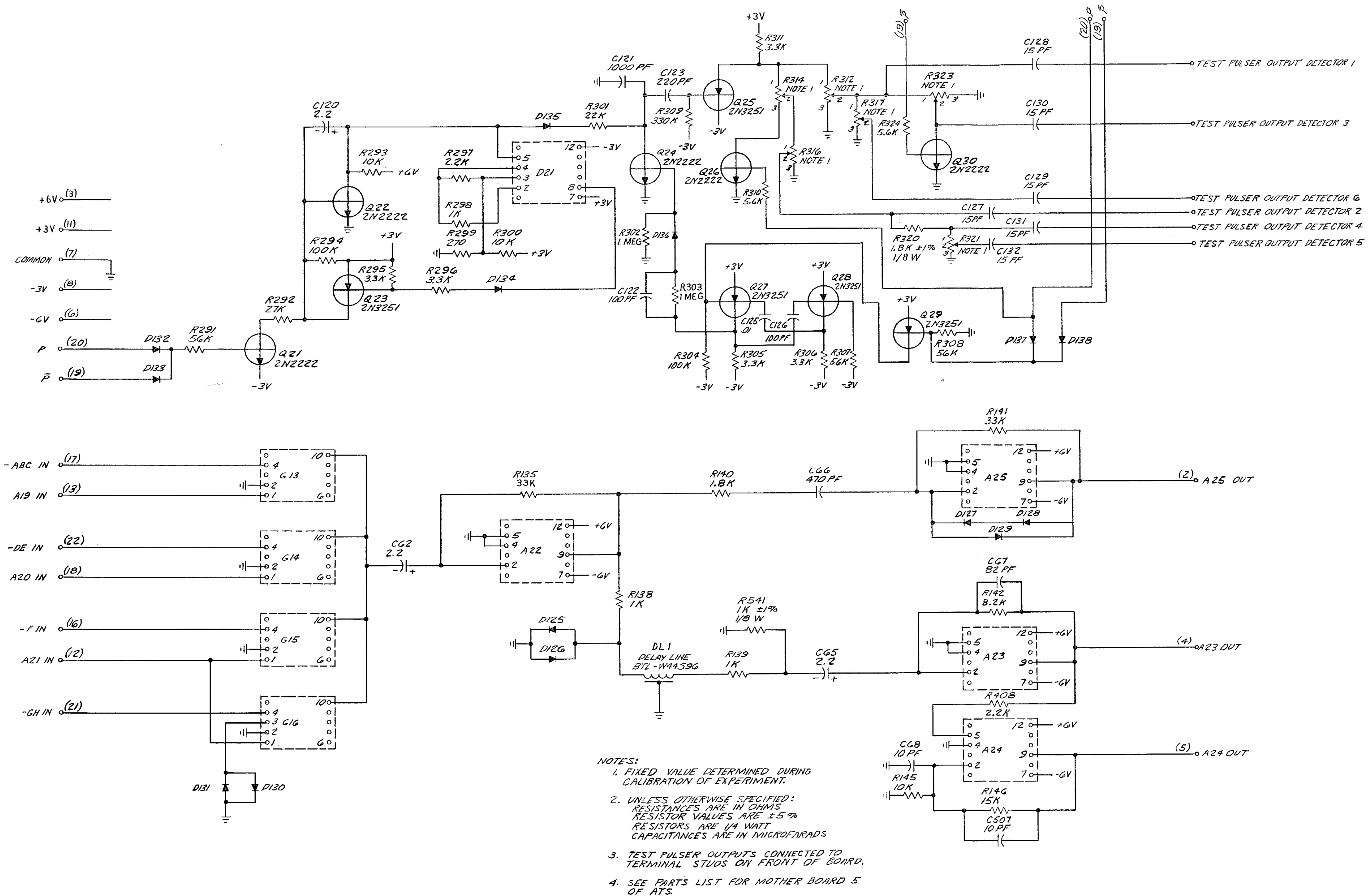

Figure 4-22. Motherboard 5, Schematic

Page intentionally left blank

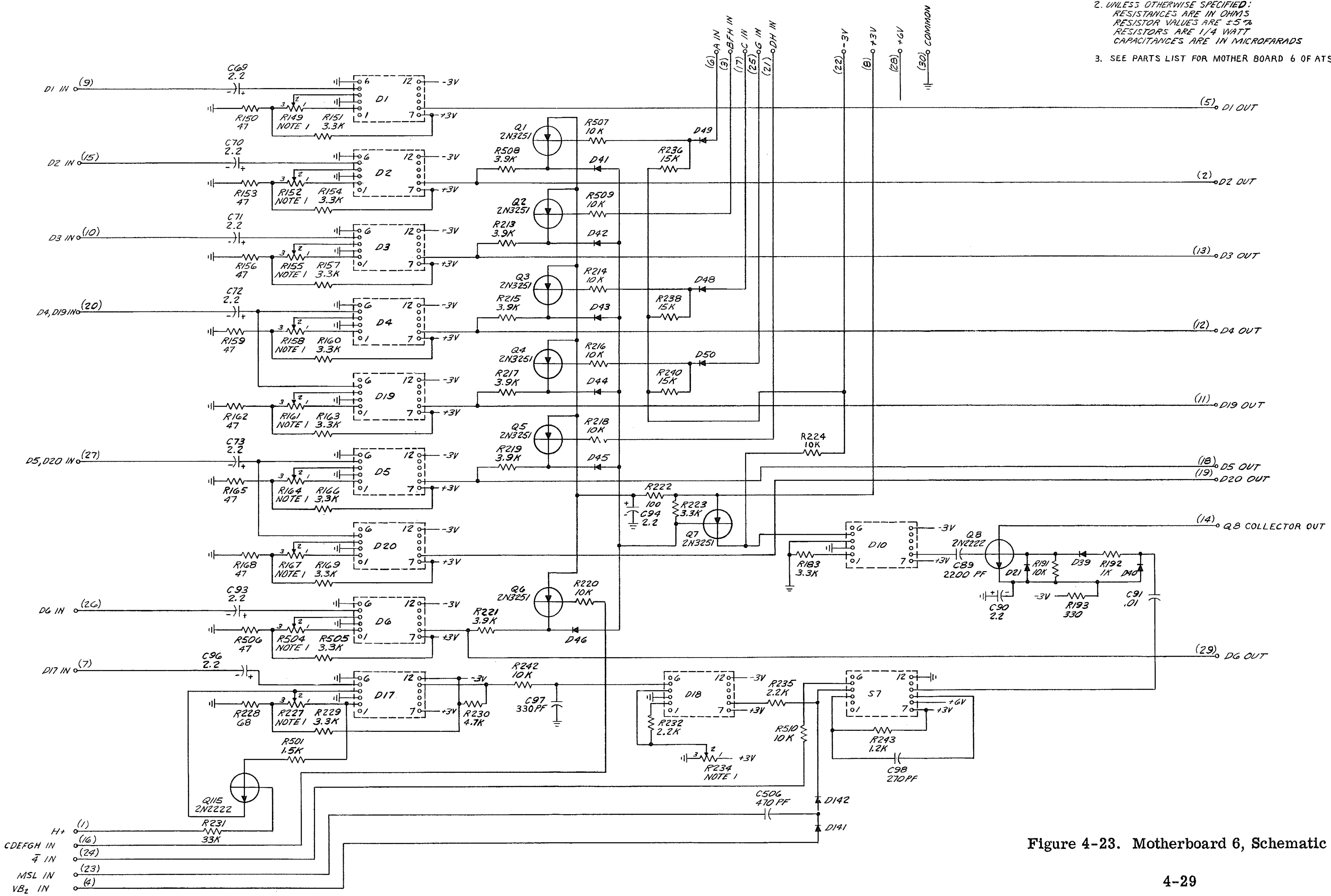

Figure 4-23. Motherboard 6, Schematic

Page intentionally left blank

NOTES:
1. TD 1,2,3 AND 4 TO HAVE SHIELDING BEAD, FERROXCUBE K500100/3B, ON LEAD
2. UNLESS OTHERWISE SPECIFIED: RESISTANCES ARE IN OHMS RESISTOR VALUES ARE ±5% RESISTORS ARE 1/4 WATT CAPACITANCES ARE IN MICROFARADS
3. TENTATIVE COMPONENT VALUE, IF USED. DETERMINED DURING CALIBRATION OF EXPERIMENT.
4. SEE PARTS LIST FOR MOTHER BOARD 7 OF ATS.

Figure 4-24. Motherboard 7, Schematic

Page intentionally left blank

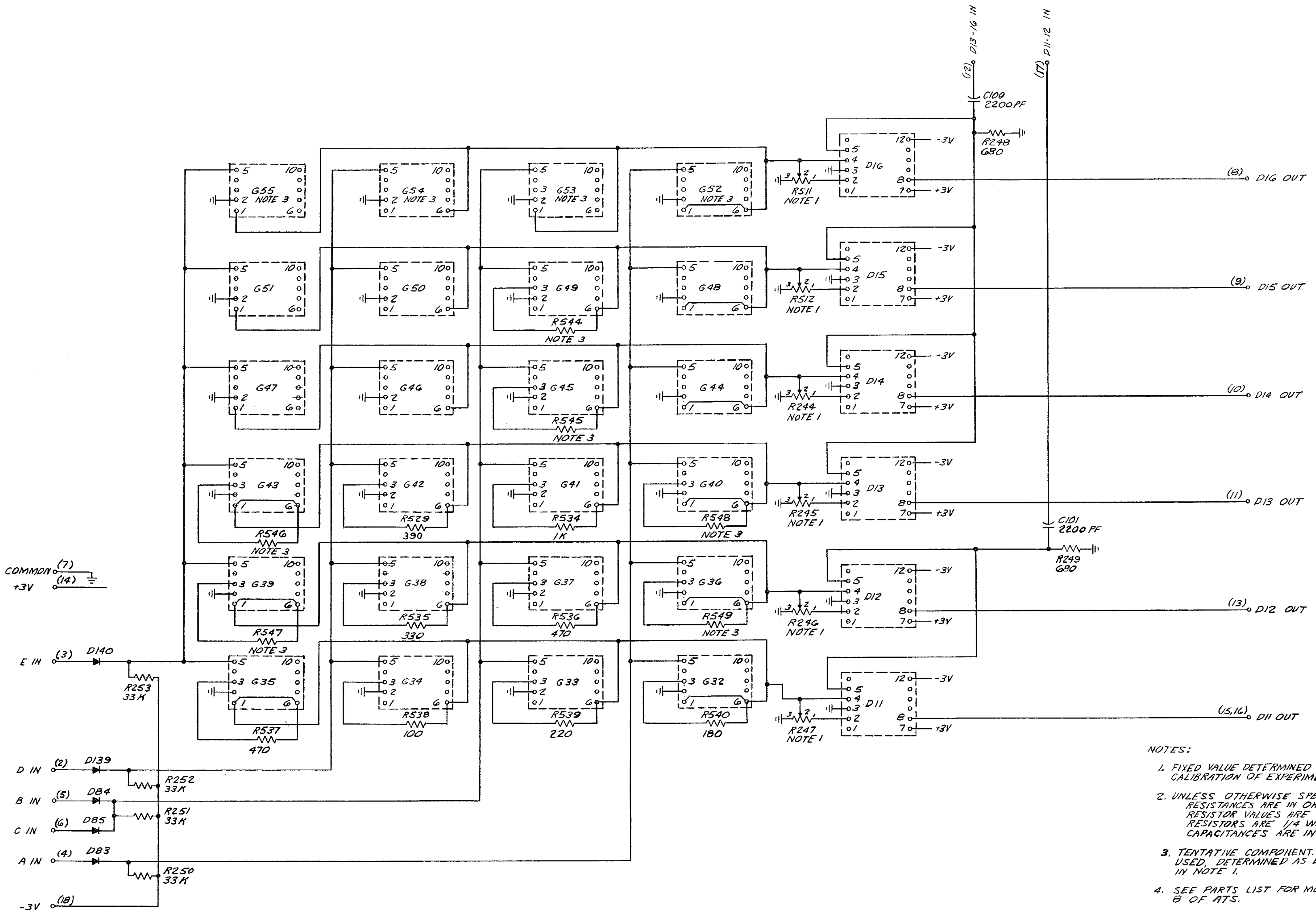

NOTES:

1. FIXED VALUE DETERMINED DURING CALIBRATION OF EXPERIMENT.
2. UNLESS OTHERWISE SPECIFIED:
   RESISTANCES ARE IN OHMS
   RESISTOR VALUES ARE ±5%
   RESISTORS ARE 1/4 WATT
   CAPACITANCES ARE IN MICROFARADS
3. TENTATIVE COMPONENT. VALUE, IF USED, DETERMINED AS DESCRIBED IN NOTE 1.
4. SEE PARTS LIST FOR MOTHER BOARD 8 OF ATS.

Figure 4-25. Motherboard 8, Schematic

Page intentionally left blank

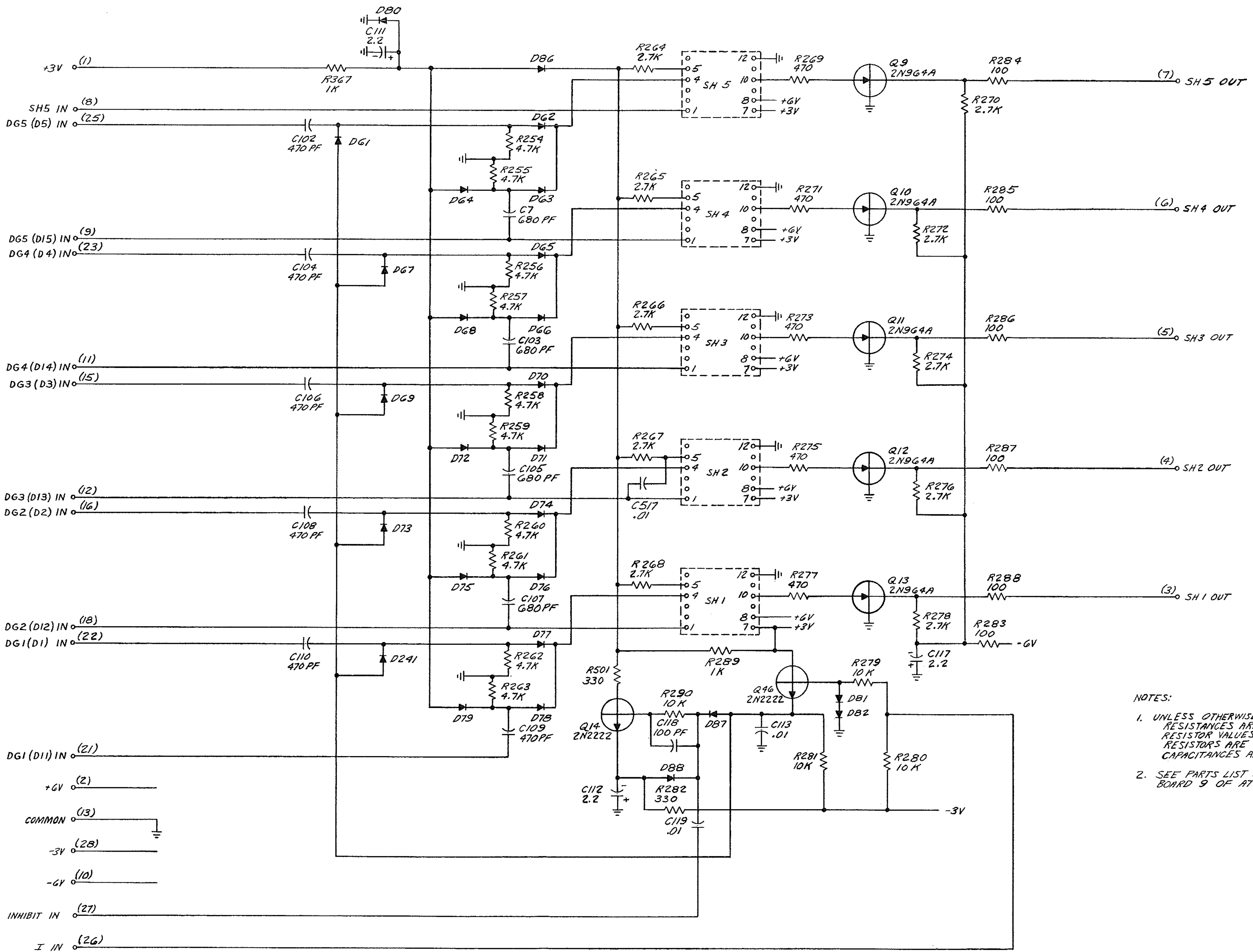

Figure 4-26. Motherboard 9, Schematic (Sheet 1 of 2)

Page intentionally left blank

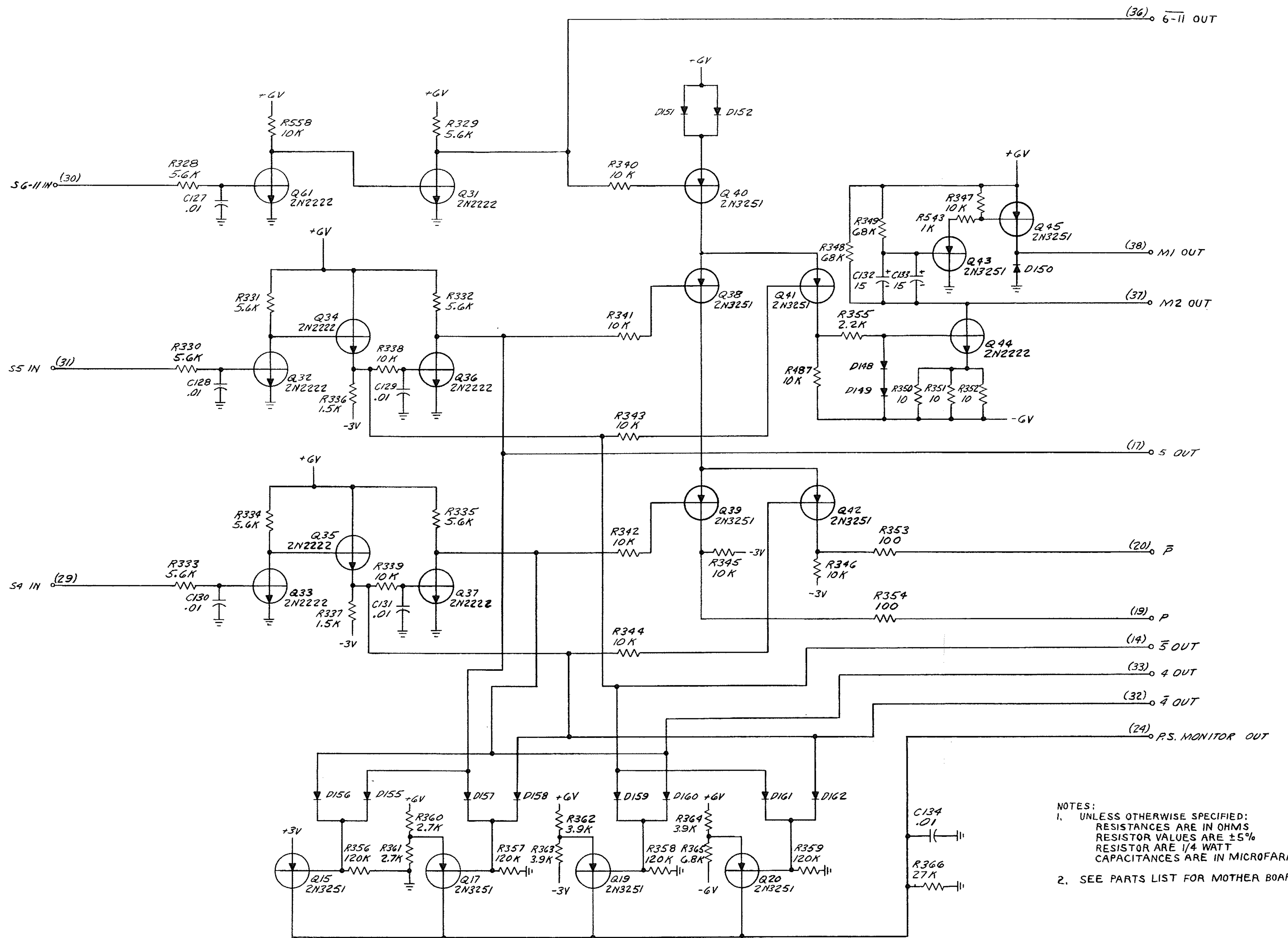

NOTES:

1. UNLESS OTHERWISE SPECIFIED:
   RESISTANCES ARE IN OHMS
   RESISTOR VALUES ARE ±5%
   RESISTOR ARE 1/4 WATT
   CAPACITANCES ARE IN MICROFARADS
2. SEE PARTS LIST FOR MOTHER BOARD 9 OF ATS.

Figure 4-27. Motherboard 9, Schematic (Sheet 2 of 2)

Page intentionally left blank

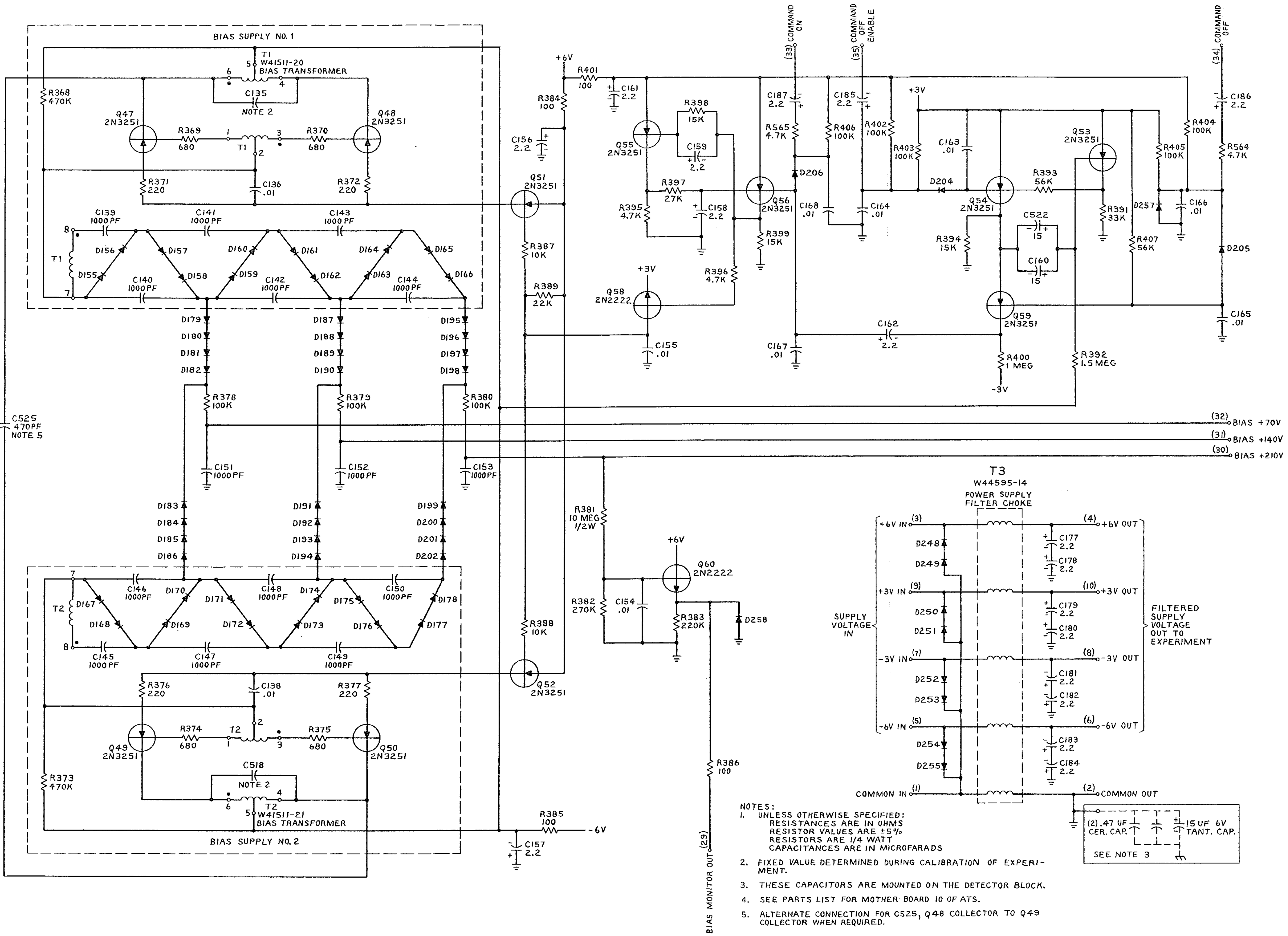

Figure 4-28. Motherboard 10, Schematic (Sheet 1 of 2)

Page intentionally left blank

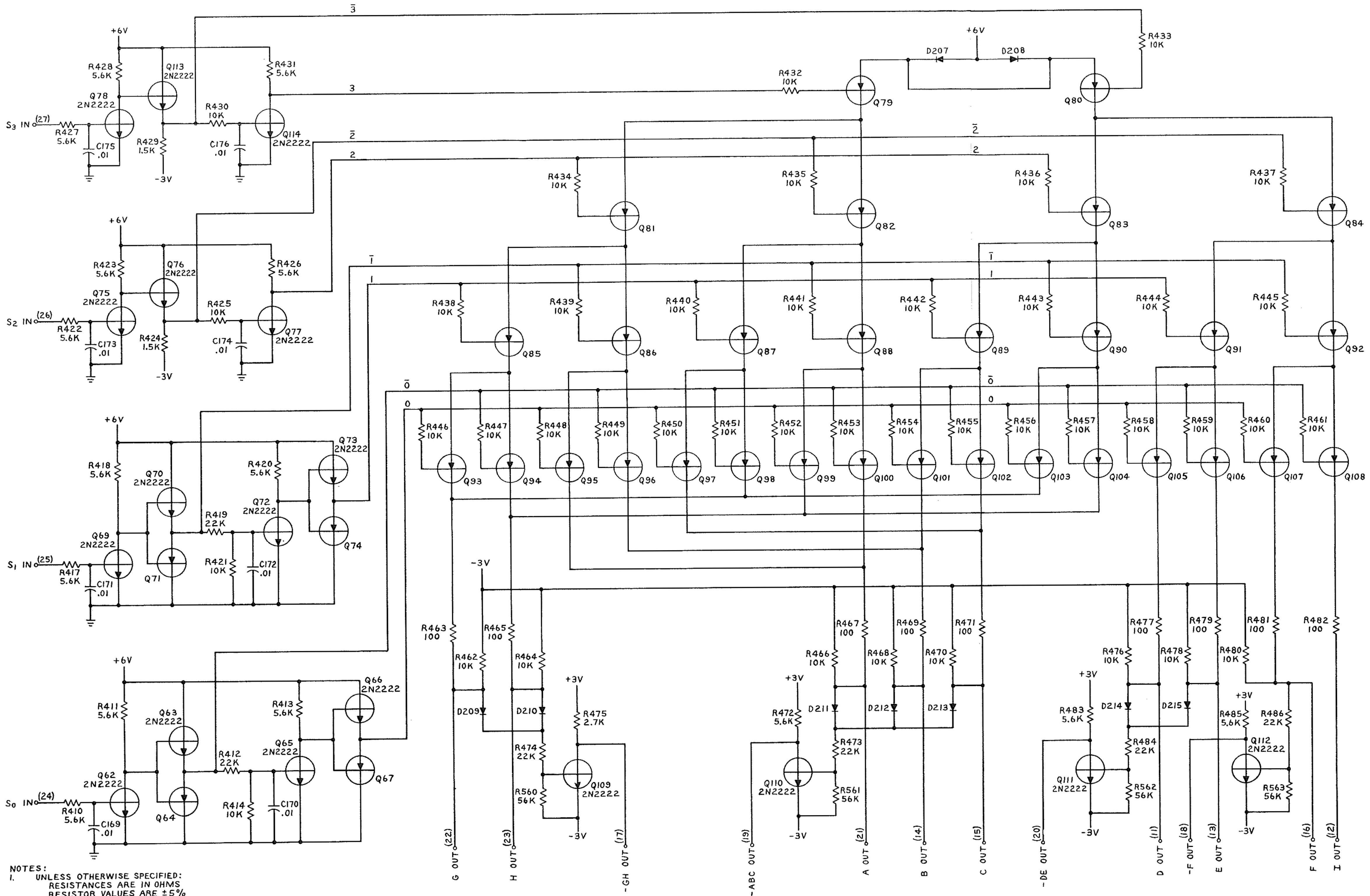

NOTES:
1. UNLESS OTHERWISE SPECIFIED:
   RESISTANCES ARE IN OHMS
   RESISTOR VALUES ARE ±5%
   RESISTORS ARE 1/4 WATT
   CAPACITANCES ARE IN MICROFARADS
   TRANSISTORS ARE 2N3251
2. SEE PARTS LIST FOR MOTHER BOARD 10 OF ATS.

Figure 4-29. Motherboard 10, Schematic (Sheet 2 of 2)

Page intentionally left blank

solved by extending tabs from board 1-3, as shown in the photographs, into the space between the top of the detector block and the cover. A slot was machined down the centers of these tabs for insertion of a similarly slotted interlocking shielding partition. This formed a shielded "egg crate" structure with six compartments, each containing a test pulse coupling network. Two additional vertical shielding baffles were added to the partition between the boards to further isolate the coupling capacitors from the printed circuit on the opposite board. A sketch of this arrangement is shown in Figure 4-4B. Terminal studs on the front end of the tabs and partition terminate the high-level test pulse inputs well away from the detector leads. Small coaxial cables connect these terminals to the test pulse generator at the front of motherboard 5 and to six miniature coaxial test jacks accessible from the front panel for input from external pulse generators. This test jack assembly was mechanically integrated with the detector mount and the front of board 5 so as to support it against the insertion forces of the mating connector, whether the electronic stack was in or out of the housing. The test jacks were divided into two groups of three to fit above and below an internal radioactive calibration source mechanism described in Section 2.2.

Motherboard 4, Figure 4-11, contains linear control gates and output amplifiers driven by the six channels on boards 1-3. Crosstalk between the input and output lines was reduced by running many of the input lines as printed circuit paths and the outputs as wires on the opposite side of the ground plane. Gates and amplifiers were oriented for minimum capacitive coupling. Mode control network components can be seen at the rear of the board. Terminal studs on a short tab at the front of the board are to connect the source motor power input and thermistor output leads to the harness terminals at the rear of the board.

The delay line, approximately in the center of board 5 in Figure 4-12, is the largest electronic component in the package. It is surrounded by its associated thin-film linear amplifiers and gates. The front one-third of this board contains the calibration pulse generator. Thin-film resistor networks, which can be seen throughout this part of the circuit in the photograph, determine the calibration pulse output amplitudes.

The complete linear system contained on boards 1-5 is separated from the pulse generating circuits comprising the remaining half of the stack by a structural metal partition in the center of the housing.

The entire coincidence system is contained on motherboards 6 and 7. A group of nine coincidence discriminators (D1-D6, D10, D19, and D20) and two others (D17 and D18) in the pile-up rejector circuit, shown in the block diagram (Figure 4-1), were laid out along the upper and lower edges of motherboard 6, shown in Figure 4-13. This configuration was necessary to place their respective level-setting

trimpots in a convenient position for adjustment during trimming operations with the board mounted in the stack. In the photograph, these have been replaced by thin-film resistor networks. Anticoincidence circuit transistors and associated components comprise the central portion of the board. Motherboard 7, shown in Figure 4-14, contains the thin-film coincidence gates, timing discriminators (D7-D9), and the five-channel analyzer gating shaper (SH6).

The five-channel pulse height analyzer discriminators and associated threshold switching gates occupy all of motherboard 8, Figure 4-15. Here, as on board 6, the discriminators are placed along the edge to facilitate trimming. Vacant spaces at the front of this board were originally for four additional gates which were deleted from the system after the layout had been completed.

The output pulse shapers and line drivers are located on the rear half of motherboard 9, Figure 4-16, directly in front of the output connector. This location reduces their output lead length inside the package since these circuits necessarily produce large current pulses. Circuits for supply voltage monitoring and actuation of the internal testing devices are located at the front of motherboard 9, along with the necessary logic for programming these events.

Motherboard 10 is unique because it contains the largest number of parts (approximately 350) and no thin-film circuits, Figure 4-17. Commandable, redundant oscillator-type bias supplies and voltage multipliers are contained on the front half of the board as far away as possible from the low-level linear system. These supplies were designed to operate above 100 kHz so as to reduce the size and weight of their components. This made possible the use of miniature 1000-pf ceramic filter capacitors and small ferrite toroidal core transformers (the two prepotted cubes at the front of the board in the photograph). Behind the bias supplies are the complete transistor mode logic "tree" and mode line driving circuits for programming the experiment. Component density was increased by packaging these items and the bias voltage multiplier as cordwood modules. The additional clearance for this arrangement was available because the minimum height in which the bias transformers could be packaged exceeded the normal board spacing used elsewhere in the stack. A five-winding noise rejection transformer externally similar to the bias transformers can also be seen in the photograph near the rear terminals. This, together with suitable filter capacitors, provides protection against external interference on all power supply lines entering the experiment.

All power inputs and timing signals enter the package through a 25-pin Cannon connector on the back plate behind motherboard 10. A miniature 37-pin connector, alongside board 10 and accessible from the front plate, is wired to many test points within the system.

4.3 MECHANICAL DESIGN

Figures 4-30 and 4-31 show, respectively, front and rear views of the fully assembled BTL experiment.

The complete package weighed 4.4 pounds and was housed in a 144-cubic-inch gold-plated magnesium enclosure 10.020 inches long, 5.750 inches wide, and 2.50 inches high. The vacancy at one side of the front plate was to accommodate the Rice University experiment on ATS-B. This volume was occupied by the BTL VLF experiment on ATS-A.

4.3.1 Mechanical Interface with the EME

Figure 4-3 shows a sketch of the EME housing, its monitoring arrangement in the spacecraft, and the location of the BTL experiment. At the beginning of the project, a request was made for our experiment to be mounted in a manner that would permit easy removal from the assembled spacecraft. The ensuing design of the EME housing was based on this feature so that its advantages were also extended to other experimenters. Ironically, at the end of the project the BTL and Rice University experiments were the only ones not removable without major disassembly of the spacecraft, due to a subsequent design change in the upper solar panels. The EME housing can best be described as similar to a vertical file cabinet; the experiments were slid into position like drawers along guide rails attached to its interior walls. This structure is mounted against the central thrust tube of the spacecraft and extends radially out to the inner surface of the solar cell panels. Large aluminum pins on the experiment back plate (shown in Figure 4-31) engage holes in the EME rear wall to bring the connectors into mating alignment and to support the back of the package. The front flanges of the experiment were attached to the EME housing with four 6-32 cap screws. Before tightening these, shims were used to adjust the gap behind the flanges to less than 0.003 inch. The screws were torqued to produce a 300-pound preload against the back plate to prevent hammering during vibration. As an extra precaution, a captive back plate locking screw was provided in the right side of the BTL housing (visible in Figure 4-31). It could be operated from outside the front panel with a special extension wrench. In its secured position, the package is lifted away from the EME guide rails so that its main areas of support are the front flanges and rear plate.

4.3.2 Thermal Control

Figure 4-32 is a copy of the Westinghouse BTL/EME interface drawing, showing critical exterior dimensions and tolerances. Stringent flatness requirements shown for the back plate were intended to ensure good mechanical contact with the

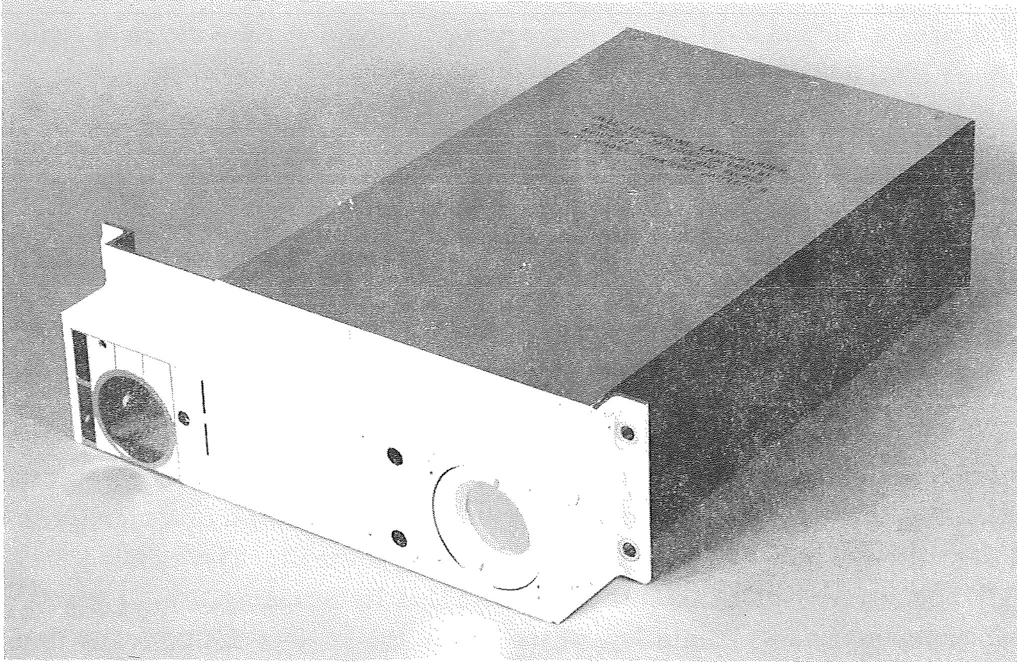

Figure 4-30. BTL Experiment Flight Model, Front View

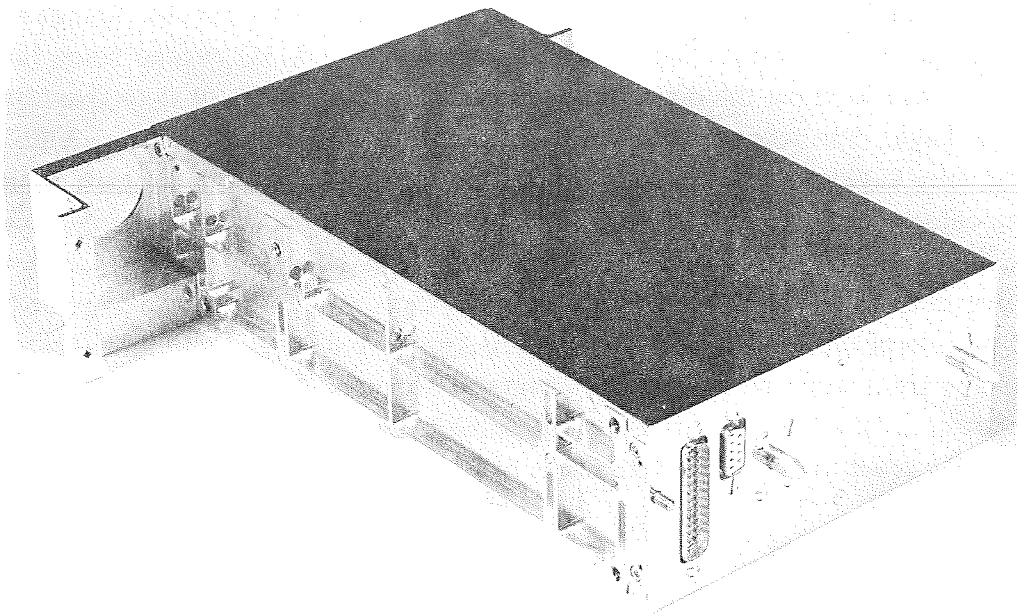

Figure 4-31. BTL Experiment Flight Model, Rear View

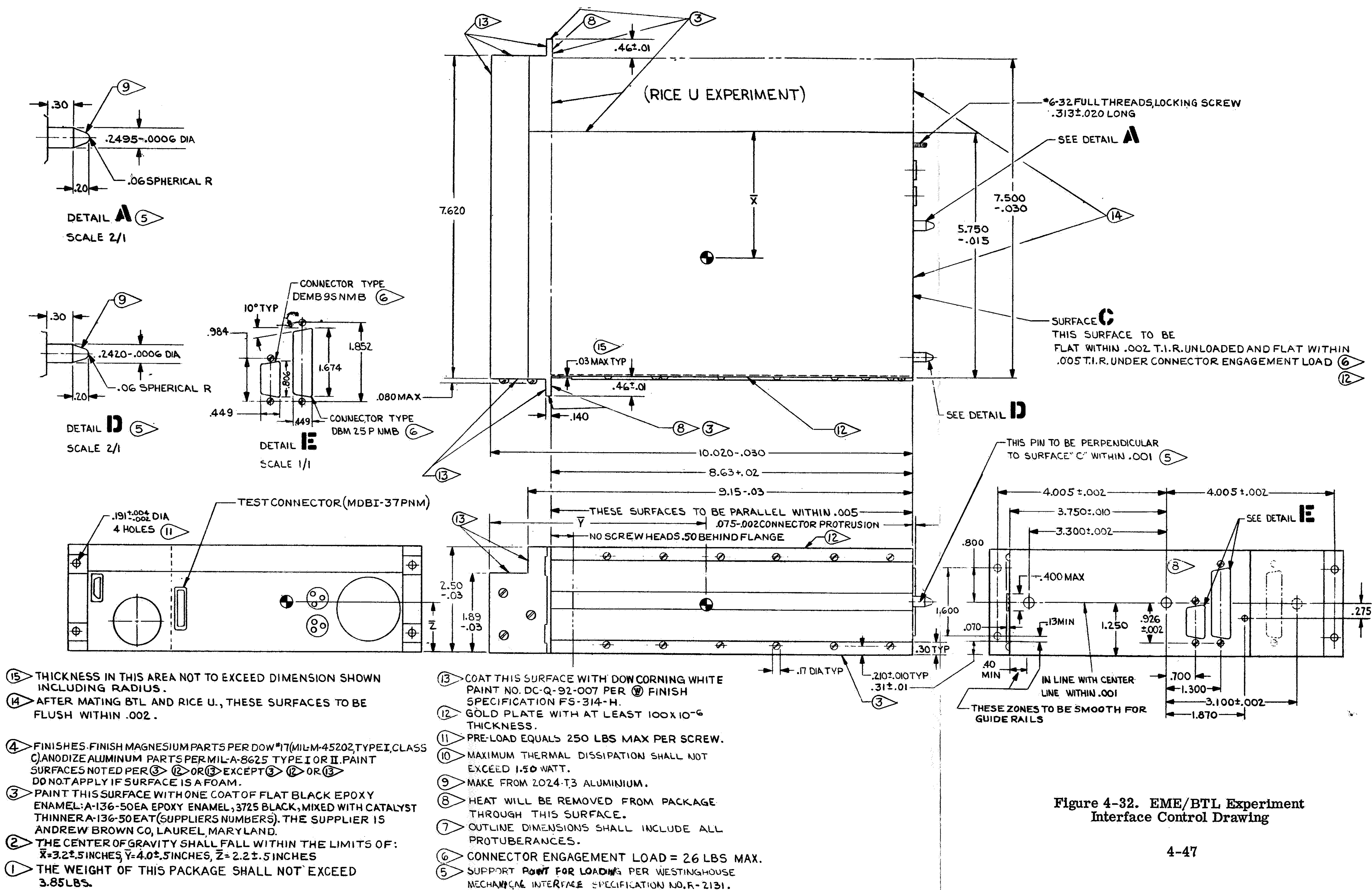

Figure 4-32. EME/BTL Experiment Interface Control Drawing

Page intentionally left blank

EME rear wall for thermal control of the experiment. Subsequent spacecraft thermal problems, indicating a higher rear-wall temperature than expected, and our need to keep the detector cool necessitated decoupling our back plate from the EME. This was accomplished with 0.005-inch-thick mylar spacers in the four rear corners. Independent thermal control of the experiment was achieved by modifying the emissivities of its surfaces. The front plate was painted with a special white paint with a low α/ϵ ratio (where α is the average absorption coefficient for the solar spectrum and ϵ is the emissivity in the infrared spectrum). The pattern in the paint around the Rice University experiment detector opening, shown on the left in Figure 4-30, was to reduce possible electric field disturbance in this area. On surfaces within the spacecraft obscured from sunlight, long wavelength infrared radiation was the main heat source. The top cover and back plate were polished gold to reflect radiation from hotter surfaces above and to the rear of the experiment. The bottom cover and the left side were painted flat black to radiate heat from our experiment to cooler surfaces. The accuracy of this thermal design (performed by Westinghouse) is proven by an operating temperature in orbit of +22°C, an almost ideal ambient for the detector.

4.3.3 Mechanical Interface with the Rice University Experiment

The main mechanical support for the Rice University experiment was provided by bolting it to our reinforced right-side plate, as shown in outlined form in Figure 4-33. This was the most compatible arrangement for vibrational behavior and for ease of interfacing and handling the combination. Cutouts were provided in the front plate for the Rice University experiment detector aperture and its two test connectors.

4.3.4 Housing Design

The mechanical design requirements for the housing were as follows:

(1) good structural integrity to withstand high vibration levels,

(2) light weight,

(3) ease of disassembly for removal of the electronic package, and

(4) dimensional accuracy.

These four goals were realized through careful design and fabrication of the housing details. Magnesium was chosen as the material for its one-third weight advantage over aluminum. All details except the covers were machined out of thick, heat-treated, magnesium tooling plates. Webbing was used wherever possible to reduce weight, while ribs were used to maintain adequate stiffness.

Figure 4-34 shows the front plate and right side details. Full dimensional information for the right side is contained in Figure 4-35. As shown in the figure, the webs between the 0.240-inch-thick ribs were only 0.020-inch thick. Four bosses, with 8-32 threaded inserts for the Rice University experiment mounting bolts, extended an additional 0.005 inch beyond the ribs for clearance between the sides of the two packages. The top and bottom edges were cut back 0.040 inch for cover flange clearance. An 0.185-inch-diameter hole was drilled concentrically from front to rear through all but the last rib for access to the back plate locking screw with an extension Allen wrench. Visible in the photograph, Figure 4-31, is the floating captive screw with its head constrained by a slot to keep it in alignment with the wrench hole.

The left side detailed in Figure 4-36 was made quite thin, since there was no external loading. Its nominal thickness was 0.050 inch, with webbing 0.020 inch thick. Additional stiffness was provided by a 0.070-inch-thick external rib. At assembly, this side is secured between the front plate flange and detector mount by screws.

Parallelism between the front and rear edges on both the left and right sides was held within 0.002-inch T.I.R. These edges interfaced with accurate surfaces on the front and back plates to assure squareness of the overall housing each time it was reassembled.

It was not possible to use webbing on the front plate due to the number of cutouts and the structural strength required of this member, Figure 4-37. The step along the top edge of the front plate provided clearance for a solar panel above the EME window in the spacecraft skin. The lower portion, containing the BTL and Rice detector apertures, extended out flush with the skin for an unobstructed view of space.

The back plate had to be quite stiff to meet the Westinghouse flatness specification, provide support for the rear guide pins, and withstand the heavy preloading transmitted by the front mounting screws.

A very strong, lightweight design was developed with a grid work of ribs and bosses with 0.025-inch-thick webs in between and a wide rim around the edge, Figure 4-38. This rim extended into the housing and provided a good mounting surface for the left and right sides and covers. Tapped bosses were suitably positioned along its inner surface for screws. The entire outer surface was machined flat to within 0.002-inch T.I.R. Flanged connectors and guide pins were attached with screws to lands provided for them on the inner surface.

A partition, shown in Figure 4-39, was originally intended only as an electrostatic shield. As an outcome of early vibration tests, it was changed to a structural

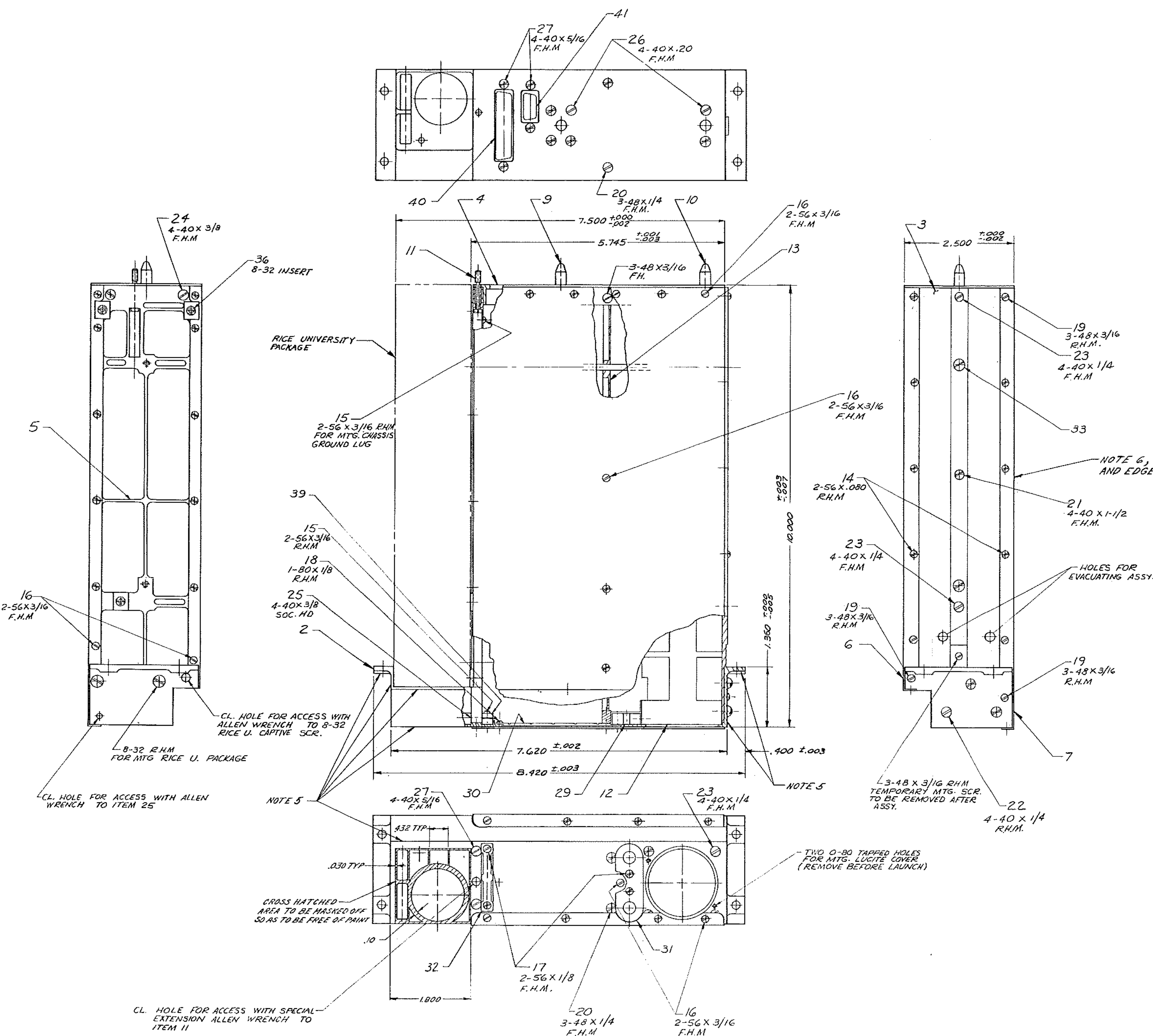

NOTES:

1. DIMENSIONS SHOWN ARE FOR REFERENCE ONLY.
2. OBTAIN FROM HELI-COIL CORP. DANBURY, CONN.
3. OBTAIN FROM CANNON ELECTRIC CO. SALEM, MASS.
4. ALL PAINTING TO BE DONE AFTER ASSEMBLY.
5. COAT THIS SURFACE WITH DOW CORNING WHITE PAINT NO DC-Q-92-007 PER WESTING HOUSE FINISH SPECIFICATION FS-314-H.
6. PAINT THIS SURFACE WITH ONE COAT OF FLAT BLACK EPOXY ENAMEL. A-136-50EA EPOXY ENAMEL, 3725 BLACK, MIXED WITH CATALYST THINNER A-136-50 EAT (SUPPLIERS NUMBERS.) THE SUPPLIER IS ANDREW BROWN CO, LAUREL, MARYLAND.
7. ALL OTHER SURFACES TO BE GOLD PLATED PER MARSHALL LAB. SPEC. NO. 40120, CLASS I (POLISHED).
8. ALL SCREW HEADS WHICH ARE VISIBLE SHALL BE THE SAME FINISH AS THE SURFACE THEY ARE MOUNTED IN.

REQ	IDENTIFICATION NO.	DESCRIPTION	REF DESIG	NOTE	ITEM
1		RECEPTACLE, CAT. NO. DEM-9S		3	41
1		PLUG, CAT. NO. DBM-25P		3	40
1		PLUG, CAT. NO. MDB-37P		3	39
					38
					37
		8-32 HELI-COIL INSERT CAT. NO. 3585-2CN0246		2	36
					35
					34
2	B-614671-1	CIRCUT BOARD SCR		7	33
1	B-615774-1	COVER			32
1	B-615773-1	COVER			31
1	B-615673	FRONT BOARD LOCKING PLATE			30
1	B-615659	TEST JACK BRACKET			29
					28
6		SCR. .112-40 X 5/16 F.H.M, CORR. RES. STL		8	27
6		SCR. .112-40 X .20 F.H.M, CORR. RES. STL		8	26
2		SCR. .112-40 X 3/8 HEX. SOC. HD, CORR. RES. STL		8	25
2		SCR .112-40 X 3/8 FHM, CORR. RES. STL		8	24
2		SCR .112-40 X 1/4 FHM, CORR. RES. STL		8	23
3		SCR .112-40 X 1/4 RHM, CORR. RES. STL.		8	22
1		SCR .112 X 40 X 1-1/2 F.H.M ALUM.		8	21
6		SCR .099-48 X 1/4 FHM, CORR. RES. STL		8	20
4		SCR .099-48 X 3/16 R.H.M, CORR. RES. STL		8	19
1		SCR .060-80 X 1/8 RHM., CORR. RES. STL		8	18
4		SCR. .086-56 X 1/8 FHM, CORR. RES. STL		8	17
41		SCR. .086-56 X 3/16 F.H.M, CORR. RES. STL		8	16
3		SCR .086-56 X 3/16 RHM, CORR. RES. STL		8	15
8		SCR. .086-56 X .080 RHM, CORR. RES. STL		8	14
1	B-615299	PARTITION			13
1	B-615215-2	DETECTOR MOUNT			12
1	B-614663	MODIFIED SCREW			11
1	B-614662	GUIDE PIN			10
1	B-614661	GUIDE PIN			9
					8
1	B-614631	BOTTOM COVER			7
1	B-614630	TOP COVER			6
1	B-614629	RIGHT SIDE			5
1	B-614628	BACK PLATE			4
1	B-614627	LEFT SIDE			3
1	B-614626	FRONT PLATE			2
					1

Figure 4-33. Mechanical Assembly Drawing

Page intentionally left blank

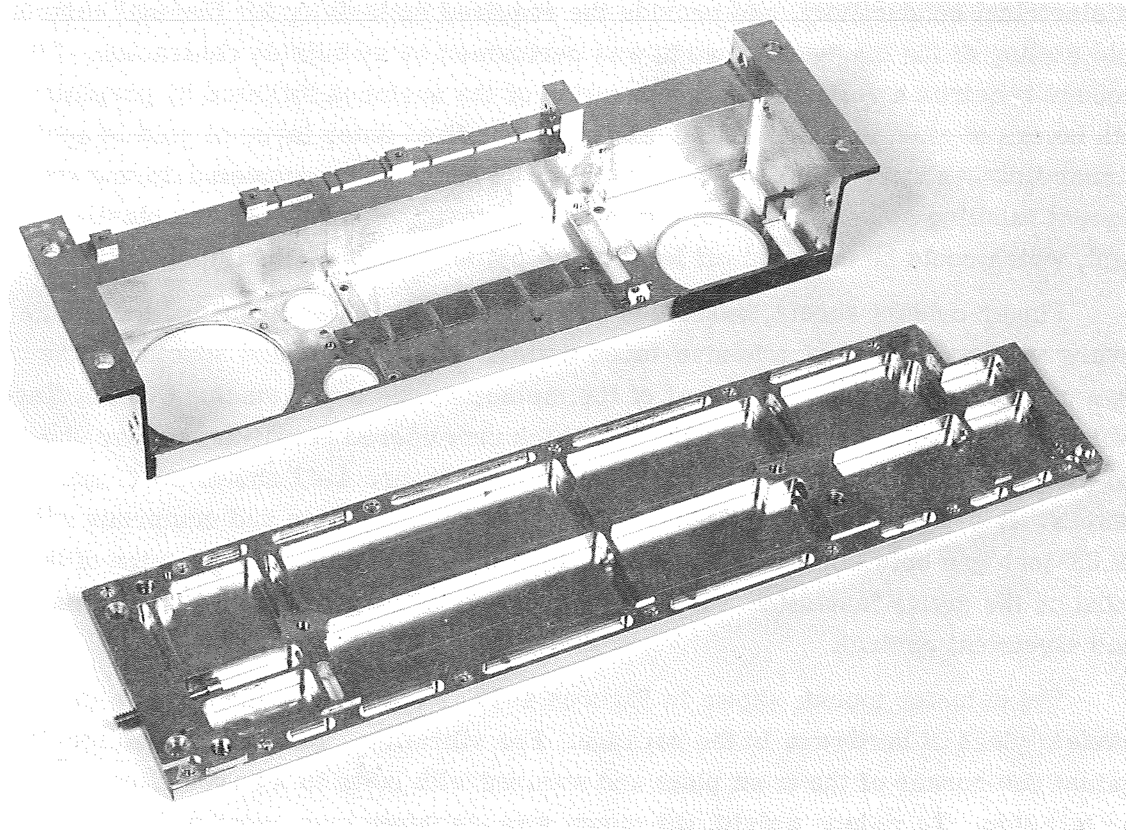

Figure 4-34. Front Plate and Right Side of the Experiment Housing

member to provide additional support for the through-bolts at the midpoint of the stack and to reduce amplification on the front plate by stiffening the housing from front to rear.

The covers, shown in Figures 4-40 and 4-41, were made from 0.020-inch-thick magnesium sheet. Flanges formed along the front and two sides helped strengthen and flatten the top surface. These had to be bent with the material heated to +500°F to prevent cracking the corners.

At the first mechanical assembly, the parts for each housing were temporarily clamped together in order to check critical dimensions and parallelism. After these requirements had been verified, 1/16-inch-diameter stainless steel locating pins were then inserted into the sides and clearance holes were drilled for them where they interfaced with the front and back plates. This "pinning" permitted a rapid return to the original fitted condition each time the housing was reassembled.

All housing parts were gold plated to protect the magnesium surface, increase its electrical conductivity, and provide the required emissivity for thermal control. Gold plating of the magnesium parts was performed by an outside contractor. The process requires a very careful preparation of the surfaces followed by preplating with layers of zinc, copper, and silver before the final outer layer of gold is applied. Mirror finishes were obtained where required. These were protected during subsequent handling by application of a thin coat of coverlac, a fast-drying plastic paint, which could be stripped off leaving the polished surface undisturbed.

Finger contact sheets, described in Paragraph 4.1.1, were bonded inside the covers with two layers of adhesive-faced mylar. The location and spacing of the rows of fingers corresponds to that of the motherboards in the stack. Contact finger outlines were photo-etched in 0.003-inch-thick untempered beryllium copper sheet and then formed and heat-treated in special dies. Figure 4-42 shows the finger contour. It was designed to extend 0.05 inch in its unload state and compress within a 0.03-inch gap between the boards and covers without digging into the edge of the board or the mylar insulation. The finished sheets were gold plated to maintain good electrical contact.

The detector mount, shown in Figures 4-43 and 6-10, was the largest and heaviest piece of hardware in the package. For vibrational reasons, it was located against one corner of the front plate and secured with bolts to the front face, flange, and left side. To reduce weight, the mount was machined over most of its length to as small a circular cross-section as possible and still provide adequate shielding for the detector. Square sections of the block were retained for mounting to the front plate and for attaching the rear cover and other accessory items (Paragraph 6.5.4). Figure 4-7 showed photographically an exploded view of all the removable internal detector telescope hardware; these items are described in Paragraph 2.2.3.

An aluminum test jack bracket, shown in Figure 4-44 and 2-20, interfaces with the detector block and front plate in alignment with the two access holes at the left of the detector aperture. Two covers, shown removed in Figure 4-7, are provided to electrostatically shield these test ports and the one for the 37-pin test connector. Both covers are vented to speed out-gassing of the experiment in space. Additional venting holes were located on each side of the rib at the front of the left side and at the rear of the right side.

A procedure for automatically producing the complex housing components through numerical control machining was explored during this project. Programs were written for the two sides (Figures 4-35 and 4-36) in time to successfully machine these details for the second flight model. A considerable cost reduction can be realized when several details of this complexity are required.

NOTES:
1. THESE HOLES SHALL BE DRILLED AT ASSY. B-614632.
2. DE-BURR THESE HOLES BOTH SIDES.
3. GOLD PLATE PER MARSHALL LABORATORIES SPECIFICATION NO. S40120, CLASS II (DULL) ALL SURFACES.
4. PART MAY BE MADE BY "NUMERICAL CONTROL MACHINING." TAPE AVAILABLE IN ENGINEERING RECORD FILES. TAPE NO B-614629.

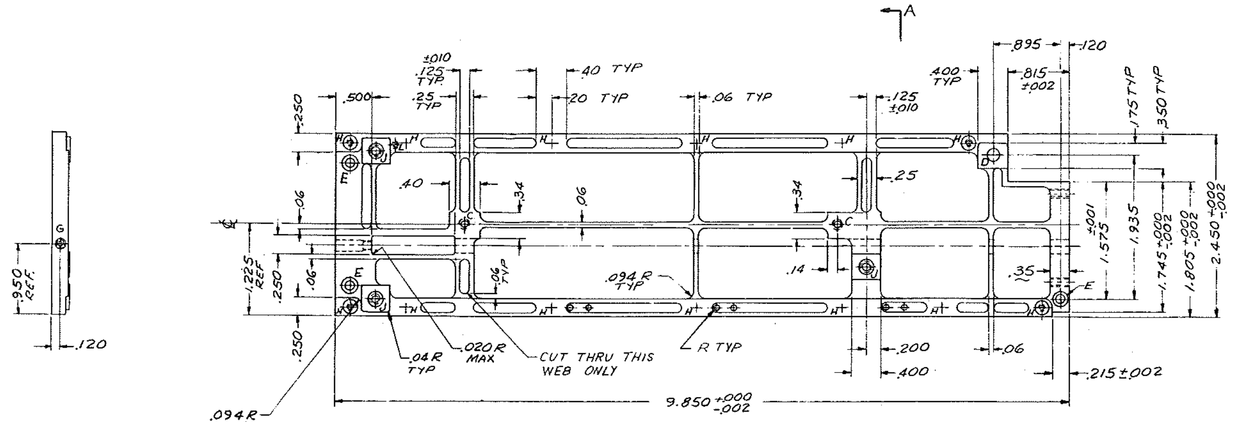

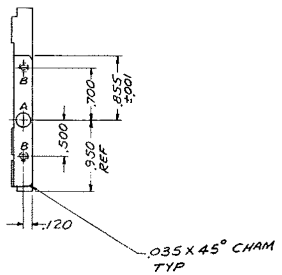

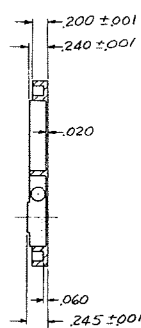

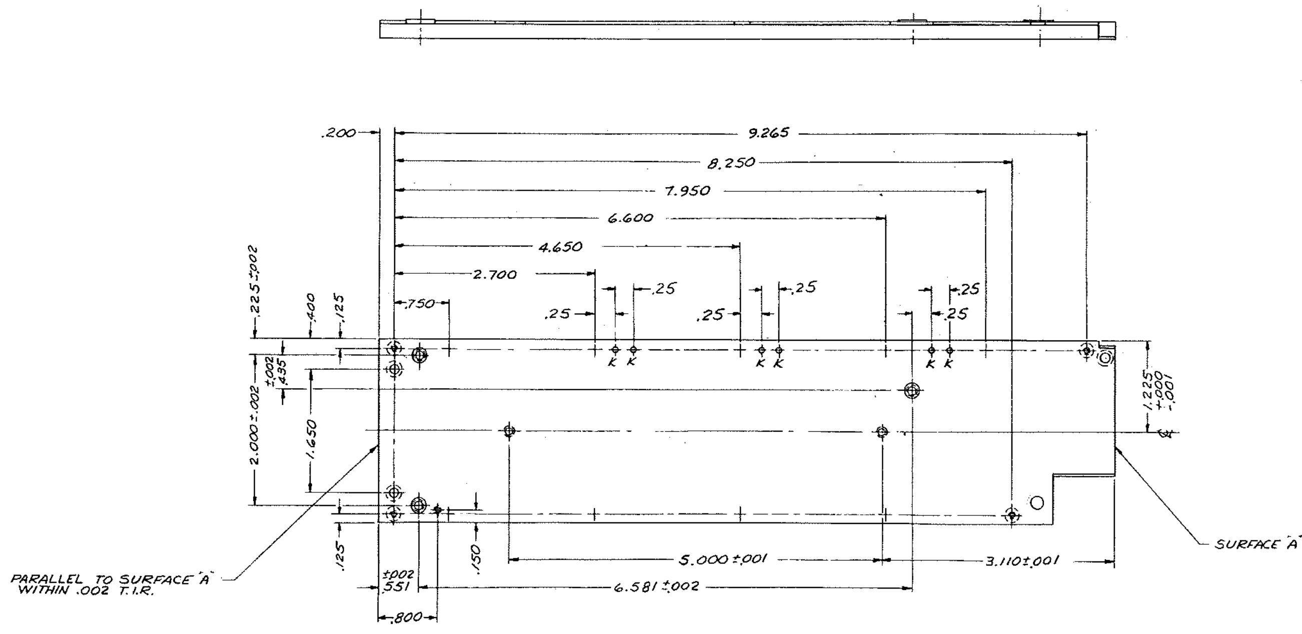

HOLE	DESCRIPTION	REQ
A	.185 DIA.	1
B	4-40 TAP (NOTE 1)	2
C	6-32 TAP (NOTE 1)	2
D	.177 DIA. (NOTE 1)	1
E	.125 DIA. & C'BORE TO .194 DIA. X .120 DP. (NOTE 1)	3
F		
G	6-32 TAP & C'BORE TO .140 DIA. X .375 DP.	1
H	2-56 TAP & CSK 80°-82° TO .113 DIA. (NOTE 1)	13
J	SPL. PLUG TAP, 32 PITCH, .2060 MAX. MAJ. DIA. .174-.180 MINOR DIA. (NOTE 1)	3
K	.070 DIA (NOTE 2)	6
L	2-56 TAP	1

MATERIAL	FINISH
MAGNESIUM, TOOLING PLATE AZ31B	NOTE 3

UNLESS OTHERWISE SPECIFIED, ALL DIMENSIONS ARE IN INCHES. NONLIMITED DIMENSIONS OTHER THAN SIZE OF RAW MATERIAL SHALL BE HELD AS FOLLOWS WHEN EXPRESSED: TO 2 DECIMAL PLACES ±.01 TO 3 DECIMAL PLACES ±.003 AS ANGLES ±~

Figure 4-35. Right Side Drawing

Page intentionally left blank

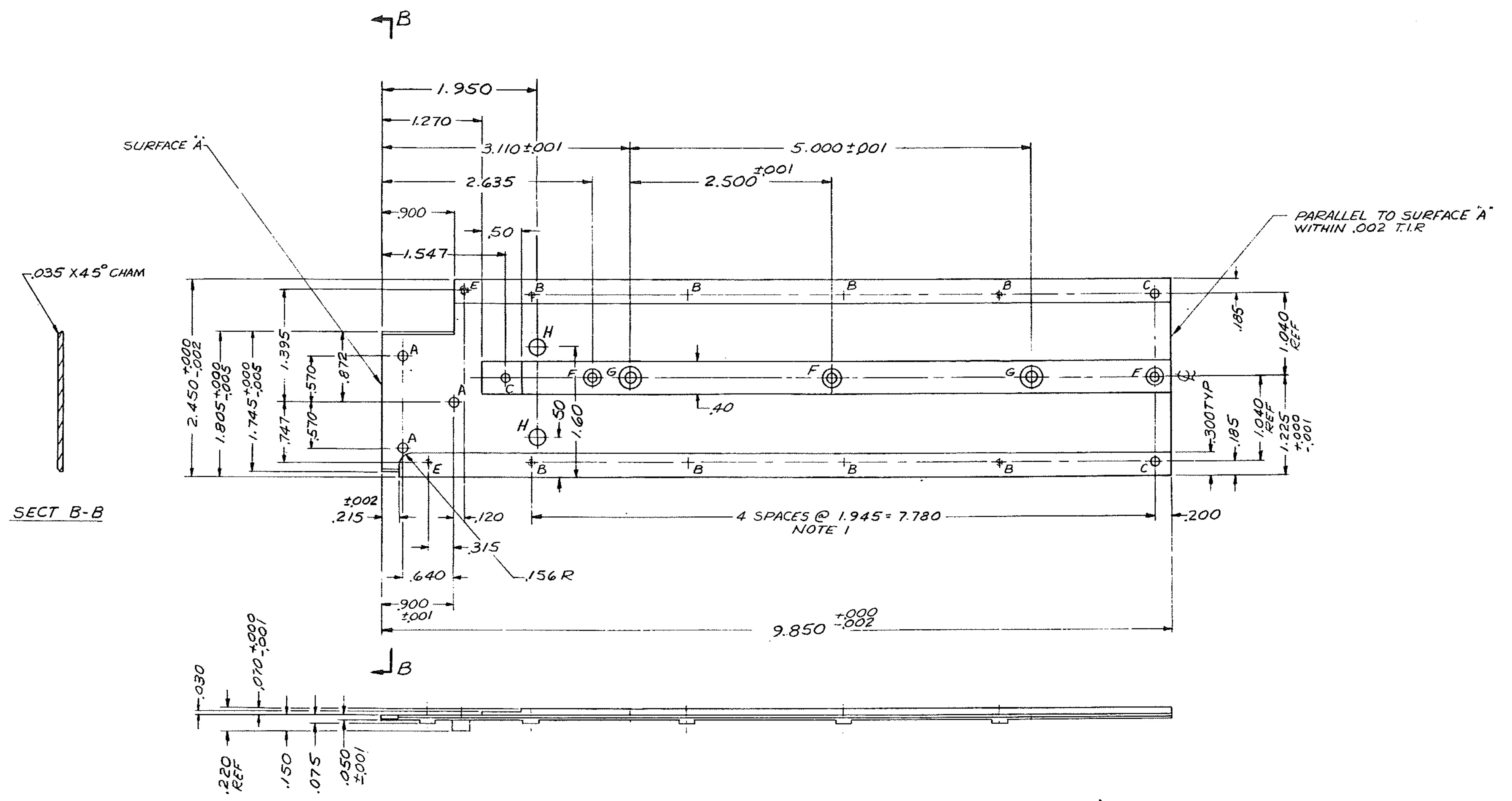

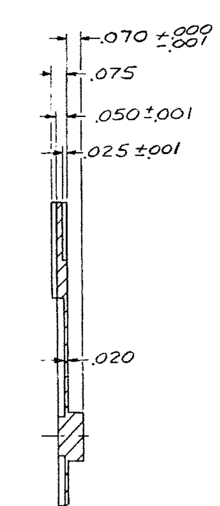

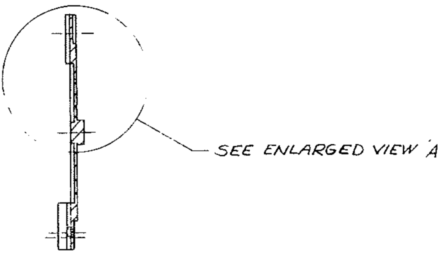

NOTES:
1. THESE HOLES SHALL BE DRILLED AT ASSY. B-614632.
2. TOLERANCES SHALL NOT BE CUMULATIVE.
3. GOLD PLATE PER MARSHALL LABORATORIES SPECIFICATION NO. S40120, CLASS II (DULL), ALL SURFACES.
4. PART MAY BE MADE BY "NUMERICAL CONTROL MACHINING." TAPE AVILABLE IN ENGINEERING RECORD FILES TAPE NO B-614627.

HOLE	DESCRIPTION	REQ
A	.125 DIA. (NOTE 1)	3
B	2-56 TAP (NOTE 1)	8
C	.109 DIA. (NOTE 1)	3
D		
E	3-48 TAP (NOTE 1)	2
F	.114-.119 DIA & CSK 80°-82° TO .228-.230 DIA.(NOTE 1)	3
G	.140-.142 DIA & CSK 80°-82° TO .275-.278 (NOTE 1)	2
H	.200	2

MATERIAL	FINISH
MAGNESIUM, TOOLING PLATE AZ31B	NOTE 3

UNLESS OTHERWISE SPECIFIED, ALL DIMENSIONS ARE IN INCHES. NONLIMITED DIMENSIONS OTHER THAN SIZE OF RAW MATERIAL SHALL BE HELD AS FOLLOWS WHEN EXPRESSED:
TO 2 DECIMAL PLACES ±.01 AS ANGLES ± ~
TO 3 DECIMAL PLACES ±.003

Figure 4-36. Left Side Drawing

Page intentionally left blank

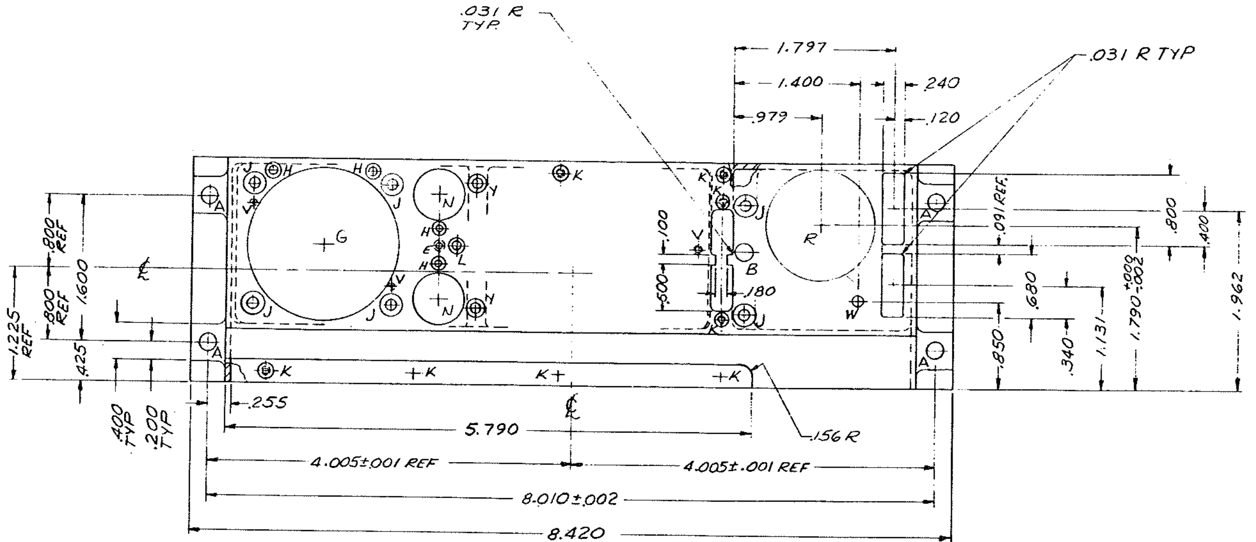

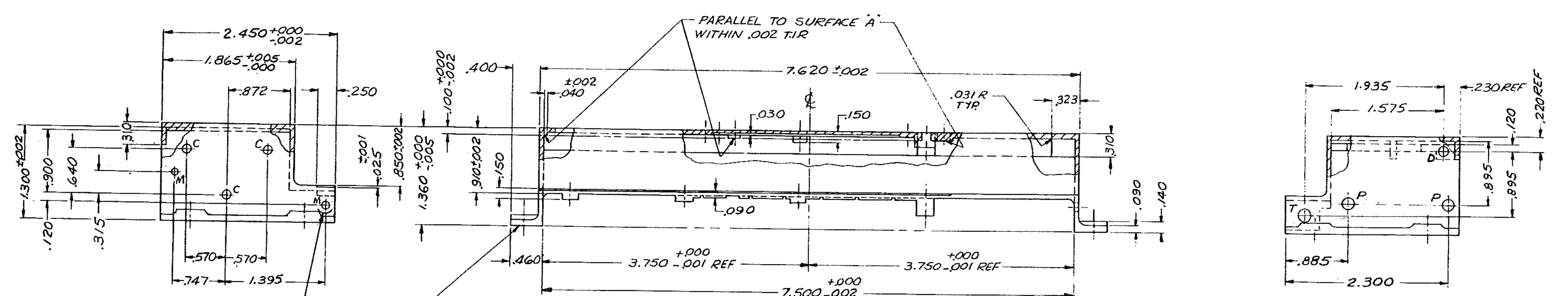

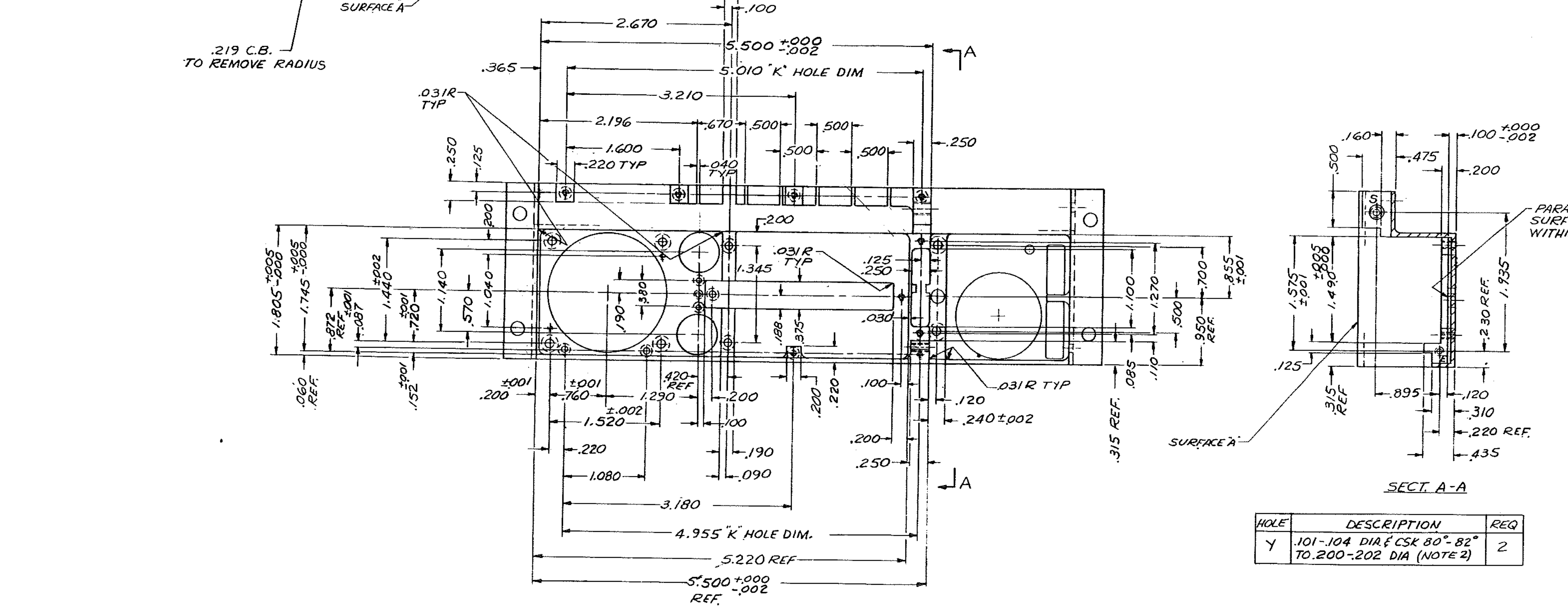

NOTES:
1. THESE HOLES TO BE DRILLED AT ASSY. B-614632.
2. THESE HOLES SHALL BE DRILLED NOW AND COUNTER-SINKING DONE AT ASSY. B-614632.
3. ALL RADII SHALL BE .094 UNLESS OTHERWISE SPECIFIED.
4. GOLD PLATE PER MARSHALL LABORATORIES SPECIFICATION. NO. S40120, CLASS II (DULL), ALL SURFACES.

HOLE	DESCRIPTION	REQ
Y	.101-.104 DIA & CSK 80°-82° TO .200-.202 DIA (NOTE 2)	2

HOLE	DESCRIPTION	REQ
A	.191 +.004 -.002 DIA.	4
B	.199 DIA.	1
C	.125 DIA.	3
D	.125 DIA (NOTE 1)	1
E	4-40 TAP (NOTE 1)	2
F		
G	1.670 DIA.	1
H	.087 DIA. & CSK 80°-82° TO .113 DIA. (NOTE 1)	4
J	.114-.119 DIA. & CSK 80°-82° TO .228-.230 DIA. (NOTE 2)	6
K	2-56 TAP & CSK 80°-82° TO .113 DIA (NOTE 1)	8
L	.087-.092 DIA & CSK 80°-82° TO .172-.176 DIA (NOTE 2)	1
M	.109 DIA.	2
N	.562 DIA	2
P	.177 DIA	2
R	1.187 DIA.	1
S	SPL. PLUG TAP, 32 PITCH, .2060 MAX. MAJ. DIA. .174-.180 MINOR DIA. (NOTE 1)	1
T	.187 DIA (NOTE 1)	1
U		
V	0-80 TAP	3
W	.140 DIA.	1

MATERIAL	FINISH
MAGNESIUM, TOOLING PLATE AZ31B	NOTE 4

UNLESS OTHERWISE SPECIFIED, ALL DIMENSIONS ARE IN INCHES. NONLIMITED DIMENSIONS OTHER THAN SIZE OF RAW MATERIAL SHALL BE HELD AS FOLLOWS WHEN EXPRESSED:
TO 2 DECIMAL PLACES ± ~ AS ANGLES ± ~
TO 3 DECIMAL PLACES ±.003

Figure 4-37. Front Plate Drawing

Page intentionally left blank

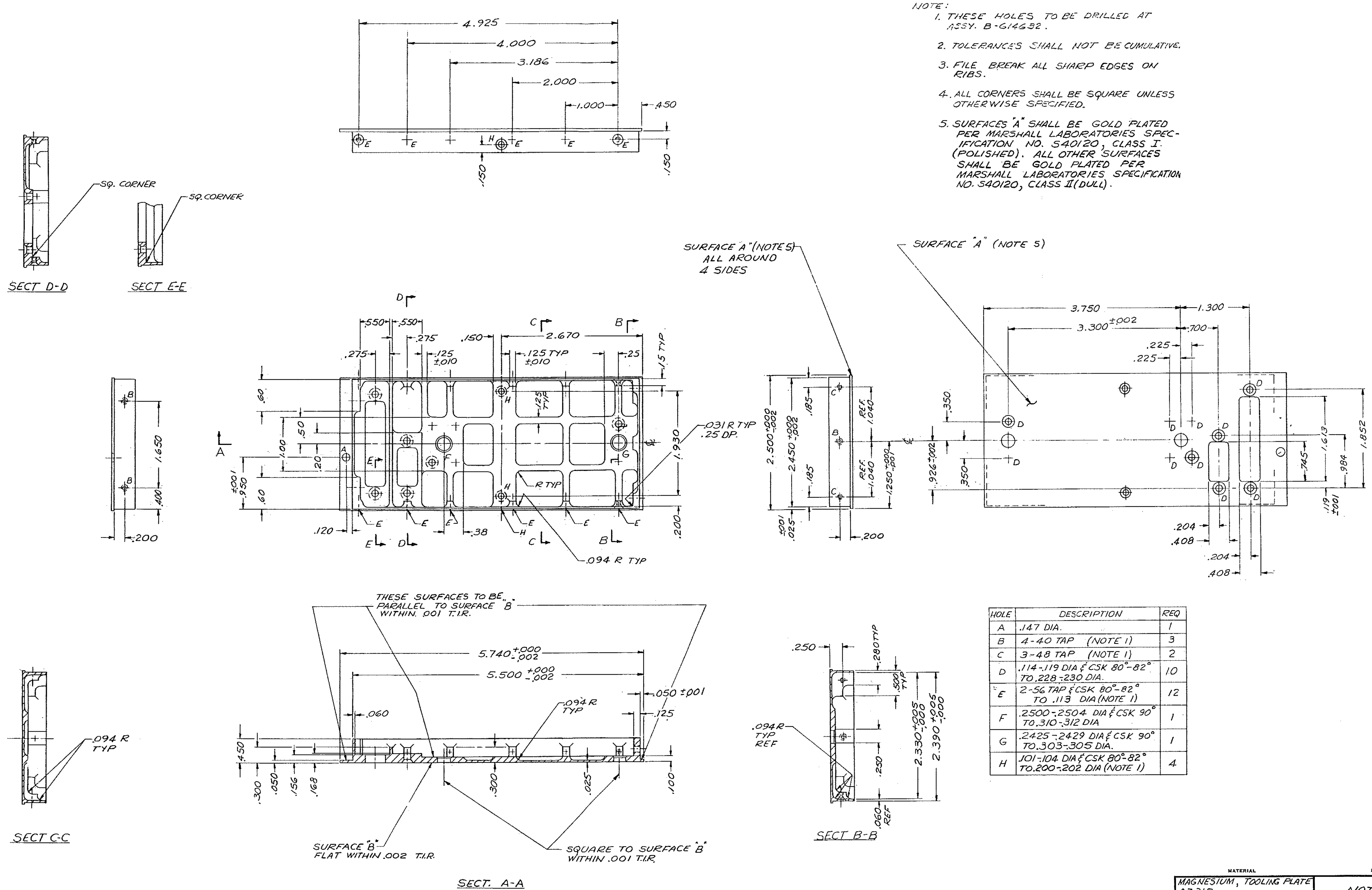

HOLE	DESCRIPTION	REQ
A	.147 DIA.	1
B	4-40 TAP (NOTE 1)	3
C	3-48 TAP (NOTE 1)	2
D	.114-.119 DIA & CSK 80°-82° TO .228-.230 DIA.	10
E	2-56 TAP & CSK 80°-82° TO .113 DIA (NOTE 1)	12
F	.2500-.2504 DIA & CSK 90° TO .310-.312 DIA	1
G	.2425-.2429 DIA & CSK 90° TO .303-.305 DIA.	1
H	.101-.104 DIA & CSK 80°-82° TO .200-.202 DIA (NOTE 1)	4

Figure 4-38. Back Plate Drawing

Page intentionally left blank

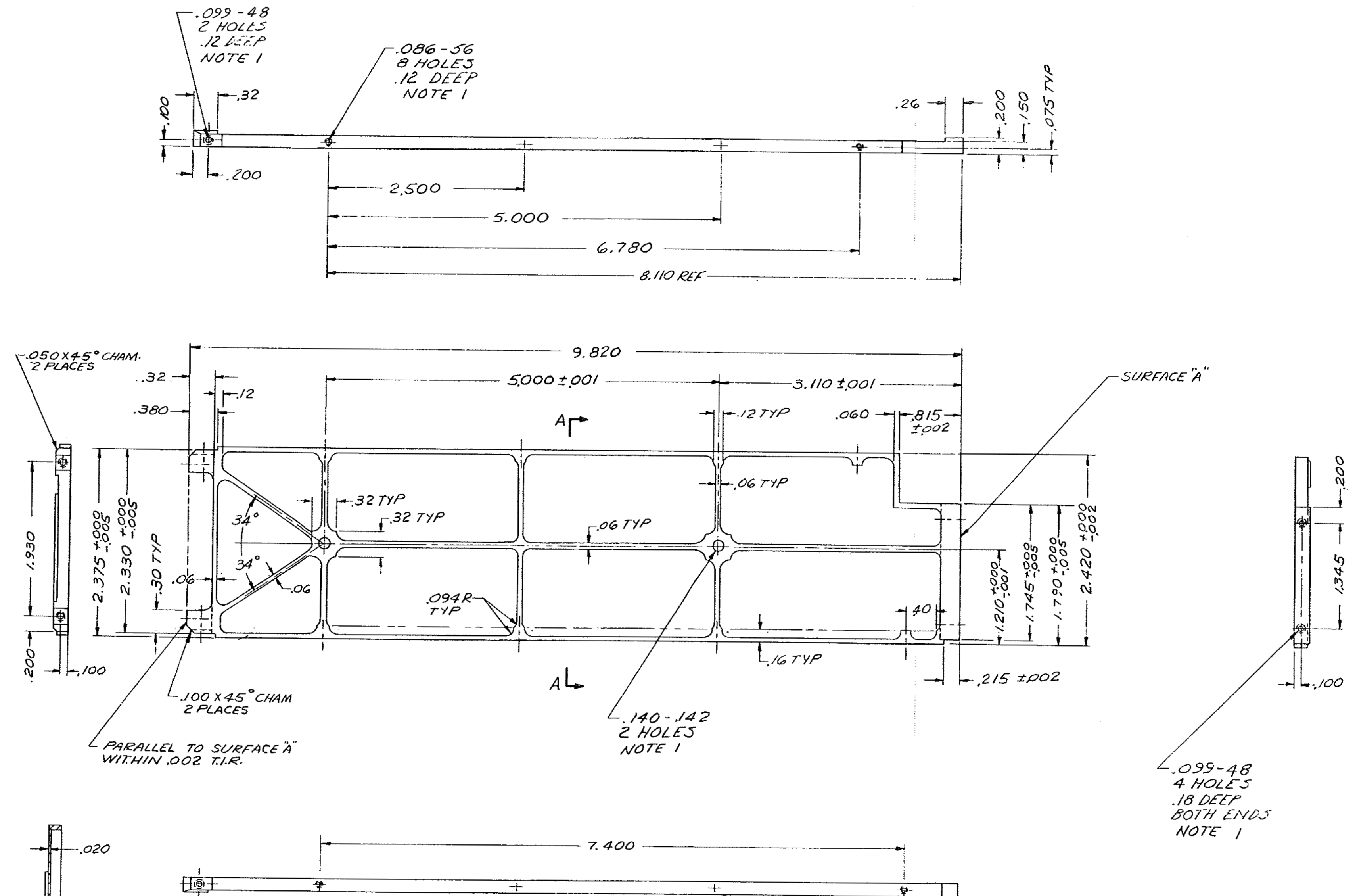

Figure 4-39. Partition Drawing

Page intentionally left blank

NOTES:

1. TOLERANCES SHALL NOT BE CUMULATIVE
2. BENDING RADII SHALL BE .005 MAX
3. ALL HOLES SHALL BE DRILLED AT ASSEMBLY B-614632
4. SURFACE "A" SHALL BE GOLD PLATED PER MARSHALL LABORATORIES SPECIFICATION NO. S40120, CLASS I (POLISHED) ALL BENT UP LIPS & INSIDE SURFACES SHALL BE GOLD PLATED PER MARSHALL LABORATORIES SPECIFICATION NO. S40120, CLASS II (DULL).

80°-82°

.147

SECT. VIEW OF "C" HOLES
SCALE 10/1

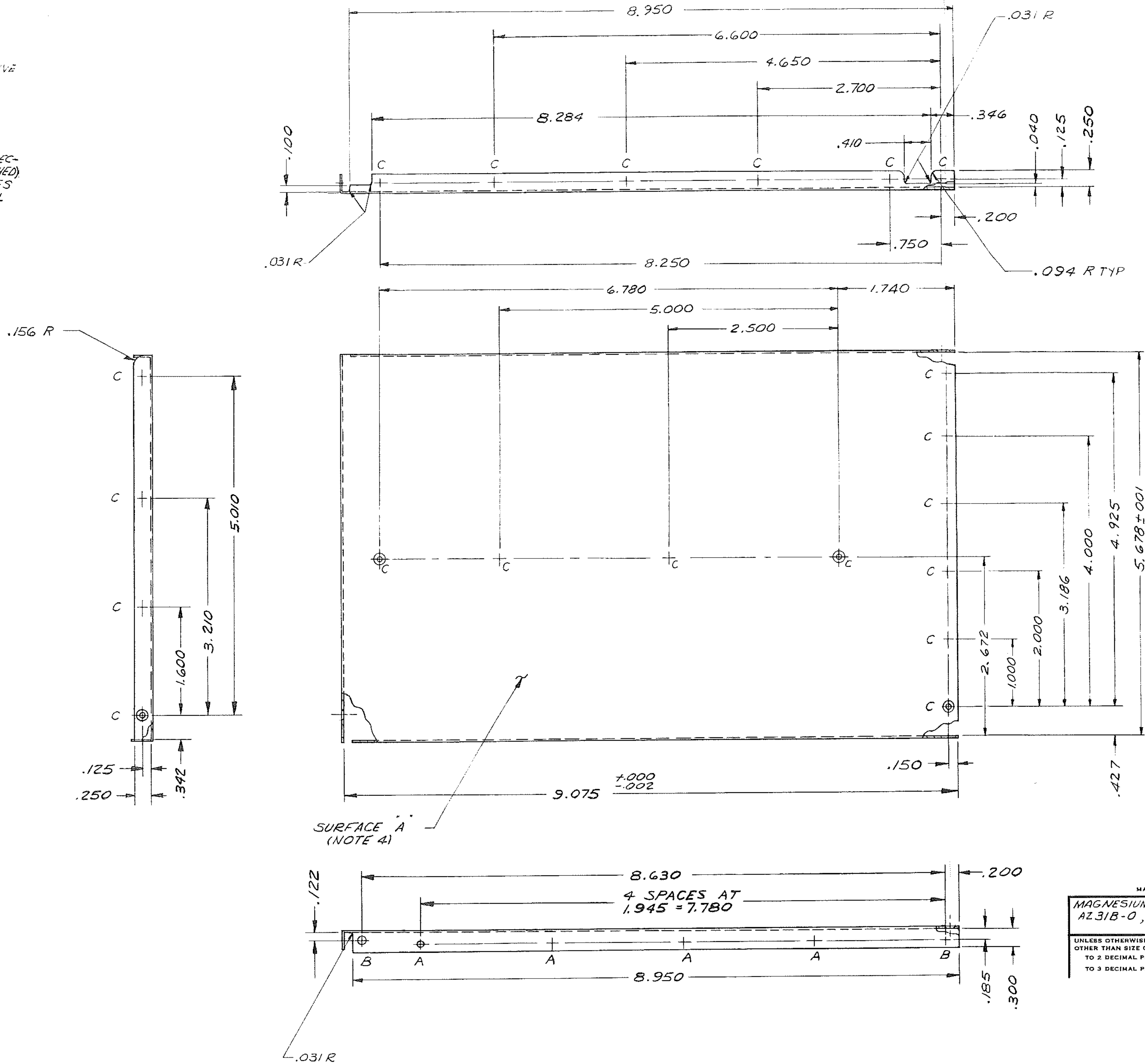

HOLE	DESCRIPTION	REQ
A	.096 DIA (NOTE 3)	4
B	.109 DIA (NOTE 3)	2
C	.087 DIA & CSK 80°-82° TO .147 DIA (NOTE 3)	20

MATERIAL	FINISH
MAGNESIUM, SHEET, .020 THK AZ31B-O, ANNEALED	

UNLESS OTHERWISE SPECIFIED, ALL DIMENSIONS ARE IN INCHES. NONLIMITED DIMENSIONS OTHER THAN SIZE OF RAW MATERIAL SHALL BE HELD AS FOLLOWS WHEN EXPRESSED:
TO 2 DECIMAL PLACES ± —
TO 3 DECIMAL PLACES ± .003
AS ANGLES ± —

Figure 4-40. Top Cover Drawing

Page intentionally left blank

NOTES:
1. TOLERANCES SHALL NOT BE CUMULATIVE.
2. BENDING RADII SHALL BE .005 MAX.
3 ALL HOLES SHALL BE DRILLED AT ASSEMBLY B-619632
4. SURFACE "A" SHALL BE GOLD PLATED PER MARSHALL LABORATORIES SPECIFICATION NO. S40120, CLASS I (POLISHED). ALL BENT UP LIPS & INSIDE SURFACES SHALL BE GOLD PLATED PER MARSHALL LABORATORIES SPECIFICATION NO. S40120, CLASS II (DULL).

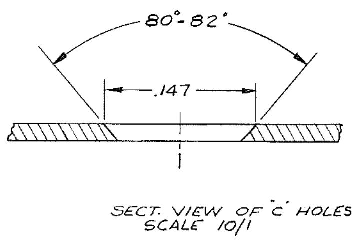

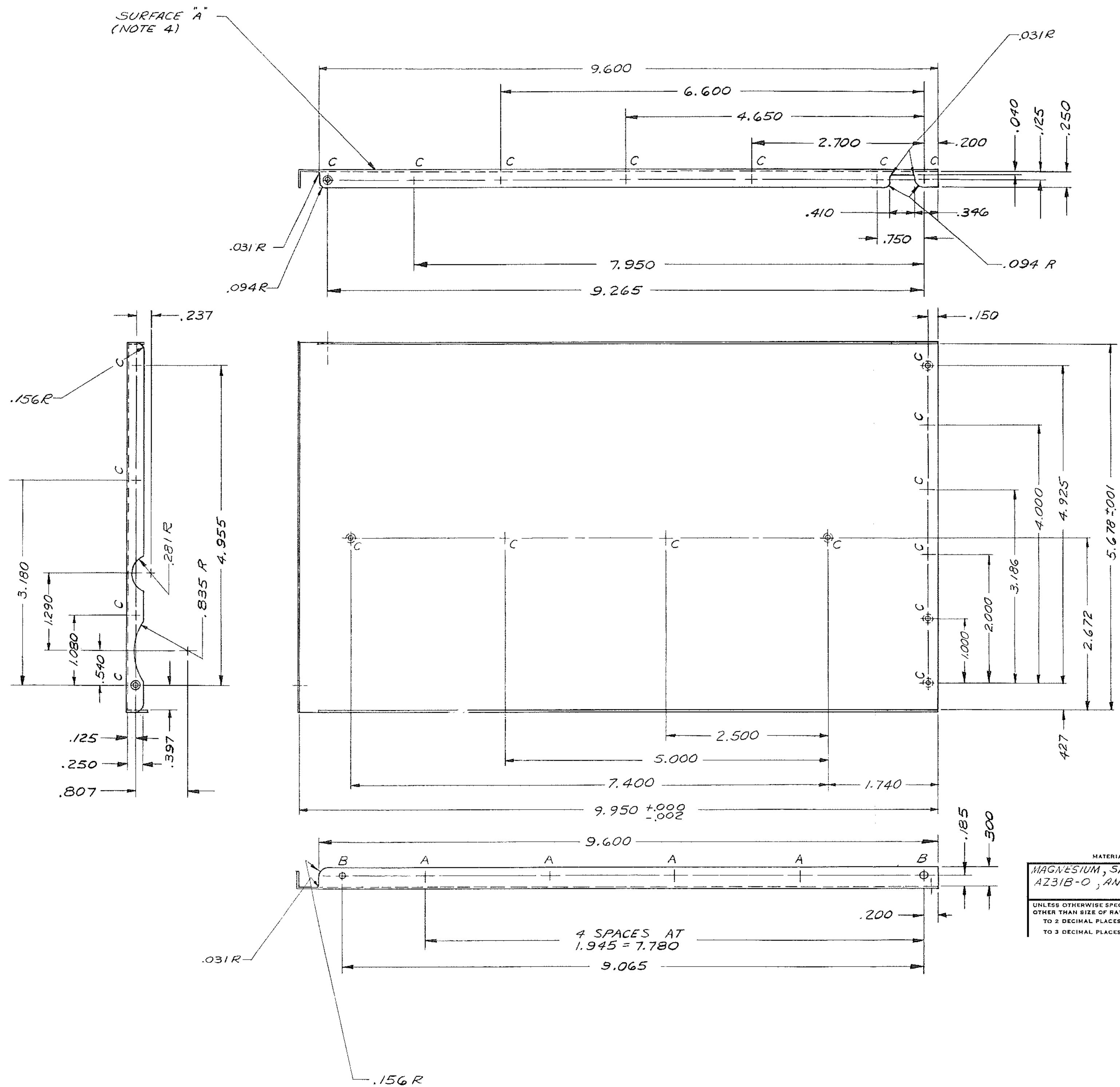

HOLE	DESCRIPTION	REQ
A	.096 DIA (NOTE 3)	4
B	.109 DIA (NOTE 3)	2
C	.087 DIA & CSK 80°-82° TO .147 DIA (NOTE 3)	21

MATERIAL	FINISH
MAGNESIUM, SHEET, .020 THK AZ31B-O, ANNEALED	NOTE 4

UNLESS OTHERWISE SPECIFIED, ALL DIMENSIONS ARE IN INCHES. NONLIMITED DIMENSIONS OTHER THAN SIZE OF RAW MATERIAL SHALL BE HELD AS FOLLOWS WHEN EXPRESSED:
TO 2 DECIMAL PLACES ± AS ANGLES ± —
TO 3 DECIMAL PLACES ± .003

Figure 4-41. Bottom Cover Drawing

Page intentionally left blank

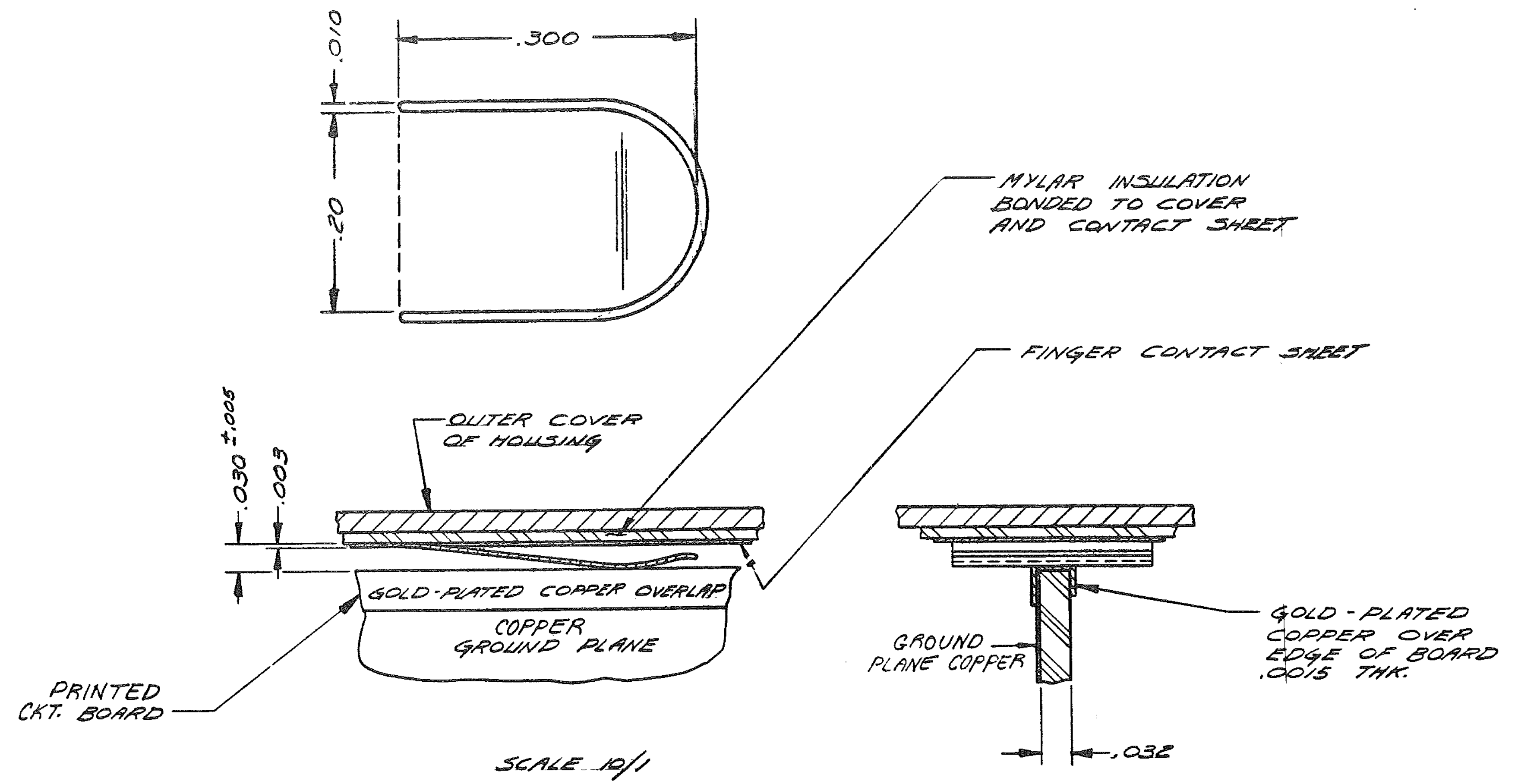

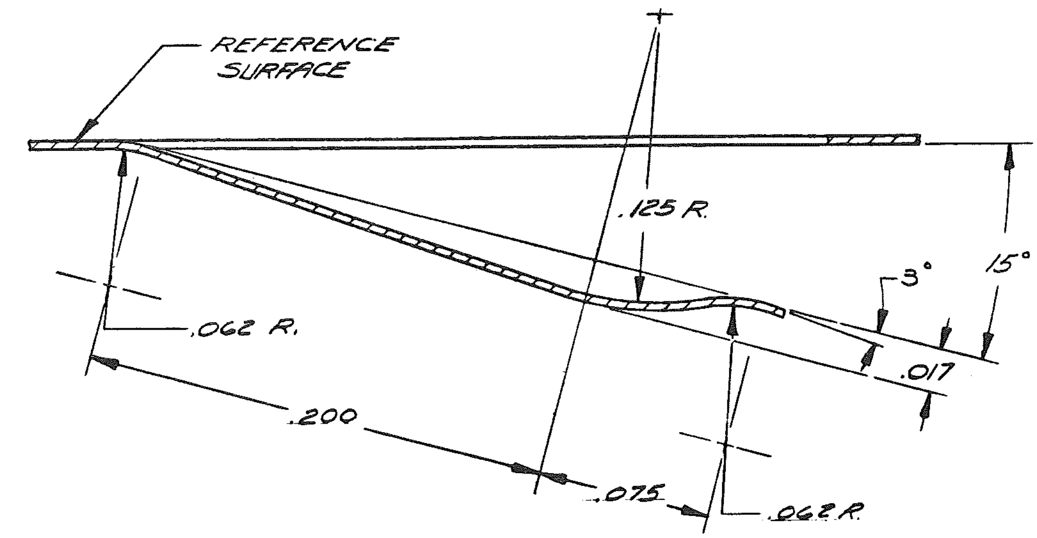

PROJECT	DWG. NO.	DESCRIPTION
ATS & IMP	B-619804-1	AS SHOWN
ATS	B-619804-2	TOP GND. CONTACT SHEET
ATS	B-619804-3	BOTTOM " " "
IMP-F	B-619804-4	GND. " " "
IMP-G	B-619804-5	GND. " " "

Figure 4-42. Ground Plane Finger Contact Drawing

Page intentionally left blank

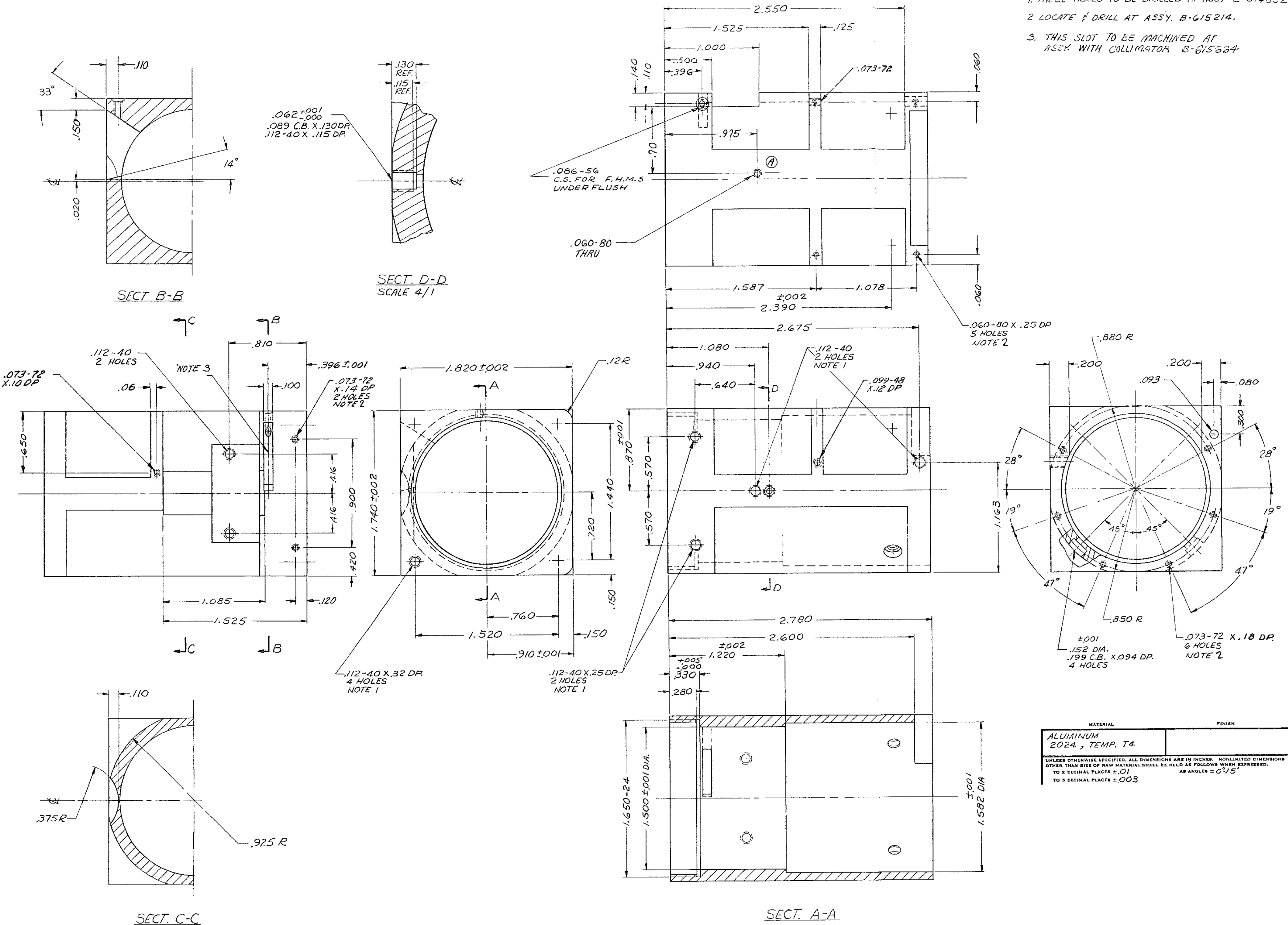

Figure 4-43. Detector Mount Drawing

Page intentionally left blank

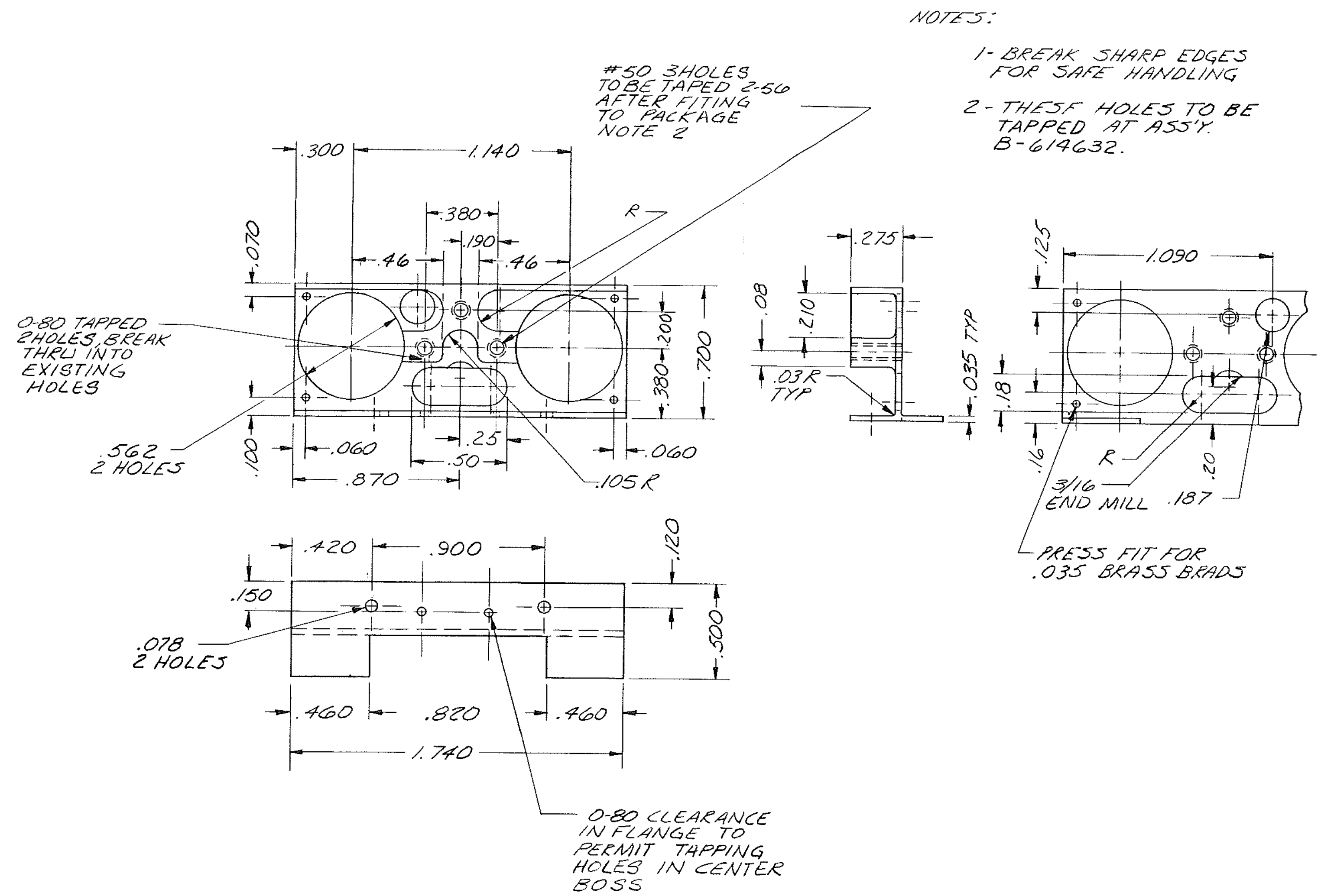

Figure 4-44. Test Jack Bracket Drawing

Page intentionally left blank

Chapter 5

COMPONENTS AND RELIABILITY

5.1 RELIABILITY

The ATS experiment was undertaken with two years operation in space as an objective. Each flight package contained 499 transistors, 341 diodes, 1348 resistors, 334 capacitors, a delay line, and 3 transformers (including all components on integrated circuits). From this information it is easy to see that only highly reliable parts could be considered. Bell Telephone Laboratories has acquired extensive experience in the use of high reliability components through programs such as Telstar and the submarine cable. The assistance of Bell Laboratories component departments in preparing specifications, advising on procurement, and in screening devices has been invaluable to this project. Only types of components which from past experience had proven consistently dependable were selected. Most of these were ordered to BTL specifications. Circuits were conservatively designed and all components operated with large deratings. Screening programs were established to eliminate early failures, unstable elements, and statistical outliers.

The reliability analysis of the particle experiment shows clearly in Figure 5-1 the value of using high-reliability parts. Some minor component changes were effected after the survey was done.

5.2 COMPONENTS

Table 5-1 shows the basic types and quantities of components used in each experiment.

5.2.1 Specifications and Screening

Table 5-2 is a summary of the specifications and screening programs for the various components.

BELL TELEPHONE LABORATORIES
INCORPORATED

SUBJECT: Reliability Analysis of BTL Particle Telescope Satellite Experiment - Case 36294-11

DATE: December 1, 1965

FROM: J. H. Bollman

MEMORANDUM FOR FILE

The purpose of this memorandum is to record the results of a reliability analysis of the BTL particle telescope experiment for the NASA ATS-B Satellite. The analysis is made under the following conditions.

1. The prediction relates to electronic equipment failures in orbit where time rather than environmental stress such as shock and vibration is the independent variable.

   It is assumed that the equipment will survive the launch stresses. This will be assured by extensive environmental tests prior to launch.

2. Only high reliability electronic parts will be used. These will be well screened to eliminate early failures. The parts failure rates furnished by Department 6222 are based on experience with similar parts[1]. It is assumed that sufficient shielding is provided so that radiation will not be a significant cause of failure.

3. It is assumed that the parts are used conservatively and adequate circuit margins for part degradation are allowed. It is estimated that approximately one-half of the inherent* life (IMTBR) of the components will be realized.

---

[1] "Operational Reliability of Components in Selected Systems" T. L. Tanner For Presentation at 1966 Reliability Symposium.

* The inherent life of components has been determined by observing their performance in the field using only data from the best systems; typically digital circuitry in roomy, air-conditioned, ground based environment with excellent maintenance, usually factory repair of large replaceable modules.

Figure 5-1. Reliability Analysis Documentation

4. There is very little real redundancy in the various modes of operation; that is, only a small number of parts are used exclusively in a given mode of operation. It is assumed that when a part in a given mode or modes fails, it will not prevent proper operation of parts not involved in that path. This permits us to calculate the probability of success for each mode without considering whether other modes are operating or not.

5. The procedures used are described in "Military Reliability Information" Section 2, Rating System A. It consists of counting the number of like parts used in a given mode, multiplying by the assigned failure rate and summing the results for all parts to obtain the inherent failure rate. The units used are failures in 10^9 hours (R.U.) hence, the inherent mean time between failures (IMTBR) is 10^9/R.U.; the mean time between failures (MTBR) is the assigned "K" factor (0.5) multiplied by IMTBR. With well screened parts and adequate pre-launch testing, the failure rates will be approximately constant with time and the probability of success for time t will be $P = \exp(-t/MTBR)$.

The assumptions and approximations involved result in a prediction which is only good to an order of magnitude (one significant figure) in MTBR and consequently in the probability of failure Q (Q = 1-P). However, two or three significant figures are given in the summary table to aid in comparisons between the various modes of operation.

A summary of the results are shown in Table 1 and the details are given in the appendix. Briefly, there is a probability of about 0.4 that there will be some failure in the two year operation period. There is a probability of about 0.2 that this will be in the common equipment and, therefore, fail all modes of operation. There is little to choose between the various modes, they all have a probability of success of about 0.75 for the two year period. To illustrate the value of using well screened, high reliability (costly) parts, the probability of success of the common equipment was calculated using experience for military equipment as given in MIL Handbook 217. The probability of lasting two years with MIL parts is about 0.12 where with high reliability parts it is 0.85.

WH-6223-JHB-OMS J. H. BOLLMAN

Att.
See next page

Figure 5-1. Reliability Analysis Documentation (continued)

SUMMARY

Probability of no failures in -	6 mo.	1 yr.	2 yr.
All equipment	.886	.784	.626
All but test equipment	.891	.794	.635
Common equipment and bias supply	.959	.919	.844
Mode A with common equipment and bias	.942	.885	.784
B	.930	.864	.750
C	.927	.860	.743
D	.921	.850	.725
E	.920	.846	.719
F	.930	.864	.750
G	.931	.870	.760
H	.928	.861	.744
I	.926	.859	.740
Common equipment (MIL HDBK 217)			.128

Figure 5-1. Reliability Analysis Documentation (continued)

Appendix A

All Equipment

Component	Number	Rate	Number X Rate
Resistor-Allen Bradley Carbon	436	1.0	436
WECo Thin Film	34	3.0	102
Corning Dep. Carbon	33	0.5	16.5
Capacitors-Erie Ceramic	55	10.0	550
Kemet Tantalum	57	5.0	285
Vitramon Ceramic	80	20.0	1600
J.F.D. Trimmers	6	100.0	600
Transistors and Tunnel Diodes	133	10	1330
Diodes	204	5	1020
Filter Choke	1	5	5
Delay Line	1	140	140
Bias Trans	2	20	40
Gates	51	20	1020
Linear Amplifier	26	130	3380
Pulse Shaper	6	200	1200
Discriminator	21	110	1310
			14034.5
	- Peripheral		828
			13206.5

IMTBF (all) = $10^9/14000$ = 71,500 hr.
(less Peripheral) = $10^9/13200$ = 75,600 hr.

MTBF (all) = 71,500 X 0.5 = 35,700
(less Peripheral) = 37,800

P (6 months) all = exp (-4380/35,700) = .886
less peripheral = .891

P (1 year) all = exp (-8760/35,700) = .784
less peripheral = .794

P (2 years) all = exp (17,520/35,700) = .626
less peripheral = .635

Figure 5-1. Reliability Analysis Documentation (continued)

Appendix A - 2

Common Equipment

Component	Number	Rate	Number X Rate
Resistors-Allen Bradley Carbon	200	1.0	200
WECo Thin Film	2	3.0	6
Corning Dep. Carbon	1	0.5	0.5
Capacitors-Erie Ceramic	3	10.0	30
Kemet Tantalum	30	5.0	150
Vitramon Ceramic	49	20	980
Filter Choke	1	5.0	5.0
Transistors and Tunnel Diodes	75	10.0	750
Diodes	67	5.0	335
Delay Line	1	140	140
Linear Amplifier	4	130	520
Pulse Shaper	6	200	1200
Discriminator	4	110	440
			4756.5

Common Equipment Only

IMTBF = $10^9/4756$ = 210,000 hr.

MTBF = 210,000 x 0.5 = 105,000 hr.

P (6 months) = exp (-4380/105,000) = .960

P (1 year) = exp (-8760/105,000) = .920

P (2 years) = exp (-17520/105,000) = .846

Common Equipment and Bias Supply

P (6 months) = .960 - .00014 = .959

P (1 year) = .920 - .00058 = .919

P (2 years) = .846 - .0022 = .844

Figure 5-1. Reliability Analysis Documentation (continued)

Appendix A - 3

Mode A (less common and power)

Components	Number	Rate	Number X Rate
Resistors-Allen Bradley Carbon	32	1.0	32
WECo Thin Film	10	3.0	30
Corning Dep. Carbon	5	0.5	2.5
Capacitors-Erie Ceramic	5	10	50
Kemet Tantalum	5	5.0	25
Vitramon Ceramic	5	20.0	100
J.F.D. Trimmers	1	100	100
Transistors and Tunnel Diodes	3	10.0	30
Diodes	10	5.0	50
Gates	10	20	200
Linear Amplifier	4	130	520
Discriminator	9	110	990
			2129.5

IMTBF = 10^9/2129 = 470,000

MTBF = 0.5 x 470,000 = 235,000

P (6 months) = exp (-4380/235,000) = .983

P (1 year) = .964

P (2 years) = .928

Mode A with common equipment

P (6 months) = .983 x .959 = .942

P (1 year) .964 x .919 = .885

P (2 years) .928 x .844 = .784

Figure 5-1. Reliability Analysis Documentation (continued)

Appendix A - 4

Mode B (less common and power)

Component	Number	Rate	Number X Rate
Resistors-Allen Bradley Carbon	57	1.0	57
WECo Thin Film	15	3.0	45
Corning Dep. Carbon	15	0.5	7.5
Capacitors-Erie Ceramic	15	10.0	150
Kemet Tantalum	11	5.0	55
Vitramon Ceramic	8	20.0	160
J.F.D. Trimmer	3	100.0	300
Transistors and Tunnel Diodes	4	10	40
Diodes	18	5	90
Gates	11	20	220
Linear Amplifier	10	130	1300
Discriminator	10	110	1100
			3524.5

IMTBR = 10^9/3524 = 284,000

MTBR = 0.5 x 284,000 = 142,000

P (6 months) = 3xp (-4380/142,000) = .970

P (1 year) = .940

P (2 years) = .884

Mode B with common equipment

P (6 months) = .970 x .959 = .930

P (1 year) = .940 x .919 = .863

P (2 years) = .884 x .844 = .745

Figure 5-1. Reliability Analysis Documentation (continued)

Appendix A - 5

Mode C (less common and power)

Component	Number	Rate	Number X Rate
Resistors-Allen Bradley Carbon	65	1.0	65
WECo Thin Film	16	3.0	48
Corning Dep. Carbon	15	0.5	7.5
Capacitors-Erie Ceramic	17	10.0	170
Kemet Tantalum	12	5.0	60
Vitramon Ceramic	7	20.0	140
J.F.D. Trimmers	3	100.0	300
Transistors and Tunnel Diodes	7	10.0	70
Diodes	21	5.0	105
Gates	11	20	220
Linear Amplifier	10	130	1300
Discriminator	11	110	1210
			3695.5

IMTBR = 10^9/3695.5 = 271,000

MTBR = 0.5 x 271,000 = 136,000

P (6 months) = exp (-4380/136,000) ≐ .968

P (1 year) = .938

P (2 years) = .880

Mode C with common equipment

P (6 months) = .968 x .959 = .927

P (1 year) = .938 x .919 = .860

P (2 years) = .880 x .844 = .743

Figure 5-1. Reliability Analysis Documentation (continued)

Appendix A - 6

Mode D (less common and power)

Component	Number	Rate	Number X Rate
Resistors-Allen Bradley Carbon	70	1.0	70
WECo Thin Film	18	3.0	54
Corning Dep. Carbon	20	0.5	10
Capacitors-Erie Ceramic	24	10.0	240
Kemet Tantalum	14	5.0	70
Vitramon Ceramic	8	20.0	160
J.F.D. Trimmers	4	100.0	400
Transistors and Tunnel Diodes	6	10.0	60
Diodes	23	5.0	115
Gates	11	20.0	220
Linear Amplifier	13	130.0	1690
Discriminator	11	110	1210
			4399

IMTBR = 10^9/4399 = 228,000

MTBR = 0.5 x 228,000 = 114,000

P (6 months) = exp (-4380/114,000) = .962

P (1 year) = .926

P (2 years) = .858

Mode D with common equipment

P (6 months) = .962 x .959 = .921

P (1 year) = .926 x .919 = .850

P (2 years) = .858 x .844 = .725

Figure 5-1. Reliability Analysis Documentation (continued)

Appendix A - 7

Mode E (less common and power)

Component	Number	Rate	Number X Rate
Resistors-Allen Bradley Carbon	80	1.0	80
WECo Thin Film	18	3.0	54
Corning Dep. Carbon	20	0.5	10
Capacitors-Erie Ceramic	24	10.0	240
Kemet Tantalum	16	5.0	80
Vitramon Ceramic	11	20.0	220
J.F.D. Trimmers	4	100.0	400
Transistors and Diodes	7	10.0	70
Diodes	28	5.0	140
Gates	13	20.0	260
Linear Amplifiers	13	130.0	1690
Discriminator	12	110.0	1320
			4564

IMTBR = $10^9/4564$ = 219,000

MTBR = 0.5 x 219,000 = 109,000

P (6 months) = exp (-4380/109,000) = .961

P (1 year) = .922

P (2 years) = .857

Mode E with common equipment

P (6 months) = .961 x .959 = .920

P (1 year) = .922 x .919 = .846

P (2 years) = .851 x .844 = .719

Figure 5-1. Reliability Analysis Documentation (continued)

Appendix A - 8

Mode F (less common and power)

Component	Number	Rate	Number X Rate
Resistor-Allen Bradley Carbon	64	1.0	64
WECo Thin Film	13	3.0	39
Corning Dep. Carbon	20	0.5	10
Capacitors-Erie Ceramic	24	10.0	12
Kemet Tantalum	13	5.0	65
Vitramon Ceramic	8	20.0	160
J.F.D. Trimmers	4	100.0	400
Transistors and Tunnel Diodes	6	10.0	60
Diodes	21	5.0	105
Gates	5	20.0	100
Linear Amplifiers	13	130.0	1690
Discriminator	6	110.0	660
			3365

IMTBR = 10^9/3365 = 298,000

MTBR = 0.5 x 298,000 = 149,000

P (6 months) = exp (-4380/149,000) = .971

P (1 year) = .943

P (2 years) = .890

Mode F with common equipment

P (6 months) = .971 x .959 = .930

P (1 year) = .943 x .919 = .864

P (2 years) = .890 x .844 = .750

Figure 5-1. Reliability Analysis Documentation (continued)

Appendix A - 9

Mode G (less common and power)

Component	Number	Rate	Number X Rate
Resistors-Allen Bradley Carbon	58	1.0	58
WECo Thin Film	11	3.0	33
Corning Dep. Carbon	15	0.5	7.5
Capacitors-Erie Ceramic	19	10.0	190
Kemet Tantalum	11	5.0	55
Vitramon Ceramic	7	20.0	140
J.F.D. Trimmers	3	100.0	300
Transistors and Tunnel Diodes	6	10.0	60
Diodes	22	5.0	110
Gates	5	20.0	100
Linear Amplifiers	10	130.0	1300
Discriminator	6	110.0	660
			3013.5

IMTBR = $10^9/3013.5$ = 332,000

MTBR = 0.5 x 332,000 = 166,000

P (6 months) = exp (-4380/166,000) = .973

P (1 year) = .948

P (2 years) = .900

Mode G with common equipment

P (6 months) = .973 x .959 = .931

P (1 year) = .948 x .919 = .870

P (2 years) = .90 x .844 = .760

Figure 5-1. Reliability Analysis Documentation (continued)

Appendix A - 10

Mode H (less power and common)

Component	Number	Rate	Number X Rate
Resistors-Allen Bradley Carbon	68	1.0	68
WECo Thin Film	13	3.0	39
Corning Dep. Carbon	20	0.5	10
Capacitors-Erie Ceramic	24	10.0	240
Kemet Tantalum	13	5.0	65
Vitramon Ceramic	8	20.0	160
J.F.D. Trimmers	4	100.0	400
Transistors and Tunnel Diodes	9	10.0	90
Diodes	27	5.0	135
Gates	4	20.0	80
Linear Amplifiers	13	130.0	1690
Discriminator	6	110.0	660
			3637

IMTBR = 10^9/3637 = 275,000

MTBR = 0.5 x 275,000 = 138,000

P (6 months) = exp (-4380/138,000) = .969

P (1 year) = .939

P (2 years) = .881

Mode H with common equipment

P (6 months) = .969 x .959 = .928

P (1 year) = .938 x .919 = .861

P (2 years) = .880 x .844 = .744

Figure 5-1. Reliability Analysis Documentation (continued)

Appendix A - 11

Mode I (less common and power)

Component	Number	Rate	Number X Rate
Resistors-Allen Bradley Carbon	55	1.0	55
WECo Thin Film	15	3.0	45
Corning Dep. Carbon	25	0.5	12.5
Capacitors-Erie Ceramic	29	10.0	290
Kemet Tantalum	16	5.0	80
Vitramon Ceramic	7	20.0	140
J.F.D. Trimmers	5	100.0	500
Transistors and Tunnel Diodes	2	10.0	20
Diodes	17	5.0	85
Linear Amplifiers	15	130.0	1950
Discriminator	5	110.0	550
			3727.5

IMTBR = 10^9/3727.5 = 268,000

MTBR = 0.5 x 268,000 = 134,000

P (6 months) = exp (-4380/134,000) = .968

P (1 year) = .936

P (2 years) = .878

Mode I with common equipment

P (6 months) = .968 x .959 = .926

P (1 year) = .936 x .919 = .859

P (2 years) = .878 x .844 = .740

Figure 5-1. Reliability Analysis Documentation (continued)

Appendix A - 12

Bias Supply

Component	Number	Rate	Number X Rate
Resistors-Allen Bradley Carbon	6	1.0	6.0
Capacitors-Erie Ceramic	6	10.0	60.0
Vitramon Ceramic	2	20.0	40.0
Bias Transformer	1	20.0	20.0
Transistors and Tunnel Diodes	3	10.0	30.0
Diodes	24	5.0	120.0
			276

IMTBF = $10^9/276$ = 3,630,000 hr.

MTBF = 0.1 x 3,630,000 = 363,000 hr.

P (2 years) = exp (-17520/363,000) = .953

Probability of both failing = $(.047)^2$ = .0022

Probability of both failing 1 yr = $(.024)^2$ = .00058

6 months = $(.012)^2$ = .00014

Figure 5-1. Reliability Analysis Documentation (continued)

Appendix A - 13

Peripheral Equipment

Component	Number	Rate	Number X Rate
Resistors-Allen Bradley Carbon	54	1.0	54
WECo Thin Film	6	3.0	18
Corning Dep. Carbon	2	0.5	1
Capacitors-Erie	6	10	60
Kemet	3	5	15
Vitramon	11	20	220
Transistors and Tunnel Diodes	28	10	280
Diodes	12	5	60
Linear Amplifier	1	130	130
			828

Figure 5-1. Reliability Analysis Documentation (continued)

Appendix A - 14

Common Equipment Using MIL-HDBK-217

(Assume 20% of rating, low ambient temperature)

Component	Number	Rate(%/1000 hr)	Number X Rate
Resistors-Allen Bradley Carbon	200	.001	0.200
WECo Thin Film	2	.025	0.050
Corning Dep. Carbon	1	.025	0.025
Capacitors-Erie Ceramic	3	.001	0.003
Kemet Tantalum	30	.005	0.150
Vitramon Ceramic	49	.001	0.049
Filter Choke	1	. 05	0.050
Transistors and Tunnel Diodes	75	.025	1.875
Diodes	67	.015	1.000
Delay Line	1	1.0	1.000
Linear Amplifier	4	.535	2.140
Pulse Shaper	6	.530	3.180
Discriminator	4	.490	1.960
			11.682

MTBR = $10^5/11.7$ = 8550 hr.

P (2 years) = exp (-17520/8550) = .128

Figure 5-1. Reliability Analysis Documentation (continued)

Table 5-1

TYPES AND QUANTITIES OF COMPONENTS USED PER EXPERIMENT

Component Type	Quantity per Experiment
CAPACITORS	
Solid Tantalum	164
General Purpose Ceramic	109
Tubular Ceramic	61
Total Capacitors	334
RESISTORS	
Carbon Composition	424
Metal Oxide Film	33
Tantalum Thin-Film (integrated circuits)	891
Total Resistors	1348
TRANSISTORS	
NPN Silicon	211
PNP Silicon	262
PNP Germanium	26
Total Transistors	499
DIODES	
Tunnel Diodes	25
Signal	316
Total Diodes	341
Transformers, Inductors, and Delay Lines	4
Total number of components:	2526

Table 5-2. SPECIFICATIONS AND SCREENING PROGRAMS

COMPONENT	TYPE	SPECIFICATION/SCREENING
Capacitors	A. Solid Tantalum	2.2-uf and 15-uf capacitors, with manufacturer's rated operating voltage of 35 volts, were supplied by Kemet Department, Linde Company, division of the Union Carbide Corporation. These capacitors were ordered under BTL Specification KS19458. All capacitors were given an additional screening at Bell Telephone Laboratories, as follows: 1. Capacitance and equivalent series resistance measurements, at 150 Hz and 10 KHz at room temperature. 2. Leakage measured at rated voltage and at 1.7 x rated voltage. 3. Temperature cycling consisting of 5 cycles between +85°C and -60°C over a 24-hour period. 4. A 100-hour life test at +85°C under rated voltage. Capacitance and effective series resistance measured at 150 Hz at room temperature. 5. Leakage measured at rated voltage. 6. A noise test consisting of a short-term leakage variation measurement at rated voltage. Rated voltage in the foregoing tests is manufacturer's rating. For our end use, we derated to one-half manufacturer's rating. Capacitors qualifying for flight use had a failure rate of less than 0.001% per thousand hours.

COMPONENT	TYPE	SPECIFICATION/SCREENING
Capacitors (continued)	B. Ceramic	1. General-purpose capacitors, ranging in value from 10 pf to 10,000 pf, with a manufacturer's rated operating voltage of 200 volts were supplied by Vitramon, Incorporated. The capacitors were manufactured and tested in accordance with BTL specifications GA9910, G300104, and G300105. 2. Temperature-compensated tubular ceramic capacitors, 5 pf to 1000 pf, with a manufacturer's rated operating voltage of 500 volts were supplied by Erie Technological Products, Incorporated. These were manufactured and tested in accordance with specification GA9910 Revision G, and Erie EP3210. Both types of capacitors were screened at Bell Telephone Laboratories by the following procedure: a. Capacitance and conductance measured at 1 KHz. b. A life test for a minimum of 100 hours at room temperature under rated voltage. c. Capacitance and conductance measured at 1 KHz. Capacitors of these types qualifying for flight use had a failure rate of less than 0.002% per thousand hours.

Table 5-2. SPECIFICATIONS AND SCREENING PROGRAMS (continued)

COMPONENT	TYPE	SPECIFICATION/SCREENING
Resistors	A. Carbon composition	Type CD and EB resistors were supplied by the Allan Bradley Corporation. All resistors were screened at Bell Telephone Laboratories in groups taken from the same manufacturing lot for each value screened. The screening procedure was as follows: 1. Resistance measured at room temperature. 2. Baked at +105°C for 96 hours. 3. Resistance measured at room temperature. 4. Ten temperature cycles between -55°C and +85°C for a period of 120 hours. 5. Resistance measured at room temperature. 6. Noise measurement. 7. Baked at 105°C for 96 hours. 8. Resistance measured at room temperature. Acceptability was based on any change in resistance occurring between step 3 and step 8 being within the norm for group, and also on the noise level measured in step 6. Resistors qualifying for flight use had a failure rate of 0.0001% per thousand hours or better.

COMPONENT	TYPE	SPECIFICATION/SCREENING
Resistors (continued)	B. Metal film	Types NA60D and RN55D resistors were supplied by Corning Electronic Products Division. The screening procedure for metal film resistors is identical to that given above for carbon composition resistors.
Transistors	A. Silicon bipolar	These were supplied by Motorola Semiconductor Products, Inc.; types 2N2222 (NPN) and 2N3251 (PNP) were chosen on the basis of their suitable electrical characteristics, reliability demonstrated through use in other BTL programs, and good tolerance to radiation damage (on the basis of several sample lots tested). All devices were ordered to meet the requirements of Mil-F-19500 and G657490 in addition to BTL specifications G383745 for the 2N2222 and G383746 for the 2N3251. (Prior experience had shown Motorola capable of delivering devices to these specifications. However, because of the short program schedule and unexpected difficulties encountered, many devices were accepted without meeting the full specifications.) Screening was done by the manufacturer on a lot basis. A prior condition for lot acceptance was a sample radiation test. All transistors in lots meeting this requirement were then subjected to the following preconditioning steps in the order listed:

Table 5-2. SPECIFICATIONS AND SCREENING PROGRAMS (continued)

COMPONENT	TYPE	SPECIFICATION/SCREENING
Transistors (continued)	A. Silicon bipolar (continued)	1. Temperature aging at +250°C for 60 hours. 2. Temperature reverse voltage at +175°C for 100 hours (PNP devices only). 3. Life defect according to G657491, Method I, 3X rated power at +25°C for two hours. 4. Temperature cycling to Mil-FTD750, Method 1051, Condition C. 5. Constant acceleration at 20,000G. 6. Shock 5 blows to Mil-FTD750, Method 2016. 7. Particle test to G657491, Method 201. 8. Leak test at 90 psi for one hour. 9. Leak test at +180°C to G657491, Method 6. A five-parameter electrical test was performed on each device following steps 1, 2, 3, 5, and 6. For lot acceptance, a PDA (percent defective allowed) of 15% applied to each step except 1, 4, and 5. In these steps, defectives were removed before proceeding. A total PDA of 30% applied for all steps following 1. All transistors in accepted lots were give a visual and mechanical examination and an electrical test which measured 16 parameters. A sample group of devices

COMPONENT	TYPE	SPECIFICATION/SCREENING
Transistors (continued)	A. Silicon bipolar (continued)	was subjected to additional environmental and mechanical tests, some of which were destructive. The supplier was unable to meet lot preconditioning requirements for the 2N3251; these devices were supplied, instead, to an expanded version of Mil-F-19500 (plus sample radiation tests). The radiation tests had to be waived for most of the 2N2222 devices; for some lots, a Mil specification was substituted for preconditioning to expedite delivery in time to meet our schedule. Those transistors for circuit applications where radiation damage was critical were screened and selected at BTL.
	B. Germanium transistors	2N964A (PNP) transistors for a special application in thin-film discriminators were also supplied by Motorola. These devices were ordered tested to BTL specification G365393.
Diodes	A. Tunnel diodes	1N3713 germanium tunnel diodes were suppled by the General Electric Corporation. The screening of these devices was performed at Bell Telephone Laboratories, Laureldale, Pennsylvania, under the following conditions: 1. Shock 5 blows 1500G as per Mil-STD750, Method 2016. 2. Constant acceleration 20,000G, one minute as per Mil-FTD750, Method 2006.

Table 5-2. SPECIFICATIONS AND SCREENING PROGRAMS (continued)

COMPONENT	TYPE	SPECIFICATION/SCREENING
Diodes (continued)	A. Tunnel diodes (continued)	3. Vibration variable frequency, 100 Hz to 2 kHz as per Mil-FTD750, Method 2056. 4. Mechanical inspection. 5. Electrical measurement of 4 parameters. 6. Life defect (high temperature accelerated aging test). All units were subjected to 250 hours at +100°C under bias. DC tests were made at 24 hours, 100 hours, and 250 hours during this step. 7. Electrical measurement of 4 parameters at room temperature. The above tests were designed to assure 0.001% per thousand hour failure rate at 50°C based on previous experiments done on diodes of the same type.
	B. Signal diodes	High reliability silicon epitaxial signal diodes were supplied by the Western Electric Company, manufactured and screened to specification GA53930, and electrically tested to GF-40163-L1-3.

COMPONENT	TYPE	SPECIFICATION/SCREENING
Transformers, Inductors, and Delay Lines		These devices were specially made by the Components Laboratory of Bell Telephone Laboratories, Whippany, New Jersey. The following types of devices were supplied. 1. Modified M-derived five-section delay line. 2. Five-winding noise rejection transformer. 3. Bias supply oscillator transformer.

5.2.2 Thin-Film Integrated Circuit Fabrication and Testing

Bell Telephone Laboratories at Allentown, Pennsylvania, in collaboration with the Allentown Works of the Western Electric Company, developed and produced the thin-film integrated circuits for this project from electronic designs supplied by Murray Hill. Each experiment required the following quantities of these devices: 25 operational amplifiers, 21 zero-crossing discriminators, 7 pulse shapers, 47 linear gates, and 37 potentiometer networks.

The first step in producing these integrated circuits was to develop the most efficient layout. Substrate size was held to the minimum which would accommodate the discrete components with adequate clearances. A standard width for the three active circuits (A, B, and C in Figure 4-2) which allowed room for two parallel rows of transistors with tantalum capacitors mounted between rows as seen in Figure 3-3 was adopted for most efficient use of the master ceramic substrate described later. Unavoidable crossovers were handled with wire straps on the component side. The thin-film resistor layouts fitted easily into the available areas with line widths well within the state of the art. The highest value resistor was 56K ohms which required a 3-mil line width. Two of these can be seen just above center on substrate A in Figure 4-3. Low-value resistors were made wide to increase their track length and minimize end effects from application of the electrolyte solution and the anodizing process. The substrate material was high-density aluminum oxide ceramic. Punching of the lead hole patterns was done with the alumina in the green state. Each type of circuit was batch processed on a 3-3/4 x 4-1/2 inch master ceramic substrate which was later diced into individual circuits with a diamond saw. After firing and glazing, the master was sputtered with an even film of tantalum nitride with a sheet resistivity of between 50 and 60 ohms per square. Thin-metal films which ultimately formed the circuit paths and terminations were evaporated on to the substrate in layers, starting with nichrome, followed by copper, and finishing with palladium on the outer surface. Next, the groups of circuit path patterns were photo-etched in the metal films. Following this, the resistor tracks were etched in the exposed tantalum between the circuit paths. After inspection of the resulting circuit patterns, each resistor on the master substrate was individually adjusted to its final value by anodizing its surface. This process converts the surface of the tantalum electrolytically into a layer of tantalum pentoxide, an insulator. The depth of anodization determines the resistance but, since it can only be raised in this process, the resistivity of the film at the beginning must be 10 to 20 percent lower than the design value. The anodizing process is automatically controlled by a bridge circuit which monitors the resistance and shuts off the current when the correct value is reached. Resistance tolerances of 1 to 10 percent were specified for these circuits, although the process is capable of far greater

accuracy. Tantalum film resistors thus formed remain stable, protected by their inert covering which is unaffected by normal handling during component assembly operations. The master substrate is finally sliced into individual circuits.

Each circuit substrate passing in-process inspection was assembled with its components, straps, and leads. Soldering was accomplished by immersing the flux-coated thin-film circuit side of each ceramic in a solder pot for several seconds. After cleaning and final inspection, the completed integrated circuits were shipped to Murray Hill. At Murray Hill, all thin-film integrated circuits received were given a follow-up inspection, assigned serial numbers and inspection cards. Electrical tests were performed on a multicircuit test stand which could accommodate half the total complement of circuits for one experiment. The test stand was designed to fit into a temperature chamber and connect to a remote test panel through a multiple feed-through connector interface. Power supply lines, inputs, and outputs of all circuits under test could be examined through selection by a system of switches. Operational checks and reference measurements of critical parameters were first made at room temperature and recorded on the inspection card. Particular emphasis was placed on pulse characteristics which were examined on an oscilloscope. Following these tests at room temperature, the complement was temperature cycled between +60°C and -20°C (10°C more in each direction than the experiment test specification), for five complete cycles of 1-hour duration each. After temperature cycling, the high- and low-temperature limits were sustained and the initial test sequence was repeated and the results recorded. One last test sequence was performed upon return to room temperature for comparison with the first to verify stability. All units completing the test were mechanically inspected for any change in appearance resulting from temperature cycling. The recorded temperature performance data for each circuit was carefully examined. Any units showing abnormal tendencies were rejected for flight use. One final operation before each thin-film circuit was released for encapsulation prior to integration with a flight motherboard was the forming of omega-shaped strain relief bends in all terminal leads. This was carefully performed on the special multiple-lead bending tool shown in Figure 5-2. These bends were necessary to prevent strains on the substrate resulting from mounting the encapsulated units directly against the printed circuit boards.

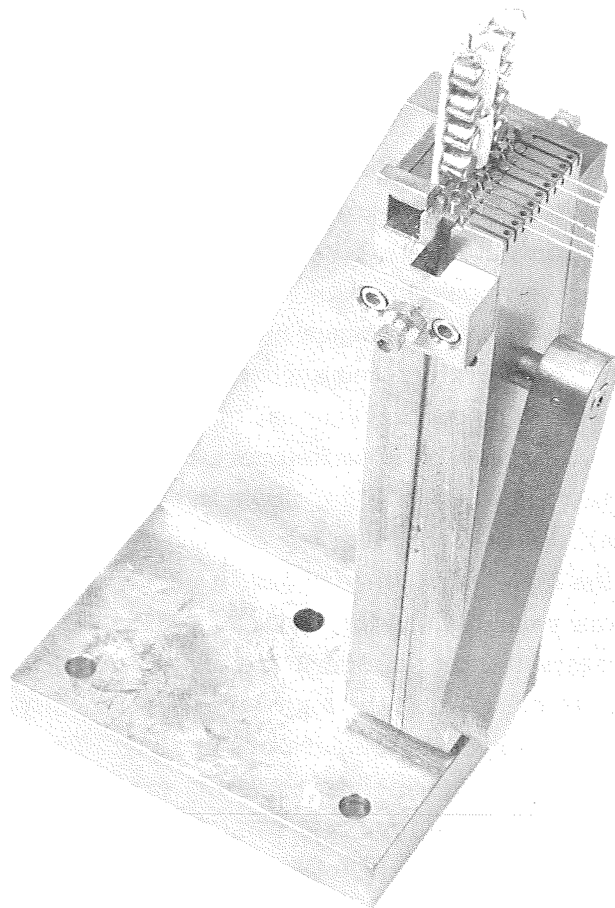

Figure 5-2. Thin-Film Circuit Lead Bending Tool

Chapter 6

CONSTRUCTION

6.1 PRINTED CIRCUIT BOARDS

6.1.1 Layout and Art Work

The production of a printed circuit board began with the preparation of a 2:1 layout drawing showing a view of the printed circuit side with the positions of components outlined as they would be seen when looking through the board. A draftsman designed each layout from schematic diagrams, working with the guidance of the packaging engineer. The assembly drawings and all printed circuit art work originated from these layouts. Except where cross-coupling or interference problems dictated, components were placed for best packaging efficiency and minimum conductor cross-over. Axial lead devices were normally laid out against the board and positioned vertically only in areas of unavoidable high density. Limits were set for minimum center-to-center lead hole spacing for each type of horizontally mounted component to allow enough length to safely form the lead bends. Printed path width was typically 0.032 inch, with a minimum of 0.020 inch. The same dimensions applied to the clearance between paths. At the board edge, a minimum of 0.050 inch was maintained. Solder lands were of the elongated circular type in various sizes depending upon the layout requirements but always providing a minimum of at least 0.08 inch clinched lead contact length. Specially shaped terminal lands at the ends of the boards were designed to mate with commercial printed circuit board connectors with either 0.10 inch or 0.078 inch center-to-center spacing.

Two reversed prints of the completed layout were made for the ground plane art work to be used on the opposite side of the board, one showing the size and location of clearance areas for component leads and the other showing the position of selectively solder plated lands for ground through-connections. Commercially available black tape, in pre-cut strips and land patterns, was used for the art work. All lands were prepunched for lead hole location; special land shapes were made by cutting or adding to the standard sizes. Taping was done on a mylar drawing form placed over the layout drawing on a large light box. Separate ground plane art work was made by cutting out clearance areas from a transparent sheet of adhesive red plastic on another drawing form laid over the appropriate reverse print.

A third piece of art work for the selectively solder-plated ground plane lands completed the set. Registry between all three pieces was assured by punched targets on each, referenced to the centers of the through-bolt holes drawn accurately on the layout.

6.1.2 Fabrication

All printed circuit boards were processed at Bell Telephone Laboratories, Murray Hill. A few special operations which were required to produce these boards will be discussed. The material used was 0.032-inch-thick Fiberglas-epoxy board with 1-ounce copper on both sides. Individual oversized blanks were supplied for each circuit board required. Every blank was predrilled for the two 0.140-inch-diameter through-bolt holes by using a drill jig to assure accurate and repeatable spacing. This step was important for proper alignment of the three printed circuit patterns and for the accuracy of the in-process machining to follow. Circuit boards were protected by cardboard separators during all machining operations and inspected for scratches or other damage before being released for the next step in the sequence.

Half-size negatives of the art work were accurately punched with 0.140-inch-diameter holes centered on the two reference targets. A frame, consisting of two lucite plates with the same hole pattern and fitted with short dowel pins, was used to align the negatives on both sides of the photosensitized circuit board blank during the exposure process.

After the circuit pattern had been etched, the blanks were carefully milled to the correct width. Electrolus copper was then deposited over the freshly milled edges and onto the ground plane side by 0.05 inch for electrical contact. These edges and the terminals at the end of the board were gold-plated to maintain a good conductivity. The printed circuit and the through-connection lands on the ground plane side were solder-plated. The remainder of the ground plane was not solder-plated to reduce circuit board weight. After the printed circuit process was complete, the ends of the boards were machined to their final dimensions and all component lead holes were drilled. Each circuit board was then thoroughly inspected for defects or damage, as described in Paragraph 6.3.5, before being accepted for flight use.

6.1.3 Preparation for Assembly

The first step in the preparation of a printed circuit motherboard for component assembly was to attach and solder the strap wires which connect the ground plane through to certain printed circuit lands. Following this, insulation consisting of a 0.001-inch-thick thermal adhesive coated mylar sheet was bonded to the ground

plane side of the board under heat and pressure. The board and mylar sheet were clamped together between two pieces of thick silicone rubber in an aluminum jig and heated to 150°C in an oven. This resulted in an excellent bond between the two with the mylar following even the contour of the etched pattern in the 0.0015-inch-thick copper. The insulating skin was trimmed and all lead holes pierced before mounting the components.

6.2 ASSEMBLY AREA

White room conditions were not a requirement of this project. The main objective was to provide a controlled area separate from other less critical laboratory activities where flight hardware could be safely assembled and stored. Figure 6-1 shows a view of the ATS experiment flight hardware assembly room. White nylon coats were worn to prevent contamination from metallic particles which might have been picked up on the clothing of the assemblers while at other locations within the building. Smoking and eating in the area was prohibited and only authorized

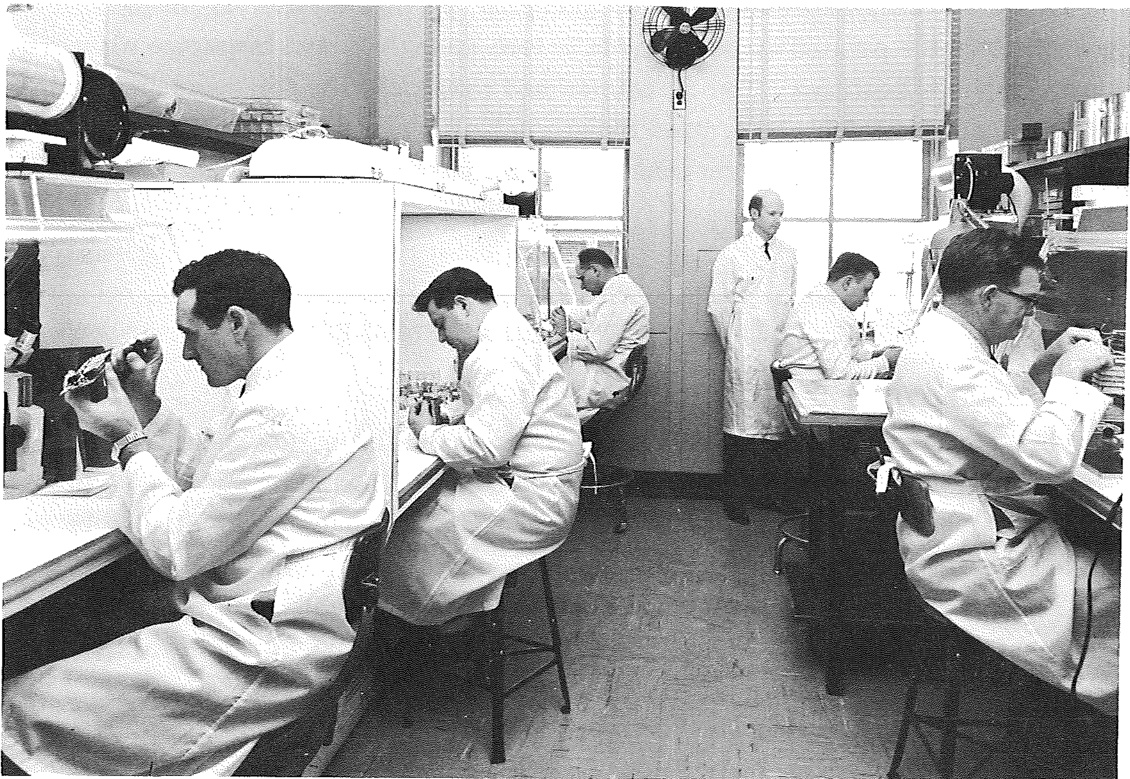

Figure 6-1. Flight Hardware Assembly Room

personnel were admitted. The room was air-conditioned by a self-contained unit and fresh air entered through a filter. A laminar flow hood containing an absolute filter was in continuous operation to reduce the overall dust level and to provide a local white working area when needed. Isolation between individual work positions was achieved with plastic bench top enclosures. These enclosures were fully open at the front and wide enough not to restrict movements of the assemblers. In this way, wire lead clippings and bits of solder were limited to each work location and were easier to control. Visibility of these stray pieces was increased by using replaceable white cardboard on the work surfaces. The hoods also kept items not essential to a particular assembly operation from cluttering the work positions and prevented possible damage from things stored overhead dropping onto the work. All flight parts and subassemblies in process were kept in plastic containers and removed from the workbenches to a locked storage cabinet at the end of the day. Polyurethane foam encapsulation of completed hardware was performed in an exhaust hood located in one corner of the room.

The assembly staff consisted of four assemblers (one of whom was the lead man and inspector), a technician, and a packaging manager. Two assemblers spent their full time mounting and soldering components to printed circuit motherboards. A third specialized in the interconnecting harness wiring. The lead man/inspector managed the work assignments and bookkeeping, performed special preparatory operations on the printed circuit boards before assembly, and inspected all work at prescribed milestones. The technician had responsibility for component procurement, stock control, integrated circuit screening, and the assembly parts kits. The packaging manager was responsible for all phases of the packing program and quality control.

6.3 MOTHERBOARD ASSEMBLY

6.3.1 Parts Kits and Records

All parts, parts lists, special instructions, and inspection sheets for each motherboard were prepared in kit form in advance of assembly and stored in plastic containers until needed. Parts kits were prepared in the form of a display by inserting the components upright into a sheet of styrofoam, as shown in Figure 6-2. This arrangement was very convenient and speeded assembly time by reducing the amount of searching and handling otherwise necessary if parts had been supplied in envelopes. The parts list with each kit identified all components by circuit number, value, tolerance, and type. Each printed circuit board was stamped with a serial number to identify it with its assigned paperwork. An inspection sheet for recording all information concerning the status of the motherboard was attached to

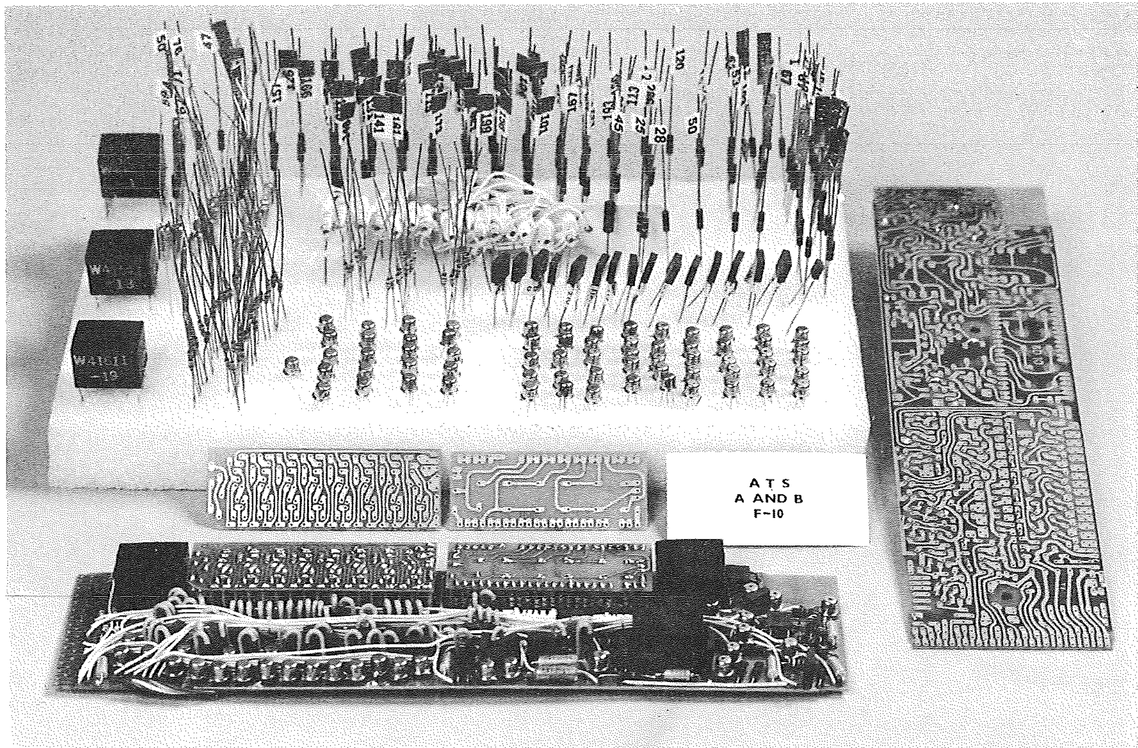

Figure 6-2. Motherboard 10 Shown with its Parts Kit

the front of the parts list. Headings and spaces on this sheet were provided for each construction milestone which were to be dated and initialed by the assembler and inspector upon completion. One of the duties of the inspector was to maintain a chart showing the status of all motherboards being processed. At the beginning of the project, a list of general assembly practices and handling procedures was issued to each assembler. Instructions for special operations on each type of board were included with the kit paper work.

Master assembly drawings for each board contained all the information necessary to identify and place the components and strap wiring. These drawings were kept up to date and no other copies were used. Each was mounted on cardboard and covered with a lucite sheet so that the assemblers could check off the components with a crayon pencil as they were installed.

6.3.2 Assembly Practices

Assembling carefully screened components onto the motherboards without degrading their reliability called for special handling precautions. Figure 6-3 shows an ATS motherboard being assembled while clamped in a handling fixture. Grooves

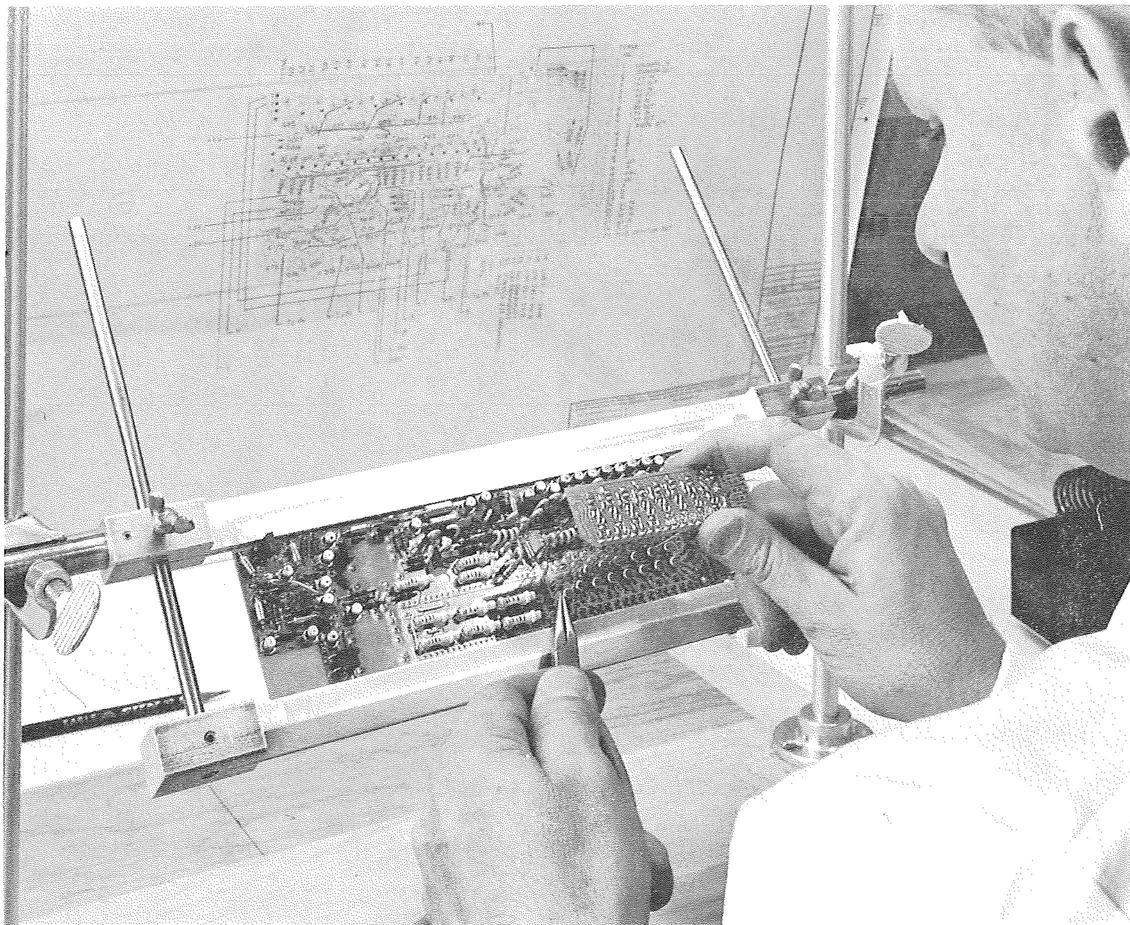

Figure 6-3. Motherboard 10 During Assembly

milled in the frame of this fixture held the board by its edges to prevent warping during component mounting and soldering operations. The fixture could be rotated axially for rapid access to either side of the board. In this way, the motherboards were placed in an ideal working position for the assembler and were protected against being dropped. Mounted components were kept out of contact with the workbench surface where they might be damaged or pick up lead clippings and solder scraps.

Component leads were bent by using specially contoured pliers to isolate bending forces from the component body and prevent marking the leads. Lead bends had a minimum radius equal to twice the lead diameter and were not closer than 1/16 inch to the component body or end seal. Mechanical shock from lead clipping was isolated from the component body with pliers clamped between it and the cutting point. Axial lead components were, in general, mounted horizontally against

the board. However, in a few areas of unusually high density, resistors and diodes were placed vertically. In these situations, the lower end of the component was spaced 0.05 inch from the board. Ceramic capacitors with end radial leads were spaced 0.1 inch from the board to permit the attachment of heat sink clips during the soldering operation. Transistors were raised by the same amount to avoid stressing the header seals during lead clinching. Special spacing gauges were provided for each type of component to speed the mounting process. Assemblers were instructed never to twist or pull on component leads during the bending or mounting operations; such stresses can break the seal between the lead and component body. In certain dense vertical mounting situations, leads were jacketed with a silicone varnished Fiberglas sleeving as a measure of protection against shorting to one another during the encapsulation process. Strap wiring was insulated No. 24 solid tinned copper wire, thermally stripped. Component leads and straps were clinched against their respective printed circuit lands and cut to a length of 0.08 inch from the mounting hole. No soldering was done until all components and wires were mounted and their correct value and placement verified by the inspector.

6.3.3 Soldering

Weller Electric Corporation's Model W-TCP temperature-controlled soldering irons, equipped with 700°F 1/16-inch screwdriver-type replaceable tips, were used exclusively. These small lightweight irons were ideally suited to printed circuit board work. A wet sponge provided a safe means for cleaning the iron-clad tips, so as to assure optimum heat transfer to each connection. The solder for most applications was 0.025-inch diameter Kester 60/40 with a pure rosin-flux core. Where connections would be subjected to low temperatures in space, special solder was used which contained a small percentage of antimony to prevent the formation of gray tin (Nassau No. RM728226, manufactured by the Nassau Smelting and Refining Company).

Components with soft solder seals or internal connections (ie: tantalum and ceramic capacitors) were protected from damage during soldering by attaching small, flat jaw, copper heat sink clips to their leads. Trimming components were temporarily mounted and tack-soldered with unclinched leads for easier removal after testing.

A rapid and effective vacuum-operated desoldering device was used for removing solder from unsatisfactory joints. It consisted of a large flask reservoir connected to a half-atmosphere house vacuum line. A glass medicine dropper was fitted to a rubber hose which was attached to a piece of glass tubing extending through a rubber stopper to the bottom of the flask. Water at the bottom of the

flask trapped and prevented solder particles from entering the vacuum line. The shape of the dropper nozzle produced a high velocity inward air flow which removed solder from a heated connection so efficiently that in most cases the lead became free. Most important, the whole operation could be performed so rapidly that no damage to the printed circuit boards occurred. Several commercial desoldering devices were tried which proved ineffective and, in some cases, detrimental to the printed circuit board. Only the assemblers were permitted to solder or desolder components. This prevented degradation of connections and components from tack-soldering by technicians during the testing and trimming operations. Although all soldering flux used was inert, it was nevertheless cleansed from the boards after assembly to facilitate inspection of the solder joints and prevent adherence of foreign particles.

6.3.4 Testing and Trimming

As mentioned in Paragraph 4.1.1, the circuit boards were designed to plug into printed circuit connectors on a large test stand which would accommodate the whole system of motherboards. By using this method, the usual hazards associated with testing a temporarily connected system of unencapsulated boards was greatly reduced. Individual boards could be quickly disconnected from the test stand, component values adjusted if necessary, and then reinserted to continue the test. The test stand provided security and stability for the boards on the bench. It was designed to simulate as nearly as possible the configuration of the system in its assembled form in order to eliminate the necessity to make further adjustments after the final assembly. Each board could be separated from the rest of the stack while still connected, permitting full access to all test points on both sides of the board. The test stand was also designed for operation within a Wiley Model C-106-3600 temperature chamber.

Trimming an experiment of this complexity involves the careful adjustment of many interacting parameters such as amplifier gains, discriminator levels, pulse shapes, and timing. Many of these adjustments were made with miniature wire-wound trimming potentiometers. No mechanically variable components were considered reliable enough for flight use. As the adjustments for each section of the experiment were completed, these potentiometers were removed from the circuit boards without disturbing their settings and carefully measured on a resistance bridge. Highly stable thin-film potentiometer networks, described in Chapter 3 and shown in Figure 4-2, were individually adjusted to match the setting of a particular trimming potentiometer. Adjustment of these networks involved bridging out elements of the resistor strong to achieve the desired value. The whole operation was performed with the aid of a microscope by an assembler trained in the

intricacies of soldering to the small plated circuit paths on these ceramic substrates. It was necessary, for a reliable connection, to place a mechanical bridge in the form of hot solder-coated No. 36 copper wire across the 0.005-inch gap before the application of solder. Liquid flux was applied to assure an even and rapid wetting of the plated paths. The assembler mastered the technique so well that these networks could be adjusted at the rate of 12 per hour. Previously adjusted networks could be changed with ease by carefully cutting out a section of the fine wire bridge with a small knife blade under a microscope. After verification of its specified resistance setting, each thin-film resistor network was permanently installed in its respective trimming potentiometer location on the circuit board. The board was then returned to the test stand to recheck the levels for agreement with the previous adjustments. Each group of adjustments was secured in this manner before proceeding to the next. In the case of capacitors, adjustable elements were removed from the boards, measured, and substituted with fixed temperature-compensated ceramic capacitors of the nearest commercially available value. The small differences sometimes resulting between the fixed and variable elements were compensated by adjustment of trimming resistors elsewhere in the circuit. Complete records of all adjustments and changes in component values during this phase of work were kept with the paper work for each board.

6.3.5 Inspection

Thorough inspections were performed at various milestones in the sequence of assembly operations beginning with the printed circuit board blanks and ending with the completed experiment package. The inspector was highly skilled in his field, having served in the same capacity during the fabrication of the electronic assemblies for the Telstar program. A wide-field binocular microscope with an adjustable range of magnification of from 7X to 80X was used as an aid for close examination of components and connections. Table 6-1 outlines the schedule.

Table 6-1. INSPECTION PROCEDURES AND SCHEDULES

AREA	OPERATION
Printed Circuit Boards	1. Inspect predrilled blanks for flaws and scratches in the copper surface before delivery to the printed circuit shop. 2. Inspect the boards after machining to the correct width, prior to edge plating, for damage to the circuit pattern, roughness of the milled edges, and correct width of the board.

Table 6-1. INSPECTION PROCEDURES AND SCHEDULES (continued)

AREA	OPERATION
Printed Circuit Boards (continued)	3. Inspect each board after completion of all printed circuit processing, final machining, and hole-drilling operations for the following: A. Scratches on (1) Paths and lands deeper than the surface of the solder plating, (2) The surface of the substrate bridging paths or lands. B. Holes and notches in the paths resulting from the printed circuit process exceeding 25 percent of the path width. C. Lifting of printed paths and lands. D. Uniformity of solder-plating. E. Metallic bridging between paths and lands. F. The condition of the over-edge plating: (1) Clearance to the nearest conductor on the printed circuit side (0.020 minimum). (2) Smoothness and uniformity. G. Dimensional accuracy. H. General condition of the board: (1) Sharpness of the printed circuit pattern and clearance areas in the ground plane. (2) Errors or omissions in the drilling of the component mounting holes. (3) Cleanliness. 4. Inspect after mounting and soldering the strap wire through connections between the ground plane and printed circuit for the quality of the soldered connections and any strap omissions. 5. Inspect each board after completion of the mylar insulation bonding process for a proper bond and general appearance.

Table 6-1. INSPECTION PROCEDURES AND SCHEDULES (continued)

AREA	OPERATION
Components and Integrated Circuits	The component technician was responsible for visual inspection of all parts prior to preparing the assembly kits.
Partially Assembled Motherboards	Inspect the partially assembled motherboards (all components excluding thin-film circuits mounted but not soldered). 1. Inspect for correct assembly. Verify components with the assembly drawing and parts list as follows: A. Value of component. B. Location of component. C. Type of component. D. Polarity. 2. Inspect the mechanical condition of components and board. A. Correct positioning and clearance of components and leads. B. Lead bends. C. Any damage to components, their leads, or the printed circuit due to mounting operations.
Inspection of Components	Inspect after all components have been soldered and strap wiring has been installed but not soldered. 1. Verify the correct connection, routing, and dress of each strap wire against the assembly drawing. 2. Damage to the components, strap wire, and insulation or printed circuit pattern as a result of installing the strap wires.

Table 6-1. INSPECTION PROCEDURES AND SCHEDULES (continued)

AREA	OPERATION
Completely Assembled Motherboards	Inspect the completely assembled motherboard following mounting of the thin-film circuits and soldering of all remaining connections. 1. Condition and appearance of all components and leads. 2. Check for the inclusion of wire clippings, solder balls, and other foreign particles which might possibly have become entrapped among the components or printed circuit. 3. Inspect all solder connections for compliance with established standards.
Trimmed and Tested Motherboards	Inspect all motherboards after trimming and testing following the installation of fixed components which replace the adjustable ones. 1. The correct placement and value of replaced components and the quality of their solder connections. 2. Damage resulting from the testing and trimming operations. 3. A final search for entrapped foreign particles on both sides of the board coupled with a general vacuum cleaning operation using the same type of device described for desoldering.
Encapsulated Motherboards	Inspect each motherboard following the foam encapsulation process. 1. The condition of the foam encapsulation. A. Uniformity and dimensions. B. Cavities exposing components or leads. 2. Damage to the printed circuit from handling during the process.

Table 6-1. INSPECTION PROCEDURES AND SCHEDULES (continued)

AREA	OPERATION
Encapsulated Motherboards (continued)	Boards having completed this final examination were signed off on the inspection sheet and were ready for interconnection with other completed boards in the harness-wiring operation. All signed inspection sheets, notes, and parts lists for each board were collected and filed in a notebook for that particular flight model.
Interconnecting Harness Wiring	Inspection is described in Section 6.5.

6.4 ENCAPSULATION

As previously described in Paragraph 4.1.2, the component side of each motherboard was individually encapsulated. The material used was Emerson & Cumming, Incorporated Eccofoam FP with catalyst 12-2. This combination cures to a rigid, thermo-setting, unicellular, polyurethane foam with a density of two pounds per cubic foot. Unlike its hard setting, high temperature counterpart, Eccofoam FPH, this foam has some degree of flexibility and can be compressed without crumbling. It was this property that was used to improve the mechanical integrity of the assembled stack.

6.4.1 Integrated Circuit Encapsulation

Since the thin-film circuits were mounted inverted on the motherboards, their components were sandwiched between it and the ceramic substrate. To insure a proper foam filling under these devices they were prepotted prior to motherboard assembly. Figure 6-4 shows a nest of special molds used for this potting operation. The foam was cast to a predetermined height above the components by inserting the substrates into flexible silastic molds which retained them around the edges in a groove near the bottom of the mold. Teflon cover plates, with close-fitting holes for the leads, prevented foam run-up and provided a nonadhering top surface for the mold. These were clamped to the mold under aluminum plates attached with screws to the sides of the mold nest. The position of both plates was determined by locating pins.

When all molds and nests had been loaded, a small quantity of foam resin was placed in a disposable container with the specified proportion of catalyst by weight

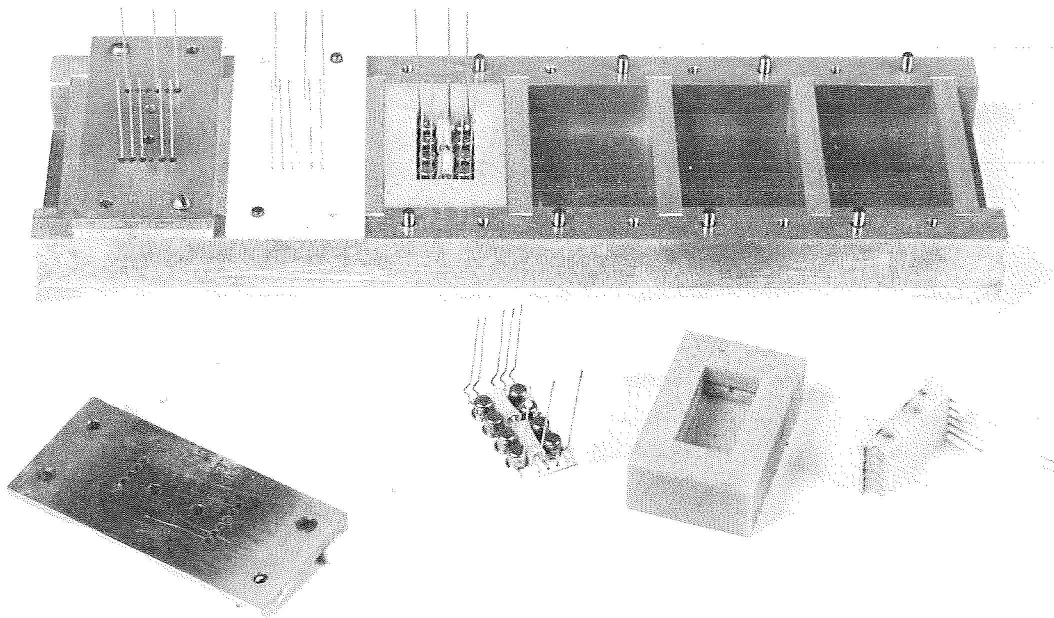

Figure 6-4. Thin-Film Circuit Foam Encapsulation Molds

and thoroughly blended by hand for one minute. This mixture was placed in a 5-cc plastic disposable syringe and a small quantity was injected into each mold in the nest. A pair of concentric relief holes in the two covers limited the amount of internal foaming pressure. Curing was accomplished in one hour at +60°C in a circulating air oven. An encapsulated substrate is shown in the lower right corner of Figure 6-4.

6.4.2 Motherboard Encapsulation

A procedure similar to the one previously described was used to encapsulate a complete motherboard. Large silastic molds were specially prepared for each type of motherboard which retained them at the required depth in a snug-fitting groove around the inner edge of the mold. The mold was made 0.1 inch narrower than the board in order to limit the foamed width to 0.05 inch in from the upper and lower edges to assure clearance for contact between the plated edges of the boards and the finger contact sheets. A greater overlap at the rear of the board masked the terminal area during encapsulation. Other clearances in the foam required for each type of board were provided by protuberances in the mold or separate inserts.

The aluminum mold nest, shown in Figure 6-5, was comprised of a number of aluminum frames of various thicknesses so that its depth could be adjusted for

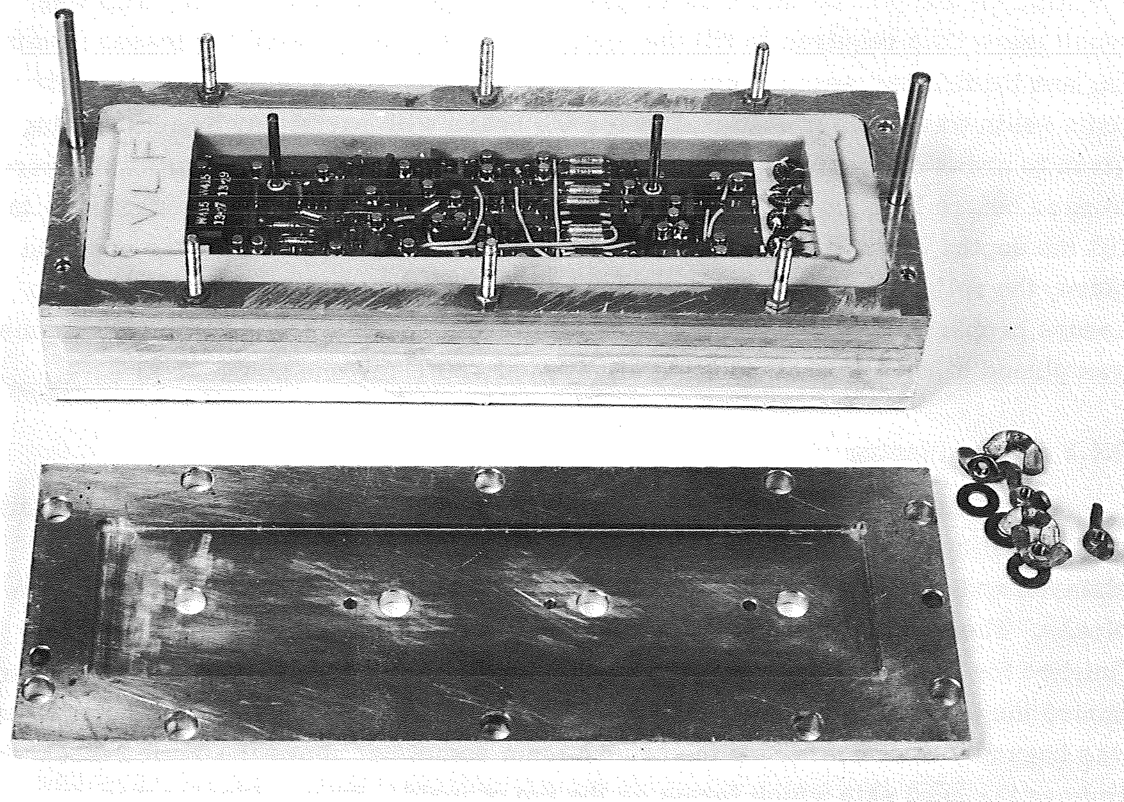

Figure 6-5. Motherboard Foam Encapsulation Mold

different molds. The motherboards were accurately positioned within the nest by close-fitting dowel pins inserted in the through-bolt holes in each board and corresponding holes accurately located in the aluminum baseplate and cover of the nest. This baseplate and cover and the various side layers comprising the nest were all aligned by two large dowel pins in the ends. The under side of the motherboard was supported against the foaming pressure by aluminum spacers around the dowel pin between the board and the bottom of the nest. Further support was provided by a piece of flexible polyfoam cut to fill this gap. Aluminum sleeves with a silicone release agent applied were slid over the dowel pins above the board after the mold was placed in the nest. These formed the necessary clearance around the through-bolt holes for insertion of the aluminum stack spacers at final assembly. The aluminum nest cover was designed to seal against the top of the silastic mold around the edges, held down by wing nuts on bolts around its parameter.

At the start of the foaming process the cover was off of the nest and in a state of readiness with its inner surfaces thoroughly coated with release agent. Approximately 30 grams of foam resin was weighed into a container thoroughly mixed with

the catalyst and poured into a 30-cc plastic syringe. This quantity of foam was much more than required to fill the mold but the excess allowed for losses in mixing and loading and assured proper foaming pressure within the mold. The mixed foam resin was injected uniformly over the board with particular attention being given to areas of greater impedance to foam flow. This operation was easily performed before installing the cover because the foam did not expand sufficiently to fill the depths of the mold for several minutes after injection. With the cover in place, the relief holes were observed for foam overflow which was necessary to assure proper filling of the mold. After the foam expansion was complete, the mold was placed to cure in a circulating air oven at +60°C for one hour.

6.4.3 Foam Planing

The foam was molded deeper than needed so that it could be accurately planed to the final height. This operation was performed in a fixture with the boards clamped and supported along their upper and lower edges by long, notched Teflon blocks. These blocks extended above the board and determined the height of the finished foam. The boards were held with screws in threaded stand-offs which supported the board in the center under the through-bolt holes. The planing operation was begun by first sawing off the excess foam somewhat above the Teflon blocks to remove the hard skin which forms on the top of molded foam. Planing was done with a very large, coarse flat file. A coarse file was used because it cut with less pressure than a fine one and produce nearly identical results. The weight of the file itself provided most of the planing pressure and the whole operation was performed gently by guiding it back and forth evenly over the foam until it was limited by the tops of the Teflon blocks. The foam surface thus obtained was moderately coarse, compressible and level to within 0.010 inch of the design height. A foamed and planed board is shown in Figure 6-6.

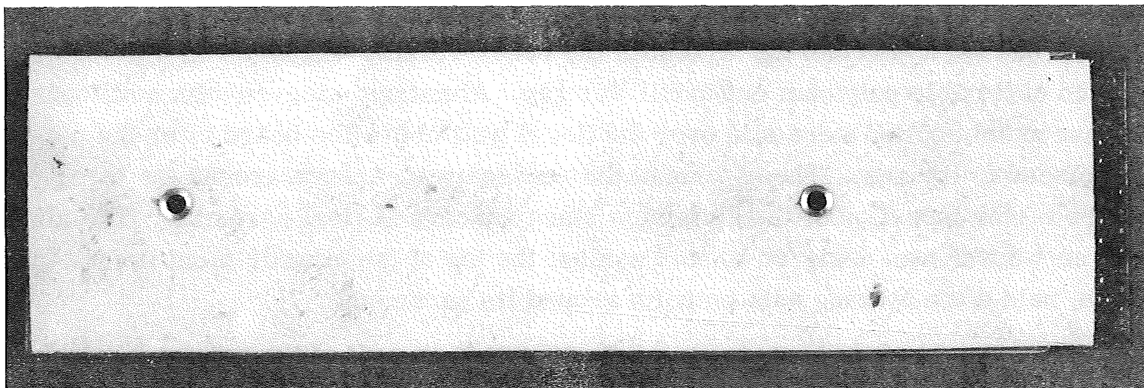

Figure 6-6. Foam-Encapsulated Motherboard

After all the motherboards and the center partition had been foamed and planed as described, they were mounted together in a stack in their correct positions between two heavy aluminum end plates. The whole stack was pressed together to seat the solder joint protrusions on the unfoamed printed circuit side of each board into the foam on the next board to achieve a board-to-foam contact throughout the stack. Pressure was supplied for this operation by tightening large wing nuts on long bolts running through the stack and the aluminum plates. Before proceeding with the harness wiring, the stack of boards was checked for proper fit into the experiment housing.

Two more foaming operations remained before the package was complete. These are described under Final Assembly in Section 6.6.

6.5 ELECTRONIC STACK ASSEMBLY

6.5.1 Preparations

After completion of the motherboard encapsulation process and a post-encapsulation inspection, the entire complement was released for permanent interconnection as a flight electronic system. Terminal lands along the rear edges of the motherboards, which had previously been used to connect them to the test stand, now served as soldering lands for attachment of the harness wires. All information for interconnecting the boards was supplied to the assembler in the form of an enlarged view of the terminal land layout and a connection chart listing the terminal number, color code, origin, and destination of every wire for each board in the stack. Some boards required 40 to 50 connections.

Wiring of the harness was done with the boards mounted on a simple jig shown together with the whole stack in Figure 6-7. The jig consisted of an aluminum bar with two long 1/8-inch-diameter rods attached to it and spaced so that they could be inserted into the through-bolt holes on each board. This was then clamped in a small wiring vise equipped with a universal joint permitting the harness work to be conveniently positioned.

Stranded No. 26 wire was used in the harness (Raychem Corp., specification 44 "Outer Space Wire"). The insulation was available only in white except by special order. In view of the large number of identifying color combinations needed, coding was done instead with colored dots of paint applied to the standard white insulation during the harness assembly.

Before starting the harnessing operation, the gold plating was removed from the terminals on each board to prevent embrittlement due to excessive gold concentration in the solder joint. Since gold dissolves very rapidly in hot solder,

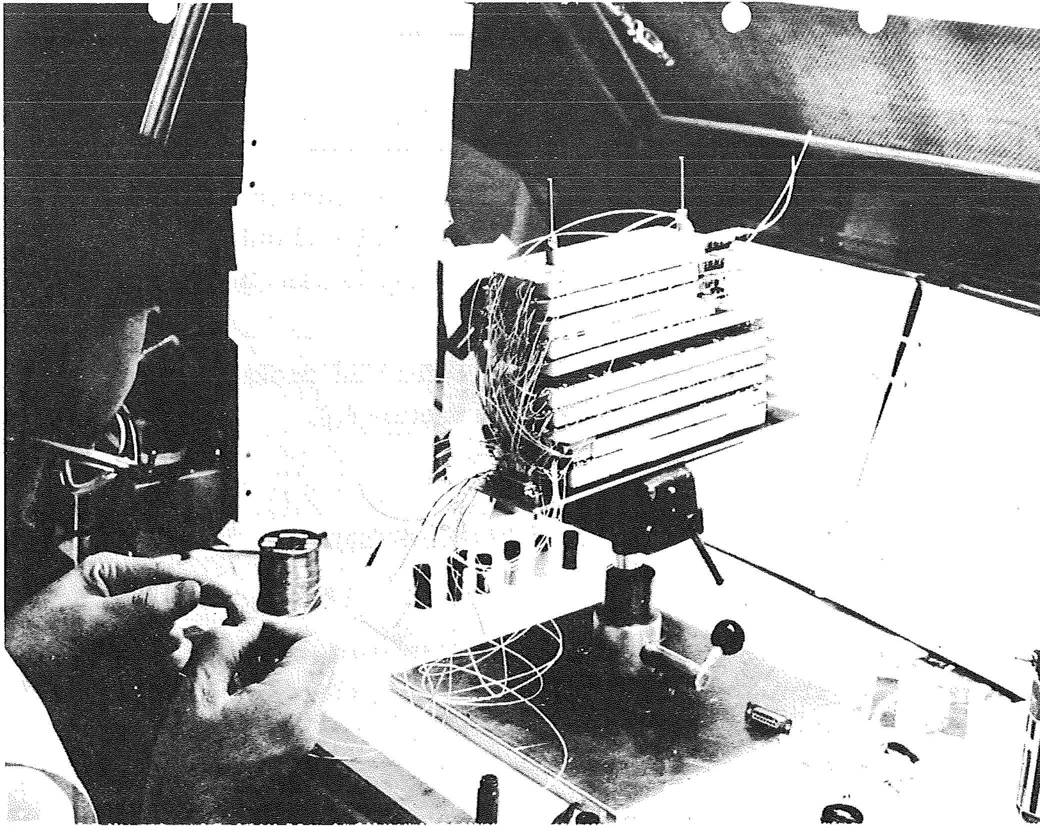

Figure 6-7. Harness Wiring During Assembly

removal was accomplished easily by wetting each terminal land thoroughly with solder and then drawing it off along with the dissolved gold with the vacuum desoldering device described in Paragraph 6.3.3. This treatment left the terminal lands with a clean and brightly tinned surface for good solderability.

6.5.2 Harness Wiring Procedure

The assembly sequence began with board 10 and proceeded towards board 1, since connections branched from higher number to lower number boards and terminal lands being connected had to be free from interfering wires. The first item to be installed on board 10 was the miniature 37-pin test connector which later mounted inside the front panel adjacent to the front of the board. The bundle of 37 test connector wires was laced and run along the lower edge of the board. Foam along this edge was beveled for the cable and reduced in height in the vicinity of the connector body so that both would fit against the right side of the housing within the outline of the foamed board. Components had been laid out for minimum height

under these areas in order to accommodate this arrangement. Both connector and cable were temporarily taped to board 10 and it was placed on the assembly jig. All test connector leads which terminate at this board were attached before proceeding with the rest of the harness. Groups of precut wires in several standard lengths were prepared for connection by thermally stripping the insulation 0.25 inch back from one end and tinning the exposed wire. As each wire was attached, color coding paint was applied to the insulation near the stripped end. Wires were inserted from the component side of the board through holes in the terminal lands, clinched against the land, cut, and soldered. All wires were dressed in a loop around the rear edge of the board for strain relief and flexibility to permit "fanning" apart the completed stack for access after assembly. After all leads had been attached to board 10, a careful inspection was made of the solder connections (since these would be obscured by the next board) and lead identification was verified. Aluminum spacers of the appropriate length were inserted in the foam cavities around the through-bolt holes on all boards. As each new board was added to the jig, additional 0.25-inch spacers were slipped between it and the one beneath to build in a controlled amount of slack in the wires. These extra spacers were removed as each board was completed so that the effect was not accumulative.

Thus prepared, board 9 was placed on the assembly jig; wires which interconnected it with board 10 were attached and soldered first. Each was color coded at its termination on board 9 with the same identification applied at the opposite end of the wire. Precut and coded wires from board 9 to lower number boards were attached and inspected as described for board 10. Because of the number of wires comprising the finished harness, the accuracy of interconnections was verified as each board was completed. Collaboration between inspector and assembler was essential during the harness wiring operation.

Interconnections to the remainder of the boards in the stack were carried out step by step in the manner described. Wires which terminated at the rear connectors were included in the harness as it progressed and were dressed into the connector area behind boards 9 and 10 (to be attached to the connectors as the last step). The two Cannon connectors were mounted on stand-offs attached to the assembly jig which positioned them conveniently for wiring and produced sufficient slack in the finished cable for proper placement in the experiment housing. The gold plating inside the connector terminal solder cups was dissolved away by filling the cups with solder and then drawing off this first filling with the vacuum desoldering device. Each wire-to-terminal connection was sleeved with Raychem heat shrinkable tubing extending from the base of the solder cup to 0.1 inch above the end of the insulation. These sleeves isolated stresses from the connections resulting from the flexing of the wires during mechanical assembly and provided insulation

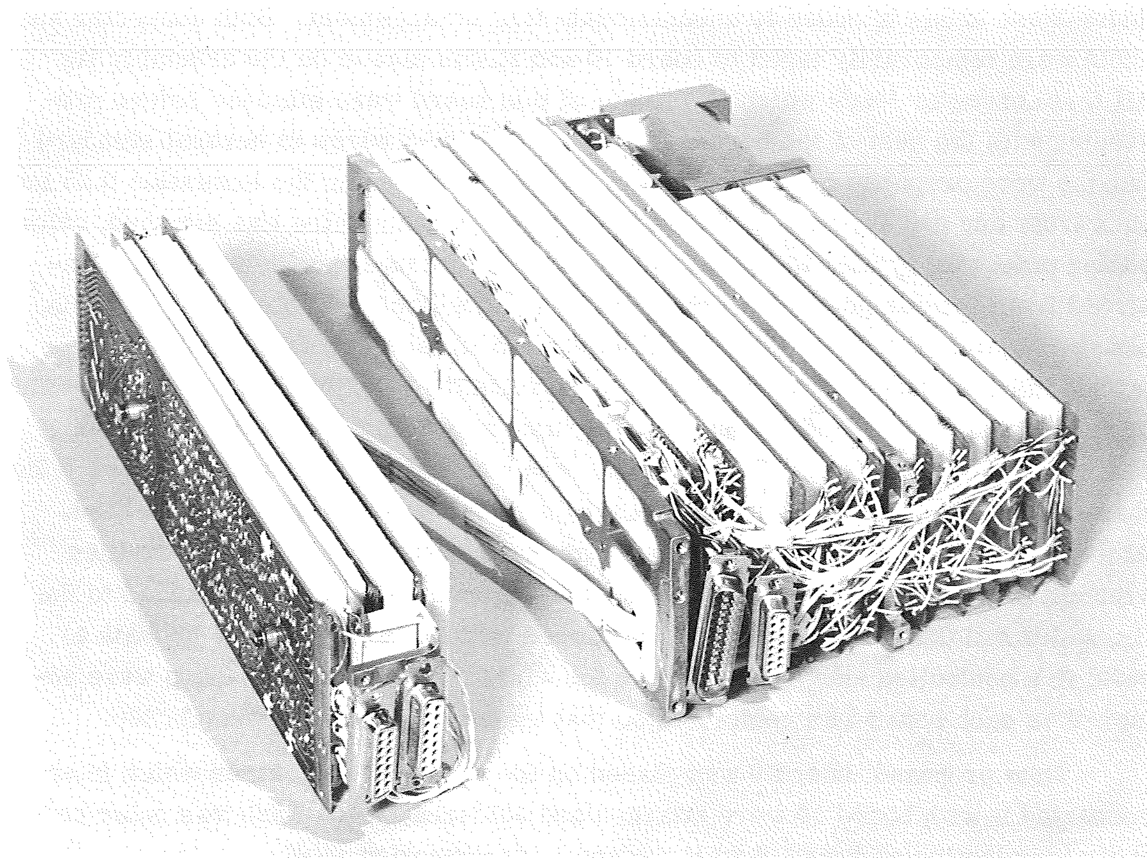

Figure 6-8. A Completely Wired Electronic Stack (ATS-A Experiment Stack Shown, the Particle Experiment Section on the Right is Identical to ATS-B)

between the closely spaced terminal cups. A view of the completed harness is shown in Figure 6-8. (This shows a view of the ATS-A experiment but the particle experiment section on the right is identical to the one in ATS-B.) The harness was dressed and tied to fit freely within the 0.24-inch gap between the ends of the boards and the inside of the housing back plate.

6.5.3 Front End Assembly

Integration with the detector mount was the final phase of the electronic stack assembly. The design of the sensitive "front end" of the experiment was described in Section 4.2. Several steps were necessary in order to prepare the stack for installation of the preassembled detector mount. First, the interlocking shield partition detailed in Figure 6-9 and shown in the sketch in Figure 4-4B was assembled. The two vertical shield baffles (Figure 6-10) and several terminal studs were mounted and soldered to the ground plane side of the piece. The unit was then

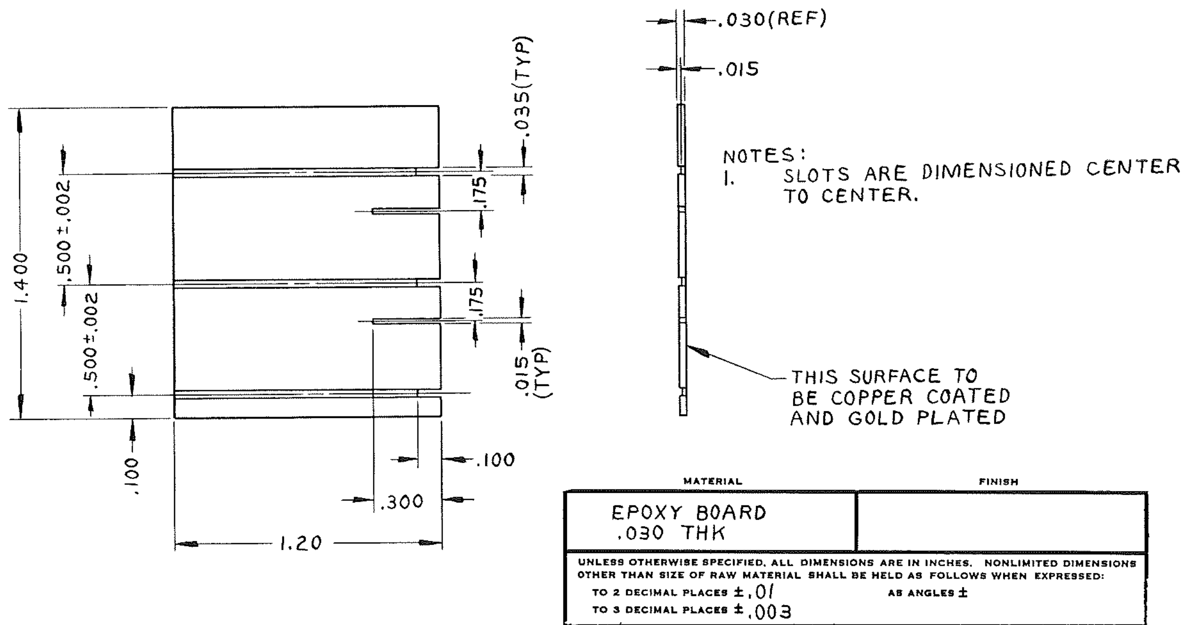

Figure 6-9. Interlocking Shielding Partition Drawing

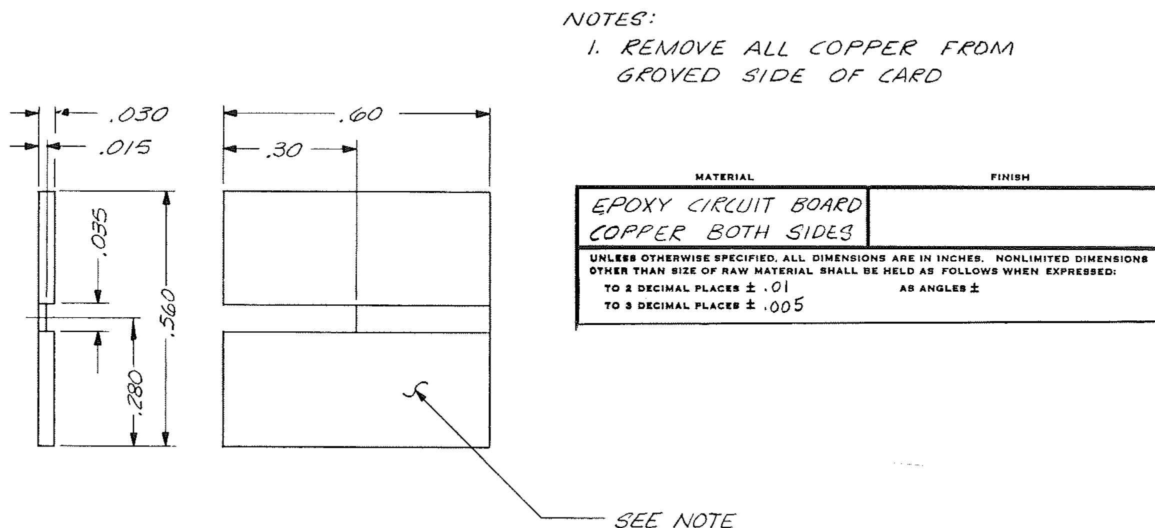

Figure 6-10. Vertical Shielding Baffle Drawing

carefully fitted into position in the slots provided for it in the input tabs on motherboards 1-3. Six miniature coaxial cables interconnect the test signal input terminal studs at the ends of the tabs to the internal pulse generator terminals on board 5. These cables were dressed against board 5 and emerged near its top edge in order to clear the detector mount. The coaxial shields were terminated to the ground studs on the shield partition to which the ground planes of boards 1-3 were also connected. Placement of these coaxial cables and the shield partition can be seen in the close-up view of the completed front end in Figure 6-11. When the detector mount was in place, the front tabs on boards 1-4 fitted into grooves in an epoxy board detail attached to the top of the mount. This, together with the interlocked tabs, forms a very sturdy mechanical arrangement for this part of the package. It was necessary only to spot-bond the front and rear intersections of these parts with epoxy to secure them.

6.5.4 Detector Mount Assembly

Figure 6-12 shows a rear view of the completely wired detector mount with the back cover plate removed to show the detector socket wiring. Wires were color coded, routed, dressed into three groups positioned to exit between the first three

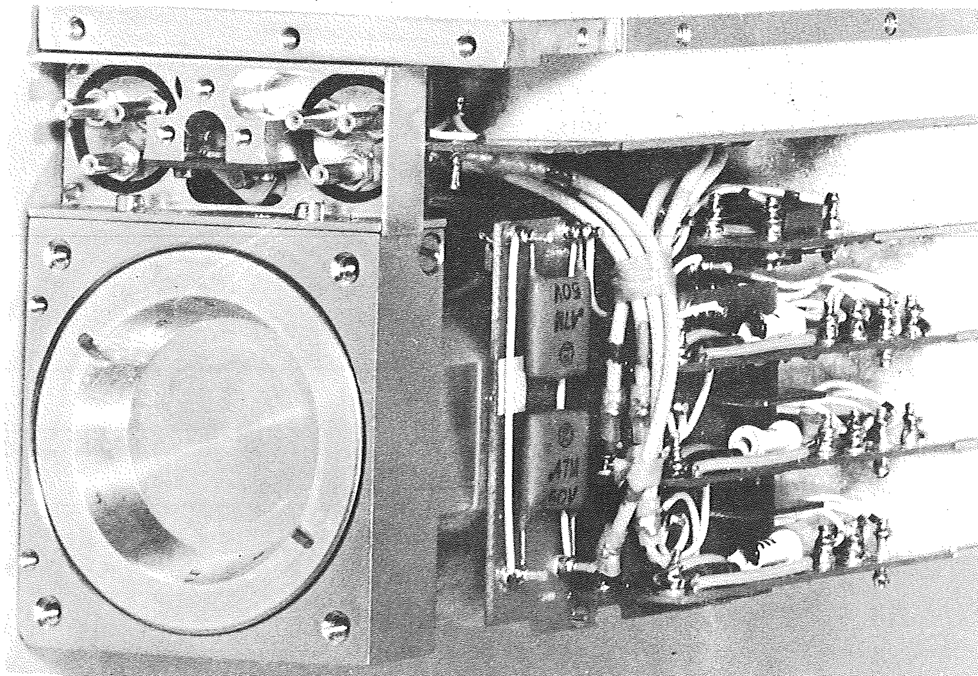

Figure 6-11. A Front-End View of the Assembled Experiment

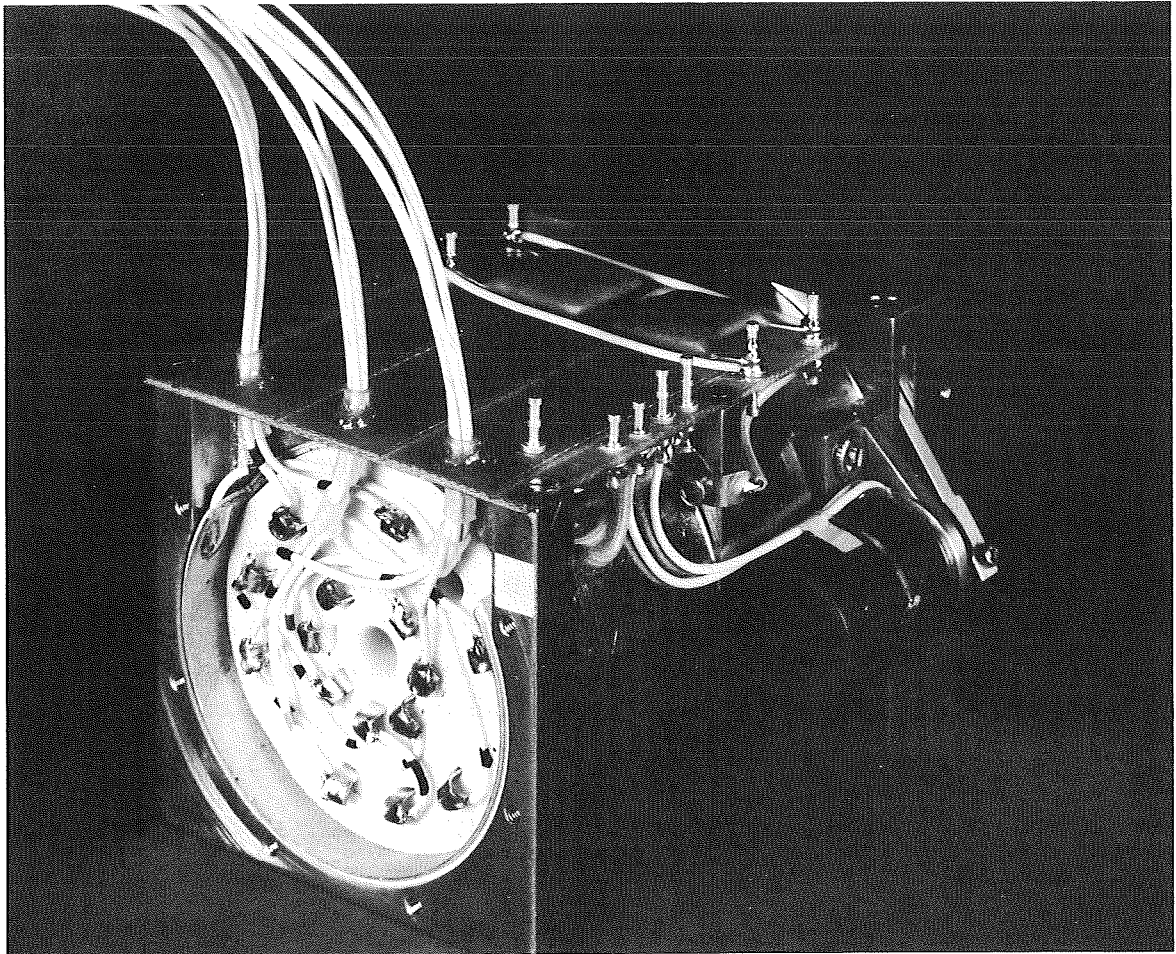

Figure 6-12. Rear View of a Partially Assembled Detector Mount

motherboards close to the preamplifier input terminals. A multipurpose epoxy board card shown on top of the mount in the photograph retained the bundles in position between grooves for the motherboard input tabs. This card also provided a mounting surface for the three chassis-ground to circuit ground bypass capacitors. Two parallel ceramic capacitors are connected to studs at the front of the card and the third, a large tantalum capacitor, is out of view underneath the card. A glass bead type thermistor for monitoring detector temperature is potted into a hole in the upper corner of the rear mounting flange of the detector block. The leads from this and the rotary solenoid are connected to terminal studs along the right edge of the epoxy board card. These items can best be seen in the front view of the detector mount shown in Figure 2-22. Assembly of the rotary solenoid is described in Paragraph 2.2.3. The coaxial test jack bracket which is attached to the side of the detector mount has been removed in the photograph to show the source arm. Figure

2-20 is an exploded diagram of the whole subassembly. Six miniature coaxial test jacks (Micon, Inc., Type 4403) were assembled to the test jack bracket insulator shown behind the bracket in the diagram. A printed circuit pattern on this insulator connects the shells of the jacks together. The pattern, in turn, is wired to the ground plane on motherboard 5. A cutout in the jack insulator seals the source arm mechanism cover to prevent entry of foam particles from the stack.

When all of these items were in place and inspected, the detector mount assembly was ready for integration with the electronic stack. Before proceeding with this, the stack was removed from the harness assembly jig and mounted in a handling frame which simulated, for fitting purposes, the sides of the housing. With all the boards in their proper relationship and the stack inverted on the bench, the detector mount was carefully fitted into position and attached to the left side of the handling frame with bolts. The detector socket wires were dressed and connected to the appropriate input terminal studs along the top edges of boards 1, 2, and 3 immediately behind the test signal input tabs. Installation was completed by wiring the coaxial test jacks to the internal test pulser studs on board 5 and connecting the rotary solenoid and thermistor terminals to studs on the front tab of motherboard 4.

6.6 FINAL ASSEMBLY

The completely wired and inspected electronic stack with all aluminum spacers in place was installed in the housing. This was, in effect, accomplished by building the housing around the stack. The first step in this procedure is to mount the left side to the stack with both through-bolts and two 0.150-inch-long spacers. The front plate is then placed face down on the bench and the stack is lowered into it vertically. Small locating pins installed on the left side are engaged in corresponding holes on the front plate flange and the stack is maneuvered into full contact with the front plate. A downward hand pressure on the side of the stack engages all the board edges in the grooved details inside the front plate. The 37-pin test connector is attached with screws from the inside before proceeding with the rest of the assembly. The back plate is fitted into place over the rear edges of the boards and secured to the left side. The right side is mounted and drawn into contact with the front and back plate mounting surfaces by tightening the through-bolts.

An inspection was made of the harness dress and clearance inside the rear plate. The rear connectors mount against the inside of the back plate attached with screws from the outside into captive nuts on their flanges. This allows the back plate to be removed after foaming the harness. Each cover was partially installed, leaving a crack between it and the rear plate. By sighting through this crack with a strong light source on the opposite end, the rows of contacting fingers could be

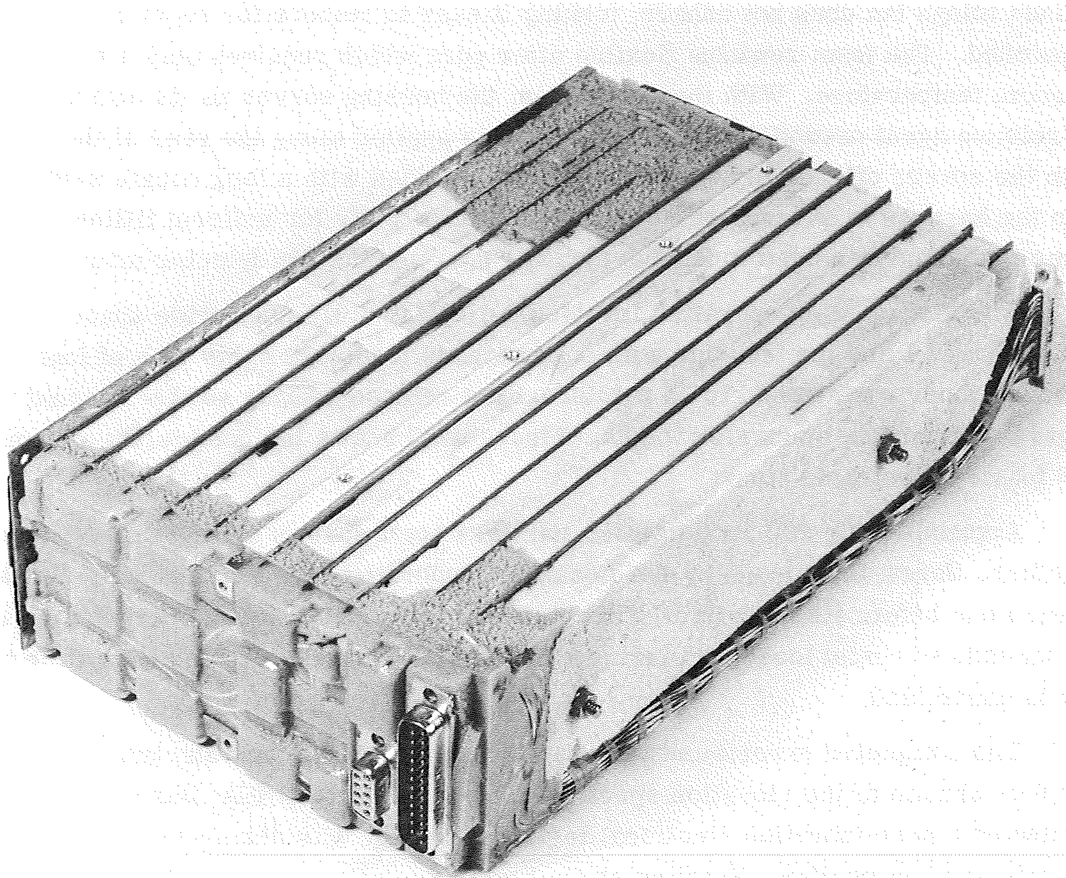

Figure 6-13. The Completely Assembled and Encapsulated Electronic Stack

observed just above the boards. If proper finger alignment and clearance was observed, the covers were screwed down. Electrical tests were performed to verify correct interconnection. These were repeated at high and low temperatures to show up defective connections. If the tests were satisfactory, the package was ready for encapsulation of all harness wiring with silicone rubber foam (Silastic RTV S-5370 Foam, 10 pounds per cubic foot density). This material fills and surrounds things but does not adhere, making it easy to remove for repairs. It can be repatched. The foam remains flexible after cure which requires only a few minutes at room temperature. With these features, the housing serves as its own mold with no release agent needed. Suitable gasketing is applied along the rear of the stack with the covers off. Catalyzed foam resin is injected with a long nozzle syringe into the harness in several places inside the back plate for uniform filling. The same technique was used to fill the cavities surrounding the detector mount.

The last foaming operation involved filling the 0.015-inch-wide space between motherboard 1 and the left side with polyurethane foam. For this type of foam, the left side inner surface had to be painted with a release coating so that it could be separated from the stack afterwards. Figure 6-13 shows the completely assembled and foamed electronic stack.

Approximately 100 nonmagnetic stainless steel screws hold the housing parts together. Screw Lock made by the Locktite Corporation was applied to the threads of each one before its insertion. This material forms a weak bond between the mating threads to resist loosening during vibration. It can be reapplied each time the box is assembled.

The completed experiment with the detector installed was electrically tested and then shaken to the vibration specifications supplied by NASA (Paragraph 8.2.2). Following a post-vibration electrical test, the package was disassembled and given a mechanical inspection. Painting of the housing details, described in Paragraph 4.1.3, was done at this time to avoid marring these surfaces during earlier mechanical integration and testing. All package components, excluding the detector, were then placed in a thermal vacuum chamber to outgas at an elevated temperature, as described in Paragraph 8.2.3. Following this step, and prior to beginning the qualifying thermal vacuum run, the final flight assembly of the experiment package was performed.

Chapter 7

GROUND SUPPORT EQUIPMENT

7.1 GENERAL DESIGN

In designing the electronic test equipment for the Bell Telephone Laboratories Particle Telescope experiment, the object was to integrate all the necessary test functions into one unit, and to build this unit into a metal suitcase for convenience of portability. Figure 7-1 shows one such unit with the suitcase lid open. Two of these units were delivered under NASA contract as Ground Support Equipment (GSE) for the ATS-B experiment.

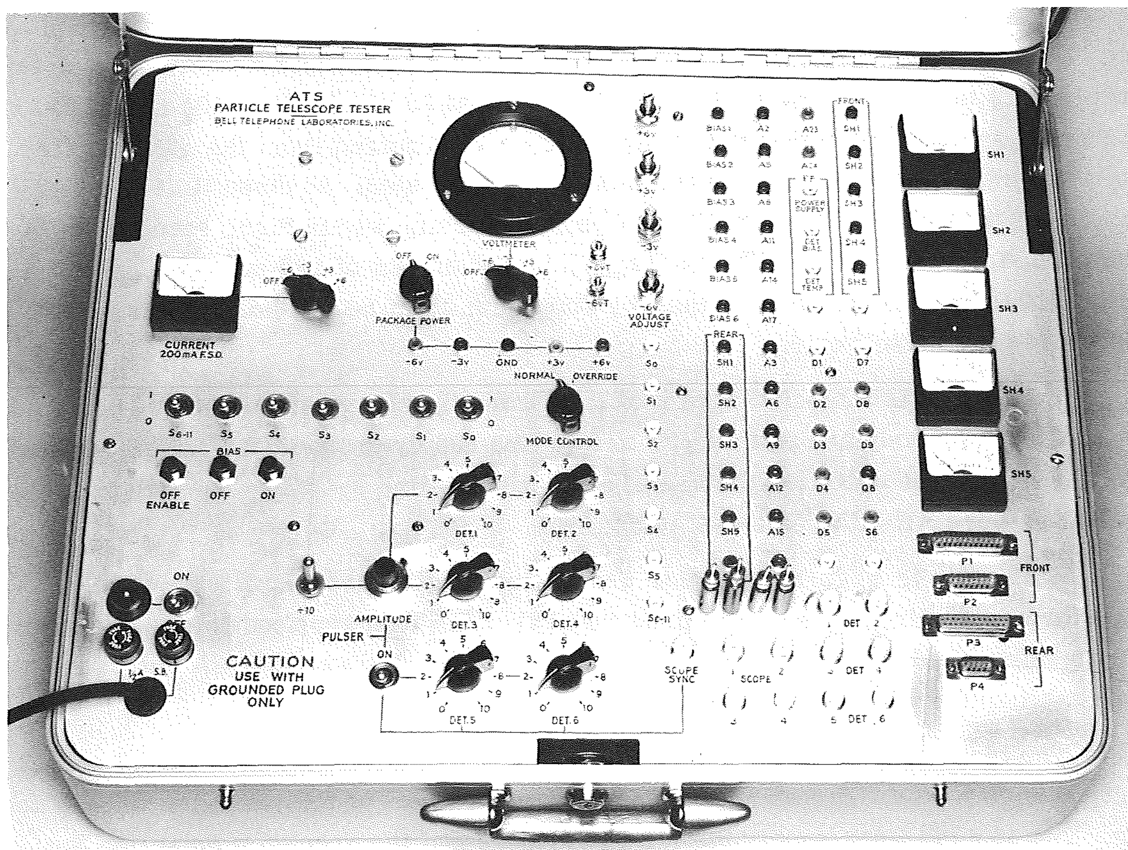

Figure 7-1. ATS Particle Telescope Tester

Normal connections to the BTL ATS-B package were made from P3 and P4 Cannon connectors to the corresponding connectors P104 and P118 (interface Specification R-2180) mounted on the rear panel of the package. Additional test points in the experiment are available through the 37-pin connector on the front of the experiment. This test connector was cabled to connectors P1 and P2 of the GSE. To provide calibration pulses to the six detector inputs to the experiment, six outputs from a precision pulser were available at six BNC connectors labelled DET 1 through DET 6. These can be coax-connected to the detector test jack array on the front panel of the package. Five Log Ratemeters provided analog representation of the pulse rates from the package output channels (shapers). These are seen along the right end edges of the GSE in Figure 7-1. Seven mode line switches provided control of the experimental modes and the calibration sequence. Three push buttons simulated the BIAS OFF ENABLE, BIAS OFF, and BIAS ON commands. A meter showed the current being drawn by each package power supply line, while another meter monitored the voltage of each package supply.

7.2 POWER SUPPLIES

Power for the package under test was supplied by the GSE tester. The power required by the package was +6V at 80 mA, -6V at 36 mA, +3V at 104 mA and -3V at 95 mA, with the exception that more power was required from the ±6V supplies when the internal calibration source motor was activated. At these times, the +6V supplied a transient current of 170 mA peak, returning within three seconds to its quiescent value of 80 mA. The -6V supplied a transient of 130 mA peak, settling within three seconds to 85 mA; thereby supplying about 50 mA holding current to the source motor solenoid.

Figure 7-2 is a block diagram of the Power Supply system. A three-wire line input allows the body and panel to be tied to line supply ground. A warning sign by the line cord input specifies the use of a three-wire line system. The live and neutral lines were RF-filtered and shielded.

As shown in Figure 7-2, two conventional full-wave rectifiers were transformer-fed from the line to produce ±18V DC. This supplied two series regulators referenced to ±12V. These regulators, in turn, fed six 250-mA regulated and stabilized supplies.

The block diagram shows that four of the six supplies provided the ±6 and ±3 volt package power. The ±3 volt lines also provided power for the mode line switching. The ±6V (T) lines supply the log ratemeters and the precision pulser in the GSE.

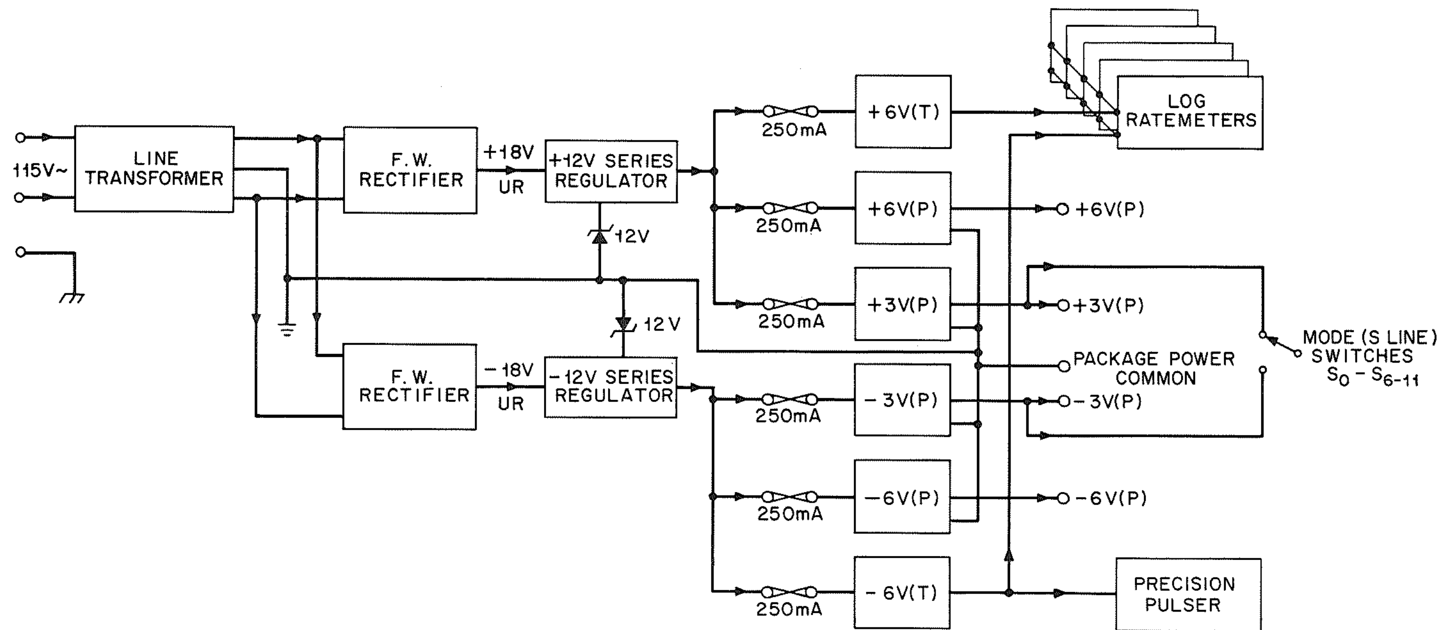

Figure 7-2. Power Supply, Block Diagram

Fuses, rated at 250 mA, were inserted between the ±12V regulators and each stabilized supply.

Figure 7-3 shows the ±12 volt regulator system and its more detailed interface to the six stabilized supplies. The ±12V lines were used to supply zeners for ±6V reference supplies. These, in turn, fed variable potentiometer chains, one for each of the six supplies. The chains were comprised of two fixed resistors and a control potentiometer which appears on the front panel of the GSE. Transistors Q3 and Q4 provide constant voltage return points for long-tailed pair stabilizing amplifiers used in the individual power supplies as shown in Figures 7-4 and 7-5.

Figures 7-4 and 7-5 are schematics of a positive and a negative supply, respectively. Q5 and Q6 form the long-tailed pair referred to above. With the base circuit of Q5 returned to ground, it is necessary to return the common emitter resistor to a negative point in the case of the positive supply and vice versa. This provides sufficient current drive for the long-tailed pair through a reasonable value of common emitter load. The Q6 base circuit senses the variations in output voltage and, through Q7, controls the base of the series regulator Q8 to correct for the output voltage changes.

A series resistor R3 was chosen in value so that when the load on the supply was 250 mA, Q8 no longer regulates the output voltage, which then deregulates, falling in value according to the IR drop across R3. At current less than 250 mA, the IR drop across R3 is inside the control loop, and does not affect the output voltage.

A shunt in the current path of each of the four package power supplies was wired to the current measuring switch (Figure 7-6) which connected each shunt in turn across the front panel current meter. The length of the shunts was adjusted to give current measurements calibrated against a Sensitive Research Milliammeter.

The output voltage of each of the four package supplies was monitored for deviation from nominal value. The Weston microammeter (labelled VOLTAGE) on the front panel, read center scale when the selected voltage was at its nominal value, full scale for 10 percent high, and zero scale for 10 percent low. Each major division on the meter therefore represented a 20 percent deviation. The wiring for this system is shown in Figure 7-7. Operation was achieved by center-tapping the 6V(P) supplies (R1 and R2 Figures 7-4 and 7-5), and tapping the 6V(T) supplies, with a potentiometer added, to ensure a tapped output in excess of 3V. Correct polarity connection to the microammeter, and selection of a series resistor (~3.9K) gave up-scale deflection on the meter, as each package supply voltage was bucked against the corresponding 6V(T) tapped outputs. The 3V(P) outputs were monitored at their full (untapped) value. Calibration of this system was achieved by first setting the ±6(V)

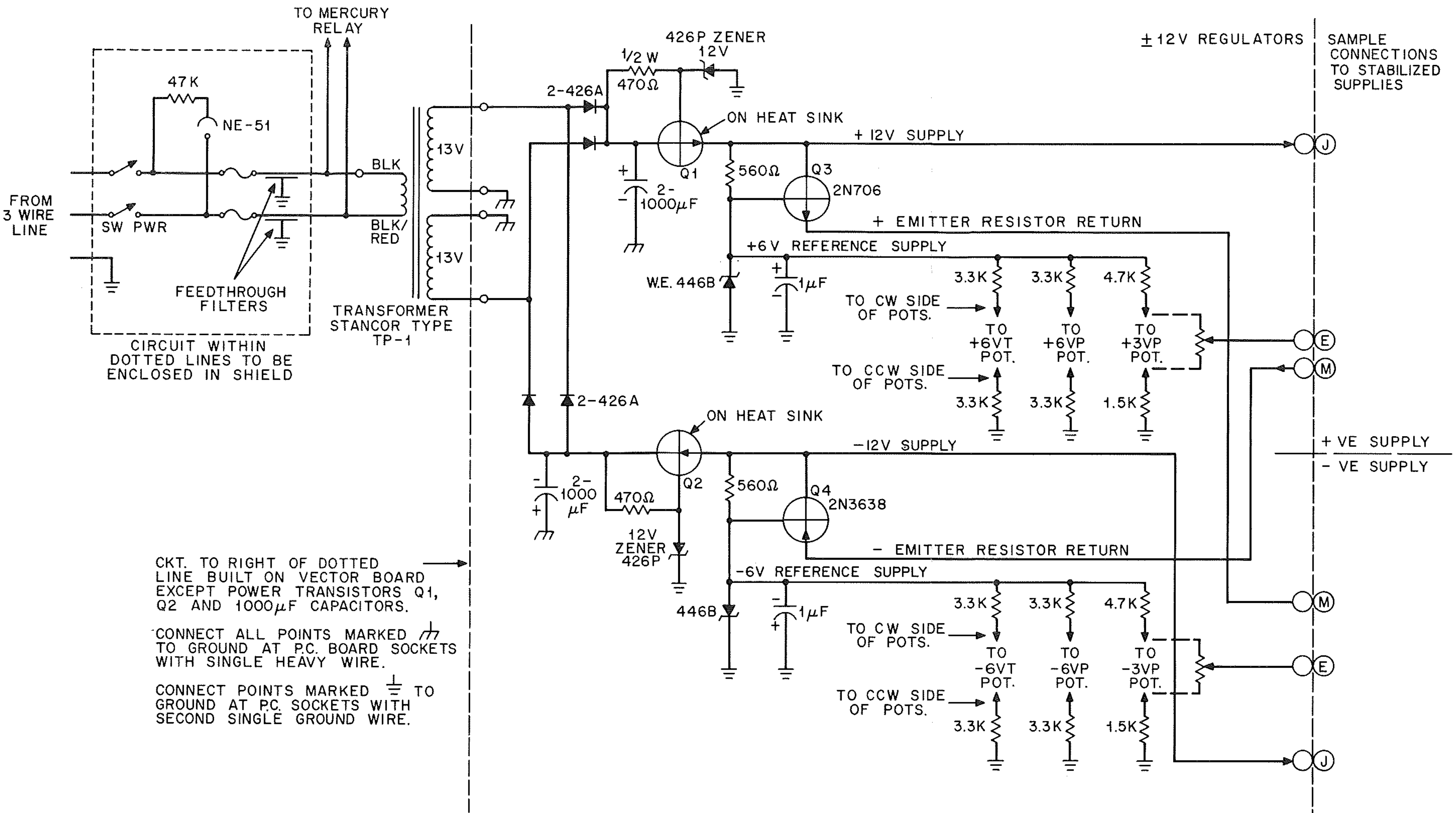

Figure 7-3. Power Supply, ±12V Regulators

Page intentionally left blank

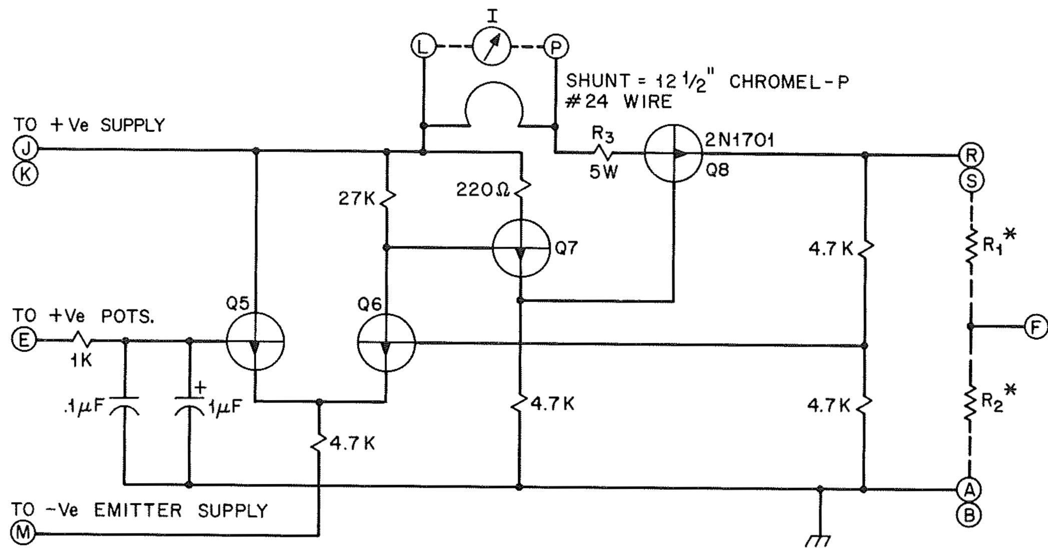

1. TRANSISTORS Q5-Q7 ARE 2N706.
2. RESISTORS ARE 10%, 1/4W UNLESS SPECIFIED.
3. * OMIT FOR +3(P), FOR +6(P) $R_1 = R_2 = 1K\Omega$, 1% FOR +6(T) $R_1 = 820\Omega$, $R_2 = 820\Omega + 500\Omega$ POT.
4. $R_3 = 20\Omega$ FOR +6(P) & +6(T), $R_3 = 32\Omega$ FOR +3(P).

+6V(T) PC#1
+6V(P) PC#2
+3V(P) PC#3

Figure 7-4. Stabilized Power Supplies

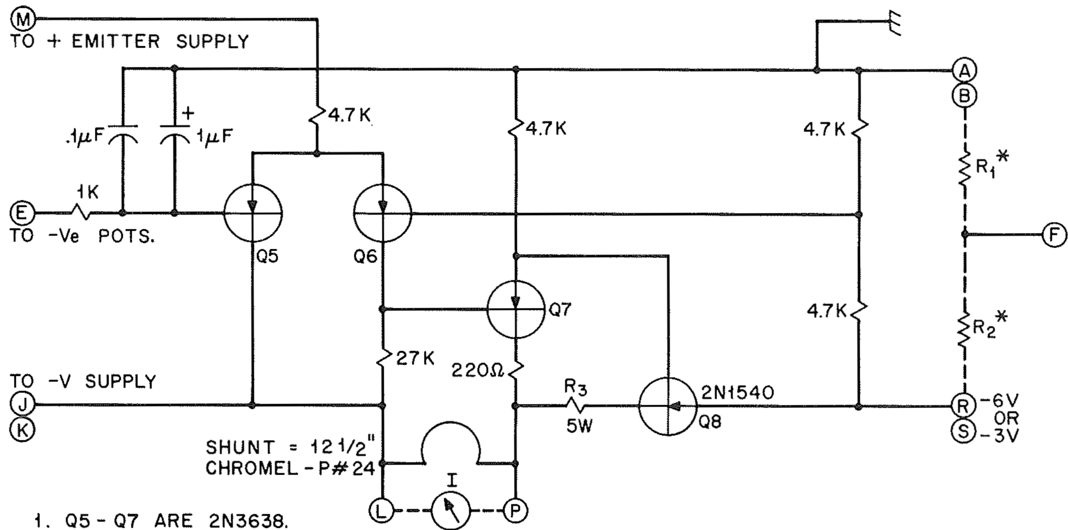

1. Q5-Q7 ARE 2N3638.
2. ALL RESISTORS 1/4W, 10% UNLESS SPECIFIED.
3. * OMIT FOR -3(P), FOR -6(P) $R_1 = R_2 = 1K\Omega$ 1%, FOR -6(T) $R_1 = 820\Omega$; $R_2 = 820\Omega + 500\Omega$ POT.
4. $R_3 = 20\Omega$ FOR -6(P) & -6(T), R = 32Ω FOR -3(P).

-3V(P) PC#4
-6V(P) PC#5
-6V(T) PC#6

Figure 7-5. Stabilized Power Supplies

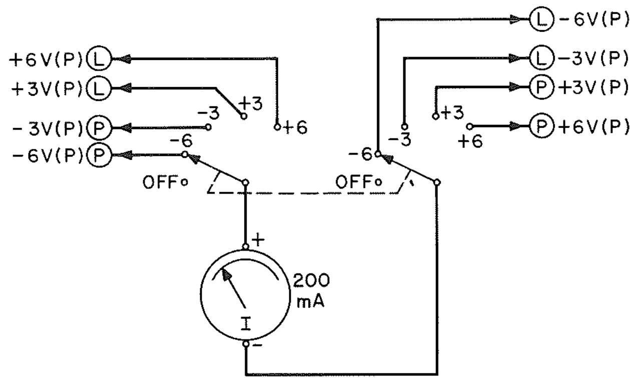

Figure 7-6. Package Current Meter Wiring

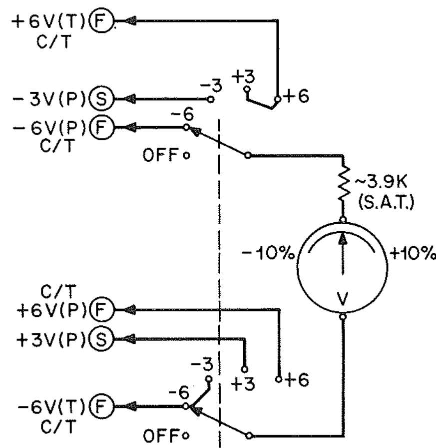

Figure 7-7. Voltmeter Switch Wiring

and ±3V(P) outputs (while on nominal load) precisely to nominal values, by use of a digital voltmeter. The potentiometer on ±6V(T) was then adjusted to give center scale on the suitcase voltmeter. Slight tolerance differences between the values of +6V(P) c/T and +3V(P), and between -6V(P) c/T and -3V(P) were nulled out by shunting the appropriate R1 or R2 on the ±6V(P) supplies.

A PACKAGE POWER ON-OFF switch was provided so that power need not be connected to the package until the voltages had been verified.

7.3 RATEMETERS

Five Log Ratemeters gave a logarithmic analog representation of the five digital outputs (SH1 - SH5) of the package under test. Each ratemeter was driven by the circuit shown in Figure 7-8.

A pulse, applied to the input, greater in amplitude than three diode forward drops, triggers the regenerative circuit formed by Q1, Q2, and C1. Q2 saturates, and its collector snaps up to +6V, discharging the bank of decade-arrayed capacitors through the connecting diodes. These capacitors then begin to charge, drawing current through the meter circuit. The 5-pf capacitor charges rapidly (~1μsec time constant), whereas the 5-μF capacitor will remain virtually discharged for input frequencies greater than 10 Hz.

If the input frequency is greater than 100 Hz, then both the 0.5-μF and the 0.05-μF capacitor remain discharged, and the contribution of current to the meter circuit is approximately doubled. At 1000 Hz, the current is approximately three times that at 10 Hz, and so on. The system is calibrated at 10 kHz by means of the 250-ohm shunt potentiometer.

7.4 MODE CONTROL

A mode control system was wired into the s-lines, see Figure 7-9. ±3V(P) was wired to seven s-line switches S_0-S_5 and S_{6-11}. Manipulation of these switches enabled the selection of any one of the possible experimental modes. S_{6-11} provided the calibration mode when set to the "1" position. A NORMAL OVERRIDE switch facility was added which provided the means for overriding the mode lines when the package was under control from the spacecraft encoder. This was achieved in the OVERRIDE position by connecting the suitcase tester mode line switches through 470-ohm resistors, to the package mode lines at the 37-pin front panel test connector.

7.5 BIAS COMMAND

Three push buttons were wired, as in Figure 7-10, to simulate the three commands; BIAS OFF ENABLE, BIAS OFF, and BIAS ON. These switches were used to test that the BIAS OFF command operated only for a 15-second period following operation of the BIAS OFF ENABLE command.

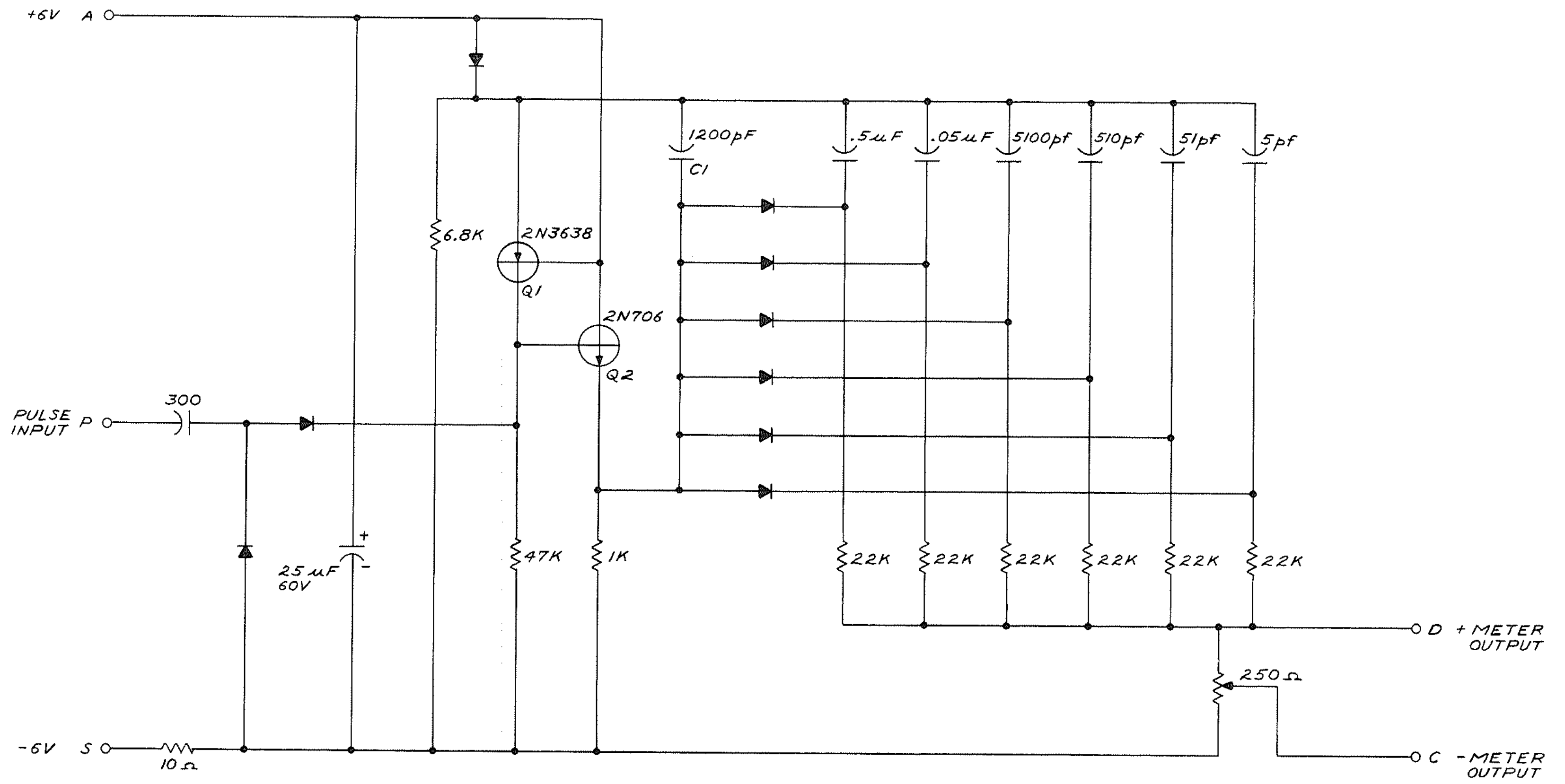

NOTE:

1. ALL DIODES 1N4009 OR 1N4154

Figure 7-8. Log Ratemeter Schematic

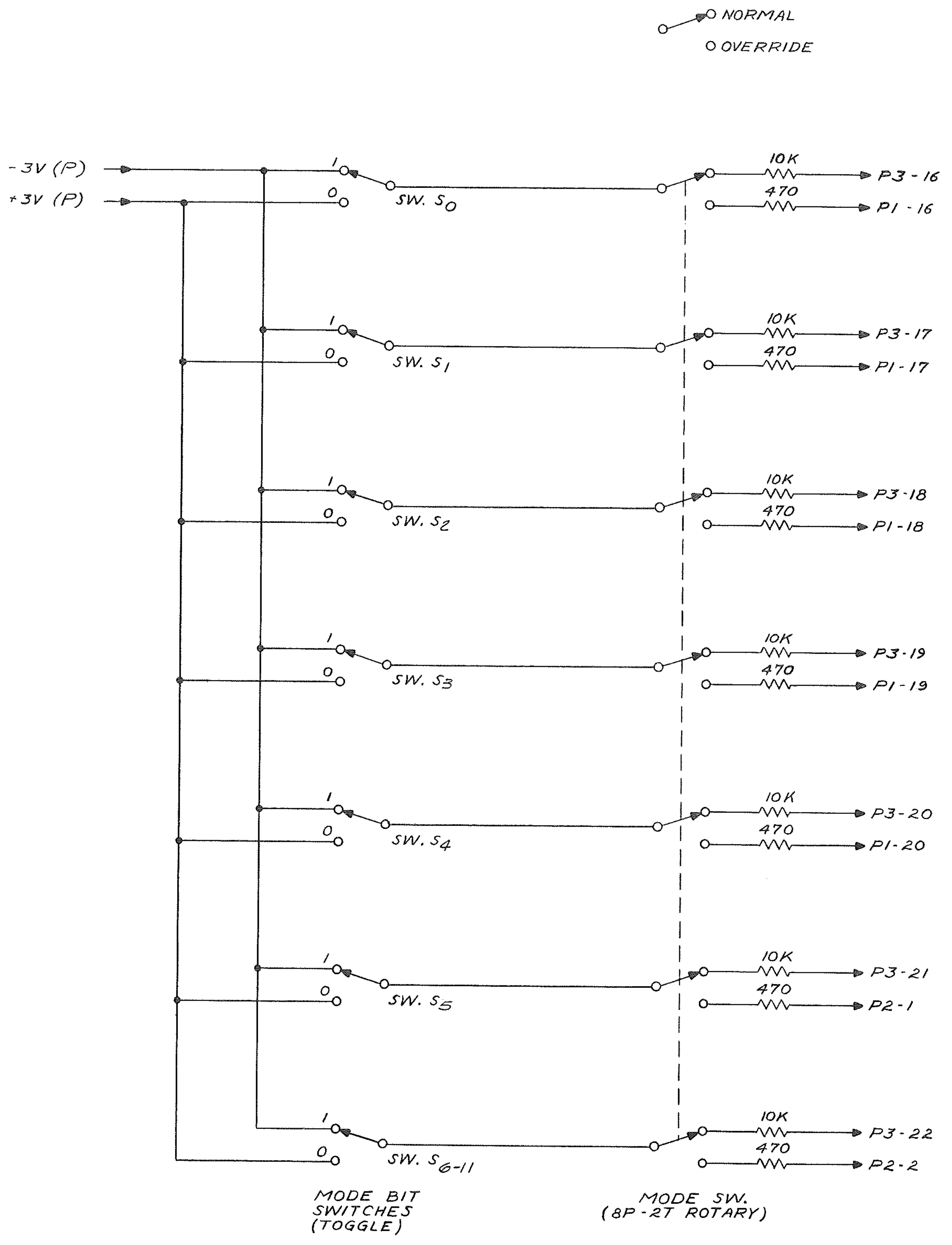

Figure 7-9. Mode and Command Switching

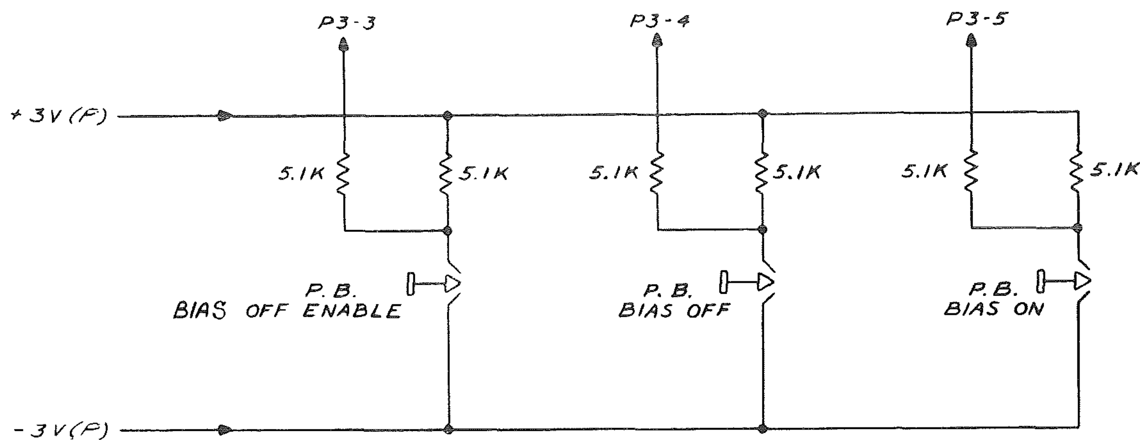

Figure 7-10. Bias Command

7.6 PRECISION PULSER

A calibrated precision pulser provided input pulses to the preamplifiers in the package, in order to calibrate discriminator levels (see Figure 7-11). Calibration is achieved by adjustment of the 1K Ω preset potentiometer, which then supplies a DC level to the relay contacts that results in a pulse height equivalent to a 100-MeV detector event. The 10-turn linear helipot now provides the attenuator system with pulse heights from zero to 100 MeV, the value being read on the 1000 division duo-dial that operates the helipot from the front panel.

First, in the attenuator system, was a divide-by-10 attenuator which was common in all six output attenuators. The effect of the ÷ 10 attenuator was to change the output range to measure from zero to 10 MeV. The ÷ 10 attenuator fed the six output attenuators, which attenuated the pulse by ten equal steps, and fed it to the corresponding BNC connector on the front panel.

For example, with the potentiometer dial set to 1000 division, and the ÷ 10 switch OFF (i.e., in the X1 position), each attenuator switch would step the output from 0 to 100 MeV in 10 equal steps of 10 MeV per step. With the ÷ 10 switch ON and the potentiometer set to 1000 division, each attenuator step was equal to 1 MeV. With the ÷ 10 switch ON, and the potentiometer set to 500 division, each attenuator switch would step the output from zero to 5 MeV in ten equal steps of 0.5 MeV, etc.

The voltage (pulse height)/electron volt calibration is derived from the fact that a 1 MeV event generates 3×10^5 electrons in a silicon detector. This is equivalent to a charge of

$$q/\text{MeV} = 1.6 \times 10^{-19} \times 3 \times 10^5 \text{ coloumb}$$

$$= 4.8 \times 10^{-14} \text{ coloumb.}$$

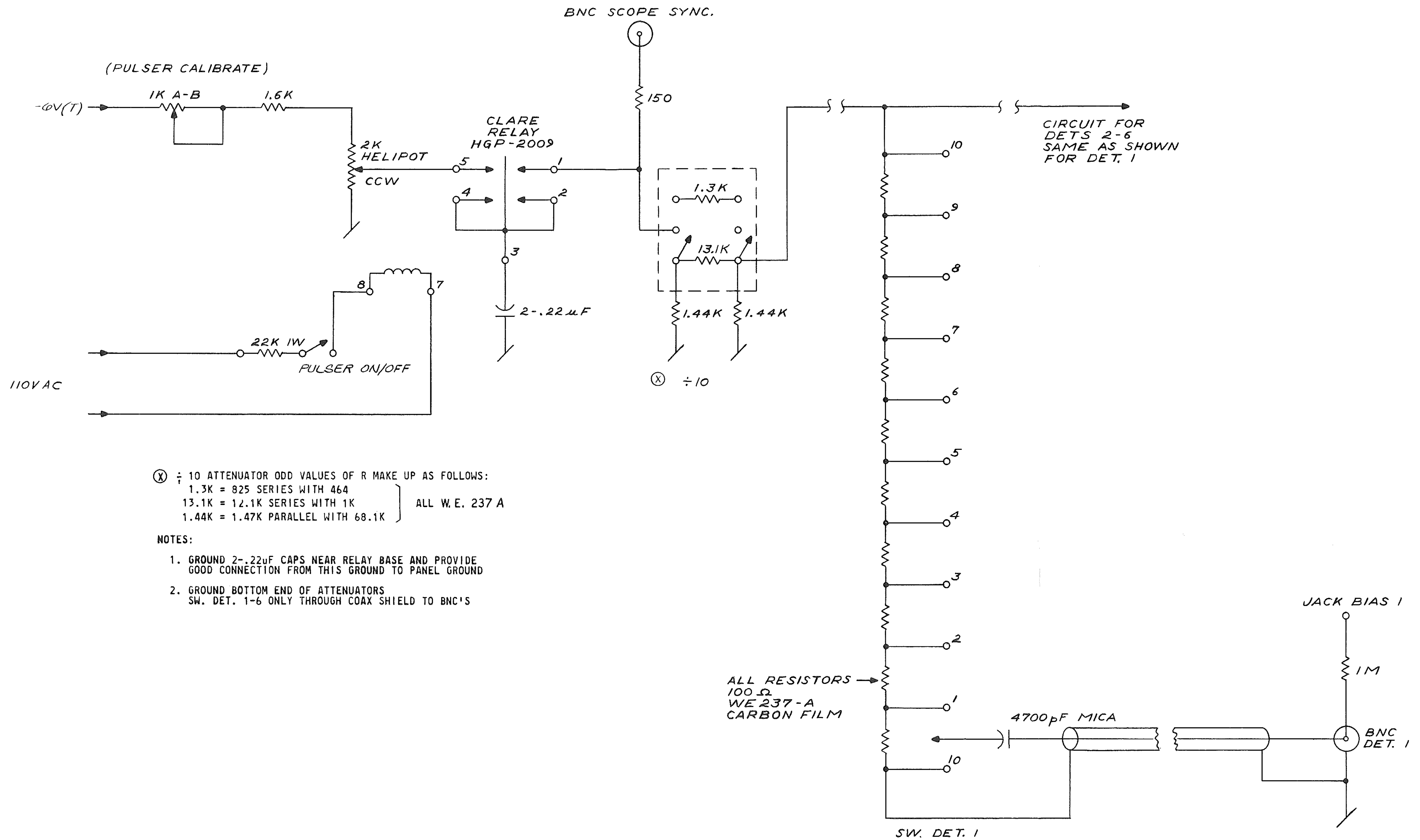

Figure 7-11. Mercury Pulser

Page intentionally left blank

Therefore, if the test pulse is applied to a 15-pf capacitor

$$v = \frac{4.8 \times 10^{-14}}{15 \times 10^{-12}} = 0.32 \times 10^{-2} \text{ volts/MeV}$$

$$v = 3.2 \text{ mV/MeV.}$$

7.7 TEST POINTS

Refer back to Figure 7-1. The 37-pin test connector on the package front panel connects with P1 and P2 on the tester front panel. P1 and P2 are, in turn, brought out to Pin Jack test points on the tester front panel. A indicates an Amplifier output signal, D indicates a Discriminator output. SH1 - SH5 are the five shaper outputs from the package, which appear twice, once from the package rear connector, and once from the 37-pin front panel test connector. Only the latter were wired into the ratemeters.

Other test points include the three performance parameter outputs: Power Supply, Detector Bias, and Detector Temperature.

The seven mode control lines from the front panel test connector were also brought out to pin jacks.

Four pin plugs were provided, wired to four BNC connectors with jumper cord, to provide four scope input points that could therefore be readily connected to any test point pin jack.

The six detector signal BNC connectors were wired respectively to six pin jacks. These connectors also carried a high impedance (a few Megohms) output of the detector bias. Hence the six pin jacks were labelled BIAS1 - BIAS6, and the detector bias could be measured at these points by a meter of sufficiently high input impedance ($\geq$ 100 Megohms), such as a Hewlett-Packard Model 412A.

In practice, when the 37-pin connector was connected to P1 and P2, stray C coupling often caused the package electronics to oscillate and cross-couple. To avoid this, a Driver/Attenuator Box was built to interface the package test signals and the tester. It consisted of 18 emitter followers to isolate the 13 test signal lines and the 5 shaper outputs from the tester cable wiring capacitance. (See Figure 7-12.)

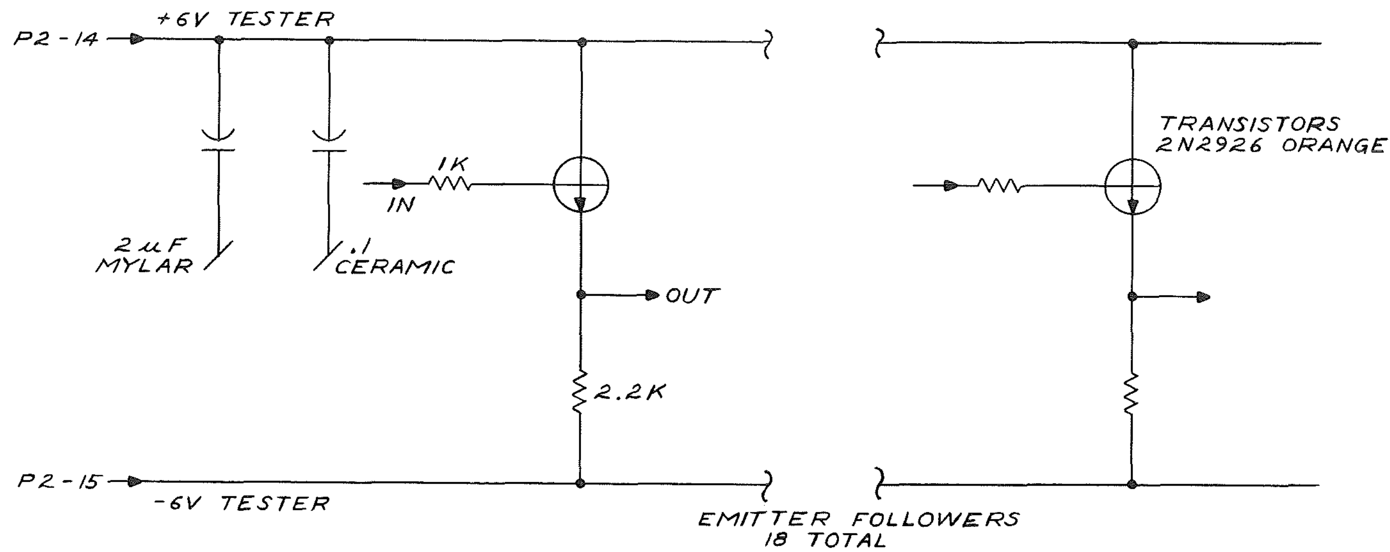

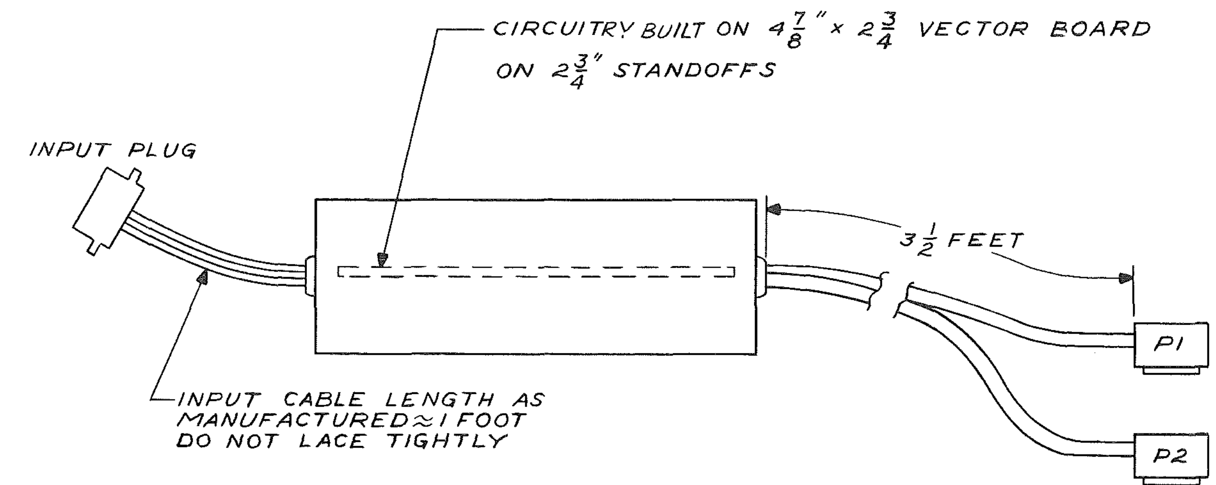

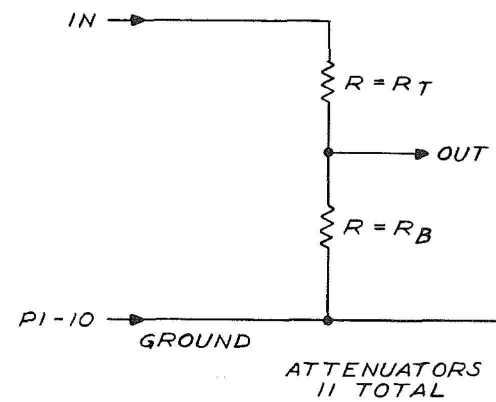

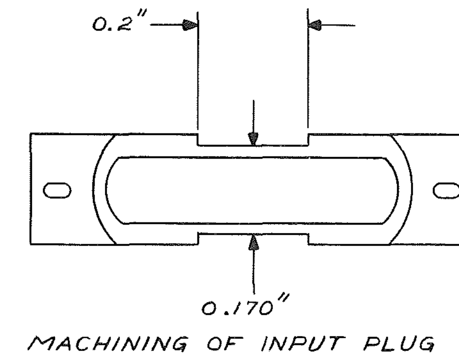

IN FIRST MODEL:	IN SECOND MODEL:
R_T = 10K	R_T = 9.1K
R_B = 1K	R_B = 1K

NOTES:

1. SEE SHEETS 1 AND 2 ATS-B DRIVER/ATTENUATOR BOX FOR WIRING LIST
2. STRAIGHT THROUGH CONNECTIONS ARE WIRED TO TIE POINTS
3. INPUT CONNECTOR IS PRE WIRED CANNON # MDB1-37SH001
4. OUTPUT CONNECTORS ARE:
   P1-CANNON DB-25S-C7
   P2-CANNON DB-15S-C7
5. POINTS MARKED "IN" COME FROM INPUT CONNECTOR
   POINTS MARKED "OUT" GO TO OUTPUT CONNECTOR

Figure 7-12. Driver-Attenuator

Page intentionally left blank

Chapter 8

ENVIRONMENTAL TESTING

8.1 TESTS

8.1.1 Specified Tests

These tests were carried out in accordance with NASA specification number S2-0102, as modified (for vibration) by Westinghouse Electric Corporation specification number R2131.

The prototype unit, Serial No. 651, was tested at Flight Qualification levels; the flight unit, Serial No. 663, and flight spare unit, Serial No. 652, were tested at Flight Acceptance levels.

8.1.2 Additional Tests

In addition to the NASA specified tests, the units were thermally cycled, during and after completion of fabrication, to check the reliability of the printed circuit soldering and the printed circuit board interconnection harness wiring.

8.2 EXPERIMENT CHECKOUT

A checkout procedure was devised to verify the operation of every electrical function of the units, and was used through all phases of the environmental tests. This procedure is best described by referring to the 15 data sheets (Figures 8-1 through 8-12) on which the checkout results were recorded.

8.3 TEST SEQUENCE

The environmental tests of each unit proceeded in the following sequence.

8.3.1 Thermal Cycling

After completion of the interconnection harness wiring and before it was encapsulated, the unit was given a complete checkout at room temperature. It was then thermally cycled three times between -20°C and +40°C for the prototype unit

NAME OF TEST: Detector Temperature

CONTROL CONFIGURATION:

Sequence Scaler							Pulser Attenuators					
S_{6-11}	S_5	S_4	S_3	S_2	S_1	S_0	Det 1	Det 2	Det 3	Det 4	Det 5	Det 6
0			1	1	0	1	DISCONNECT					

DESCRIPTION: This test monitors the voltage from the thermistor temperature sensor on the detector block.

RESULTS:

NOTES: This measurement taken before and after all other measurements.

Figure 8-1. Detector Temperature Checkout Sheet

NAME OF TEST: Bias Command

CONTROL CONFIGURATION:

Sequence Scaler							Pulser Attenuators					
S_{6-11}	S_5	S_4	S_3	S_2	S_1	S_0	Det 1	Det 2	Det 3	Det 4	Det 5	Det 6
0	√		1	1	0	1	DISCONNECT					

DESCRIPTION: This constitutes a check on the bias "off enable," "off," and "on" commands.

RESULTS: The presence of bias is observed at the bias monitor point.

Does the command operate with a ~10 second delay between "off enable" and "off"?	
Does the command operate with a ~15 second delay between "off enable" and "off"?	

NOTES: It is intended that the "off enable" and "off" commands be sent within 8 seconds of one another to be effective. S_5 must be in the (1) state for commands to affect bias.

Figure 8-2. Bias Command
Checkout Sheet

NAME OF TEST: Bias Monitor

CONTROL CONFIGURATION:

Sequence Scaler							Pulser Attenuators					
S_{6-11}	S_5	S_4	S_3	S_2	S_1	S_0	Det 1	Det 2	Det 3	Det 4	Det 5	Det 6
0	1		1	1	0	1	DISCONNECT					

DESCRIPTION: This test checks the reading of the bias monitor.

RESULTS:

	Bias Off	Bias On
Bias Voltage		

NOTES:

Figure 8-3. Bias Monitor Checkout Sheet

NAME OF TEST: Detector Bias Voltage

CONTROL CONFIGURATION:

Sequence Scaler							Pulser Attenuators					
S_{6-11}	S_5	S_4	S_3	S_2	S_1	S_0	Det 1	Det 2	Det 3	Det 4	Det 5	Det 6
0	0						CONNECT					

DESCRIPTION:

RESULTS:

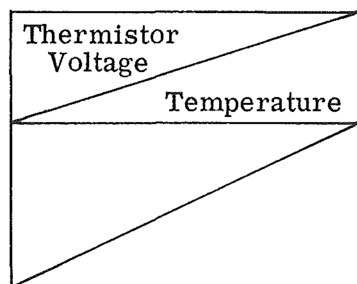

Detector	Bias Voltage
1	
2	
3	
4	
5	
6	

NOTES:

Figure 8-4. Detector Bias Voltage Checkout Sheet

NAME OF TEST: Mode Logic

CONTROL CONFIGURATION:

Sequence Scaler							Pulser Attenuators					
S_{6-11}	S_5	S_4	S_3	S_2	S_1	S_0	Det 1	Det 2	Det 3	Det 4	Det 5	Det 6
√	√	√	√	√	√	√	√	√	√	√	√	√

DESCRIPTION: The logical coincidence and anticoincidence requirements of each mode are checked.

RESULTS:

Mode	S_6	Q_8
A_1		
A_2		
B_1		
B_2		
C_1		
C_2		
D		
E		
F		
G_1		
G_2		
G_3		
H_1		
H_2		
H_3		

NOTES:

Figure 8-5. Mode Logic Checkout Sheet

NAME OF TEST: Power Consumption

CONTROL CONFIGURATION

Sequence Scaler							Pulser Attenuators					
S_{6-11}	S_5	S_4	S_3	S_2	S_1	S_0	Det 1	Det 2	Det 3	Det 4	Det 5	Det 6
0	1	1	√	√	√	√	DISCONNECT					

DESCRIPTION: The test box current monitor is switched between the various supplies in each of the experimental modes.

RESULTS:

Mode	+6V	-6V	+3V	-3V
A_1				
A_2				
B_1				
B_2				
C_1				
C_2				
D				
E				
F				
G_1				
G_2				
G_3				

Figure 8-6. Power Consumption
Checkout Sheet (Sheet 1 of 2)

NAME OF TEST: Power Consumption (continued)

Mode	+6V	-6V	+3V	-3V
H_1				
H_2				
H_3				
I				
			← Current drawn with source drive on, $S_5(0)$, $S_{6-11}(1)$	

NOTES: S_5, S_4 both (1). This state draws maximum current in all modes. Make sure bias is switched on. (Command before testing.)

Figure 8-6. Power Consumption Checkout Sheet (Sheet 2 of 2)

NAME OF TEST: Power Supply Monitor

CONTROL CONFIGURATION:

Sequence Scaler							Pulser Attenuators					
S_{6-11}	S_5	S_4	S_3	S_2	S_1	S_0	Det 1	Det 2	Det 3	Det 4	Det 5	Det 6
0	√	√	1	1	0	1	DISCONNECT					

DESCRIPTION: The power supply commutating check system is examined with the package operating in a characteristic mode.

RESULTS:

Supply	+6V	-6V	+3V	-3V
Reading				

NOTES:

Figure 8-7. Power Supply Monitor Checkout Sheet

NAME OF TEST: Threshold of Coincidence Discriminator

CONTROL CONFIGURATION:

Sequence Scaler							Pulser Attenuators					
S_{6-11}	S_5	S_4	S_3	S_2	S_1	S_0	Det 1	Det 2	Det 3	Det 4	Det 5	Det 6
0	0	1	0	0	0	0	√	√	√	√	√	√

DESCRIPTION:

RESULTS:

	Attenuator	Helipot	MeV
D_1			
D_2			
D_3			
D_4			
D_5			
D_6			

NOTES: Use I Mode. Check D_6 by using D_{noise}: $34\overline{56}$. Just use $\overline{6}$ with 34 at high amplitude.

Figure 8-8. Threshold of Coincidence Discriminator Checkout Sheet

NAME OF TEST: Threshold of 5-Channel Discriminator

CONTROL CONFIGURATION:

Sequence Scaler							Pulser Attenuators					
S_{6-11}	S_5	S_4	S_3	S_2	S_1	S_0	Det 1	Det 2	Det 3	Det 4	Det 5	Det 6
0	0	1	√	√	√	√	DISCONNECT					

DESCRIPTION:

RESULTS:

		Attenuator	Helipot	MeV	
Mode	D_{11}				
	D_{12}				
	D_{13}				
	D_{14}				
	D_{15}				
	D_{16}				
Mode	D_{11}				
	D_{12}				
	D_{13}				
	D_{14}				
	D_{15}				
	D_{16}				

Figure 8-9. Threshold of 5-Channel Discriminator
Checkout Sheet (Sheet 1 of 3)

NAME OF TEST: Threshold of 5-Channel Discriminator (continued)

		Attenuator	Helipot	MeV	
Mode	D_{11}				
	D_{12}				
	D_{13}				
	D_{14}				
	D_{15}				
	D_{16}				
Mode	D_{11}				
	D_{12}				
	D_{13}				
	D_{14}				
	D_{15}				
	D_{16}				
Mode	D_{11}				
	D_{12}				
	D_{13}				
	D_{14}				
	D_{15}				
	D_{16}				
Mode	D_{11}				
	D_{12}				
	D_{13}				
	D_{14}				
	D_{15}				
	D_{16}				

Figure 8-9. Threshold of 5-Channel Discriminator Checkout Sheet (Sheet 2 of 3)

NAME OF TEST: Threshold of 5-Channel Discriminator (continued)

		Attenuator	Helipot	MeV	
Mode	D_{11}				
	D_{12}				
	D_{13}				
	D_{14}				
	D_{15}				
	D_{16}				
Mode	D_{11}				
	D_{12}				
	D_{13}				
	D_{14}				
	D_{15}				
	D_{16}				

NOTES: If more than one detector is associated, ratio of the amplitude into each detector has to be noted. (Normally equal amplitude.)

Figure 8-9. Threshold of 5-Channel Discriminator Checkout Sheet (Sheet 3 of 3)

NAME OF TEST: Internal Pulser I

CONTROL CONFIGURATION:

Sequence Scaler							Pulser Attenuators					
S_{6-11}	S_5	S_4	S_3	S_2	S_1	S_0	Det 1	Det 2	Det 3	Det 4	Det 5	Det 6
1	1	1	√	√	√	√	DISCONNECT EXTERNAL PULSER AT THE PACKAGE					

DESCRIPTION: Check modes using the internal pulse generator.

RESULTS:

Mode	Sh 1	Sh 2	Sh 3	Sh 4	Sh 5
A_1					
A_2					
B_1					
B_2					
C_1					
C_2					
D					
E					
F					
G_1					
G_2					
G_3					
H_1					
H_2					
H_3					
I					

NOTES:

Figure 8-10. Internal Pulser I
Checkout Sheet

NAME OF TEST: Internal Pulser II

CONTROL CONFIGURATION:

Sequence Scaler							Pulser Attenuators					
S_{6-11}	S_5	S_4	S_3	S_2	S_1	S_0	Det 1	Det 2	Det 3	Det 4	Det 5	Det 6
1	1	0	√	√	√	√	DISCONNECT					

DESCRIPTION:

RESULTS:

Mode	Sh 1	Sh 2	Sh 3	Sh 4	Sh 5
A_1					
A_2					
B_1					
B_2					
C_1					
C_2					
D					
E					
F					
G_1					
G_2					
G_3					
H_1					
H_2					
H_3					
I					

NOTES:

Figure 8-11. Internal Pulser II
Checkout Sheet

NAME OF TEST: Calibration Source

CONTROL CONFIGURATION:

Sequence Scaler							Pulser Attenuators					
S_{6-11}	S_5	S_4	S_3	S_2	S_1	S_0	Det 1	Det 2	Det 3	Det 4	Det 5	Det 6
1	0	0	√	√	√	√	DISCONNECT					

DESCRIPTION: Checks detector 1 with an Am^{241} α source and detector 4 with a Sr^{90} β source.

RESULTS:

Mode	Sh 1	Sh 2	Sh 3	Sh 4	Sh 5
A_1					
A_2					
H_1					
H_2					
H_3					
I					

NOTES: No significant number of α particles are detected by counter I unless the system is in a vacuum. $S_4 = (0)$ - Pileup Rejector Enabled.

Figure 8-12. Calibration Source Checkout Sheet

and -10°C and +40°C for the flight units. (The upper limit of +40°C was held due to the presence of the solid state detector in each unit.) During the last cycle, after allowing the high and low temperatures to stabilize, a complete set of checkout measurements was obtained for each temperature extreme. The harness wiring was then encapsulated and the unit was rechecked at room temperature.

8.3.2 Vibration

A complete set of the specified vibration tests was then performed. If time permitted, a further temperature cycle was given after vibration, at the extremes of which (+40°C and -10°C) a functional checkout* was performed to verify the wiring connections.

8.3.3 Bakeout

Preceding the next specified test, thermal vacuum, each package with detector removed, was mounted in a hot plate box, placed in a thermal vacuum chamber and pumped on for several hours. This was found necessary to avoid detector contamination from the volatile organic molecular species that evolved from the package during its first extended exposure to vacuum. After 10 or 12 hours of pumping, heat was applied by the hot plate, and the package foam was baked out. Discoloration of the foam took place if it was pumped on and baked out too soon after the foam was applied. To avoid this it was found necessary to allow foam to cure at least 24 hours before pumping on it.

8.3.4 Thermal Vacuum

After "bakeout," each unit was removed from the thermal vacuum chamber so that a detector could be installed. This procedure avoided contamination of the detectors and allowed thermal vacuum testing of each unit to follow at this point.

Finally, the units were completely tested at room temperature and pressure just prior to shipment.

*A functional test to check wiring, omitted the tests of Figures 8-6, 8-8, and 8-9.

8.4 THE INDIVIDUAL TESTS

8.4.1 Thermal Tests Apparatus and Procedure

The apparatus used was a Wyle Laboratories chamber, with temperature control facilities and an automatic timer-sequencer unit. Instrumentation connections were made by feed-through connectors in the chamber door. Adapter cables were made to connect the unit to the feed-through connectors, and the feed-through connectors to the ground support equipment (GSE). Liquid CO_2 was auto control-switched into the chamber to provide low temperatures. In order to prevent contamination of the detectors by the CO_2 (which was not free of volatile hydrocarbons), and by carbonic acid which formed in the presence of water vapor, each unit was placed in a plastic bag. Dry nitrogen was piped into the bag throughout the tests, maintaining a positive pressure of nitrogen inside the bag.

For thermal cycling, the Wyle Sequence-Timer unit was set for 30 minutes cold and 30 minutes hot. For temperature test results, the unit was allowed to stabilize in temperature for at least 30 minutes before checkout results were recorded. The Package Detector Temperature performance parameter output was monitored for this purpose.

A complete set of results was recorded on the Test Result Checkout Sheets 1-15 (Figures 8-1 through 8-12) for each temperature extreme, and also at intermediate temperatures, in order to track the variation of discriminator levels with temperature.

8.4.2 Thermal Test Results

All units operated satisfactorily over the range -20°C to +40°C for Serial No. 651 and -10°C to +40°C for Serial Nos. 663 and 652.

8.4.3 Vibration Test Apparatus and Procedure

A fixture was fabricated from 1" aluminum pieces, bolted together with 3/8-inch socket-head screws (see Figure 8-13). A connector-carrying back plate was provided to enable the unit under test to be plugged in, when mounted, as in the EME package of the ATS-B satellite. Two 1 by 1-1/2 inch stiffeners were provided at the front of the box to reduce resonance in the Z and X modes of vibration. Accelerometer mounting holes were drilled and tapped in the corner of the fixture located closest to the detector telescope.

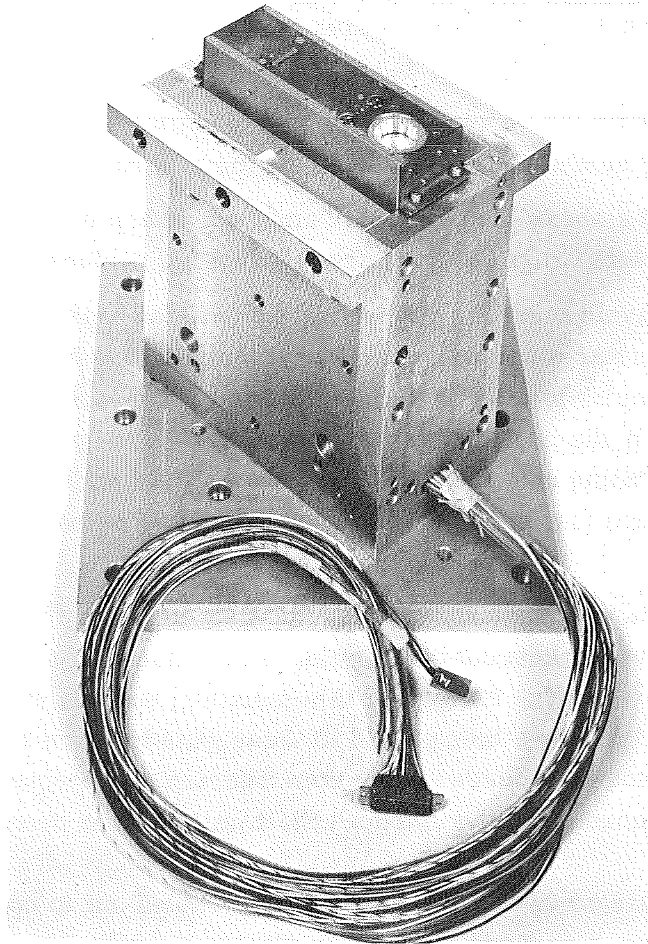

Figure 8-13. Vibration Fixture

A 13 by 13 inch mounting plate was also fabricated from 1-inch aluminum, to mate the vibration fixture to the vibrator armature head. All assembly and mounting screw holes were designed to assure at least 3/8-inch of thread to engagement.

In order to obtain a large area of contact between the three mounting surfaces of the box with the mounting plate, the following fabrication specifications were made:

(1) The mounting surface of the mounting plate was milled until the lowest point on the surface was machined at least 2 mils.

(2) With the box assembled, each mounting surface was milled until the lowest point was machined at least 2 mils.

(3) All corners of each piece were bevelled a few mils.

(4) The rims of all holes appearing on the mounting surface were chamfered a few mils to eliminate sharp edges.

Points 1 and 2 above provide good flush-mounting surfaces, which are important in minimizing mechanical resonances during vibration.

Points 3 and 4 above help to avoid damage to sharp edges and corners, which results in small dents, hills, and craters in mounting surfaces.

In order to avoid metal-to-metal contact between a package and the back plate, 0.008-inch-thick mylar discs were adhered to each of the back plate corners. Another 0.008-inch mylar washer was mounted around the back plate captive nut clearance hole, in which the package rear-panel captive locking-screw engaged. Then, in mounting the floating connectors, spacers were used under the connector mounting holes, to ensure that mating of the connectors was between 15 mils and 25 mils from bottoming.

To ensure back plate loading, the mounting surfaces under the package mounting flanges were undercut by 40 mils. When mounting a package, the gap between the package mounting flange and this mounting surface was gauged over each mounting hole. Shims were then placed in these gaps to leave 1-mil gaps under each mounting hole. Mounting screws were then inserted and torqued to 30 in-lbs, compressing the mounting flange through the 1-mil gap and thereby loading the back plate.

The back plate connectors were wired and cabled out to connectors that mated with the GSE. Thus, a package mounted in vibration fixture could be tested without being removed from the fixture.

The breakdown of the weights of the complete vibration fixture are as follows:

Box with one stiffener	31 lbs
1" aluminum mounting plate	17 lbs
ATS package	6 lbs
Bolts and hardware	2 lbs
	56 lbs
2" magnesium damping plate	22 lbs
	78 lbs

NOTE: 78 lbs at 55 g (maximum level during qualification) = 4290 lbs.

A dummy load was fabricated, and was used in resonant surveys before subjecting the package to unknown environments. It consisted of two brass cylinders of 3-1/2 inches diameter and 8-1/4 inches long, mounted between two aluminum

plates. The rear plate was fitted with guide pins to locate in the fixture back plate, and the front plate with clearance holes, to allow mounting in the fixture with four mounting screws.

While using the dummy load to conduct a resonance survey on December 10, 1965, a 7:1 resonant peak was found at 1.6 kHz. The addition of a 2-inch thick mg plate between the mounting plate and the armature head, modified this peak to be 2:1 at 2 kHz. Subsequent vibration fixtures were designed to mount directly to this magnesium plate to avoid an extra mounting plate in the system.

8.4.4 Vibration Test Results

The prototype unit Serial No. 651 was vibrated at Associated Testing Laboratories, Wayne, New Jersey on September 29, 1965, on a Ling Model A275 Shaker (rating 10,000 lb). The levels applied are shown in Table 8-1.

Table 8-1. PROTOTYPE QUALIFICATION VIBRATION SPECIFICATIONS

1. Sinusoidal

Axis	Frequency (Hz)	Applied Vibration Level
X & Y	10-30	0.5" D.A.
	30-250	±22.5 g
	250-400	±45.0 g
	400-2000	±7.5 g
Z	10-30	±2.3 g
	30-250	±34.5 g
	250-400	±55.5 g
	400-2000	±7.5 g

NOTE: Sweep rate at two octaves per minute.

2. Random

Test Duration	Frequency (Hz)	Accel. (g-rms)	PSD (g^2/Hz) Level
4 min. per axis	20-150	9.2	0.0225
	150-300		Increased to 0.045 at 3 db/octave
	300-2000		0.045

The silicon detectors, Pack #5, were damaged by this test and were replaced. The electronics operated satisfactorily after the test and the package did not suffer any mechanical or external physical damage.

The two flight units were vibrated at Bell Telephone Laboratories, Whippany. Serial No. 652 was tested on December 10, 1965, and Serial No. 663 on April 20, 1966. A Ling Model 275 Shaker was used in each case. The levels of vibration applied for both flight units are shown in Table 8-2.

Table 8-2. FLIGHT ACCEPTANCE VIBRATION SPECIFICATIONS

1. Sinusoidal

Axis	Frequency (Hz)	Applied Vibration Level
X & Y	10-30	0.33" D.A.
	30-250	±15.0 g
	250-400	±30.0 g
	400-2000	±5.0 g
Z	10-30	±1.6 g
	30-250	±23.0 g
	250-400	±36.9 g
	400-2000	±5.0 g

NOTE: Sweep rate at 4 octaves per minute.

2. Random

Test Duration	Frequency (Hz)	Accel. (g-rms)	PSD Level (g^2/Hz)
2 min. per axis	20-150	7.3	0.01
	150-300		Increasing to 0.02 at 3 db/octave
	300-2000		0.02

This test damaged the dE/dX Detectors 72 and 74, and the first lithium-drift detector in unit Serial No. 652.

After unit Serial No. 663 was tested in the Y mode, a fault in the detector telescope (a plug-in module) was observed. This was found to be an intermittent spring contact connection to dE/dX Detector #1. No other electrical or physical damage occurred to either unit Serial No. 663 or Serial No. 652.

8.4.5 Vibration Build-up in the Package

On May 5, 1966, after unit No. 663 had been selected to be the first-choice flight unit, No. 652 was used to investigate the mechanical system of the detector plug-in module. This was done by mounting three accelerometers in mutually perpendicular axes in a dummy detector package. This arrangement was installed in unit No. 652 and vibrated at flight acceptance levels on May 20, 1966.

Visicorder charts and reports are available on all of these tests.

The investigation of the detector mechanical mounting system showed resonant build-ups of significant magnitude. These were 2:1 at 400 Hz and 3:1 at 1100 Hz in the axis of thrust. Reference to the vibration level specifications show that the detector will experience at 400 Hz, 110 g during qualification and 74 g at acceptance level tests.

Vibrations in the X axis generated resonant buildups in the detector assembly of 1.2:1 between 250-400 Hz, and 6:1 over a narrow range at 1000 Hz. At ATS acceptance levels, this indicates the detector will be subjected to 60 g at 250-400 Hz and 50 g at 1000 Hz. This mode also generated cross-axes coupling into the Y axis, where (in the X mode) 20 g at 250-400 Hz and 40 g at 1000 Hz was observed.

A similar situation existed for the Y axis mode, where a 1.2:1 buildup occurred between 250-400 Hz. At 400 Hz, this buildup increased to 1.5:1. Cross-coupling to the X axis generated a 40 g peak at 400 Hz. In the 1000 Hz range, the magnification extended from 1000 Hz to 1500 Hz. It was 2.5:1 from 1000 Hz to 1200 Hz and 5:1 from 1200 Hz to 1400Hz, then tapered off to unity at 1500 Hz. Again, cross-coupling into the X axis occurred, where 20 g at 1000 Hz and 30 g at 1400 Hz was generated.

In subsequent separate vibration tests of individual detector assemblies, this information was used to modify the test specifications.

8.4.6 Thermal Vacuum Test Apparatus and Procedure

8.4.6.1 Chamber

A cylindrical Thermal Vacuum (T.V.) chamber was constructed from 1/2 inch aluminum, type 60/61. It was 18 inches long and 11 inches inside diameter. One end was closed by a 1/2-inch plate, with a 2-inch outlet for connection to the vacuum pumps (see Figure 8-14). The other end was open, and was sealed during test by a 1.25-inch lucite (cast acrylic) plate against an O-ring (see Figure 8-15). This lucite plate also carried all the feed-throughs necessary for the experiment, package signals, power supplies, thermocouples, hot-plate power, etc.

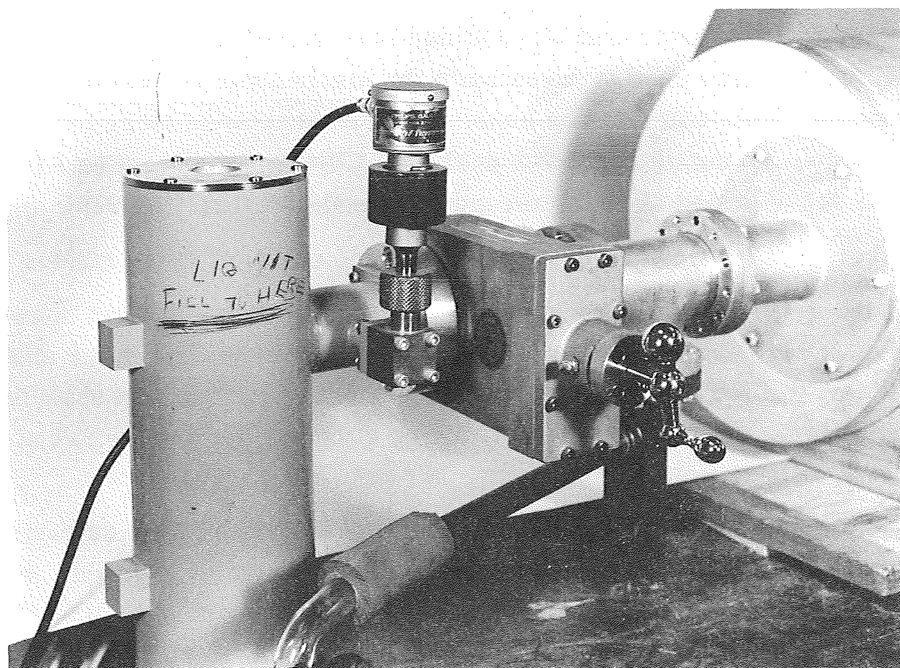

Figure 8-14. Thermal Vacuum Chamber, Rear View

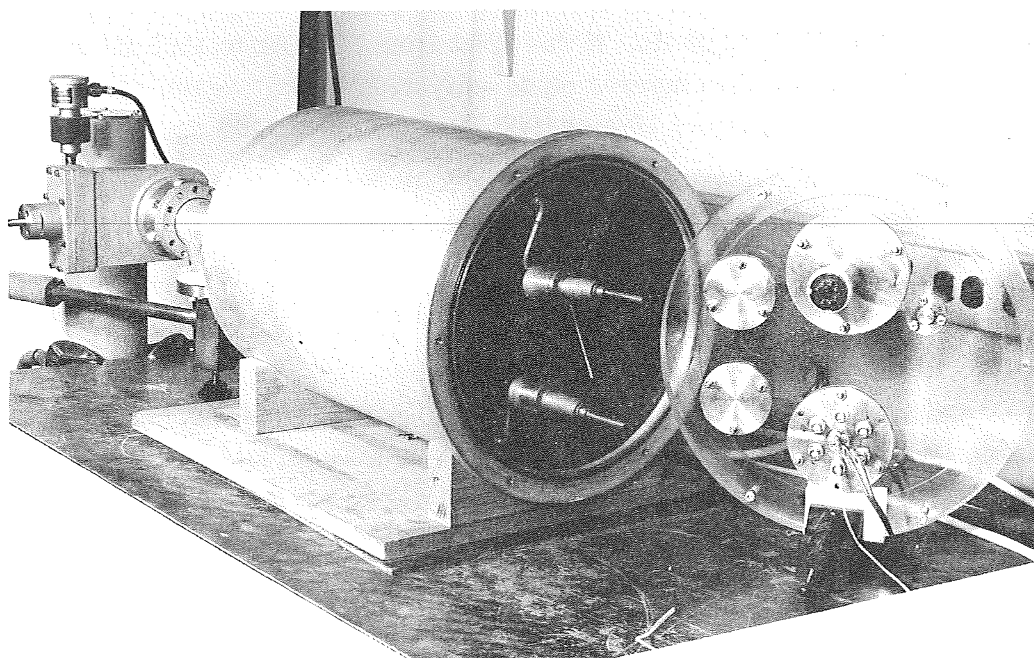

Figure 8-15. Thermal Vacuum Chamber, Front View

A cylindrical cold wall was constructed from 1/32-inch thick copper. A 3/16-inch copper pipe was coiled length-wise, and soldered to the inside of the cold wall. During tests, vaporized liquid nitrogen was forced through this pipe, the exhaust temperature running about -100°C for -10°C package temperature, and about -80°C for +40°C package temperature. The inlet and outlet to this pipe were also fed through the lucite plate with bellows. Liquid nitrogen vapor was forced through the cold wall piping, by connecting the piping to a 50-liter dewar of liquid nitrogen. Inserted in the dewar was a filament of resistance wire in two porous layers of fiberglass sleeving. This filament was driven by a variac at 30-40 VA. The cold wall enabled the achievement of the low temperatures specified, and also acted as a cyrogenic trap, thereby assisting in attainment of pressures inside the chamber of less than 10^{-6} mm Hg. (The silastic foam used as the encapsulant, contain considerable amounts of volatile material of high vapor pressure. It was this material in particular that was difficult to pump out without the cold wall.)

A hot plate was constructed from 3/16-inch aluminum with a resistance wire filament mounted on the underside (see Figure 8-16). A horseshoe shroud was constructed to mount on the hot plate to form a box into which the units under test could be inserted and mounted (see Figure 8-17). The inside surfaces of this box were painted with black epoxy paint to effect a radiant source. The hot plate filament was constructed by winding nichrome wire on a quartz plate and insulated in mica for a hot resistance of 75 ohms. This filament was conveniently driven by a Harrison 881A Power Supply, and provided more than adequate power to achieve a package temperature of +40°C.

An additional feature of great convenience to the T.V. system was a thermal coupling between the horseshoe box and the cold wall. This was a copper braid strap soldered to the cold wall on one end. The opposite end terminated in a copper block machined with a hole. A long stainless steel rod with a threaded end was made captive in this hole. The threaded end mated with a threaded aluminum block mounted on a horseshoe. The opposite end was fed through the lucite plate and fitted with a knob. Turning this knob clockwise increased the thermal coupling between cold wall and hot plate box, and vice versa. This device was most useful in reducing the time taken to achieve package temperatures below ambient.

8.4.6.2 Pumping System

The 2-inch pipe was made with a Y joint which branched to a Welsh 1402B 140 liter/min forepump used to rough out the chamber. This branch contained a glass cold-trap tube which was immersed in liquid nitrogen once the chamber pressure was 200 microns or less. This enabled pressures of about 15 microns to be achieved, at which time the forepump branch was shut off, and the other branch (connected to

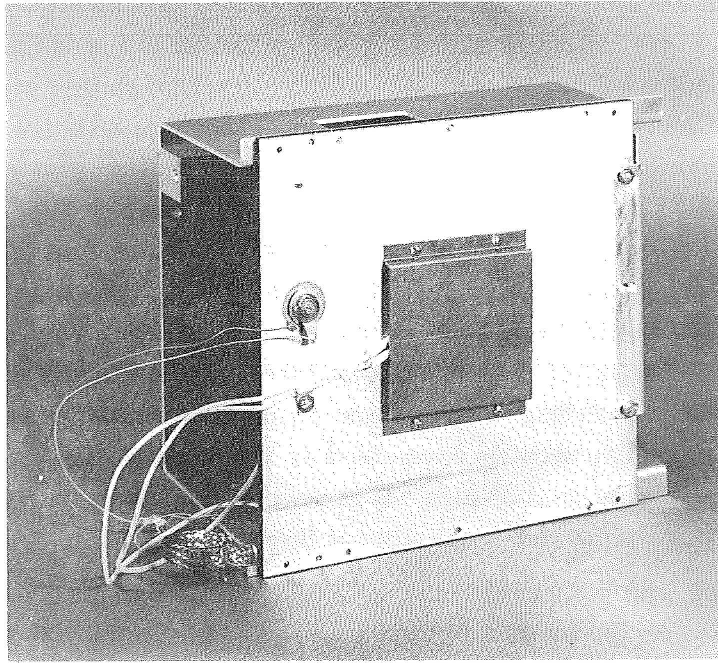

Figure 8-16. Hot Plate Filament and Thermistor

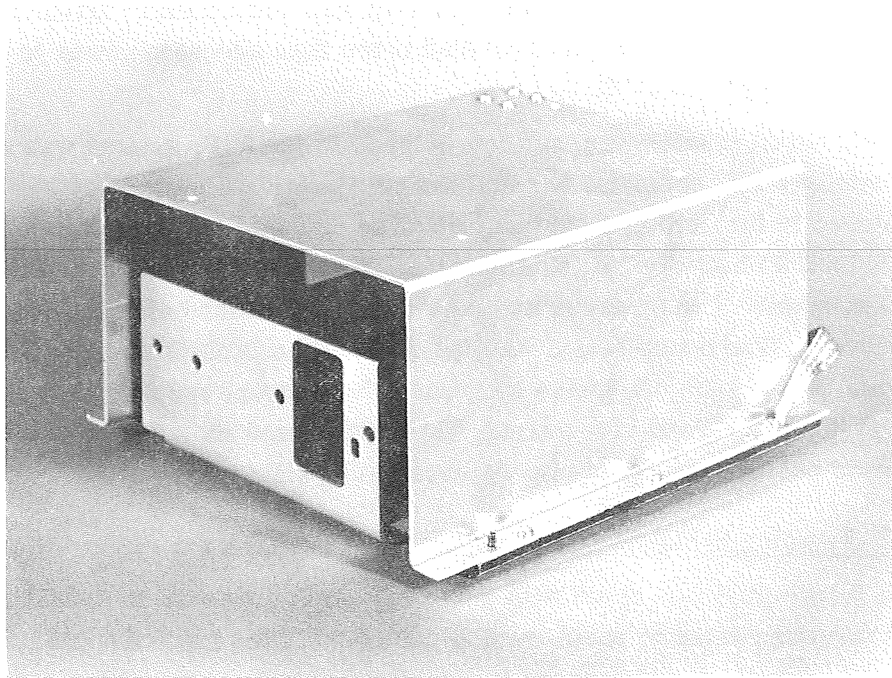

Figure 8-17. Hot Plate with Horseshoe Shroud

a diffusion pump system) was opened. This system consisted of a liquid nitrogen trap, which was filled about 15 minutes before this branch was opened, a CVC oil diffusion pump of 115 liter/sec capacity, and a Welsh 1405B 58 liter/min backup pump. A room temperature Chevron-baffle was inserted between the diffusion pump and the liquid nitrogen trap. Phillips vacuum gauges monitored the pressures at strategic points in the system, and the metering system contained a meter full-scale trip, which turned off the power to the diffusion pump heater in case the vacuum failed.

The temperature of the package under test was monitored at all times by use of a copper constantan thermocouple, mounted under a package mounting screw head, on the detector side. An ice-water bath was used as reference for this thermocouple. The output of the thermocouple was recorded on the Leeds & Northrup recording potentiometer, and measured for accurate temperature determination by a Rubicon potentiometer #2745.

The temperature of the hot plate was monitored, as a guide to temperature control, by a thermistor mounted on the hot plate (Figure 8-16). The thermistor value was read by using a Leeds & Northrup resistance bridge, and the temperature was then determined from the temperature/resistance calibration curve for the thermistor.

8.4.6.3 Data

During the T.V. tests of all units, temperature and pressure histories were recorded, and charts of the temperature history are available for each unit. Pressure in the chamber was at all times less than that called for in the test specifications (1×10^{-5} mm Hg). A Leeds and Northrup stripchart recording potentiometer, with a temperature tripping device, was used to switch the current to the hot plate filament. Current was switched off when a preset high temperature was reached (a useful safety precaution), and switched on when a preset low temperature was reached.

In order to obtain more calibration data, a Photo-data system was devised and used during the T.V. test of Serial No. 663. It was made up of the following items (see Figure 8-18):

(1) A sequence generator to control the S-lines and hence the experimental modes. The sequence count was advanced by one on application of an input trigger pulse to this unit. The S_{6-11} line was locked in the "one" state, so that the package under test, remained in the calibrate mode. This gave rise to the following continuously repeated cycle of events.

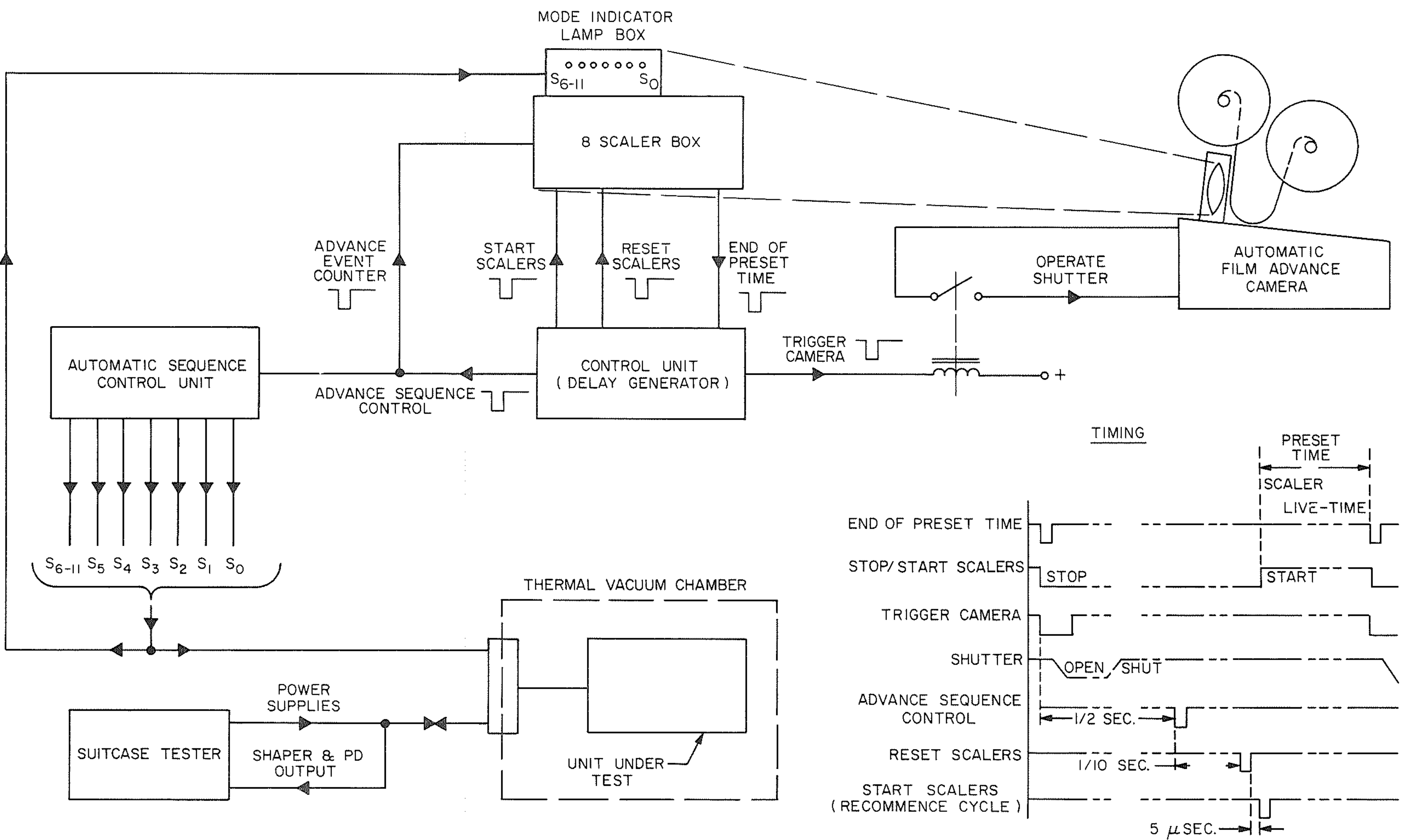

Figure 8-18. Photo Data System, Block Diagram

Each of the 16 experimental modes was cycled through twice while the internal source was activated. The modes were then cycled through once while the Test Pulser II was turned on. Finally, the modes were cycled through while the Test Pulser I was turned on, after which the sequence was repeated with the activation of the internal source, and so on.

(2) A scaler box that contained eight separate scalers and their individual Nixie displays (see Figure 8-19). These were used to scale and display the five channel outputs from the package under test, the number of experimental modes sequenced (event counter), and live time. The live time counter had a preset control which generated the automatic STOP of all scalers.

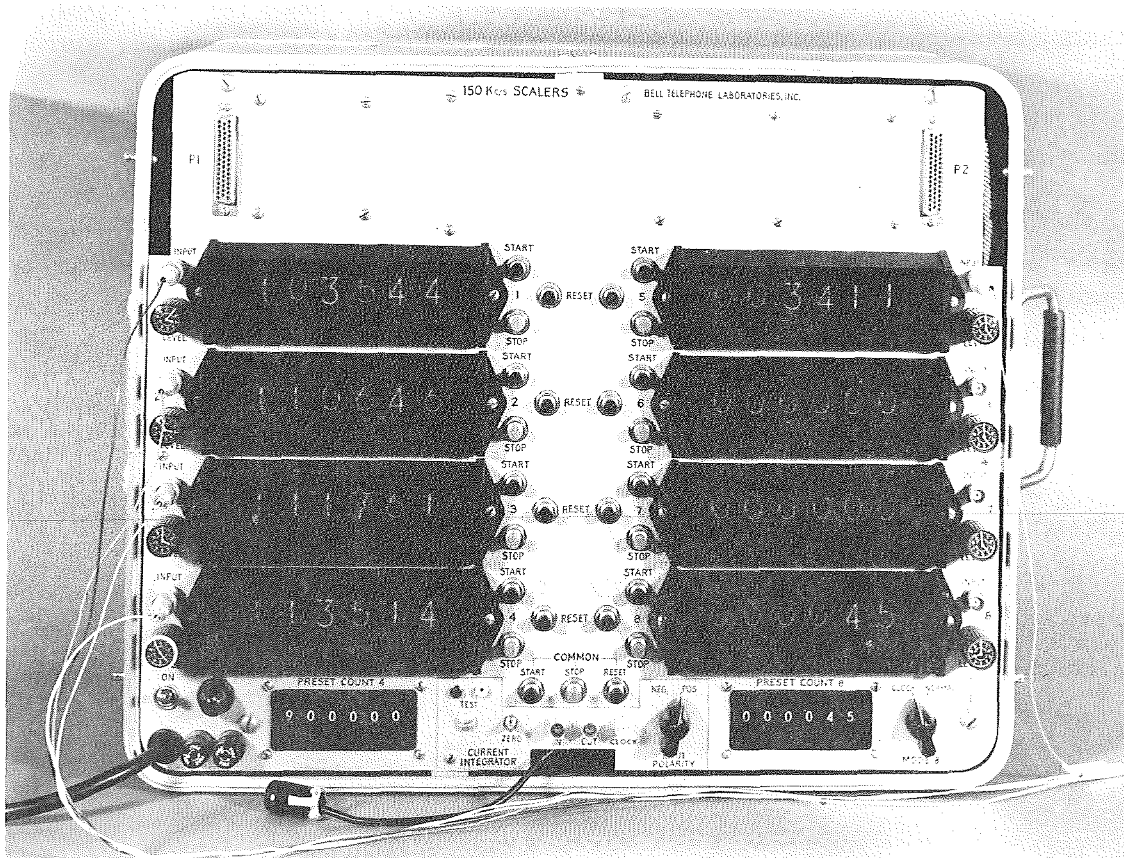

Figure 8-19. Eight-Scaler Box

(3) An automatic Kymograph camera type C4F which could be triggered remotely by an electrical signal, and would then operate its shutter and automatically advance the film to the next frame. Kodak 4-x film was used at 1/25 sec and f16-22.

(4) A control unit in which a system of delay univibrators was triggered by the preset time pulse in the scaler box. This initiated the following sequence of commands:

a. Trigger camera.
b. Advance sequence generator by one and event counter by one.
c. Reset scalers.
d. Start scalers.

At preset time later, the preset pulse in the scaler unit would trigger the next of these control cycles. The preset time was selected to be 5 seconds. The S_5 line was broken and used to activate a circuit which drove a relay coil. The relay contacts paralleled the source motor switch in the GSE suitcase. Hence, the source motor was activated at the correct sequence times.

8.4.7 Thermal Vacuum Test Results

During T.V. test of unit No. 651, the solid-state detectors became noisy, and it was subsequently determined that this was due to outgassing material from the encapsulant condensing on the detectors. This initiated the "bake-out" procedure as described in Paragraph 8.3.3 above.

Operation of the electronics was fault free. Unit #652 operated correctly throughout the T.V. test.

During the T.V. test of unit #663 detector #6 became noisy. This was lithium assembly No. 138. The electronics operated without fault.

Some 10,000 frames of photo-data were taken for subsequent detailed evaluation of temperature calibration.

Chapter 9

EXPERIMENT CARRYING CASE

All experiment packages were protected against damage during shipment by a specially outfitted carrying case (shown with the experiment in place in Figure 9-1).

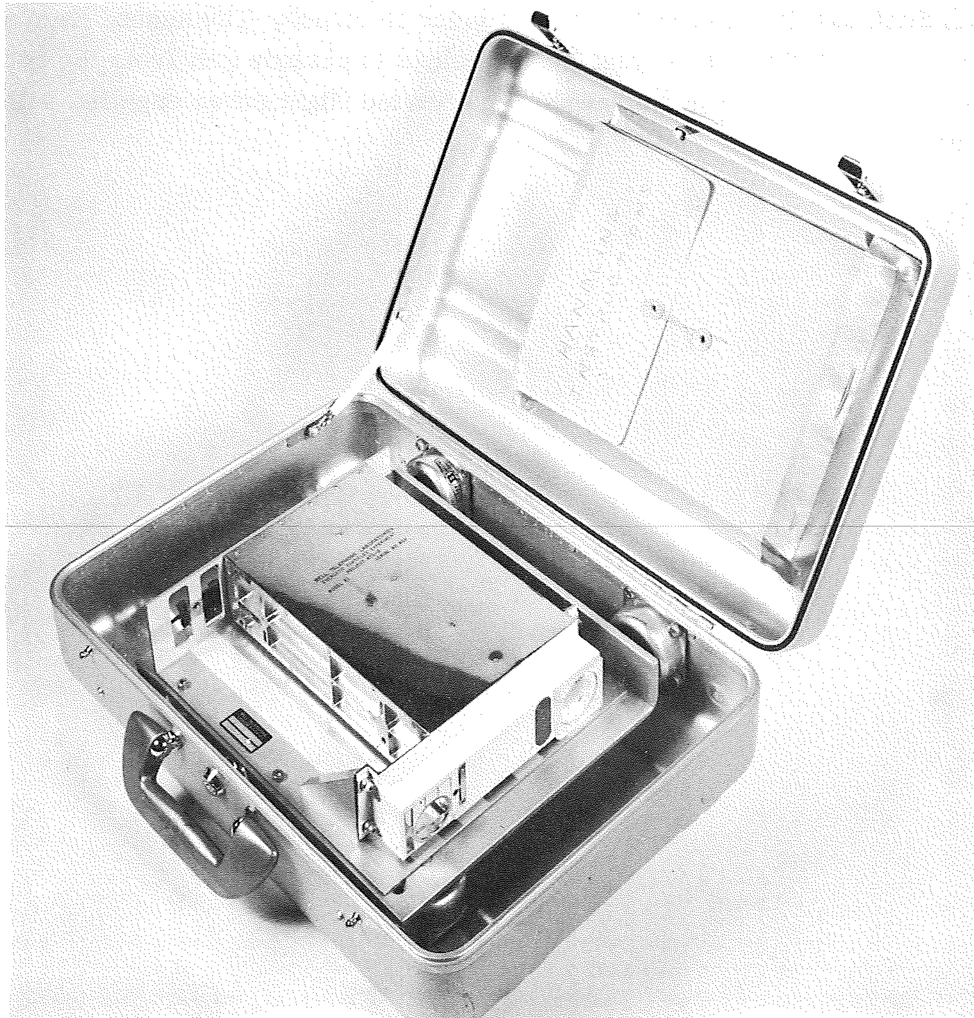

Figure 9-1. Experiment Carrying Case

A 6 x 13 x 18 inch aluminum case, made by Halliburton, Incorporated, was equipped with a heavy L-shaped aluminum plate, supported on large rubber shock mounts secured to the bottom and one side of the case. The experiment was mounted in a handling fixture designed to protect the housing finishes during bench testing prior to spacecraft integration. The package was suspended in this fixture in a manner similar to the EME mounting arrangement and provisions were made to accommodate the Rice University experiment. All rear connectors were accessible through cutouts. This fixture was bolted to the carrying case plate for shipment. A rear locking screw tool and Allen wrenches for removing the shipping bolts were secured inside the carrying case along with a copy of the BTL integration and prelaunched mechanical handling instructions.

Two nonflight protective covers on the front plate required countdown action. One of these was a lucite cover over the detector aperture to protect its 85 millionths of an inch thick titanium foil from damage prior to launch. The second item was an unvented plate over the coaxial test jack openings to exclude grit from the rotary solenoid bearings. This was exchanged for a vented flight cover supplied with each experiment.

BELL
SYSTEM